VORTEX STRUCTURE AND DYNAMICS OF FLORIDA KEYS WATERSPOUTS

1974 Field Experiment

Final Report

Principal Investigator: P. C. Sinclair

DEPARTMENT OF ATMOSPHERIC SCIENCE
COLORADO STATE UNIVERSITY
FORT COLLINS, COLORADO

TABLE OF CONTENTS

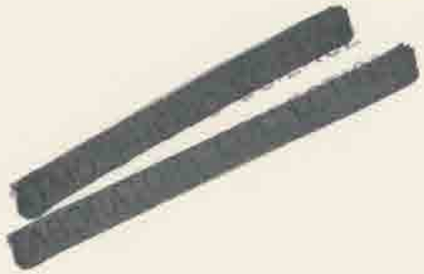

ABSTRACT

From direct penetrations of the waterspout funnel by specially instrumented aircraft, a quantitative description of the dynamic-thermodynamic structure of the waterspout has been developed. The Navier-Stokes equations of motion for the waterspout vortex are simplified by an extensive order of magnitude analysis of each term in the equations. The reduced set of equations provides a realistic mathematical model of the waterspout vortex. Further simplification shows that the cyclostrophic-Rankine combined vortex model accounts for, on the average, approximately 63% of the measured pressure drop from the environment to the waterspout core.

The penetration measurements show that the waterspout funnel consists of a strong rotary and vertical field (radial component is smaller) of motion which results in a combined flow pattern similar to that of a helical vortex. In general, the measurements indicate that this one-cell vortex structure is the dominate configuration. However, several penetrations suggest reduced positive vertical velocities near the funnel core, and in one case, a downdraft core with vertical velocity of -0.8 $msec^{-1}$. These measurements indicate that waterspout vortex may in some stages of development have a structure more closely described by the two-cell vortex such as discovered by Sinclair (1966, 1973) for the dust devil vortex. The temperature and pressure structure show that the waterspout, like the dust devil, is a warm core (ΔT = 0.1 to 0.5°C), low pressure (ΔP = -0.6 to -8.4 mb) vortex. All aircraft penetrations of the visible funnels were made within 150 m of cloud base at speeds of 55-65 $msec^{-1}$.

ACKNOWLEDGEMENTS

I wish to express my appreciation to the many people who over the years prior to and during the 1974 waterspout field program were responsible for its ultimate success. Special regards go to Dr. Joe Golden, who introduced me to the waterspout research area, and Mr. Verne Leverson who carried out the detailed analyses of the aircraft measurements which were later used as the basis of his Master of Science Thesis.

As a matter of record, the key personnel that were responsible for the instrumentation and aircraft development, the 1974 waterspout field program, and the following data analysis and interpretation are listed below along with their primary work area responsibility(s).

Personnel	Research Responsibility(s)
P. C. Sinclair	Project Director Field Experiment and Aircraft Modification Design Flight Test Data Analysis and Interpretation
V. H. Leverson	Graduate Research Assistant Field Manager: 1974 Program Aircraft Observer Data Analysis and Interpretation
G. B. Edelen	Computer Programming
D. Younkin	North American T-6 Pilot Flight Test
J. Wilkie	Aircraft Mechanic Instrumentation and Installation
R. Remilong	Chief Electronics Technician Aircraft Instrumentation and Development
J. Burton	Electronics Technician Aircraft Instrumentation and Development
L. Lilie	Electronics Technician Aircraft Instrumentation Installation and Check Out: 1974

Personnel	Research Responsibility(s)
T. Grove	Electronics Technician Aircraft Instrumentation Installation and Check Out: 1974
D. Hill	Electronics Technician Aircraft Instrumentation Field Maintenance and Check Out: 1974
R. Ellis	Machinist Instrumentation Pod
C. Wilkins	Machinist Aircraft Instrumentation
J. Wilson	Secretary: Thesis typing
K. Malewicz	Secretary: Thesis typing
R. Urbanak	MIC Key West Weather Station
G. Faraldo	Key West Airport Manager
Dr. F. Smith	Instrumentation Pod Stress Analysis
U. S. Air Force	Instrumentation Pod (T-33 fuel tank)
Martin Marietta	Instrumentation Calibration and Instrumentation Pod Modifications

THE VORTEX STRUCTURE AND DYNAMICS OF THE FLORIDA KEYS WATERSPOUT

The 1974 Waterspout Field Program Synopsis

I. INTRODUCTION

The primary purpose of our waterspout research program has been essentially twofold: (1) develop in-situ and remote sensing techniques and observational platforms that can be used to determine the dynamical-thermodynamical structure of the waterspout vortex, and (2) from these measurements and analysis results, design and implement a similar tornado vortex observation system. We anticipate, the waterspout research, along with an earlier dust devil vortex measurement program, will act as a two-step, building block approach to the design and implementation of the tornado vortex investigation. Our previous and present measurements near and within dust devils (Sinclair, 1966, 1969a, 1973b) and waterspouts, (Leverson, Sinclair, Golden, 1977 and [1]Sinclair et al, 1977) along with the relatively meager tornado vortex measurements (Hoecker, 1960, Golden, 1976), indicate that the vortex structures may be quite similar even more so than that indicated visually (Figs. 1, 2, and 3).

The detailed analysis of the waterspout data obtained under NOAA Grant 04-5002-8 and NRC Grant AT49-24-0197 for the Final Report has been largely accomplished by Mr. Verne Leverson, who received his Master's Degree in Atmospheric Science from Colorado State University (CSU) in June 1978. Consequently his Master's Thesis "Waterspout Structure and Dynamics" is included since it is the most complete, single document of the 1974 waterspout

---

[1]Sinclair, P. C., V. H. Leverson, and R. F. Abbey Jr., 1977: The Vortex Structure of Dust Devils, Waterspouts, and Tornadoes. Tenth Conference on Severe Local Storms, Oct. 18-21, Omaha, Neb., AMS, Boston, Mass.

Figure 1: Tornado

Figure 2: Waterspout

Figure 3: Dust Devil

field research program. Several papers by Leverson and Sinclair, et al, have also been published, and they are included in the Appendix. It is worthy to note, however, that this entire waterspout field program was primarily dependent on available expertise and research equipment within the CSU Atmospheric Science Department Airborne Research Flight Facility (Sinclair, 1969b, 1973a, 1974). This Facility instrumented the North American T-6 Research Aircraft and provided the trained technicians, flight and ground crews for the field experiment. In addition, the Facility provided important data recording and processing techniques and computer programs which had evolved during the six year period prior to the waterspout program. The Facility capability was available primarily because of our previous severe storm measurement and analysis programs with instrumented aircraft (Figs. 4, 5, and 6). Because of this available capability, high quality measurements and analyses could be provided at minimum cost.

II. FIELD EXPERIMENT LOCATION

The selection of the field experiment site was based primarily on the pioneering waterspout research by Dr. Joe Golden of NOAA/ERL. Golden (1970, 1971, 1973a,b, 1974a,b,c) had shown that the Florida Keys area in the vicinity of Key West experiences a high and bimodal frequency of waterspout occurrence during the summer months - primarily during June and August. Also, the Key West area provided an ideal location for the research flight operations because of the relatively low-density air traffic environment. This was an extremely important factor since the waterspout penetrations required almost unrestricted airspace for the penetration tracks. Consequently, all flights could be conducted VFR with altitude and flight direction completely under control of the

Figure 4: McDonnel F-101B Severe Storm Penetration Aircraft

The F101B is owned by CSU and has been extensively modified to carry the AADS-4A data system. The 16 ft nose boom supports the 3-D gust velocity probe which is referenced to a strapped-down gyro system in a temperature controlled chamber in the nose of the aircraft.

Figure 5: Canadair Mark IV (T-33) Severe Storm Penetration Aircraft

The Mark IV has an earlier (AADS-3A) but similar measurement system as used on the F-101B research aircraft.

Figure 6: North American T-6 Severe Storm Cloud Base and Waterspout Research Aircraft

The T-6 system (AADS-2A) is very similar to that of the F-101B and Mark IV research aircrafts, except the entire gust probe package is mounted below the right wing in a modified T-33 drop tank pod. This system was specially modified for the waterspout penetration program.


N90650

flight crew.

In addition, there were excellent support facilities at and near the Key West International Airport. The National Weather Service station (MIC, Mr. Richard Urbanak) provided the project with current observations, analyses and forecasts for the waterspout project area. Also, the FAA Flight Service Station provided the research aircraft crew with updates on current and forecast weather during the entire flight phase of the experiment. Lastly, the Key West site provided us with relatively inexpensive living quarters within approximately one block of the airport fixed based operator where the research aircraft was parked. This arrangement allowed us to perform our daily calibrations and aircraft maintenance with a minimum of travel and logistics support. We feel that the selection of the Key West airport site was instrumental in the successful waterspout field operations and in the subsequent data analyses and results presented in this report.

III. FIELD OPERATIONS

A. Waterspout "Hunter" Technique

Since an important goal of the research program was the development and field testing of suitable instrumentation and efficient penetration techniques, a game plan of "hunting" waterspouts was formulated. Because virtually no documented accounts of aircraft penetrations of waterspouts were available in the literature, only small to medium sized funnels were chosen as targets of the "hunt". The entire process leading up to the successful penetration(s) of a waterspout involved a degree of forecasting, a considerable amount of nowcasting, and trained observers both in the air and on the ground.

The first step involved careful inspection of synoptic charts, synoptic and aviation observations, and the Key West soundings. The ideal weather for waterspout-producing cloudlines included: (1) few or no middle and high clouds during the maximum diurnal heating period - approximately 0900 to 1600 EDT, (2) surface winds less than about 10-15 kt (generally accompanied by a surface pressure gradient of 2-3 mb or less from Miami (MIA) to Key West (EYW)), (3) low level winds approximately easterly in direction, (4) stability indices (SI) between +3 and -5, (5) low velocity shear in the vertical below 400 mb, (6) warm low level temperatures, and (7) warm water temperatures. If a synoptic scale disturbance was present, the frequency of waterspout-producing cloudlines and the strength of the disturbance were generally inversely related.

Certain definable features of cloudlines provided distinct clues as to waterspout production and existence. The "hardest" and fastest growing cumulus congestus cells in a line were the most favorable locations for waterspout development. A mature or dying cell in the same cloudline was often raining out within several kilometers of the waterspout. Small protuberances on the usually flat cloud bases often indicated regions of suspected rotary motions.

Once in the vicinity of possible funnel activity, several physical indications both on the sea surface and at cloud base suggested incipient waterspout formation. The significance of these features had resulted from comprehensive studies of the Florida Keys waterspout by Golden (1973b). A dark spot on the water surface indicated the concentrated rotary motions of an invisible vortex column extending from cloud base to sea surface. If not already visible, a funnel cloud often subsequently developed. On occasion a spiral pattern on the water surface was an indication of

boundary layer air converging into a yet-invisible waterspout vortex. This pattern occurred most often when a rain shaft was very close to the suspected area of waterspout formation. Any rotations or pendants at cloud base also provided clues to future waterspout development. The research aircraft usually remained in these areas of suspected waterspout formation until either funnels formed or the cloudline began to dissipate.

B. Summary of Field Operations

Table 1 presents a summary of field project activities. Out of a total 12-day period, waterspouts were sighted on 7 days from Key West International Airport, the base of operations. The research aircraft flew and penetrated funnels on six of the seven waterspout days. The aircraft was down for maintenance on the remaining day. A total of 15 individual waterspout were penetrated; of these, 7 waterspouts were penetrated more than once. This provided a total of 49 penetrations for the field program. It should be noted that we are defining a waterspout as any event that exhibits the physical features associated with concentrated vortical or helical motion (e.g., dark spots, spiral patterns, incipient funnel pendants, etc.).

Flight time hours for the research program totaled 74.7 hours. Of these, 53.3 hours were ferry hours to and from Key West, 20.0 hours were field experiment hours involved in either searching out or penetrating waterspouts, and 1.4 hours were utilized in flight testing.

Table 1. Summary of the Field Project Period and Total Research Aircraft Hours.

TOTAL FIELD PROJECT DAYS	WATERSPOUT DAYS	NUMBER OF WATERSPOUT FLIGHT DAYS	NUMBER OF WATERSPOUTS PENETRATED	NUMBER OF PENETRATIONS	TOTAL FLIGHT HOURS		
					FERRY	FIELD EXPERIMENT	FLIGHT TEST
12	7	6	15	49	53.3	20.0	1.4

IV. SUMMARY OF RESULTS

Seven penetrations of three individual waterspouts were selected for detailed case study examinations. The three were chosen for the following specific reasons:

1. all were multiply penetrated at various altitudes,
2. penetrations were accomplished in the visible funnel portion of the vortex, thus affording estimates of the off-center distance by the instrument probe penetration,
3. both cyclonic and anti-cyclonically rotating vortices were included, and
4. extensive photographic and aircrew log documentation of the three funnels were available.

The remaining waterspout penetrations were associated with either much weaker and sometimes invisible funnels which were difficult, if not impossible, to analyze because of suspected large off-center penetration tracks. However, the selected waterspout cases provided consistent results for the development of a conceptual vortex model.

The primary conclusions of the waterspout measurement and analysis program are summarized as follows:

1. Suitably instrumented and stressed aircraft are capable of successfully penetrating weak to moderately intense waterspouts and obtaining measurements of the vortex flow and thermodynamic fields. By this method, measurements in the radial direction are spatially detailed; however, the vertical structure can only at best be coarsely resolved. Improved penetration techniques and faster responding instrumentation should supply data of greater accuracy than that presented here.
2. Waterspout wind, temperature, and pressure structure in the near cloud base environment can be described as follows:
   a. The vortex is defined by a concentrated region of strong tangential and vertical velocities upon which is superimposed radial velocities of slightly lesser magnitude. Maximum values of $\bar{v}$ range from $\sim$5 ms^{-1} to 22 ms^{-1}, while largest values of $\bar{w}$ range from +2 ms^{-1} to $\sim$+8 ms^{-1}. In the weaker waterspouts $\bar{v}_{max} \approx \bar{w}_{max}$, but the departure of $\bar{v}_{max}$ above $\bar{w}_{max}$ increases with more intense waterspouts. Radial

velocities exhibit maximum values of $\sim$+2 ms^{-1} to -5 ms^{-1}. The average radial velocity profile shows inward motion of $\sim$-1 ms^{-1} to -3 ms^{-1}; however, the environmental winds can apparently disrupt the convergent velocities and produce regions of either outflow or amplified inflow.

b. The measurements indicate general upward vertical motion near the core (one-cell vortex); however, several penetrations suggest reduced positive vertical velocities, and in one case, a definite downdraft of -0.8 ms^{-1} was measured at a radius of 1.5 m. The lack of more evidence of the central core downdraft (two-cell vortex) in the measurements may be due to consistent, but small, off-center penetrations by the aircraft.

c. The tangential velocity radial profiles do not in general fit the Rankine-combined vortex model very well. Profiles of $\bar{v}$ show an increase in relative angular momentum outward of the radius of maximum $\bar{v}$ (non-zero relative vorticity). The closest fit to the Rankine model occurs in the strongest waterspout penetrated. Few core measurements of $\bar{v}$ are available; however, those that are, indicate a region rotating approximately in solid body fashion with a rotation rate that decreases from r = 0 to r_{max}/where r_{max} is at $\bar{v}_{max}$. The $\bar{v}_{max}$ extrema are appreciably eroded from that predicted by the (inviscid) Rankine model.

d. The temperature structure exhibits increases on the order of 0.1 to 0.5 K from large radii to the waterspout core. Such a small relative warming in or near the core gives little evidence for either rising or sinking air motion on the vertical axis. Warm boundary-layer air is certainly transported vertically by the waterspout circulation system, remaining essentially undiluted due to the vortex's resistance to entrainment/detrainment. By the same token, axial downflow could warm an air parcel adiabatically, the amount depending on its initial temperature and pressure. No apparent decrease in temperature has been detected in the vortex core.

e. The pressure structure indicates core deviations of -0.6 to -8.4 mb. The measured tangential wind maxima, assuming cyclostrophic flow, account for as little as 25% to as much as $\sim$94% of the measured core pressure deficits with an average value of 63% for all six penetrations. These results are in general agreement with the dust devil wind-pressure measurements (Sinclair, 1966, 1969a, 1973b).

3. Anticyclonic waterspouts of the weak to moderate intensity appear to occur as often as cyclonic ones. Of the 15 waterspouts penetrated during the field program 4 rotated cyclonically, 7 anticyclonically, and 4 in an undetected direction.

4. The order of magnitude analysis shows that the cyclostrophic relation ($\bar{v}^2/r = \bar{\rho}^{-1} \partial\bar{p}/\partial r$) provides a valid first approximation to the complete radial momentum equation. Likewise, the hydrostatic assumption appears valid near the core, but the lack of accurate and numerous measurements in the core and along the vertical axis precludes knowledge of the vertical momentum balance there. In general, retention of the inertial terms necessitates likewise retention of the turbulence terms in all three momentum equations. The continuity equation for imcompressible, axisymmetric flow is a valid approximation for the waterspout vortex. An order of magnitude analysis of the thermodynamic energy budget shows that in addition to strictly vertical ascent; non-vertical ascent, non-hydrostatic effects, and condensation processes can be important in considering parcel temperature changes in the waterspout.

The data and conclusions in this paper should provide additional useful insights into waterspout structure and dynamics. Together with previous field measurements of other naturally occurring vortices (i.e., Sinclair, 1966, 1973b), these results can form a solid foundation upon which new and more accurate concepts and models of geophysical vortices can be built.

Of utmost importance in the area of future research is the necessity for continued efforts at detailed observations of concentrated atmospheric vortices. Such observations should include not only the atmospheric structure antecedent to and concurrent with the occurrence of such vortices, but also examinations of the detailed circulation and energetics of the parent cloud-vortex system. The frequently occurring and usually more docile waterspout (particularly Florida Keys and Gulf Coast types) should continue to be a subject of detailed observational programs; the goal(s) being not so much a determination of maximum kinematic and thermodynamic anomalies, but more a quantitative description of the hydrodynamic processes and life cycle dynamics that in general should be transferrable, at least qualitatively, to the tornado. These efforts should be directed to

the entire waterspout system - - from parent cloud to surface boundary layer.

V. FUTURE RESEARCH

We feel that without question the fine success of this first year's exploratory waterspout measurement and analysis program indicates that significant progress has now been made in understanding the vortex structure of small atmospheric vortices (i.e., dust devil and waterspout) to undertake the planning phases of a future tornado measurement program. Subsequent (1975 and 1976) waterspout field program results substantiate these results and analyses presented herein.

While the waterspout and the dust devil present a relatively insignificant threat to property and mankind, the tornado, on the other hand, kills hundreds of people and results in many millions of dollars damage annually. Severe weather phenomena statistics show that the eastern half of the United States can expect an annual: 1000 to 1500 tornado sighting, $\$1\text{-}2 \times 10^8$ dollars property damage, and 100-200 deaths. In 1973 six major tornado outbreaks accounted for $\$2 \times 10^6$ dollard property damage. As the population density in the U. S. increases, tornado deaths and property damage will increase markedly. Consequently, a significant increase in our understanding of tornadic storms by direct observations is urgently needed to assist the development of adequate warning systems and more protective home, schools, and industrial buildings. Also, the design of new structures, such as nuclear power plants and oil drilling towers, requires much more intimate knowledge of tornado funnel flow fields and pressure variations.

Although direct and passive measurements near and within the

tornado vortex will require at least 1-3 years of instrumentation and vehicle development, our first efforts will be to develop, from the measurements and results presented herein, a full size spectrum of physically relevant analytical and numerical models of small-scale geophysical vortices. These models will have a direct application in the structural engineering and operation of the proposed off-shore, floating nuclear power plants and oil drilling platforms. The models will also provide meaningful estimates of similar parameters of the more intense tornado system and thereby act as a guide to the formation of a safe and meaningful tornado field measurement program.

VI. WATERSPOUT MEASUREMENTS AND ANALYSES

This section of the Report presents the detailed discussion and analyses of the 1974 waterspout research program. It represents in its entirety Mr. Verne Leverson's Master of Science Thesis "Waterspout Structure and Dynamics". Since Leverson's Thesis is the most complete, single document of the 1974 waterspout field research program, it appeared most appropriate that it be included in its original form in this Report.

THESIS

WATERSPOUT STRUCTURE AND DYNAMICS

Submitted by

Verne H. Leverson

In partial fulfillment of the requirements

for the Degree of Master of Science

Colorado State University

Fort Collins, Colorado

Spring, 1978

ABSTRACT OF THESIS

WATERSPOUT STRUCTURE AND DYNAMICS

A quantitative description of the kinematic and thermodynamic structure of the Florida Keys waterspout is presented. The description is based on field measurements of the three-dimensional winds, pressure, and temperature obtained by a penetrating, specially instrumented research aircraft. The experimental procedures, aircraft instrumentation, and analysis techniques are discussed and appraised. A set of hydrodynamic governing equations for the waterspout vortex is derived. Utilizing the aircraft measurements, an extensive order of magnitude analysis is performed on the equations to obtain a realistic mathematical model of the waterspout.

Waterspout winds were derived by measuring the atmospheric motion relative to an airborne platform, the attitude and motion of the platform relative to the earth, and the visible funnel's translation and tilt. Pressure and temperature were measured using commercial units. Visible funnel characteristics were recorded on film and in aircrew data logs. Penetrations of visible funnels were accomplished within 150 m of cloud base and at speeds of 55 to 65 m s^{-1}.

Penetration measurements reveal the waterspout as a small area of concentrated rotary circulation upon which is superimposed general rising motions - the one-cell vortex. However, several penetrations suggest reduced positive vertical velocities near the funnel core, and in one case, a downdraft of -0.8 m s^{-1} was measured at a radius of 1.5 m - the two-cell vortex. The temperature and pressure structure is depicted by maximum core deviations ranging from 0.1 to 0.5 K and

-0.6 to -8.4 mb, respectively. Additional aspects of waterspout structure are discussed.

The order of magnitude analysis shows that the cyclostrophic relation is a valid first approximation to the radial balance of forces, and that the hydrostatic assumption appears valid near the core in view of the available measurements. The retention of all inertial forces requires the inclusion of turbulence effects in the three momentum equations. The assumption of incompressible, axisymmetric flow appears valid for the weak to moderate waterspout, upon which the emphasis of this study was focused.

Verne H. Leverson
Atmospheric Science Dept.
Colo. State University
Fort Collins, Colo. 80523
Spring, 1978

ACKNOWLEDGMENTS

The author extends sincere thanks and appreciation to his advisor, Dr. Peter C. Sinclair, for his guidance and support during the course of this work. For his encouragement and suggestions, the author expresses gratitude to Dr. Joseph H. Golden. Special thanks go to Professor Lewis O. Grant and Dr. Jack E. Cermak for their valuable input in the final preparation of the manuscript.

The success of the Florida Keys field program is to be shared by many people. Mr. George Faraldo, Airport Manager of Key West International, and Mr. Richard Urbanak, Meteorologist-in-Charge of the Weather Service Office in Key West provided assistance and cooperation during the field program that is gratefully acknowledged. The capable maintenance and technical support of the aircraft and instrumentation systems during the field program by Messrs. Jerrell Wilkey and Donald Hill are sincerely appreciated. The author wishes to specially thank Messrs. Lyle Lilie and Thomas Grove for their expert preparation of the AADS-2B for the field program.

The author expresses considerable gratitude to Mr. Gary B. Edelen who provided professional programming expertise from the initial AADS-2B calibration to the final waterspout output. Quality typing of the manuscript was performed by Ms. Karen Greiner and Ms. Julie Wilson. The drafting was professionally done by Mr. Kenneth Streeb. The author especially thanks Ms. Kathy Malewicz for the excellent job of final manuscript typing and preparation, and Mr. David "Honkin" Younkin, the research pilot, for his excellent flying talents and good eyes.

Finally, the author thanks his wife, Mary, whose patience and understanding made this thesis possible.

This research was funded by the National Oceanic and Atmospheric Administration under Grant 04-5002-8 and by the Nuclear Regulatory Commission under AT(49-24)-0197.

TABLE OF CONTENTS

TABLE OF CONTENTS (cont'd)

LIST OF TABLES

LIST OF FIGURES

1. INTRODUCTION

1.1 History

The understanding of the behavior of small scale atmospheric vortices presents a formidable task yet unachieved. Dust devils, waterspouts, and tornadoes, all related by their unique concentrated vortical structure, occupy positions at the lower end of the spectrum of geophysical vortices based on the dimensions of their horizontal flow fields. Notwithstanding, tornadoes can produce the most locally damaging effects. From 1955 to 1969 tornadoes killed an annual average of 125 persons and caused an annual average of $75 million in property damage (Kessler, 1970). While operational forecasting techniques have drastically improved over the past twenty years, tornado prediction is still limited to successful severe thunderstorm forecasting, since a direct relationship usually exists between the thunderstorm energetics and tornado formation. Furthermore, the forecasting of maximum wind speeds, pressure drops, path lengths and widths, etc. is virtually impossible with present available information. This lack of understanding not only impedes better forecasts, but also restricts the design of tornado-proof structures and the generation of expedient tornado modification schemes.

The deficiencies in the knowledge of these small scale atmospheric vortices are mainly due to the absence of accurate observational data. The difficulty in making precise forecasts of their occurrence severely limits the ability to obtain on-the-spot observations. In addition, the environment near destructive vortices is hazardous to life and property. The only observational data have been acquired through

photogrammetric analyses of eyewitness movie films of tornadoes and tornadic waterspouts (e.g., Hoecker, 1960; Fujita, 1975; Agee, et al., 1975; Golden and Purcell, 1976; Zipser, 1976; Blechman, 1975) and from post mortem damage analyses (Mehta, et al., 1975; Fujita, 1970). These data have given quantitative values for only the tornado flow fields; the pressure and thermal structure remain virtually unknown except for cases when a tornado funnel has passed near a barograph (Outram, 1904; Lewis and Perkins, 1953; Ward, 1964).

Many experimental and numerical models have been developed with some success. Using laboratory apparatus, usually rotating tubs of water or air chambers outfitted with exhaust fans, concentrated vortices that resemble atmospheric vortices have been produced (Long, 1958, 1961; Turner and Lilly, 1963; Ward, 1972; Ying and Chang, 1970; Fitzgarrald, 1973; Dessens, 1972; Maxworthy, 1972; Hsu and Fattahi, 1975). In addition, mathematical and numerical models based on solutions to the governing equations have been obtained that simulate such possible geophysical vortex characteristics as one and two-cell flows, buoyant convection, and inviscid or turbulent flows (e.g., Gutman, 1957; Burgers, 1948; Sullivan, 1959; Kuo, 1966, 1971; Leslie, 1971; Bode, et al., 1975). However, many of the assumptions inherent in these models (e.g., initial and boundary conditions, constant eddy coefficients of momentum and heat transfer, and inviscid flows) remain open to doubt until they can be tested with observational data (Lilly, 1965).

1.2 Background Information

A waterspout is defined as a concentrated columnar vortex of small horizontal extent over water (Golden, 1974a). Morton's (1966)

definition loosely includes water devils, small vortices with no apparent link to clouds and comparable to dust devils in formation and intensity; waterspouts, columnar vortices stronger than dust devils yet weaker than tornadoes; and tornadic waterspouts, vortices ranking in intensity and appearance to tornadoes. In the context of this study, the intermediate definition will apply. That is, all waterspouts studied rank in intensity between dust devils and tornadoes, with the majority being generally more akin to dust devils in intensity.

Golden (1974a,b) has suggested that tornadoes and waterspouts are qualitatively similar, but differ in only certain quantitative characteristics. These differences comprise the intensity and size of the vortex, the structure of the meso and synoptic scale environment, and the characteristics of the parent convection. Furthermore, waterspouts occur in a relatively small area, the Florida Keys, with a higher frequency than other documented areas in the world, and their very nature usually allows close range observations (Golden, 1974a). For these reasons, the Florida Keys waterspout is susceptible to detailed scientific examination. Golden (1973b) has completed a thorough study of the life cycle, scale interactions, and climatology of the Keys waterspout that, together with recent photogrammetric analyses of tornado films (see review by Golden, 1976) and comprehensive in situ measurements of desert dust devils (Sinclair, 1966, 1973b; Ryan and Carroll, 1970) should provide a strong foundation upon which more detailed observations can be added in order to formulate relevent theoretical models of atmospheric vortices.

In order to capitalize on the accessible character of the Florida Keys waterspout, an airborne measurement program was conducted by Colorado State University in the early fall of 1974 in the Lower Florida Keys. Using a specially instrumented aircraft, direct penetrations of mature waterspouts were accomplished. The airborne data system was designed to record the waterspout's three dimensional flow field, temperature and pressure structure, the visible funnel characteristics, and the near-environmental wind and temperature structure. These data are analyzed and synthesized into a composite mathematical model of a waterspout based on an extensive order of magnitude analysis of the governing hydrodynamic equations.

1.3 Objectives

The primary objective of this paper then is four fold:

1. Discuss the experimental procedures and techniques developed to successfully probe waterspout funnels with a research aircraft;

2. Present a quantitative picture of the Florida Keys waterspout kinematic and thermodynamic structure deduced from the airborne data;

3. Discuss implications of the measurements on the dynamics of the waterspout vortex;

4. Present a realistic mathematical model of the waterspout based on the airborne measurements.

Hopefully from the above, clearer insight into conceptual knowledge and modelling attempts of geophysical vortices will be gained.

2. EXPERIMENTAL PROCEDURES

2.1 Design of the Field Program

In order to achieve a successful waterspout measurement field program, it was necessary to consider several crucial factors. The choice of a suitable location and time for implementation of the field program was imperative. Measurement requirements called for the development of accurate airborne data collection systems and techniques. Finally, careful planning and coordination of field operations were required in order that revelent measurements be obtained efficiently.

Location and Time. A review of the appropriate literature shows that waterspouts, by the general definition, can occur over almost any of the world's bodies of water (e.g., Gordon, 1951; Rossman, 1958; Price and Sasaki, 1963). This definition includes water devils, often termed fair weather waterspouts, and tornadic waterspouts. The "pure" waterspout, intermediate to the dust devil and tornado in intensity, generally forms most frequently where air and sea surface temperatures are relatively high (Gordon, 1951). The Gulf of Mexico, the Mediterranean Sea, the Bay of Bengal, the South China Sea, and the mid-Atlantic are, according to Gordon's analysis of waterspout reports from British ships, hot spots for waterspout formation. These results must be tempered with the realization that only British ships following specific shipping lanes were used as the statistical sample. However, other reports do indicate that the Gulf of Mexico and the Mediterranean Sea are favored waterspout locations (Rossman, 1958; Hyde, 1971; Gerrish, 1967; Garza, 1971).

Climatological analyses of the Florida Keys waterspout by Clemons (1969) and Golden (1973a) reveal this area of the Gulf of Mexico as

one with a high frequency of waterspouts. Golden (1973a) has catagorized waterspout events by the number of funnel days per month and the number of funnels per month observed from the Key West Weather Service Office. A funnel day is defined as a day during which at least one funnel was sighted. Figure 1 shows that for the period 1958 to 1968 June had the most funnel days, with August and July as close seconds. The most active month in terms of total funnels observed (Fig. 2), however, is August followed closely by June, while a relative minimum occurs during July. May and September are transitional months, but observed funnels still average above thirty for those periods.

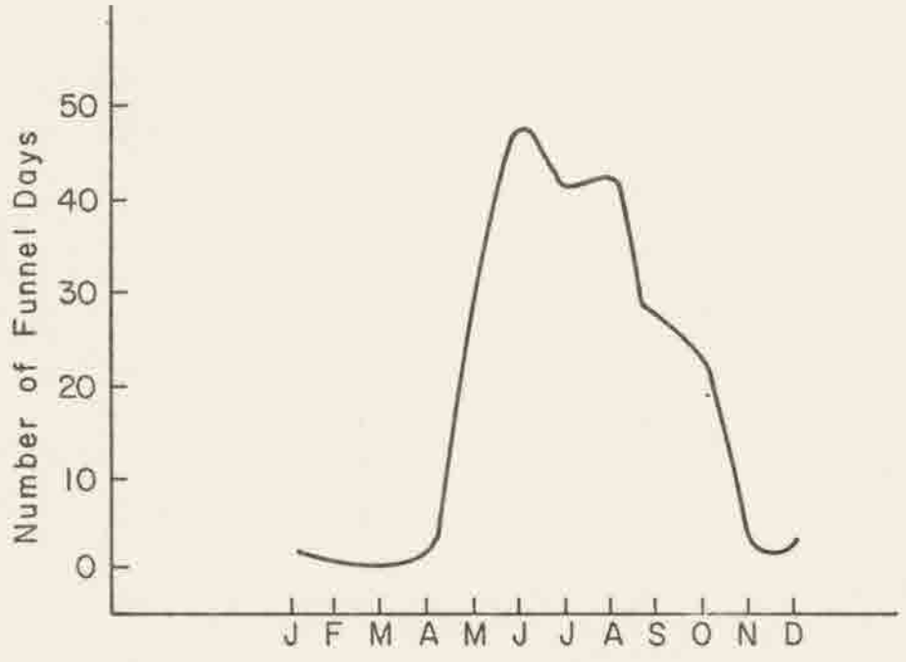

Fig. 1. Number of funnel days per month for the period 1958 - 68 determined from Key West WSO data (from Golden, 1973a).

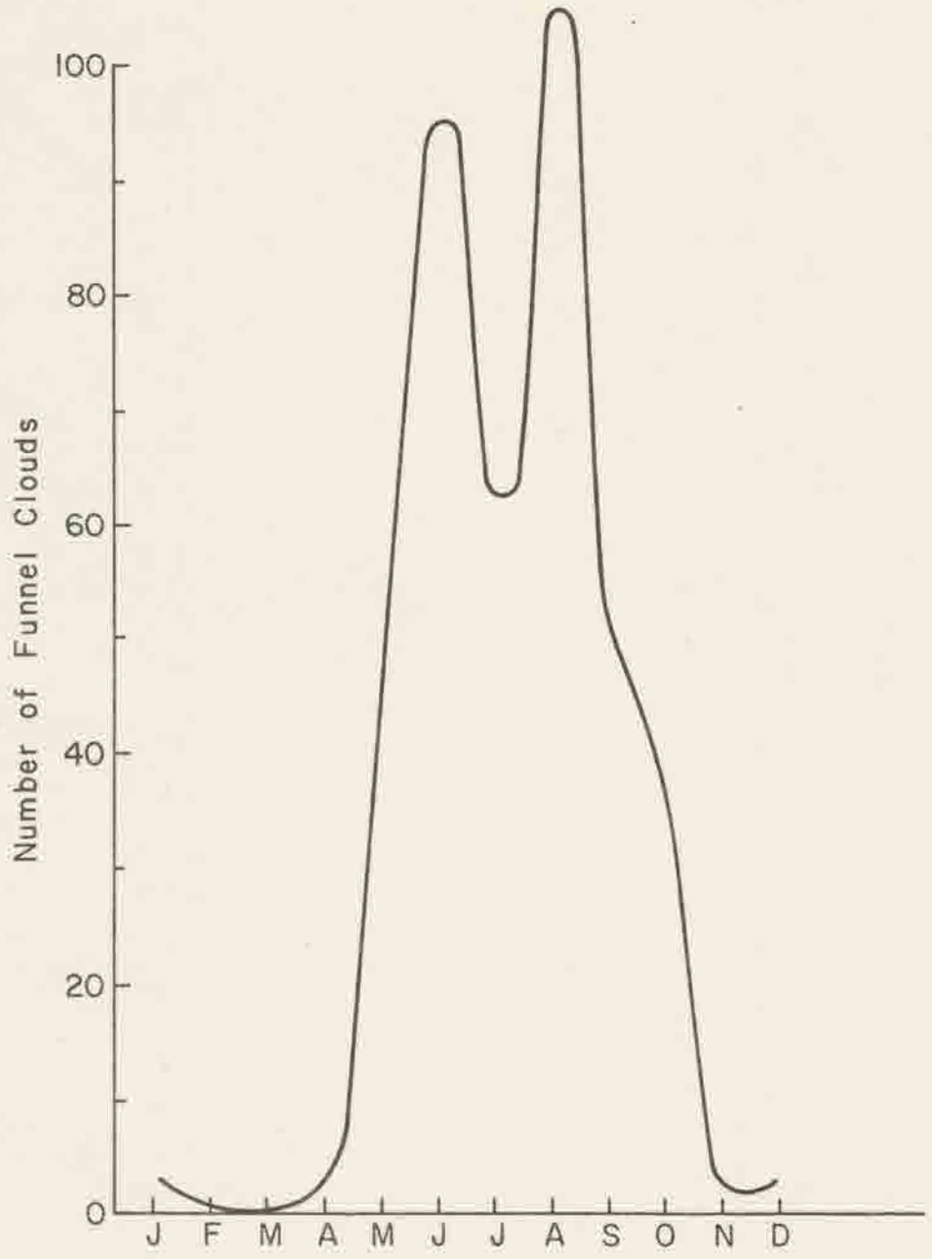

Fig. 2. Number of funnel clouds observed per month for the period 1958 - 68 determined from Key West WSO data (from Golden, 1973a).

Based on the climatological waterspout data and the time necessary to build-up and calibrate the airborne instrumentation system, the optimal period for the 1974 waterspout field measurement program was chosen to be late August and early September.

The entire Florida Keys chain (from Key Largo to the Marquesas Keys) is approximately 140 miles long and 25 miles wide. Key West is located at the outermost (southwestern most) portion of the Keys chain. The large number of waterspouts observed from the Key West WSO (Golden, 1973a) and the evidence presented by Golden (1973b) indicating waterspouts' preference for the shallow waters of the Keys, suggested the Key West International Airport as an ideal base for the field operations. Furthermore, the research aircraft's rapid in transit time and ability to remain airborne for four to five hours brought the entire Lower Keys (Fig. 3) into the field program area, thus increasing the total possible number of waterspouts available to investigation. In addition, the services of the National Weather Service Office at Key West were generously made available, and the airport management granted the research team access to the many airport facilities.

Data Requirements. The requirements for the type, quality, and quantity of data were based on achieving a detailed picture of the waterspout vortex structure. Accurate spatial and temporal acquisition of the data would then allow the formulation of theories relevant to waterspout vortex dynamics. The measurement program was subsequently designed to, above all, obtain accurate detailed measurements of the vertical and horizontal variations of the three-dimensional wind field (u, v, w) and the atmospheric thermodynamic variables across and within the visible funnel boundaries. In addition, it was expedient

Fig. 3. The Lower Florida Keys waterspout field program area extending from Big Pine Key on the east to the Marquesas Keys on the west.

to measure the waterspout near-environmental wind and temperature fields. Last of all, adequate visual and photographic documentation of each waterspout's visible funnel characteristics, along with the parent convection and any surrounding landmarks, was necessary.

An airborne instrumentation platform was decidedly the ideal *in situ* probe for the Keys waterspout. The mobility of an airplane provides the capability of rapidly probing the three-dimensional mesostructure of the atmosphere, and the small scale nature of the waterspout optimized this quality. An airplane was able to provide rapid, successive, multi-level penetrations of the vortex and its near-environment. In addition, airborne instrumentation packages could be large and varied depending on aircraft size, flying and load-carrying characteristics, and available power. The measurement of the waterspout dynamic and thermodynamic variables necessarily involved a variety of sensors plus data processing and recording electronics that a suitable aircraft could support.

Nevertheless, the aircraft measurement concept is only as good as the instrumentation system and the measurement techniques. The high electromagnetic interference and acoustical noise environment of a powered airplane demands sufficient filtering of the raw signals, in addition to adequate insulation of the sensors from excessive vibration. Other problems arise from the airplane's rapid motion through the atmosphere. Sensors must be placed so as to measure the character of the atmosphere unaltered by the aircraft motion. Waterspout measurements were further aggravated by the relatively short sampling time (i.e., the time the aircraft is in the vortex, $\sim$ 1-3 seconds). Therefore, sensor response times had to be sufficiently fast to permit

accurate measurements with exact spatial resolution. For a small waterspout vortex of diameter 10 meters and a typical penetration airspeed of 60 ms^{-1}, instrument response times of 0.1 second would provide, at best, a very coarse picture of the vortex structure. It was therefore decided to utilize sensors with response times of at least 0.1 second or faster. Fortunately, sensors of this quality were available both commercially and through the CSU Severe Storm Measurement and Analysis Group (SSMAG). Considerable expertise had been developed at CSU over the previous five years in terms of airborne measurement accuracies required by numerical model designs and cloud modification schemes (Sinclair, 1969b, 1973a). This experience indicated similar measurement accuracies for the waterspout program, accuracies of ± 0.5 ms^{-1} for relative wind velocity measurements and $\pm 0.1^{o}C$ for temperature measurements.

2.2 Aircraft and Aircraft Instrumentation

Over the past thirty years the airplane has developed into an effective and indispensable tool for atmospheric research. Early pioneering efforts included measurements of cumulus and thunderstorm cloud vertical velocities and temperatures (Malkus, 1954; Byers and Braham, 1949) and investigations of the turbulent motions in the lower atmosphere (Bunker, 1955). Amidst growing applications, the Tornado Research Airplane Project (TRAP) was instigated in 1956 and, continuing through 1959, was the forerunner of "Rough Rider", the airborne phase of the National Severe Storms Project (NSSP) (Goddard, 1962). During "Rough Rider", penetrating jet aircraft obtained detailed measurements of the turbulent structures of severe thunderstorms during various stages of growth (Steiner and Rhyne, 1962). As experience grew,

airborne measurements became more refined until almost all atmospheric phenomena have become subject to aircraft investigations (e.g., Dutton, 1967; Axford, 1968; Holmes, 1972; Lilly and Kennedy, 1973).

Research Aircraft. The primary mission of the waterspout research aircraft was to fly successive penetrations of the waterspout vortex at varying altitudes, usually within 2000 ft. (610 m) above sea level. In addition, the aircraft was to provide accurate spatial probing of the waterspout near-environment on each penetration. Because of the strong shears and turbulent motions presumed to exist in the waterspout vortex, the penetration aircraft had to meet certain stringent requirements in structural integrity and flying capabilities. To minimize possible control and structural problems during a funnel penetration, it was necessary for the aircraft to be suitably stressed and fully aerobatic. Furthermore, it had to possess adequate space for the research instrumentation and crew, plus suitable flying capabilities to safely carry the additional weight.

The penetration aircraft for the 1974 waterspout project was a North American AT-6. The AT-6 (Fig. 4a,b) is a two-place, single-engine, low-wing monoplane originally designed and built as an advanced training plane. Its capabilities as a low level, stable research aircraft have been demonstrated in the past. The particular AT-6 used in the Keys was among the inventory of research airplanes previously utilized in Colorado State University's involvement in the National Hail Research Experiment (NHRE). There it was used as a cloud base research aircraft and had proven itself suitable in the often extremely turbulent environment beneath northeastern Colorado hailstorms. Furthermore, with sufficient lead-time forecasting, the

Fig. 4a. Waterspout Penetration Research Aircraft, the North American AT-6, is shown in its research configuration, modified for waterspout penetrations. The pod and boom assembly mounted under the right wing supports the primary sensors of atmospheric pressure, temperature and motion.

AT-6 was capable of flight durations of four to five hours at average ground speeds of 110 to 130 kts. This facilitated thorough investigations of waterspouts while permitting adequate flight time for return to Key West from anywhere within the designated project area. Research flights were usually limited rather by the available recording times of the data tapes. Finally, the AT-6 rear cockpit provided ample space for instrumentation layout and good visibility for the scientist-observer, while structural hard points under the right wing furnished an ideal location for the instrumentation pod that housed the remainder of the research package.

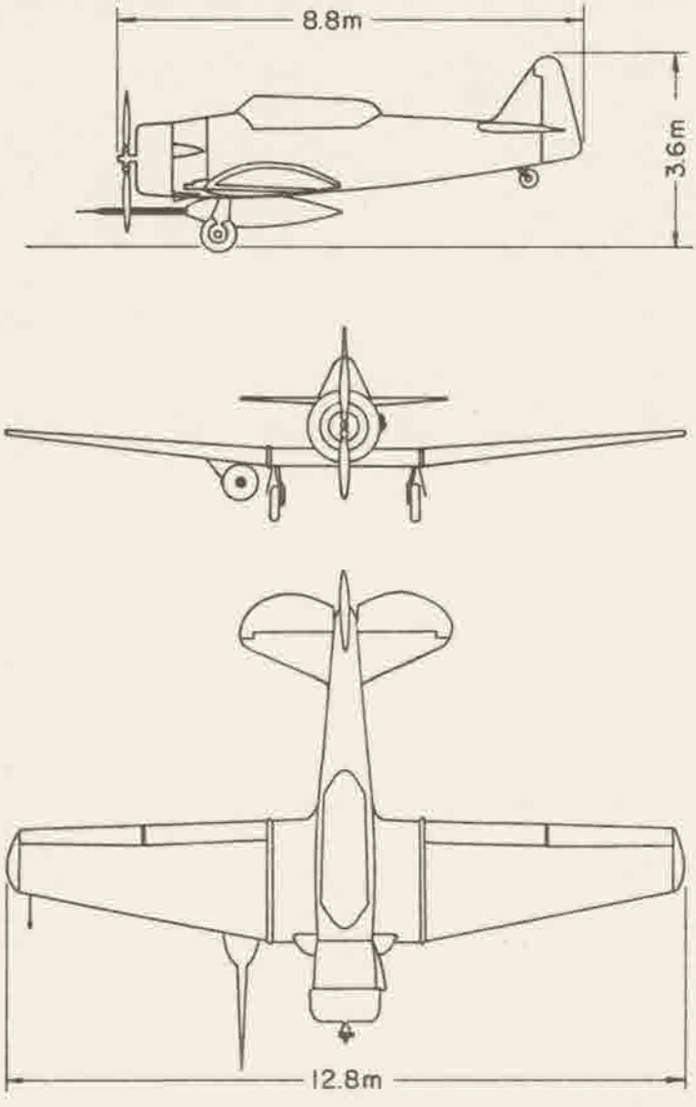

Fig. 4b. Three-view diagram of AT-6 research aircraft.

Aircraft Data Systems. The formulation of a detailed picture of the waterspout vortex kinematic and thermodynamic structure required a sophisticated airborne data acquisition system. A variety of Airborne Atmospheric Data Systems (AADS) have been developed and utilized in airborne severe storm research by Colorado State University's Severe Storm Measurement and Analysis Group over the previous five years (Sinclair, 1969b, 1973a, 1974). In its final configuration, the North American T-6 AADS-2B was a combination of the technology and some of the instrumentation from three other Airborne Atmospheric Data Systems, an earlier T-6 AADS-2B, a Canadair T-33 AADS-3B, and a McDonnell F-101B AADS-4A. The system was designed by Sinclair (1978) and fabricated by in-house personnel for this particular waterspout application.

The AADS-2B is designed to measure the atmospheric air motions, with respect to the earth, $\vec{V}_{a,g}$. The measurement principle is based on measuring the air velocity relative to the airplane, $\vec{V}_{a,p}$, and the velocity of the aircraft relative to the earth's surface, $\vec{V}_{p,g}$. The equation relating the three vector velocities is, after Sinclair (1969b):

$$\vec{V}_{a,g} = \vec{V}_{a,p} + \vec{V}_{p,g} \ . \qquad (1)$$

$\vec{V}_{p,g}$ is measured by a three-axis aircraft accelerometer that gives the aircraft velocity in three-dimensional space with respect to an earth-based coordinate system. Measurements of $\vec{V}_{a,p}$ are first obtained relative to an aircraft coordinate system and then are subsequently referenced to the earth's surface by using measurements of the airplane's attitude with respect to the earth. The final calculation of $\vec{V}_{a,g}$ is in terms of its three components (u_f, v_f, w_f). The horizontal air

velocities u_f, v_f are positive in the direction of the airplane's positive x_f and y_f axes (Fig. 5), but corrected so as to be orthogonal to the earth's local vertical. The vertical air velocity w_f is positive in the normal meterological sense and oriented along the earth's local vertical.

The complete equation for the vertical velocity, $w_f = \hat{k} \cdot \vec{V}_{a,g}$, is, after making the small angle approximation (Sinclair, 1969b, 1973a),

$$w_f = V_T\alpha - V_T\theta + V_T\beta\phi + \int_o^t a_z \, dt + w_{p,g}(0) + L_1\dot{\theta}. \qquad (2)$$

V_T is the aircraft's true airspeed, α is the angle of attack[1], β is the angle of sideslip[2], and θ and ϕ are the aircraft's pitch and roll angles respectively. The integral gives the aircraft's vertical velocity over the integration time interval, where a_z is the vertical acceleration of the aircraft. $w_{p,g}(0)$ is the vertical velocity of the airplane at time $t = 0$. $\dot{\theta}$ is the pitch rate of the aircraft (degrees s^{-1}), and L_1 is the longitudinal distance separating the aircraft accelerometers and the airstream angle measurement point.

The equation for the (small angle approximation) lateral or crosstream velocity (v_f) is written as:

$$v_f = V_T\beta - \int_o^t V_T\dot{\psi} \, dt + V_T\alpha\phi + \int_o^t (\ddot{y} + \ddot{z}\phi) \, dt + v_{p,g}(0) + L_2\dot{\psi} \, . \qquad (3)$$

[1]The angle of attack is defined as the angle of the airstream with respect to the longitudinal axis of the aircraft measured in the airplane's vertical plane.

[2]The angle of sideslip is the angle of the airstream with respect to the longitudinal axis of the aircraft measured in the airplane's horizontal plane.

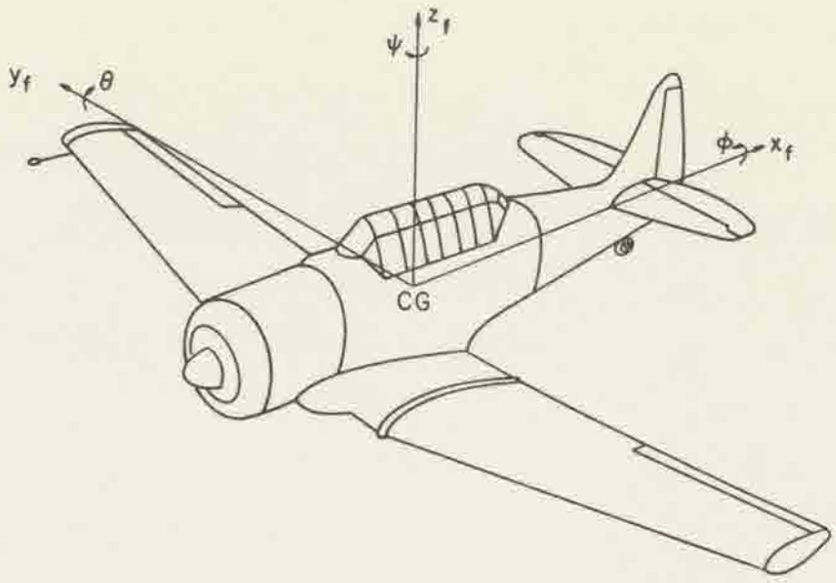

Fig. 5. Aircraft-oriented cartesian coordinate system utilized in calculations of $\vec{V}_{a,g}$.

The symbols in (3) have the same meaning as in (2) with the addition of $\dot{\psi}$ as the aircraft yaw rate, $\ddot{y}$ and $\ddot{z}$ as the output of the lateral and vertical aircraft accelerometers respectively, $v_{p,g}(0)$ as the lateral velocity of the aircraft at time t = 0, and L_2 as the lateral distance from the accelerometers to the airstream angle measurement point.

Finally, the (small angle approximation) longitudinal velocity (u_f) is given by:

$$u_f = V_T - \int_o^t (\ddot{x} + \ddot{z}\theta)\, dt - u_{p,g}(0) \qquad (4)$$

where $\ddot{x}$ is the output of the longitudinal aircraft accelerometer and and $u_{p,g}(0)$ is the longitudinal velocity of the aircraft at time t = 0.

The angles of attack and sideslip are measured by specially coated balsawood flow vanes. Measurements of θ, ϕ, $\dot{\theta}$, and $\dot{\psi}$ are accomplished by precision vertical and rate gyros. The true airspeed (V_T) is

determined from pitot-static tube measurements of the ram (total) and static pressure, and temperature sensor measurements of total temperature. The aircraft accelerations $\ddot{x}$, $\ddot{y}$, $\ddot{z}$ are obtained from a three-axis accelerometer system mounted at the airplane's center of gravity. Values of initial aircraft vertical velocities $w_{p,g}(0)$ are calculated for each waterspout penetration from measurements of fine static pressure change over a reference interval. By the same token, $u_{p,g}(0)$ and $v_{p,g}(0)$ are determined for the reference interval from calculations of the aircraft ground speed using a standard pilot's flight computer. This can be a rather coarse calculation; known variables in the computation are true airspeed, magnetic headings, compass variation, and wind direction and velocity. In our case, reference values for the environmental wind was assumed the same as that measured by the Key West raob at the approximate penetration altitude.

The AADS-2B is designed to measure all parameters relative to the aircraft coordinate system shown in Fig. 5, with the following sign designations being utilized: pitch up, right roll, right yaw, angle of attack vane deflections upwards, and sideslip angle vane deflections to the right (of the airplane's direction of travel) are all defined as positive angles. All velocities and accelerations in the direction of the positive aircraft coordinate axes are likewise defined as positive.

The first three terms on the right side of (2) and (3) and the first term on the right side of (4) represent the measured values of $w_{a,p}$, $v_{a,p}$, and $u_{a,p}$ respectively. The vertical air velocity with respect to the airplane is always along the earth's local vertical, but is along the airplane's vertical axis only if the pitch and roll

angles are 0. The two components of the horizontal air velocity with respect to the airplane are orthogonal to the local vertical and, as calculated in (3) and (4), are respectively perpendicular and parallel to the initial aircraft true heading at time $t = 0$. Therefore, it is advantageous (using this particular system) to fly each penetration at a constant heading so that the heading at the time of funnel penetration is the same as the initial heading. In deriving (2), (3), and (4) the assumption is made that measurements of pitot (ram) pressure by the AADS-2B pitot tube are essentially unaffected by angles of attack or sideslip up to $\sim \pm 15^{o}$.

The remaining three terms in (2) and (3) and the last two terms in (4) give values of the airplane's velocity relative to the earth ($w_{p,g}$, $v_{p,g}$, and $u_{p,g}$). Since the three axis accelerometer system is unstabilized against aircraft pitch, roll, and yaw (unlike inertial nav systems), gravity and cross-component contamination will result whenever the aircraft deviates from straight and level flight. As a result the extra terms, $\ddot{z}\phi$ and $\ddot{z}\theta$, are included under the integrals in (3) and (4) respectively. Note that accelerometer cross-component contamination due to aircraft yawing motions has been neglected since yaw angles were typically small during a penetration. The vertical aircraft velocity is calculated from a combination of accelerometer and static pressure data. Since it is actually necessary to know the velocity of the flow vanes relative to the earth, the additional terms, $L_1\dot{\theta}$ and $L_2\dot{\psi}$, must be added to (2) and (3) respectively.

Theoretically, the AADS-2B is so designed that pilot induced motions will not contaminate accurate measurements of atmospheric air motions (Sinclair, 1969b and 1978). In reality, however, this

principle cannot be fully satisfied because of small errors in each of the atmospheric and/or aircraft sensors. Consequently, in order to minimize the total system error, data sampling flights are commonly flown at constant attitude with constant power settings to reduce the probability of experiencing large angles of pitch, attack, sideslip, and to prevent large deviations in airspeed.

The AADS-2B instrumentation pod and boom assembly is mounted under the right wing of the T-6 (Fig. 4). The pod houses the pressure transducers, a pressure reference chamber, precision vertical and rate gyros, and associated inverters, power supplies, and demodulators for the various sensors. The pressure reference chamber is designed so that, prior to penetration, an air sample with atmospheric pressure corresponding to that flight level is captured by closing a solenoid valve. Comparisons of static pressure in the funnel are then made with the air sample's pressure, thus facilitating accurate measurements of the waterspout's core pressure deficit. The vertical gyro is maintained parallel to the earth's local vertical through a gravity-sensitive, liquid damped device. The slow erection rate is 5^{o}/min.

Extending forward approximately 2.5 m from the instrumentation pod is the AADS-2B sensor boom. At the tip of the boom is mounted the pitot-static tube, a commercial unit aerodynamically compensated to nullify position errors and suitably designed to effectively eliminate attack and yaw angle errors up to approximately $\pm$ 15^{o}. Immediately to the rear of the pitot-static tube are located the airstream angle vane sensors. The vanes were developed in-house under the SSMAG and are coated with a special abrasive coating to provide durability. In addition, they are internally mass balanced to negate acceleration

affects on their response characteristics. Both the pitot-static tube and vanes are positioned at a point ahead of the plane of the propeller such that the atmospheric flow/turbulence measured is considered unaffected by the aircraft's present. The boom's natural frequency is 11 Hz.

Farther to the rear on the boom are located the platinum wire total temperature sensor and a mount available for a dew point hygrometer. The Rosemount total temperature sensor is designed to measure the sum of the static air temperature and the entire dynamic heating affect due to the kinetic energy of the airflow (recovery factor equal to 1). In addition, the resistance wire sensor is mounted in a housing which forces part of the inflowing air around a 90^{o} bend. This is to protect the sensor from wetting from liquid water in the form of cloud droplets or rain. In reality small droplets may be able to turn the corner, wetting part or all of the wire element. Furthermore, this particular model has an additional delayed response to a temperature change due to thermal contact between housing and element (Lenschow and Pennell, 1974). Further information regarding the AADS-2B instrumentation is listed in Table 1.

The remainder of the AADS-2B is situated in the rear cockpit of the T-6. Here the three-axis accelerometer system (lateral, longitudinal, ± 2 g and ± 5 g vertical accelerometers) is mounted at the aircraft center of gravity. The remainder of the system electronics, including eight-pole Butterworth filters, signal conditioners, and power supplies, are mounted for easy access and calibrations. The AADS-2B control and display section is designed to provide complete operation and in-flight monitoring of the entire research package. Monitoring is accomplished

Table 1. AT-6 AADS-2B Sensors

Parameter	Instrument Type	Manufacturer	Range	Error	Time Constant
Angle of attack and sideslip α, β	Vane synchro	Developed by SSMAG	$\alpha \pm 21°$ $\beta \pm 40°$	±0.05°	0.07 sec
Pitch and roll θ, ϕ	Vertical gyro	Kearfott T2109	$\theta \pm 82°$ $\phi \pm 360°$	±0.1°	0.1 sec
Pitch and yaw rate $\dot{\theta}$, $\dot{\psi}$	Rate gyro	$\dot{\theta}$ Whittaker, R170 $\dot{\psi}$ Honeywell, JRS101A2	$\pm 20°s^{-1}$ $\pm 7°s^{-1}$	±0.1°	<0.1 sec
Coarse static pressure P_S	Variable reluctance transducer	Pace CP60A	0 to 15 psi	±0.5% FSO	0 to 10^3 Hz frequency response
Fine static pressure P_F	Variable capacitance transducer	Rosemount	±0.2 psid	±0.5% FSO	<0.02 sec
Airspeed P_R	"	Wiancko	0 to 0.6 psid	±0.2% FSO	<0.02 sec
Vertical acceleration $\ddot{z}$	Linear force-balance servo accelerometer	Donner Systron 431F-S-AG	±5g ±2g	±0.025g ±0.012g	0.05 sec
Lateral acceleration $\ddot{y}$	"	Donner Systron 4310-1-AG	±1g	±0.005g	0.05 sec
Longitudinal acceleration $\ddot{x}$	"	Donner Systron 4310-1	±1g	±0.005g	0.05 sec
Total air temperature T_T	Platinum wire element	Rosemount 10232AL	-50° to +55° C	±1% FSO	$\geq$0.1 sec

by an oscilloscope and a 15 position selector switch that provides a display of each sensor's output signal after filtering and conditioning. Included in the control and display section is a digital magnetic tape recorder, the heart of the system. The tape recorder formats the sensor's analog inputs into a computer-compatible data format and incrementally records the data on magnetic tape at the rate of 1000 characters per second. Accommodations are provided for insertion of real time on the data tapes, and a digital clock readout on the recorder panel displays the time from milliseconds to days, allowing absolute time referencing of research flight events.

The entire AADS-2B is shown in block diagram form in Fig. 6. Fourteen sensors supply inputs of atmospheric and flight parameters to the system. After six of the signals are demodulated, all fourteen pass through low pass Butterworth filters to eliminate fluctuations in the analog data greater than 10Hz. Subsequently, conditioning is performed on the fourteen channels (signals) to match them to the A/D converter input requirement of ± 2 volts. The Incredata Mark II tape recorder contains a twenty channel analog multiplexer, and A/D converter, a programmable data formatter, a time code generator, an internal digital clock, and an incremental magnetic tape recorder. Five of the sensor signals are sampled (recorded) every 0.02 seconds, the remaining nine signals every 0.04 seconds. The fastest sampling rate is performed on the quickest responding sensors (vanes, ram pressure, fine static pressure, and ± 2 g vertical accelerometer) that measure the critical parameters for determining waterspout flow and pressure fields. Rapid sampling of the total temperature sensor signal would be futile since its response time is probably never faster than 0.1 second.

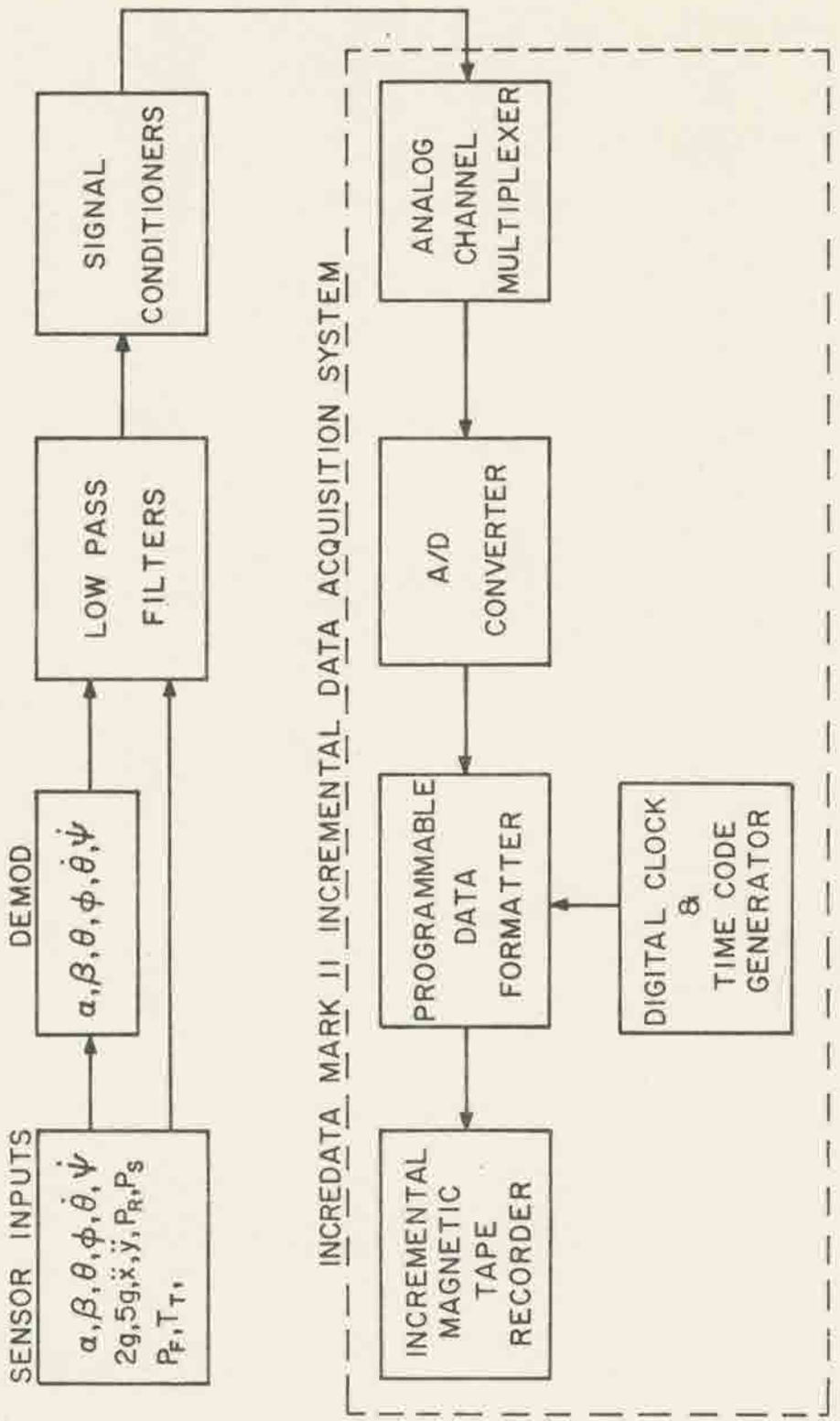

Fig. 6. Flow chart of the AADS-2B data acquisition process.

2.3 Data Collection

Field Operations. The waterspout field measurement program commenced September 16, 1974, and continued through September 27. During the field operations, 15 waterspouts were penetrated by the T-6 with multiple penetrations flown on 7 of the total 15. Table 2 gives a detailed breakdown of field operations for the 1974 program.

Field Program	Total Days Flown	Waterspout Days	Number of Waterspouts Penetrated	Number of Waterspouts Multiply Pene.	Total Pene.
Sept. 16-27, 1974 (12 days)	6	7	15	7	49

Table 2. Breakdown of field operations for 1974 waterspout field measurement program. (Waterspout days are days during which at least one funnel cloud was sighted by either National Weather Service or research personnel from Key West Airport).

The research aircraft was parked at Key West International Airport with access to the Flight Service Station and national Weather Service facilities in addition to ground electrical power for daily instrumentation calibrations. Personnel usually remained on station at the airport throughout the day if conditions appeared favorable for waterspout formation. Research flight forecasts, made by research personnel, were issued in the morning and during the day based on the existence of several conditions conducive to cloud line development: (1) generally light surface winds (< 10 kts) from the southwesterly or easterly direction, (2) relative absence of middle and high clouds, (3) warm low level temperatures, and (4) lifted indices between +3 and -5. Not all cloud lines produced waterspouts, but the aircraft were more often than not launched with success on lines that appeared to be formed by the surface

heating effects of the Keys rather than on lines produced by a passing synoptic scale disturbance. Golden (1973b) has indeed shown the "surface heating" cloudline to be a more efficient producer of waterspouts than the line formed by a larger (synoptic) scale disturbance (see Chapter 3). After some experience, it was not difficult to visually delineate between the two lines. The "surface heating" cloudline was distinct (cu-congestus), yet not overly large, in an uncluttered sky. On the other hand, the synoptic-scale disturbance cloudline was a more indistinct line of cu-congestus in a generally cloud scattered (semi-isolated cumulus, patchy middle clouds) sky. The majority of research missions launched based on these somewhat subjective techniques were successful in locating waterspouts.

Based on Golden's (1973a) analysis of the diurnal occurrence of Keys waterspouts (Fig. 7), primary flight times were concentrated between the hours of 1100 and 1600 EDT. An average research flight lasted approximately 1.5 to 2 hours. The maximum number of flights for any 24 hour period was 3.

Penetration Procedures. The primary section of the funnel and parent cloud system selected for study was that area at and immediately below cloud base. This was done so as to provide relatively safe elevations at which the aircraft could recover from any possible effects of strong turbulence. It must be pointed out that this was a testing program for aircraft and instrumentation. Although waterspouts had previously been penetrated by, for example, military aircraft (Rossow, 1970, and Phillips, 1950), no systematic, consecutive penetrations by aircraft especially instrumented to measure wind, pressure, and temperature fields had been accomplished. The original plan was to

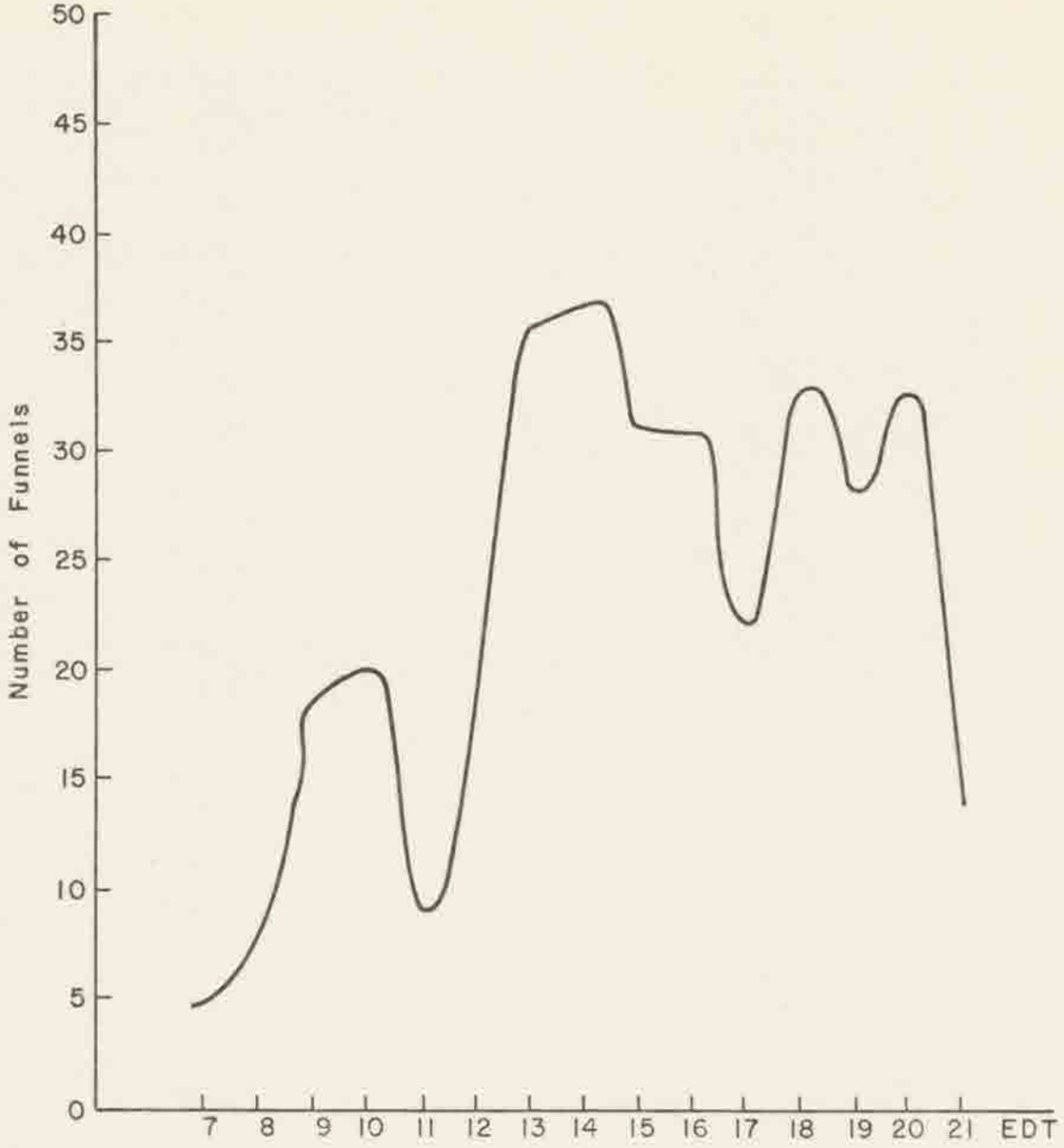

Fig. 7. Number of funnel clouds observed per hour for the period 1958-68 determined from Key West WSO data (from Golden, 1973a).

begin by penetrating small waterspouts that produced either no or minimal disturbance on the water below. Then, decisions on attempting larger, supposedly stronger funnels would subsequently be made based on the previous penetrations. Joseph Golden, thoroughly versed in the characteristics and life-cycle of the Keys waterspout, was the initial

scientist-observer and briefed the pilot on characteristic water surface features indicating incipient waterspout formation, e.g., dark spots, spiral patterns. It was, perhaps, quite fortuitous that during the 1974 twelve day field program each waterspout that formed was essentially stronger and more developed than any before it had been. This allowed almost complete realization of the originally planned procedures. Mean penetration airspeeds were initially between 125 and 135 kt, but as the pilot gained experience, they were successively lowered to a point at which there was a balance between aircraft stability and maximum data collection in the vortex, generally between 110 and 125 kt. In addition, minimum penetration altitudes were gradually lowered to approximately 500 feet below cloud base (1000 to 1500 feet above MSL) so as to provide a more complete picture of the vertical structure of the upper portion of the waterspout.

Expedient penetration techniques were gradually developed during the field program. Upon the decision to penetrate a specific waterspout, an attempt to fly the following ideal pattern was made. The aircraft flew to a point outside the waterspout-parent cloud sphere of influence, i.e., outside the visible cloud or cloud-line boundaries, whereupon a flight path on a course line of constant magnetic heading was initiated. Subsequent to this Initial Point (I.P.), a reference run in clear air at essentially constant pressure altitude was flown to reference the AADS-2B, i.e., to record, w_o, v_o, and u_o. Then, upon approach to and following penetration of the waterspout, the aircraft was flown in a constant attitude-constant power settings profile. Necessary alterations to this basic profile sometimes occurred due to existing rain shafts, other clouds, and even other waterspouts. For example, on some

penetrations tight turns were negotiated before and after the penetration. For most penetrations, however, an average time interval of 0.5 to 1 minute elapsed during the entire penetration run. Once a waterspout was selected for study, penetrations continued on that waterspout until either it dissipated or the data tape was filled. Since the available recording time for each tape was approximately 40 minutes and average waterspout lifetimes were on the order of 10 to 20 minutes, multiple penetrations of a particular waterspout were possible, providing the event was sighted sufficiently early in its life cycle.

Ground Observations. An important addition to the aircraft waterspout data was the accumulation of photographs, visual observations, and notes provided by research ground crews. When the aircraft was in the air, the remaining personnel stationed themselves in advantageous observational positions such as the roof of the airport terminal building. From here, contact was kept with the Flight Service Station, which generally knew the aircraft's location. If incipient waterspouts were subsequently sighted, and the aircraft was in a different location where there were no waterspouts, word was often relayed through the Flight Service Station to the aircraft. Movie and still pictures of any waterspout parent-cell/cloudline were taken, providing valuable visual documentation of locations, distances, cloud top heights, etc., that complemented radar and aircraft data.

National Weather Service Support. The professional services offered by the Key West Weather Service Office (WSO) considerably simplified the waterspout forecasting process and furnished valuable supplementary information for final data reduction and analysis. The

entire inventory of N.W.S. facsimile and teletype products were available for examination by research scientists. Surface and radar observations, soundings, and area forecasts were studied daily and used as primary input for waterspout probability forecasts in the field and as historical records of environmental conditions for data analysis.

2.4 Data Reduction and Error Analysis

Data Reduction. The first step in the data reduction process was to acquire accurate calibrations of the AADS-2B. Prior to and following the field program, extensive static calibration procedures were performed on each of the fourteen data channels. To provide field validation, spot-check static and in-flight calibrations were carried out several times while at Key West. From these data, fifth-order polynomial calibration curves were computed for each channel (sensor) by a least squares regression technique.

Each data tape was indexed and catalogued according to dates and penetrations. Then, based on the flight logs, voice tapes, and photographs, preliminary selection of specific penetrations was made, and signal voltage levels for those penetration time intervals were printed out. This allowed an examination of each sensor's output for accuracy and reliability.

Based on the preliminary examination of the voltage printout, final selection was made of the waterspout penetrations that would serve as case studies for analysis. The data from each case study was then converted to engineering units via the calibration curves. Since true airspeed V_T and static temperature T_s were not directly measured,

values were calculated from measurements of ram pressure P_R, static pressure P_S, and total temperature T_T using the compressible, subsonic flow equations (Sinclair, 1973a)

$$\frac{P_R}{P_S} = \left(1 + \frac{\gamma - 1}{2} M^2\right)^{\left(\frac{\gamma}{\gamma - 1}\right)} - 1 \tag{5}$$

$$\frac{T_T}{T_s} = 1 + \frac{\gamma - 1}{2} \eta M^2 \tag{6}$$

$$V_T = T_T^{\frac{1}{2}} \left[gR / \left(1 + \frac{\gamma - 1}{2}\right)\right]^{\frac{1}{2}} \tag{7}$$

where M is the Mach number, γ is the ratio of the specific heats of dry air, $c_p/c_v = 1.4$, and $\eta = 1.0$ is the recovery factor of the total air temperature probe. M was calculated from (5), T_s from (6), and V_T from (7). A digital filter was subsequently applied to the data to remove further spurious fluctuations due to boom vibrations and/or electronic noise.

Following conversion of the data to engineering units, values of u_f, v_f, and w_f were calculated from (2), (3), and (4) every 0.04 seconds of penetration flight time. The sensors that were sampled every 0.02 seconds were averaged to obtain one value every 0.04 seconds. The spatial increment corresponding to 0.04 seconds obviously depended on the aircraft ground speed, while the number of data points obtained through the funnel was related to the funnel diameter and aircraft penetration speed. Typically, 15 to 30 data points were recorded for most penetrations. In addition to calculating the three-dimensional velocity components, horizontal profiles of the waterspout pressure field or core pressure deficit (CPD) and the static temperature field were computed. Finally, values of each term in (2), (3), and (4) together with u_f, v_f, w_f, CPD, and T_s were printed out and plotted

for each penetration. Usually this penetration time interval was from 10 to 20 seconds, thus providing a horizontal profile of the three-dimensional flow field, pressure, and temperature at the penetration altitude through and $\sim$ 0.3 to 0.5 km either side of the waterspout vortex.

Measurement Error Analysis. Primary errors in u_f, v_f, w_f as calculated from (2), (3), and (4) result from two sources. The first is the small angle approximation made in deriving the final forms of (2), (3), and (4). These errors are systematic and will always increase the measured values of u_f, v_f, and w_f. The second area is the accuracy with which the AADS-2B measures the actual wind field. These errors involve the sensor and system errors, and inaccuracies arising from the measurement (penetration) technique.

Errors due to the small angle approximation are greatest when the airstream and attitude angles are largest, hence u_f, v_f, and w_f measured in the funnel contain larger errors than wind components measured outside the funnel. Using the maximum values of airstream and attitude angles for two sample funnel penetrations, the maximum absolute error from this source can be calculated for each penetration. The first penetration is one of the strongest waterspouts encountered during the program (Table 3, column 2). The second (Table 3, column 3) lists parameters for a waterspout of weaker relative intensity. The majority of all penetrations accomplished were generally similar to the weaker case.

Maximum errors from the small angle approximation for vertical velocities calculated from equation (2) are $\sim 0.8 ms^{-1}$ and $\sim 0.1 ms^{-1}$ for the strong and moderate penetrations respectively. Similarily, errors

Table 3. Measured Parameters and Associated Maximum System and Measurement Errors for Strong and Moderate Waterspout Penetrations

Parameter	Measured Maximum Values (Strong)	Measured Maximum Values (Moderate)	System and Measurement Error (δ) (Strong)	System and Measurement Error (δ) (Moderate)
V_T	$75 ms^{-1}$	$75 ms^{-1}$	$1.4 ms^{-1}$	$0.3 ms^{-1}$
α	6.3°	7.6°	0.05°	0.05°
β	21.1°	9.5°	0.05°	0.05°
θ	3.9°	2.8°	0.1°	0.1°
ψ	6.0°	6.2°	0.1°	0.1°
ϕ	15°	2.1°	0.1°	0.1°
$\dot{\theta}$	$14.5°s^{-1}$	$6.2°s^{-1}$	$0.1°s^{-1}$	$0.1°s^{-1}$
$\dot{\psi}$	$8.7°s^{-1}$	$7.4°s^{-1}$	$0.1°s^{-1}$	$0.1°s^{-1}$
$\int a_z dt$	$5 ms^{-1}$	$2 ms^{-1}$	$0.1 ms^{-1}$	$0.1 ms^{-1}$
$\int a_y dt$	$10 ms^{-1}$	$6 ms^{-1}$	$0.5 ms^{-1}$	$0.5 ms^{-1}$
$\int a_x dt$	$5 ms^{-1}$	$2 ms^{-1}$	$0.5 ms^{-1}$	$0.5 ms^{-1}$
$w_{p,g}(0)$	$1 ms^{-1}$	$1 ms^{-1}$	$0.5 ms^{-1}$	$0.5 ms^{-1}$
$v_{p,g}(0)$	$5 ms^{-1}$	$2 ms^{-1}$	$\sim 2 ms^{-1}$	$\sim 2 ms^{-1}$
$u_{p,g}(0)$	$65 ms^{-1}$	$70 ms^{-1}$	$\sim 2 ms^{-1}$	$\sim 2 ms^{-1}$

of $\sim 0.1 ms^{-1}$ and $< 0.1 ms^{-1}$, respectively, exist for values of longitudinal velocity calculated from equation (4). However in the case of lateral velocities (equation (3)), maximum errors are as high as $\sim 2 ms^{-1}$ for the strong waterspout, due primarily to the large measured angle of sideslip (21.1^{o}). For the moderate case the maximum error drops to $\sim 0.3 ms^{-1}$. Since the maximum small angle approximation errors in equations (2), (3), and (4) for the moderate waterspout are on the order of $0.1 ms^{-1}$, which is considered less than the resolution of the AADS-2B, the approximation is reasoned to be valid for this study.

Maximum measurement errors in u_f, v_f, and w_f can be calculated from the data in Table 3. Values listed in column 4 and 5 are the estimated combined system and measurement technique errors for the strong and moderate penetration cases.

For vertical velocity, maximum errors can be estimated for the strong case from

$$V_T\delta\alpha + \delta V_T\alpha + V_T\beta\delta\phi + V_T\delta\beta\phi + \delta V_T\beta\phi + V_T\delta\theta + \delta V_T\theta +$$

$$\delta\int a_z dt + L_1\delta\dot{\theta} + \delta w_{p,g}(0) \sim 1.3 ms^{-1}.$$

A similar calculation for the moderate waterspout gives $\sim 0.9 ms^{-1}$ as the maximum error in the measured vertical velocity.

The maximum error in measurements of v_f is

$$V_T\delta\beta + \delta V_T\beta + V_T\alpha\delta\phi + V_T\delta\alpha\phi + \delta V_T\alpha\phi + V_T\delta\psi + \delta V_T\psi +$$

$$\delta\int a_y dt + L_2\delta\dot{\psi} + \delta v_{p,g}(0) \sim 3.0 ms^{-1}.$$

For the moderate case, maximum error is $\sim 2.5 ms^{-1}$.

Finally, the maximum error inherent in measurements of the longitudinal velocity u_f is given by

$$\delta V_T + \delta \int a_x dt + \delta u_{p,g}(0) \sim 3.5 ms^{-1}$$

for the strong case and $\sim 2.5 ms^{-1}$ for the moderate case.

The greatest contributor to the large maximum measurement errors in u_f and v_f is the aircraft's initial horizontal velocity. Due to the method of calculation (using airspeed, true heading, and wind speed and direction), large errors are inherent. However, maximum errors with respect to the airplane's initial horizontal velocity are approximately half as large, $\sim 1 ms^{-1}$. Since $v_{p,g}(0)$ and $u_{p,g}(0)$ are constants for each penetration, the errors associated with their measurement have the affect of increasing the maximum error band for equations (3) and (4) respectively.

Measurements of the coarse static pressure (P_S) (pressure altitude) may contain errors up to $\sim$ 30m (100 ft) at average waterspout penetration altitudes (1000 to 2000 ft). However, fine static pressure (P_F), which is used to obtain the waterspout's core pressure deficit (CPD), has at most a total error of $\simeq$ 0.1mb with respect to the air sample in the pressure reference chamber.

Values of static temperature (T_s) contain errors primarily due to errors inherent in ram and static pressure measurements used in equation (5). In a droplet environment, however, the temperature sensor may become a partial wet bulb, giving lower values of total temperature. For flight in "dry" air (air free of liquid water) maximum errors in T_s are $\simeq 0.1^oC$. Temperature errors during penetrations of visible funnel clouds will be discussed in Chapter 4.

3. PREVIOUS RESEARCH OF FLORIDA KEYS WATERSPOUTS

Before discussing the 1974 waterspout penetration data, it is necessary to briefly review the previous research conducted on the Florida Keys waterspout. The most comprehensive work to date is that performed by Golden (e.g., 1970, 1971, 1973 a,b, 1974 a,b,c). Rossow (1970) has conducted observational programs designed primarily to measure the electric and magnetic fields associated with the Keys waterspouts. Gerrish (1967) analyzed occurrences of tornadoes and waterspouts in the South Florida area.

3.1 Life Cycle

One of the most important discoveries to come from Golden's research was the existence of a recognizable life cycle associated with all Keys waterspouts (Golden, 1974 a,b). The life cycle, according to Golden, is composed of five distinct but overlapping stages:

1) the dark spot stage characterized by a light colored area on the sea surface, surrounded by an annulus of dark, apparently disturbed water;

2) the spiral pattern stage during which dark and light colored bands on the sea surface surround the dark spot in a curling manner;

3) the spray ring or incipient spray vortex stage characterized by a concentrated ring of spray around the dark spot, with a distinct funnel cloud above;

4) the mature waterspout or spray vortex stage during which the visible spray vortex at the sea surface reaches maximum intensity, and the funnel cloud attains maximum length and diameter;

5) the decay stage during which the waterspout dissipates, usually from the arrival of a nearby shower-induced gust front.

A particular waterspout need not pass through all five stages in its lifetime, but almost always begins in the dark spot stage.

Golden has found the dark spot to be the surface termination of a complete waterspout vortex column. Even though there are more dark spots than funnel clouds, movie loops of marine smoke flares indicate the dark spot to be the focus of localized, converging boundary layer air. The lower structure of the vortex appears to be composed of an outer cylinder of ascending, rotating air surrounding an inner region of sinking motion (Fig. 8).

Dark spots appear to form in multiples (favoring even rather than odd). Golden suggested the formation of multiple dark spots approximately along a quasi-vertical vortex sheet and therefore may be formed by a shearing instability. Observations from the 1974 waterspout project lend credence to the existence of even multiples of dark spots. Often, two funnel clouds formed with two dark spots on the sea surface.

Dark spot lifetimes observed by Golden lasted from 1 to 22 min. He found no physical features to distinguish a dark spot that evolved into a mature waterspout from one that did not. However, if a funnel cloud formed above the dark spot, the possibility of further intensification was strong.

Golden's spiral pattern stage represents the primary growth phase of the waterspout (Fig. 9). During this time the localized convergence of boundary layer air increases dramatically in intensity and areal influence. The local vorticity increases as the converging flow concentrates the air's angular momentum until finally the waterspout evolves into stage 3. During stage 2, the visible funnel generally increases in length and diameter.

The spiral pattern is generally much larger than the dark spot and often propagates around it from a nearby pre-existent shear band on the

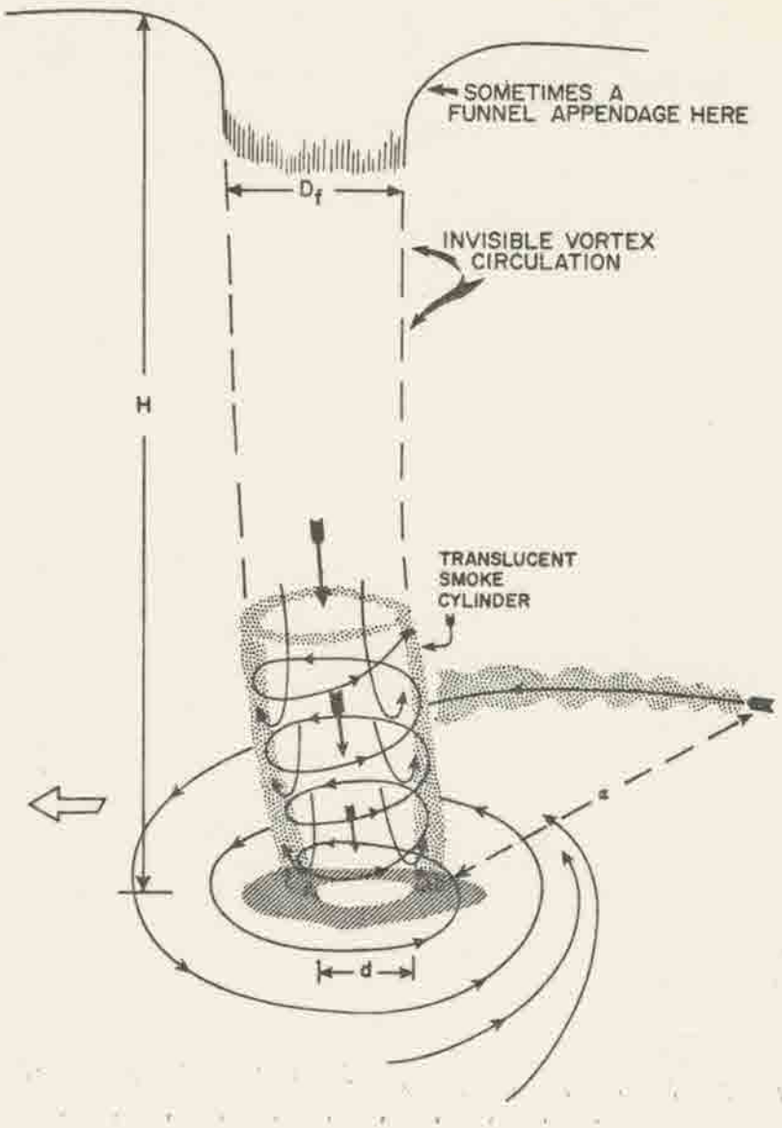

Fig. 8. Golden's composite structural-flow model for the dark spot stage of the waterspout life cycle. Characteristic scales are: H = 550 - 670m; D_f = 3 - 150m; d = 3 -45m; and α = 15 - 760m (reproduced with author's permission, from Golden, 1974a).

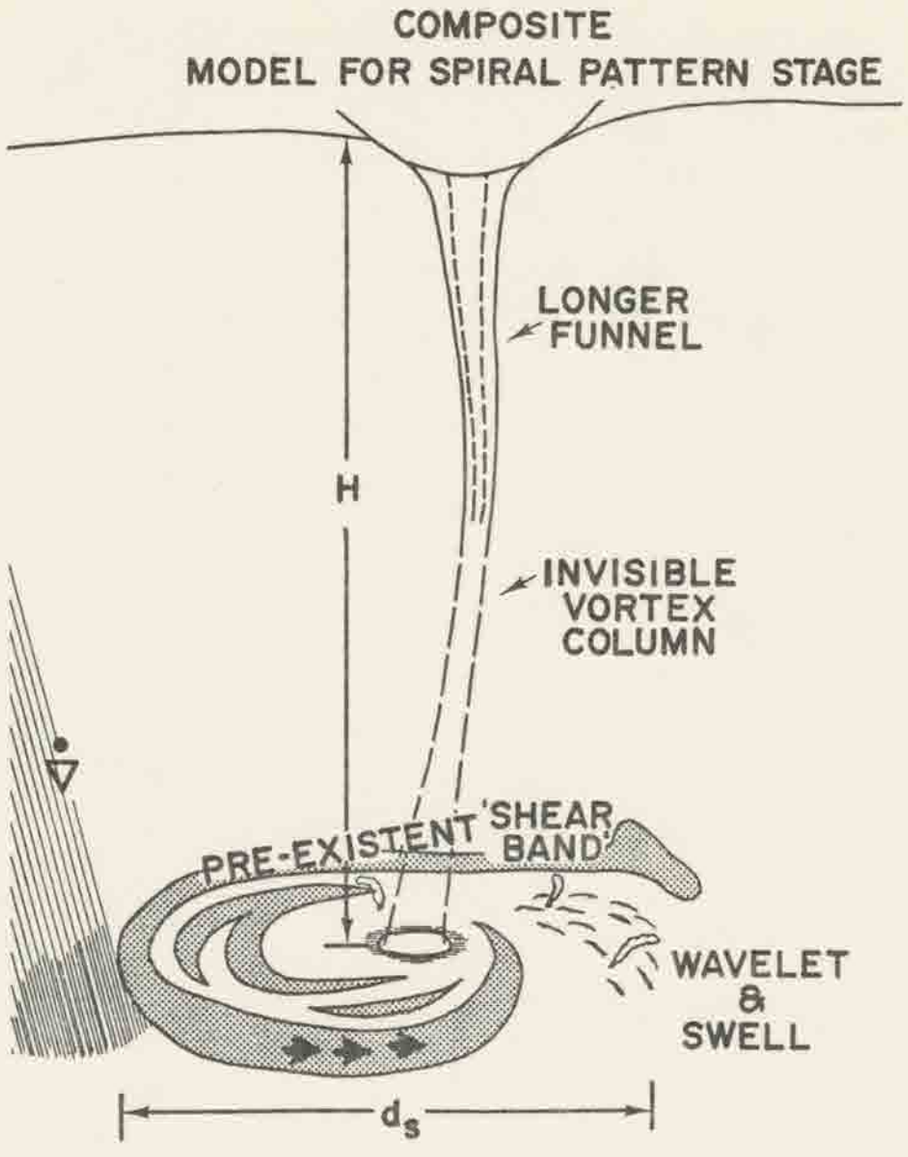

Fig. 9. Golden's composited schematic model for the spiral pattern in the waterspout life cycle. The major spiral band (heavy arrows) evolves around the dark spot during this stage. Characteristic scales are: H = 550 - 670m and d_s = 150 - 920m (reproduced with author's permission, from Golden, 1974a).

sea surface. Golden has found the spiral pattern stage not to occur as often as the other four life cycle stages. However, waterspouts that did pass through the spiral pattern stage almost always evolved through the complete waterspout life cycle.

The third stage (Fig. 10) is the period during which the waterspout wind speeds reach values high enough to pick up spray from the sea surface ($22.5 ms^{-1}$). A spray ring forms at the waterspout's lower

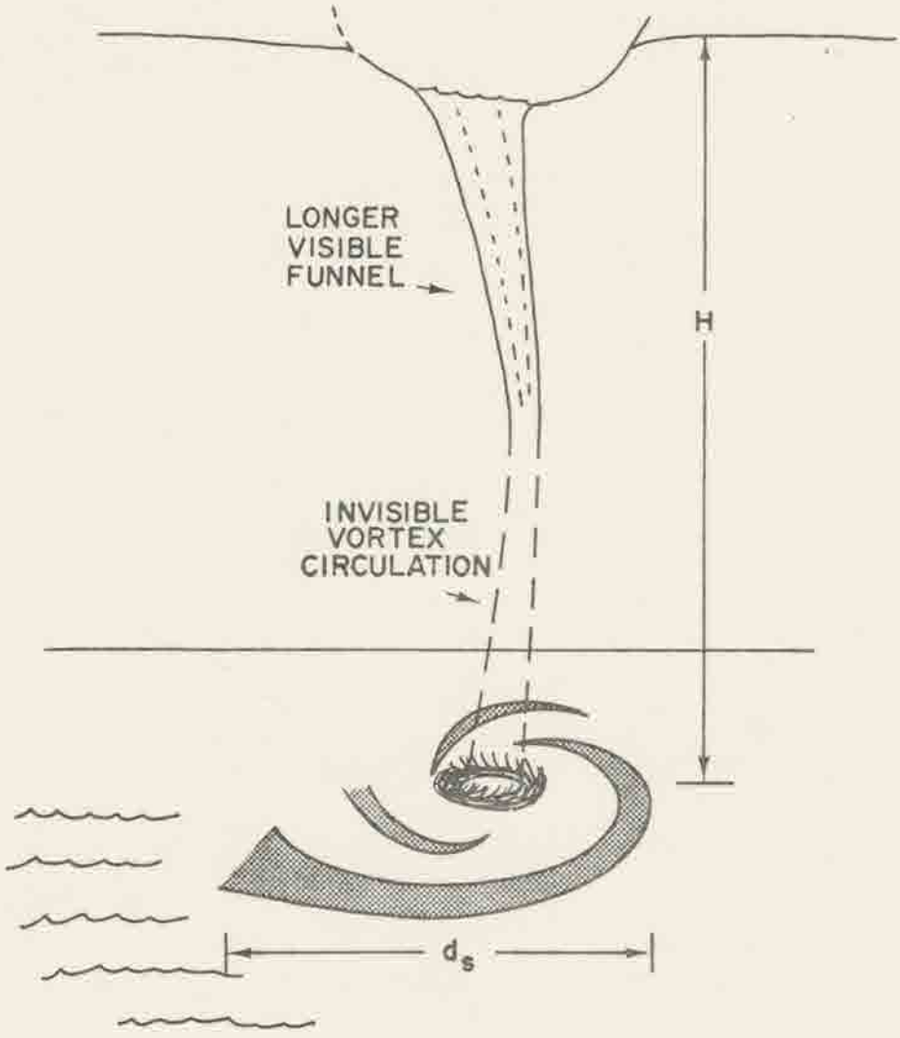

Fig. 10. Golden's composited schematic model for the spray ring stage of the waterspout life cycle. Characteristic scales are: H = 550-670 m and d_s = 45-260 m (reproduced with author's permission, from Golden, 1974a).

boundary and gradually tightens its diameter. As the vortex wind speeds increase, the funnel continues its expansion in length and diameter begun during stage 1 and/or 2. The funnel also begins to translate over the water, and its tilt increases. The spiral pattern (if present) gradually begins to shrink.

The mature waterspout or spray vortex stage occurs when the waterspout attains maximum wind speeds (vertical and horizontal) and grows to its largest size. Translational speeds of the lower funnel increase to usually between 3 to 8ms^{-1}, and the vortex tilt increases due to the disparity of translatory motion between the upper and lower portions of the funnel. The tilt may be partially due to the overtaking of the lower funnel portions by a nearby shower-induced gust front. The mature stage can exist from 2 to 17 min and, together with the dark spot stage, usually makes up approximately 70 to 80% of the lifetime of a specific waterspout (Golden, 1974a).

Golden has documented specific structural features associated with the mature waterspout (Fig. 11). These include a visible double-walled structure with a relatively hollow funnel core, a spray vortex at lower levels extending upward to form a spray sheath surrounding the visible funnel, and a distinct wake of disturbed sea water. The maximum tangential winds appear to exist just above the spray vortex at the approximate radius of the sheath. The sheath itself represents an annulus of intense rising motions. In many cases an entire visible funnel does not exist from cloud base to sea surface.

Golden's final stage or decay stage in the waterspout's life cycle usually lasts about 1 to 3 min. During this time a rain shower may overtake and engulf the funnel, or a shower-induced gust front may

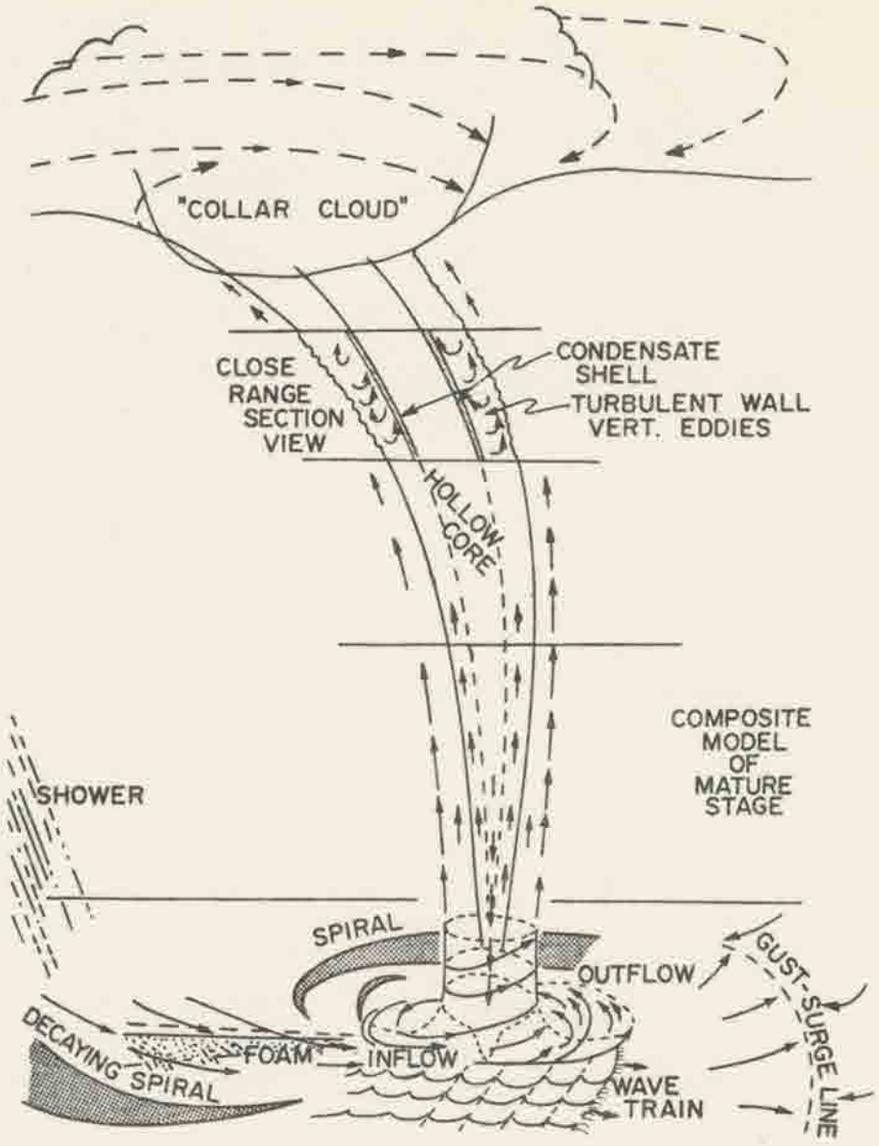

Fig. 11. Golden's composite schematic model of a mature waterspout, slightly modified by the author. Funnel diameters just below the "collar cloud" range from 3 - 140m (reproduced with author's permission, from Golden, 1974a).

destroy the vortex circulation. Often, the funnel becomes contorted with an extreme tilt; in other cases the funnel merely widens and withdraws towards cloud base. The spiral pattern, which usually decreases in size through stages 3 and 4, now shrinks and disappears as the waterspout decays.

3.2 Meso-synoptic Scale Characteristics

Waterspouts typically form from convective cloudlines that develop over the warm land areas and surrounding shallow waters of the Keys. Most waterspout-active cloudlines are in the cumulus congestus stage while individual waterspout-producing cells are usually in the mature stage (Golden, 1974a). In many cases a rainshower is falling within 1 to 2 km of the waterspout(s). The cell(s) spawning waterspout(s) are often the most rapidly growing in the cloudline. Golden determined photogrammetrically cloud top growth rates and heights for several waterspout events. He found average growth rates around 4 to 7ms^{-1} with maximum rates as high as 11ms^{-1}. Cloudline cells appeared to pulsate with waterspout formation or intensification often related to rapid individual cell growth. Cloudline cloud top heights generally averaged between 2900m (9500 ft) and 5700m (18700 ft) during waterspout occurrences. Rossow (1970) observed waterspouts protruding from isolated cumulus clouds and cloudlines with tops at 1830m (6000 ft) to 3050m (10000 ft). Cloud bases varied from 305m (1000 ft) to 610m (2000 ft).

During the summer months, the Keys and surrounding waters attain very warm temperatures from the increased solar insolation. As a result the area can become a strong source of convective activity. The orientation of the Bermuda High maintains the wind field from the east-southeast, quasi-parallel to the Keys chain. Convective cloudlines

are usually oriented approximately parallel to the Keys (ENE to WSW) and translate to the west under the influence of the easterly flow. Aircraft radiometer measurements of sea surface temperatures have detected values as high as 33.5°C over some of the shallower waters (Golden, 1974a). In other cases Golden measured air temperatures 500 ft over one of the larger Keys (Big Pine) of 1° to 2°C higher than outlying air temperatures. Aircraft and rawinsonde (especially 00Z) soundings often reveal neutral or unstable conditions with respect to dry convection in the lower 50 to 100mb of the atmosphere.

Although convective cloudlines are plentiful in the Keys, Golden (1973b, 1974a) asserts that certain synoptic scale features appear necessary for formation of waterspout-active cloudlines. He has enumerated these conditions as:

1) an approaching weak synoptic scale disturbance (easterly wave or short wave in the westerlies) in the lower troposphere accompanied by weak convergence and positive absolute vorticity;

2) weak vertical wind shear in the lower 400mb of the troposphere;

3) moist convectively unstable conditions between the surface and 700mb with dryer air above.

If conditions other than those listed above exist, such as strong subsidence or the passage of a strong disturbance, then waterspout activity will cease or at least be greatly diminished. While subsidence will inhibit convection, strong synoptic disturbances will intensify convection over a large area. As a result the increased cloudiness, strong winds, and vertical wind shear will diminish the surface heating effect on convection. Individual cells in a cloudline will not exist long enough to concentrate pre-existing ambient vorticity.

4. STRUCTURE

Waterspout event case studies discussed in this chapter represent typical waterspouts penetrated during the 1974 field program. A total of 15 waterspouts were penetrated by the instrumented aircraft. The life cycle stages of the penetrated waterspouts included all of Golden's (1974 a,b) five documented stages except the spiral stages. Multiple penetrations occurred on 7 of the total 15. The majority of the waterspouts ranged from weak to moderate in intensity, i.e., maximum vertical velocities $\leq$ 10m/sec and maximum tangential velocities $\leq$ 30m/sec. Table 4 chronologically lists waterspout penetrations, life cycle stages during the penetrations, and the measured rotation sense. The term "waterspouts" refers to any event exhibiting physical characteristics of the concentrated rotary motions of a waterspout vortex, e.g., dark spots, incipient funnel clouds, etc. Unknown rotation senses usually arose from flights over dark spots when it was impossible to tell if or where the aircraft penetrated the invisible vortex. Penetrations of the largest waterspout observed during the field program occurred on September 22, but a temporary malfunction of the instrumentation prohibited any data acquisition other than visual.

4.1 Transformation of Coordinates

All wind velocities calculated from equations (2), (3), and (4) in Chapter 2 are relative to a measurement coordinate system whose vertical axis is parallel with the local vertical. These quantities are measured by the aircraft along an essentially horizontal track that does not necessarily pass through the funnel center. The digitization of the filtered analog signals places the measured quantities at increments of

Table 4. Waterspout events penetrated during 1974 field program. Brackets indicate waterspouts occurring in close proximity, i.e., <1 km horizontal separation.

DATE	WATERSPOUTS PENETRATED	LIFE CYCLE STAGE	NUMBER OF PENETRATIONS	ROTATION SENSE
9-16	1	Funnel	3	CW
9-18	3	Funnel with Dark Spot	2	CW
		Dark Spot Only	1	Unknown
		Funnel with Dark Spot	4	CCW
9-19	3	Dark Spot Only	1	Unknown
		Dark Spot Only	1	Unknown
		Dark Spot Only	1	CCW
9-20	8	Funnel with Dark Spot	17	CCW
		Funnel with Dark Spot	9	
		Funnel with Dark Spot	2	CW
		Funnel with Dark Spot	1	
		Funnel to Surface with Spray Vortex	1	CW
		Funnel to Surface with Spray Vortex	4	
		Funnel to Surface with Spray Vortex (Decaying)	1	CW
		Funnel with Dark Spot (Decaying)	1	Unknown

distance along the aircraft path, the distance increment magnitude depending on the airplane's longitudinal velocity relative to the earth.

It is relevant to a discussion of waterspout structure that the winds be presented in a cylindrical coordinate system moving with the vortex. As a result, a series of transformations involving the tilt, translational velocity, and tilt heading of the funnel with respect to the aircraft heading must be applied to the measured winds.

The first transformation involves conversion of the wind vector in a fixed coordinate system (subscript f) to one relative to a coordinate system moving with the waterspout (subscript s). This is accomplished by simply subtracting out the waterspout's translational velocity (assumed to be constant) from the AADS-2B derived wind vector. Therefore, designating the measured wind vector as $\vec{V}_f = (u_f, v_f, w_f)$ (from equations (2), (3), and (4)) and the wind vector relative to the moving funnel as $\vec{V}_s = (u_s, v_s, w_s)$, then

$$\vec{V}_s = \vec{V}_f - \vec{C} \ . \tag{8}$$

$\vec{C}$ is the waterspout's translational velocity vector (relative to the earth) and has two components, c_{x_f} and c_{y_f}, in the measurement cartesian coordinate system such that $\vec{C} = (c_{x_f}, c_{y_f}, 0)$ (Fig. 12a). Rewriting (8),

$$\vec{V}_s = (u_f - c_{x_f})\hat{i} + (v_f - c_{y_f})\hat{j} + w_f\hat{k} \ . \tag{9}$$

From Fig. 12b it can be seen that $c_{x_f} = -C \cos \chi$ and $c_{y_f} = C \sin \chi$, where χ is the angle measured clockwise from the -x axis (aircraft nose) to $\vec{C}$, and (9) can then be written as

$$\vec{V}_s = (u_f + C \cos \chi)\hat{i} + (v_f - C \sin \chi)\hat{j} + w_f\hat{k} \ . \tag{10}$$

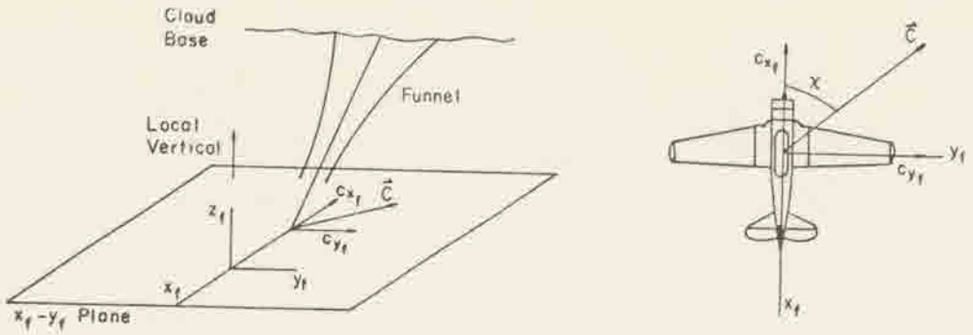

Fig. 12a. Resolution of the waterspout translational velocity vector ($\vec{C}$) into its components in the AADS-2B measurement coordinate system. 12b. Relationship of $\vec{C}$ to its component magnitudes.

The translational waterspout velocity $\vec{C}$ was calculated from photographic sequences and aircraft crew observations of the surface water disturbance and funnel cloud taken as close to the time of penetration(s) as possible. Errors might possibly be as large as several meters per second; however, in the penetrations considered here, the waterspout translation appeared approximately constant, and a mean $\vec{C}$ was determined from the photographic and visual data. If no detectable changes in funnel tilt occurred during a penetration, the movement of the surface dark spot/spray vortex was considered to approximate the funnel's translational velocity ($\vec{C}$) at penetration altitude.

The second transformation converts wind velocities relative to a non-tilted cartesian coordinate system to a tilted cartesian system, both moving with the funnel. This involves two rotations of the non-tilted coordinate axes such that the end result is a set of axes whose z axis is tilted toward some goegraphical heading by an angle γ. The first rotation (Fig. 13a) is around the y_s axis through an angle λ ($\lambda > 0$ for a right-handed rotation; $\lambda < 0$ for left). The second rotation (Fig. 13b) is around the new x' axis through an angle η ($\eta > 0$

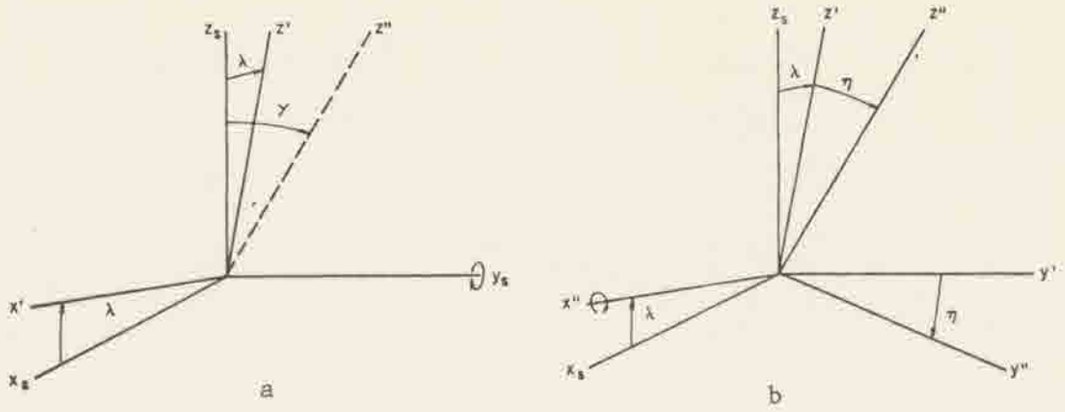

Fig. 13a. Rotation of the non-tilted coordinate system (x_s, y_s, z_s) around its y_s axis to produce a new tilted coordinate system (x', y', z'). 13b. Rotation of the (x', y', z') system around its x' axis to produce the final coordinate system (x", y", z") whose z" axis is tilted γ degrees from the original z_s axis.

for right-handed rotation; $\eta < 0$ for left). Each rotation involves a transformation matrix operating on the scalar components of $\vec{V}_s$ such that the new velocity vector $\vec{V}''$ is written as

$$\vec{V}'' = \begin{pmatrix} 1 & 0 & 0 \\ 0 & \cos\eta & -\sin\eta \\ 0 & \sin\eta & \cos\eta \end{pmatrix} \begin{pmatrix} \cos\lambda & 0 & \sin\lambda \\ 0 & 1 & 0 \\ -\sin\lambda & 0 & \cos\lambda \end{pmatrix} \vec{V}_s \qquad (11)$$

or, combining the two matrices, as

$$\vec{V}'' = \begin{pmatrix} \cos\lambda & 0 & \sin\lambda \\ (\sin\eta\sin\lambda) & (\cos\eta) & (-\sin\eta\cos\lambda) \\ (-\cos\eta\sin\lambda) & (\sin\eta) & (\cos\eta\cos\lambda) \end{pmatrix} \vec{V}_s \; . \qquad (12)$$

Measurements of the funnel tilt (γ) were also obtained (like $\vec{C}$) from air crew photographs and visual observations of the waterspout. Knowledge of the funnel cloud heading as seen from the aircraft (camera), the aircraft heading, and the direction the funnel tilts allowed

calculations of the actual tilt (γ) from the tilt angle measured on the photograph(s). Errors in these calculations appeared to be caused most frequently by the determination of the heading of the funnel cloud as seen from the aircraft. No precise method was available for this measurement and estimates had to be made when each photo was taken. Errors in γ could be as much as $\sim \pm 10^{o}$, but are likely more consistent at $\sim \pm 5^{o}$.

Values of λ and η were calculated for each penetration using funnel tilt, tilt direction, and aircraft penetration heading. Simple mathematical relations for spherical right triangles (whose three sides are traced out by the axes rotations in Fig. 13 and given by γ, λ, and η) were employed.

Equations (10) and (12) provide a complete transformation of the wind velocities measured by the AADS-2B ($\vec{V}_f$) to wind velocities relative to a translating, tilted waterspout ($\vec{V}''$). Combining equations (10) and (12) the scalar velocity components become

$$u'' = (u_f + C \cos \chi) \cos \lambda + w_f \sin \lambda \tag{13a}$$

$$v'' = (u_f + C \cos \chi) \sin \eta \sin \lambda + (v_f - C \sin \chi) \cos \eta - w_f \sin \eta \cos \lambda \tag{13b}$$

$$w'' = (u_f + C \cos \chi) \cos \eta \sin \lambda + (v_f - C \sin \chi) \sin \eta + w_f \cos \eta \cos \lambda . \tag{13c}$$

Equations (13) express velocity components in a cartesian system. The final transformation converts u", v", and w" to components in cylindrical coordinates centered at the funnel's vertical axis, i.e., radical, tangential, and vertical velocities. Since the AADS-2B gust probe usually penetrated the funnel off-center, u" and v" each

contain components of the true radial and tangential velocities. The true waterspout vertical velocity is considered to be w". The standard equations relating cartesian vector components to cylindrical vector components are utilized:

$$u = u'' \cos\theta + v'' \sin\theta$$
$$v = -u'' \sin\theta + v'' \cos\theta \qquad (14)$$
$$w = w''.$$

The azimuth angle θ is measured in the normal sense in cylindrical coordinates and determined from the equation

$$\theta = \pm \tan^{-1} [(R \pm x \sin\lambda \sin\eta)/x \cos\lambda]. \qquad (15)$$

Figure 14 shows plan and side views of the geometry of a funnel penetration and the graphical description of the terms in (15). The choice of plus or minus signs depends on what side of the funnel the "pseudo-center" is located relative to the direction of penetration, e.g., for the Fig. 14 configuration, $\theta = \tan^{-1} [(R + x \sin\lambda \sin\eta)/x \cos\lambda]$. Since the AADS-2B instrumentation boom was mounted offset to the right of the airplane's longitudinal axis which was used by the pilot to "sight" on the funnel center, the majority of pseudo-centers were located to the right of funnel center. The value of R is the minimum funnel radius the aircraft reaches during a penetration, i.e., the pseudo-center. Note that the pseudo-center is not the spatial center of the vortex but is the approximate point at which the maximum deviation in airspeed and the minimum pressure occur as measured by the AADS-2B. Its value is calculated somewhat subjectively from visual observations and relative changes in airspeed and core pressure deficit for successive penetrations, assuming negligible intensity changes and approximate

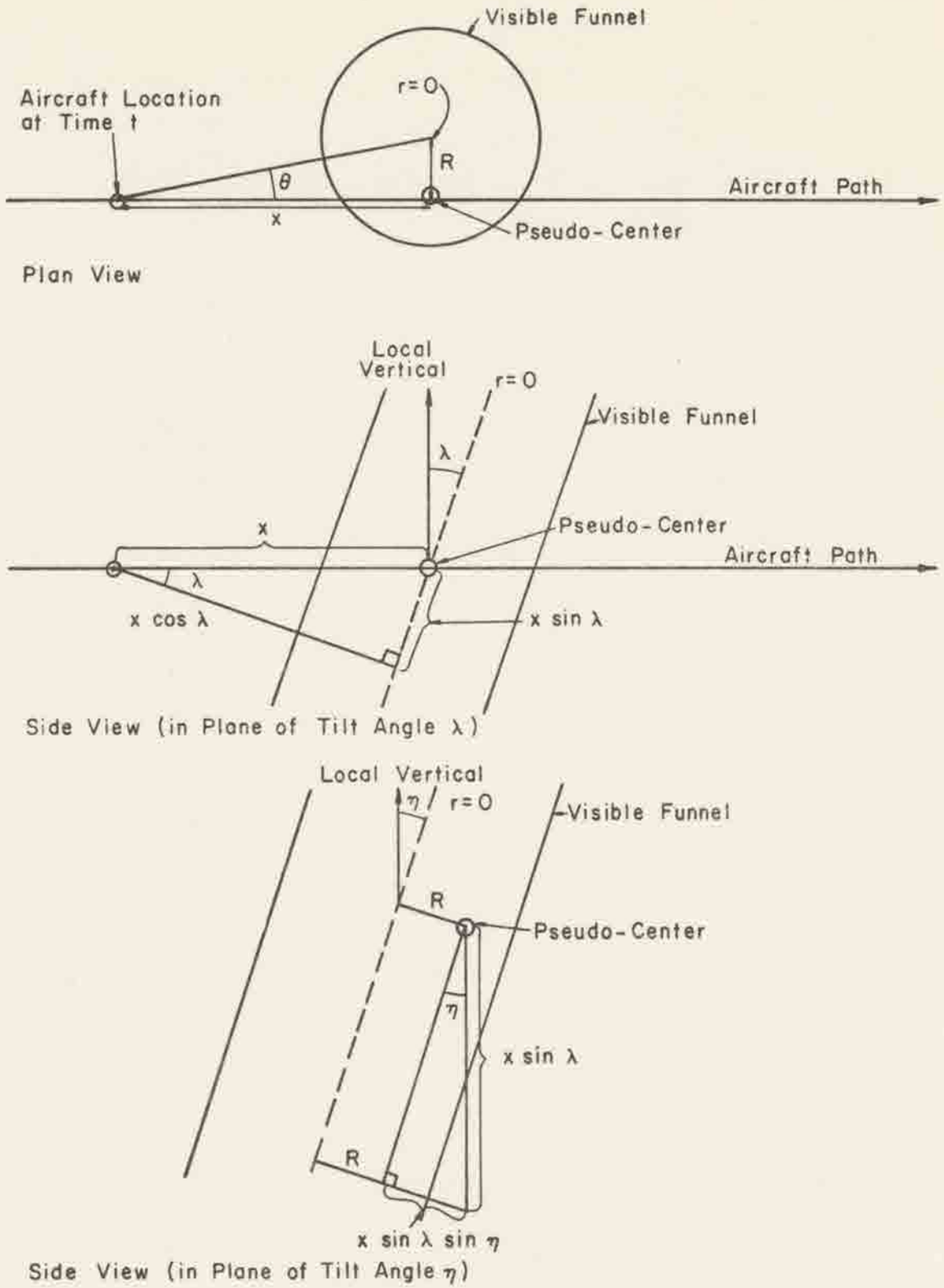

Fig. 14. Plan and side schematic views of a funnel penetration. The aircraft path in the lower side view is into the page.

Rankine vortex flow. The variable x is the distance at time t from the T-6 along the aircraft path to the pseudo-center. The term x cos λ is included to obtain the component of x in the waterspout's rθ plane. x is calculated from the aircraft longitudinal velocity relative to the funnel and the time to/from the pseudo-center.

Because of the waterspout's component of tilt (λ) along the airplane's direction of motion, measurements of wind, temperature, and pressure are not possible in a constant rθ plane of the funnel. That is, the aircraft, as seen from the waterspout cylindrical coordinate system, is climbing or decending during a penetration. This problem is considered unimportant because of the short distances along a typical penetration track and the usually small waterspout tilt angles; therefore, no attempt is made to correct for these apparent changes in geometric altitude relative to the funnel's vertical axis. (If $\lambda = 0$, the problem does not exist for that specific penetration).

As a graphic illustration of how funnel tilt and translational motion affect the measured wind profiles, wind data obtained from a typical penetration are presented in Figs. 15 and 16. Component wind velocities (ordinate) are plotted as a function of distance along the aircraft path from the pseudo-center. The airplane's direction of travel is from left to right. In Fig. 15 the wind components in the measurement coordinate system (u_f, v_f, w_f) are shown. The result of applying equations (13) to (u_f, v_f, w_f) to obtain wind velocities relative to the tilted waterspout (u", v", w") is shown in Fig. 16. For this specific penetration the aircraft heading was 250° and the funnel tilt γ was $\sim$ 30° (see Fig. 13) towards a heading of $\sim$ 330°. The funnel translational velocity at the penetration altitude was determined to be $\sim$ 4-5ms^{-1} towards a heading of $\sim$ 275°.

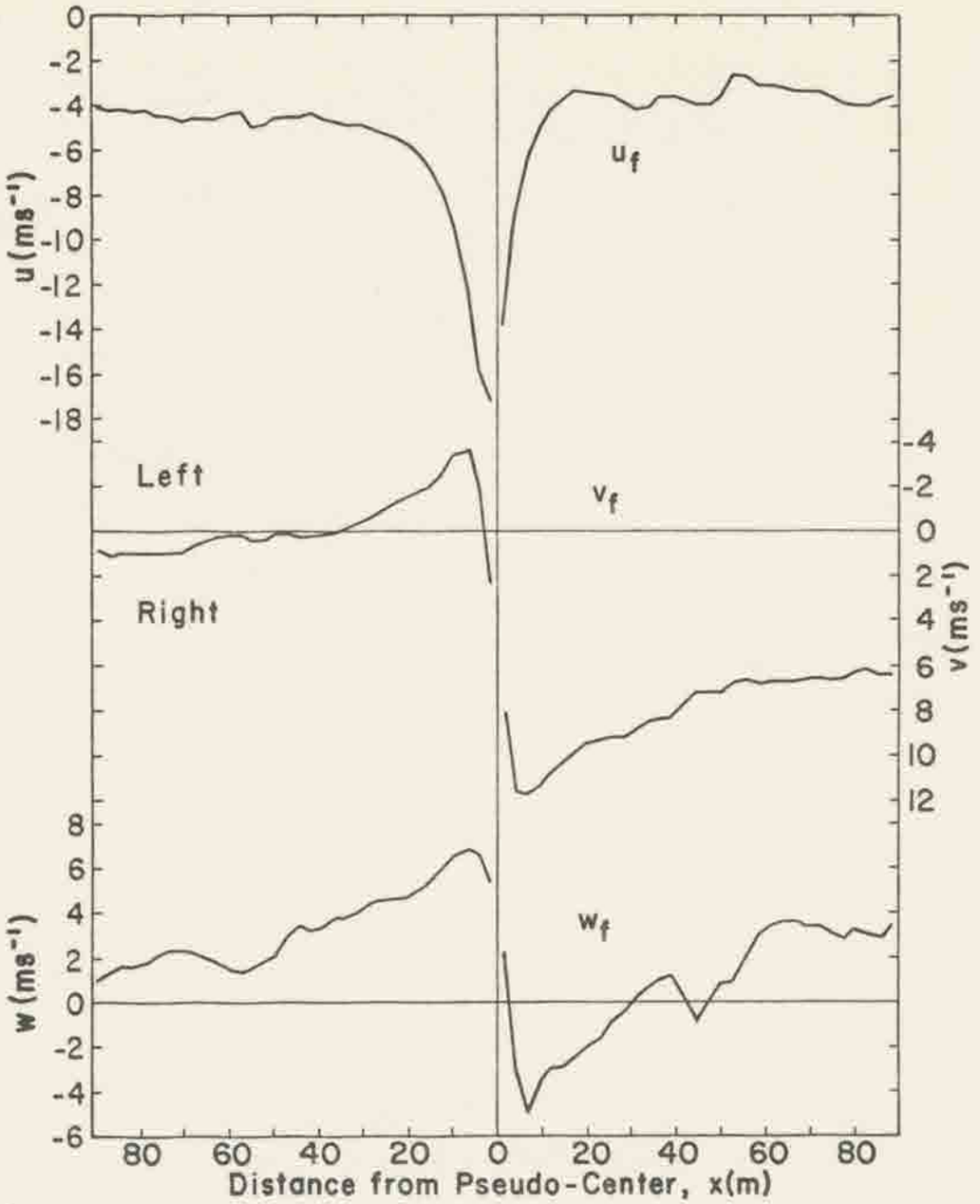

Fig. 15. Three-dimensional wind velocities measured by the AADS-2B (equations (2), (3), and (4)) as a function of aircraft distance (x) from the pseudo-center.

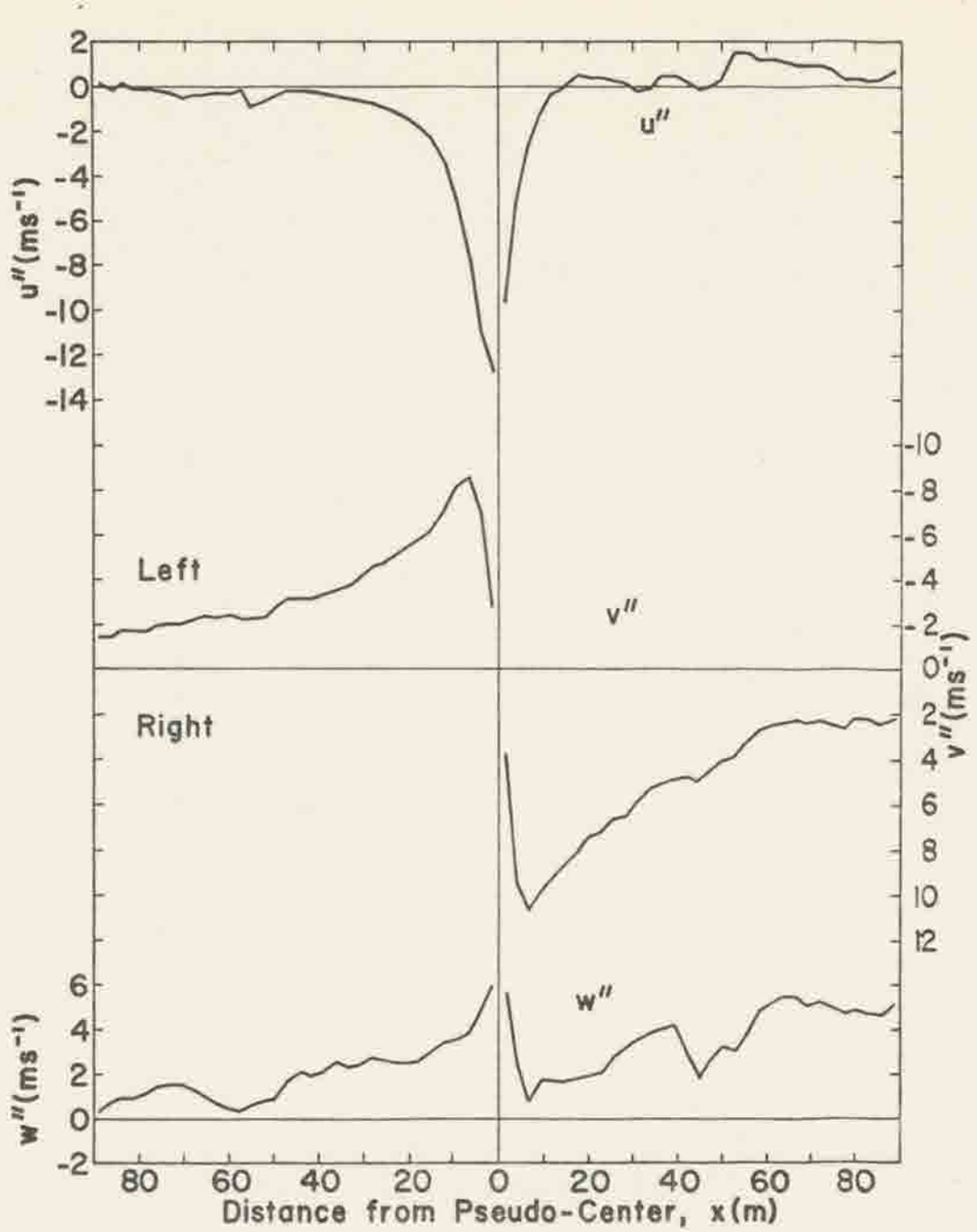

Fig. 16. Three-dimensional wind velocities resulting from application of equations (13) to wind components in Fig. 15. $|\hat{C}| \sim$ 4-5ms^{-1} and $\gamma \sim 30^{\circ}$.

Upon comparing Figs. 15 and 16, it becomes apparent how asymmetries in the measured wind field can arise due to the tilt of a waterspout. The correction for funnel translational velocities in u_f and v_f also reduces the extreme asymmetries into relative winds more symmetric about u" = 0 and v" = 0. Notice that the measured vertical velocity (w_f) trace has a maximum positive value on the front[3] side of the funnel and a maximum negative value immediately on the back. This is a result of the alpha vane measuring a component of the horizontal wind field due to the funnel tilt. In the w" trace both positive and negative maxima have been diminished to reflect the actual vertical velocity with respect to the funnel. Similar comparisons apply for v_f and v", and u_f and u".

4.2 Case I

The penetration data presented in this section were all obtained by successively penetrating one waterspout funnel over a time interval of approximately 10 min. The waterspout was one of two adjacent cases that formed about 10km south of the Saddlebunch Keys at 1200 EDT on September 20 (Fig. 17). Although penetrations were flown thru both funnel clouds and the data were very similar for each, only one funnel was selected for discussion because its winds were $\sim$ 10-20% stronger than the second vortex. The Case I waterspout initially developed approximately 16 min (1216 EDT) after the aircraft crew sighted the first funnel cloud. The total lifetime of the visible vortex,

[3]Reference to the front and back sides of the waterspout is with respect to the aircraft penetration track, i.e., front is left and back is right of x = 0, respectively.

Fig. 17. Photograph of the Case I waterspout funnel and dark spot early in its life cycle. The funnel cloud extends ∿ 140m below cloud base altitude of ∿ 520m. Funnel diameter ranges from ∿ 4-8m.

manifest by a funnel cloud and a dark spot on the water, was 13 min. During the period when both funnels coexisted, the Case I vortex was situated ∿ 700m to the northeast of the second waterspout. The cloud-line was oriented NE-SW and was largely composed of towering cumulus (TCu) with one large cell raining out ∿ 3km southwest of the two waterspouts (Fig. 18). Both funnels translated to the west-southwest (hdg: 250°) at ∿ 2-3ms^{-1}. The Case I funnel was measured photogrammetrically to have a tilt (γ) of 15° towards a true heading of 300°. Subcloud layer mean winds were determined from the 1200 GMT EYW sounding to be 80° at ∿ 4ms^{-1}. During their lifetime, the two vortices existed only in the dark spot stage with visible funnels extending downward from cloud base ∿ 100-150m (Fig. 19). Their dissipation featured a

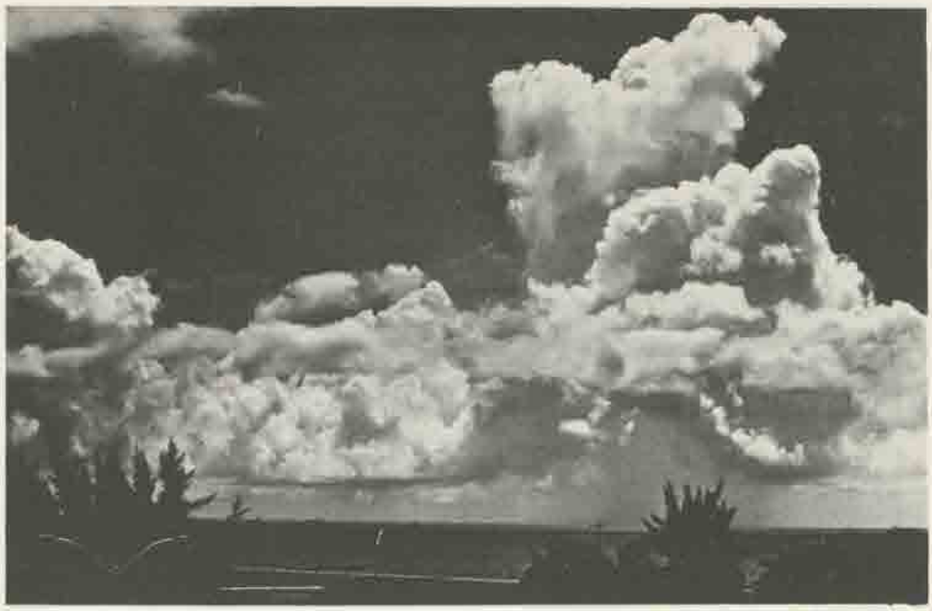

Fig. 18. Photograph of the Case I waterspout cloudline taken from the EYW airport terminal roof. Photo looks ESE.

Fig. 19. Photograph of the Case I waterspout funnel and dark spot nearing the end of its life cycle. Funnel diameter is $\sim$ 10-12m.

withdrawal of the visible funnel to cloud base and disappearance of the dark spot on the water. No noticeable change in funnel tilt was observed during the decay process.

Penetration 1. The three cylindrical components ($\bar{u}$, $\bar{v}$, $\bar{w}$) of the waterspout wind velocity vector $\vec{V}$ as measured by the AADS-2B are shown in Fig. 20. The radial ($\bar{u}$), tangential ($\bar{v}$), and vertical ($\bar{w}$) velocities are plotted on the ordinate against waterspout radius (r) on the abscissa. The measured wind components are considered to represent the mean three-dimensional wind field of the waterspout, hence the addition of the average bars. The aircraft track is from left to right (pagewise) with the "front" ("back") of the funnel specified as left (right) of r = 0. Remember that these measurements are not obtained along a constant radius vector, but that the aircraft usually penetrates the funnel slightly off-center. As a result, in presenting wind velocities, pressure, and temperature as a function of funnel radius, a gap in the data will appear inside r = R, i.e., at radii less than the radius of the pseudo-center R (see section 4.1). The standard sign designations for radial and vertical velocities are utilized, i.e., $\bar{u} > 0$ ($\bar{u} < 0$) for motion towards larger (smaller) r, and $\bar{w} > 0$ ($\bar{w} < 0$) for upward (downward) motion in the normal meteorological sense.

The presentation of tangential velocities ($\bar{v}$) requires an additional explanation. In Fig. 20 velocities are plotted on the ordinate as left or right (paperwise) of $\bar{v} = 0$. Right (left) denotes tangential velocities with a positive (negative) v" component (see equations 14). These direction definitions arise from the aircraft coordinate system (see Fig. 5) where v_f (hence v") is positive (negative) for air motions towards the right (left) of the airplane's direction of travel. As

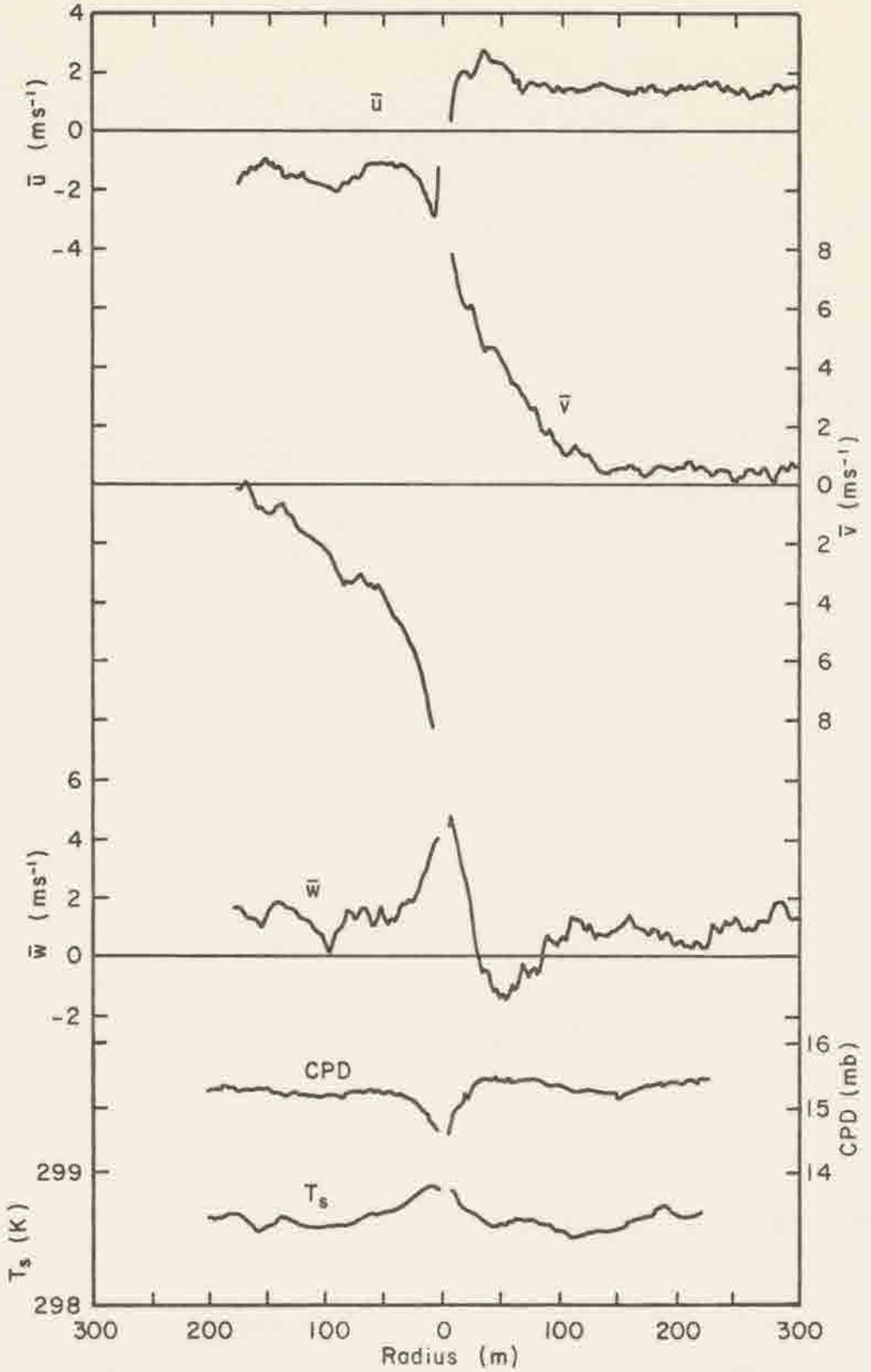

Fig. 20. Radial profiles of $\bar{u}$, $\bar{v}$, $\bar{w}$, CPD, and T_s for penetration 1, Case I waterspout. Penetration altitude was 466m; penetration heading was 220°.

the aircraft approaches the pseudo-center, an increasing percentage of the tangential velocity will be contributed by the u" component of the wind, but as long as v" is positive (negative), $\bar{v}$ is defined as right (left). Obviously, the shift in the $\bar{v}$ profile across the 0 line should not be construed as a change in sense of rotation of the mean tangential winds, but only as a change in sign of the v" wind component. A positive (negative) $\bar{v}$ indicates cyclonic (anticyclonic) rotation. This manner of graphical display was chosen so as to aid in visualizing the waterspout's swirling flow.

Profiles of the absolute static temperature (T_s) and the core pressure deficit (CPD) are also shown in Fig. 20. All values are measured along the airplane's flight path; that is, no corrections to a constant reference altitude are made. T_s (K) is calculated from equation (6) (Chapter 2), and the CPD (mb) is measured directly by the AADS-2B. Both values are plotted as functions of waterspout radius.

a. Three Dimensional Wind Profiles. The three dimensional waterspout wind field as measured by the penetrating aircraft is shown in Fig. 20. The most noticeable characteristic is the dramatic increase in relative wind velocities in the vertical and tangential fields of motion. Examination reveals an area of enhanced upward vertical motion superimposed on a field of concentrated rotary motion. The vertical velocity ($\bar{w}$) increases positively inwards towards the waterspout center, with a maximum of $\sim$ 4-5ms^{-1} found at the smallest radii (for this penetration $\sim$ 5.5m). The tangential velocity ($\bar{v}$) reveals the cyclonic rotation of this waterspout. Values of ($\bar{v}$) increase with decreasing radius to a measured maximum of $\sim$ 8ms^{-1} at r = 5.5m. The radial velocity profile shows an increase in inflow on the front

side of the funnel at about r = 8m, and a broader outflow area of slightly less magnitude on the back side of the vortex. Considering the penetration heading of 220° and the mean subcloud layer easterly winds, the entire $\bar{u}$ profile shows that the waterspout is translating at a slower rate than the environmental winds. Hence, on the penetration front side or, roughly, the waterspout's right rear quadrant (relative to the direction of translation), there is relative inflow of $\sim$ -1 to $-2ms^{-1}$ that increases to $-3ms^{-1}$ at r = 8m. The opposite is true on the penetration back side or the waterspout's forward quadrants, where relative outflow of $\sim$ $1-2ms^{-1}$ exists at radii far from the funnel.

It should be noted that errors in $\bar{u}$ and $\bar{v}$ as calculated from equation (14) and (15) may increase as the radius decreases. If the radius of the pseudo-center (R), or off-center penetration distance is in error by several meters, values of the azimuth angle (θ) will also be in error, the magnitude of which could be as much as $\sim$ 10° to 20° at minimum radii. For typical values of u'' and v'' at these radii, this could produce errors in the radial and tangential velocities of $\sim$ $1-2ms^{-1}$. At greater distances from the waterspout, x sin λ sin η is much larger than R in equation (15), and errors will be minimized. Apparent areas of relative inflow and outflow near r = 0 should be considered with caution realizing that large errors of $1-2ms^{-1}$ may be present. By the same token, values of $\bar{v}$ at small radii may also be in error by like amounts, the end effect being reduction or amplification of the profile peak where $\bar{v} = \bar{v}_{max}$.

The tangential winds reveal a broad circulation extending out to a radius of approximately 150m on either side of the funnel. The visible funnel diameter at the penetration altitude was photographically

determined to be ∿ 10m, hence the horizontal extent of the tangential circulation is much larger than the funnel size. It appears as though the AADS-2B boom-vane system penetrated the waterspout near the boundary of the visible vortex. The maximum measured values of $\bar{v}$ appear just at or inside the radius of the visible funnel, but that is not to say velocities are not stronger at radii less than R.

Vertical velocities in the near-funnel environment are of the order $1ms^{-1}$. There is an area of negative vertical velocity centered near r = 50m on the back side of the vortex. This is believed to be real and not a product of the measurement system, e.g., overshooting alpha vane.

b. Temperature and Pressure Profiles. Profiles of static temperature and core pressure deficit reveal the waterspout core as a warm, low pressure region. The maximum measured temperature deviation from mean values in the near environment (∿ 298.6 K) amounts to ∿ 0.3 K. The extent of the warmer temperatures reaches to r ∿ 70m on the front side and to r ∿ 30m on the back.

It is believed by the author that essentially two outside factors affect the temperature measurements. First, the waterspout's small horizontal extent combined with the rapid aircraft motion calls for a faster responding temperature probe than the Rosemount unit in order to obtain accurate values of T_s in the waterspout. Secondly, it is believed that the small water droplets formed in the visible funnel are not entirely separated from air flow past the element by the 90^o bend designed into the sensor. As a result the platinum wire may become partially wet thus giving erroneous total temperature values (Lenschow and Pennell, 1974). No estimate of the magnitude of this error is available.

The CPD profile again substantiates the broad horizontal extent of this waterspout's kinematic and thermodynamic anomalies compared to the size of the visible funnel. Pressure begins to drop below the ambient value at a radius of approximately 30m and reaches a maximum deviation of -0.6mb at the minimum radius of measurements, r = 5.5m. As in the case of the wind measurements, the off-center penetration only allows conjecture concerning the temperature and pressure profiles at r < 5.5m. Possibly, there may be a double peak in the T_s profile, and most likely, lower pressures would exist at the funnel's core.

Penetration 2. Data from the second penetration of the Case I waterspout is shown in Fig. 21. The penetration occurred one minute and nine seconds after penetration 1 and 34m lower (429m). The penetration heading was 110°, approximately 30° off an upwind heading of 80°. The front side of the waterspout in Fig. 21 is now its downwind side, and the back side is in its upwind sector. The minimum funnel radius reached during this penetration was calculated to be ∿ 5m to the right of r = 0. The visible funnel diameter was still a relatively constant 10m.

a. Three Dimensional Wind Profiles. The relative wind profiles are similar in shape and intensity to those of penetration 1. The characteristic tangential wind field extends outward to radii of approximately 100m. Maximum values of 7.8ms^{-1} and 8.0ms^{-1} are found at radii of 6-7m on the front and 10-11m on the back side, respectively.

The vertical velocity increases from near-funnel values of ∿ 2ms^{-1} to a measured maximum of 6.0ms^{-1} at a front side radius of ∿ 7m. Immediately on the back side of the funnel, $\bar{w}$ drops to a minimum of

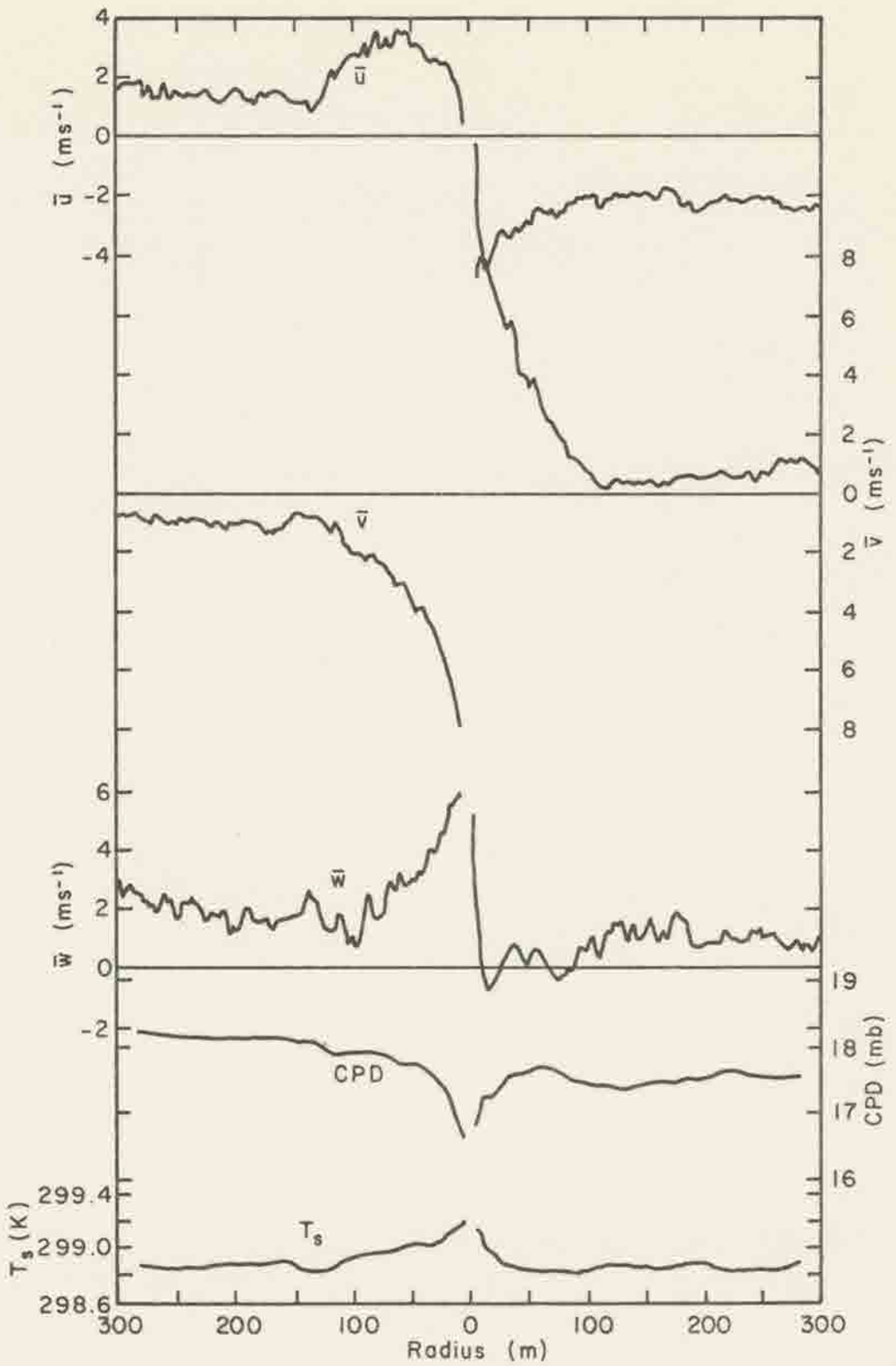

Fig. 21. As in Fig. 20 except for penetration 2. Penetration altitude was 429m; penetration heading was 110°.

$-0.8ms^{-1}$ before climbing back to $\sim 1ms^{-1}$ in the upwind near-funnel environment.

Due to the penetration heading, radial velocities contain the largest component of the environmental wind field. Positive (negative) values downwind (upwind) of r = 0 indicate relative outflow (inflow). Near the vortex, regions of apparent enhanced outflow and inflow exist out to radii of $\sim$ 50-100m. As r decreases radial winds tend toward zero similar to the penetration 1 profile.

b. Temperature and Pressure Profiles. Temperature and pressure profiles again show the broad warm, low pressure core of the waterspout. The maximum temperature anomaly in the funnel of $\sim$ 0.4 K is found at the smallest radii (r = 5m). Increases above environmental values of T_s begin at approximately 100m on the waterspout's front side; whereas T_s drops almost immediately to environmental values on the backside.

The CPD reaches a maximum drop in the waterspout of -1.2mb, again at the smallest radii. The low pressure area extends out to radii of about 30 to 40m on either side of the funnel. The drop in ambient pressure from the front side of the funnel to the back is due to an aircraft altitude gain of about 5-10m as the penetration was made.

Penetration 3. This waterspout penetration was executed four minutes, twenty seconds after penetration 2. In that interim, the adjacent waterspout, which formed first, dissipated. Also, two additional penetrations were made on the Case I waterspout. The first occurred at 12:22:35 or approximately 1.3 min after penetration 2. Its kinematic and thermodynamic structure is very similar to penetration 2. Maximum measured anomalies of $\bar{w}$, $\bar{v}$, T_s, and CPD are approximately $6.5ms^{-1}$, $8.0ms^{-1}$, 0.2K, and -0.8mb respectively. The second

penetration was flown at 12:24:31, but the data is not presented because the radius (R) of the pseudo-center was nebulous. It appears as though the penetration was farther off-center than the previous three, since maximum wind, temperature, and pressure values are 10 to 50% smaller.

The third penetration's altitude (492m) was 30 to 60m higher than penetrations 1 and 2. This altitude was the nearest to cloud base ($\sim$ 520m) of all penetrations accomplished on this specific waterspout. Funnel diameter was determined to be $\sim$ 10-12m just prior to penetration. Within 30 sec after the penetration, the dark spot on the water surface grew smaller and the visible funnel withdrew to about 30m below cloud base and widened out appreciably. Funnel tilt did not appear to change.

a. Three Dimensional Wind Profiles. Waterspout winds are illustrated in Fig. 22. Once again tangential flow extends to radii of approximately 100m. Maximum measured values in the vortex are 7.7 and 9.2ms^{-1} on the front and back side, respectively. The tangential winds at radii beyond about 100m show relative wind flow towards the southwest (aircraft heading + 90^{o}) since the waterspout's translational velocity was measured to be less than the mean subcloud environmental winds, $\sim$ 4ms^{-1}.

The relative radial velocity in the near-funnel environment is positive (outflow) and negative (inflow) on the front and back sides of the vortex, respectively. This is similar to penetration 2, whose heading was 110^{o}, and opposite to penetration 1 with a heading 220^{o}. In the vortex itself, the measurements show slight inflow on the front side, but alternating regions of in and outflow at the back. These

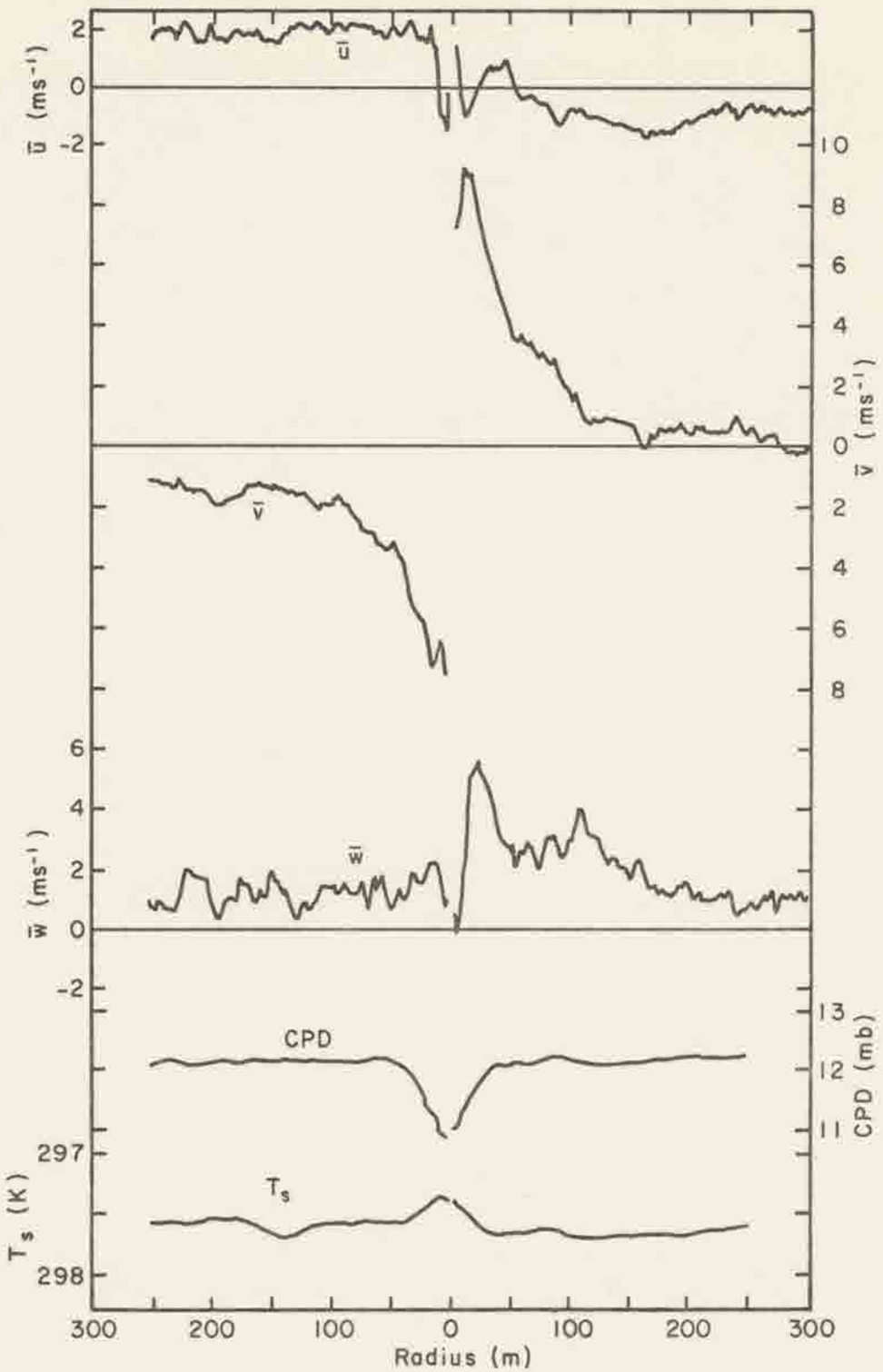

Fig. 22. As in Fig. 20 except for penetration 3. Penetration altitude was 492m; penetration heading was 130°.

should be interpreted with caution due to possible large measurement errors at these small radii.

The interesting feature of the vertical velocity profile is the area of apparently suppressed positive vertical motion near the funnel core. Surrounding this region the characteristic strong upwards motion of the vortex exists. Similar patterns, termed two-cell circulations, have been measured in desert dust devils (Sinclair, 1973b and Kaimal and Businger, 1970) and simulated in laboratory vortices (e.g., Ying and Chang, 1970, and Ward, 1972) and numerical experiments (e.g., Kuo, 1966; Bellamy-Knights, 1971; and Harlow and Stein, 1974). The two positive velocity maxima are, respectively, 2.2 and 5.5ms^{-1} on the front and back sides, while the $\bar{w}$ minima at r ≈ 6m is -0.2ms^{-1}. It is interesting to note the existence of the relative downflow on the r = 0 axis coincides in this case with the mature stage of the waterspout.

b. Temperature and Pressure Profiles. The CPD and T_s traces are also shown in Fig. 22. A maximum pressure change of -1.3mb was measured between near-funnel environmental radii and the minimum funnel radius reached by the aircraft. Values of the CPD begin to decrease at radii of about 40m.

The static temperature increases in the funnel to a maximum anomaly of ≈ 0.2 K above values measured outside the waterspout's sphere of influence. Maximum changes in T_s begin at radii of approximately 30-40m.

Penetration 4. The last penetration of this waterspout was negotiated as a pass over the small dark spot remaining on the ocean surface. No funnel pendent was apparent below cloud base. As a result, the

radius of the pseudo-center (R) could not be measured, but due to the apparent magnitude of the measured wind speeds, it was assumed the aircraft passed quite close to the center of rotation, and R = 7m was quite arbitrarily chosen.

a. Three Dimensional Wind Profiles. The most noticeable characteristic from this set of waterspout wind velocities (Fig. 23) is the apparent increase in the turbulent intensity, especially in the $\bar{u}$ and $\bar{v}$ components. The smooth increase in tangential winds to a sharp peak near the waterspout vertical axis that appeared in the preceding three penetrations is not so evident in penetration 4. The velocity peaks appear eroded into weaker broader maxima of ≈ 3.0 to 3.3ms^{-1}. The near-back side of the vortex exhibits stronger turbulent gusts than the front for all three wind components. Maximum vertical velocities obtained at small radii reach 4.2 to 4.5ms^{-1}. Radial velocities with respect to the vortex are outflowing ($\bar{u} > 0$) on the front side, and mostly inflowing ($\bar{u} < 0$) on the back. These data seem to indicate that the decay of the waterspout may be well correlated with an increasingly turbulent near-funnel wind field. The turbulence may, for example, be induced by the superposition of a nearby shower-induced gust front on the waterspout flow field (Golden, 1974a). Golden suggested that waterspouts being overtaken by shower-induced outflow usually exhibit increases in funnel tilt and contortions and/or suddenly change their translational velocities. However, as previously mentioned, none of these tendencies were visually observed as the waterspout decayed.

b. Temperature and Pressure Profiles. Comparing the traces of T_s and CPD in Fig. 23 with those of the previous three penetrations,

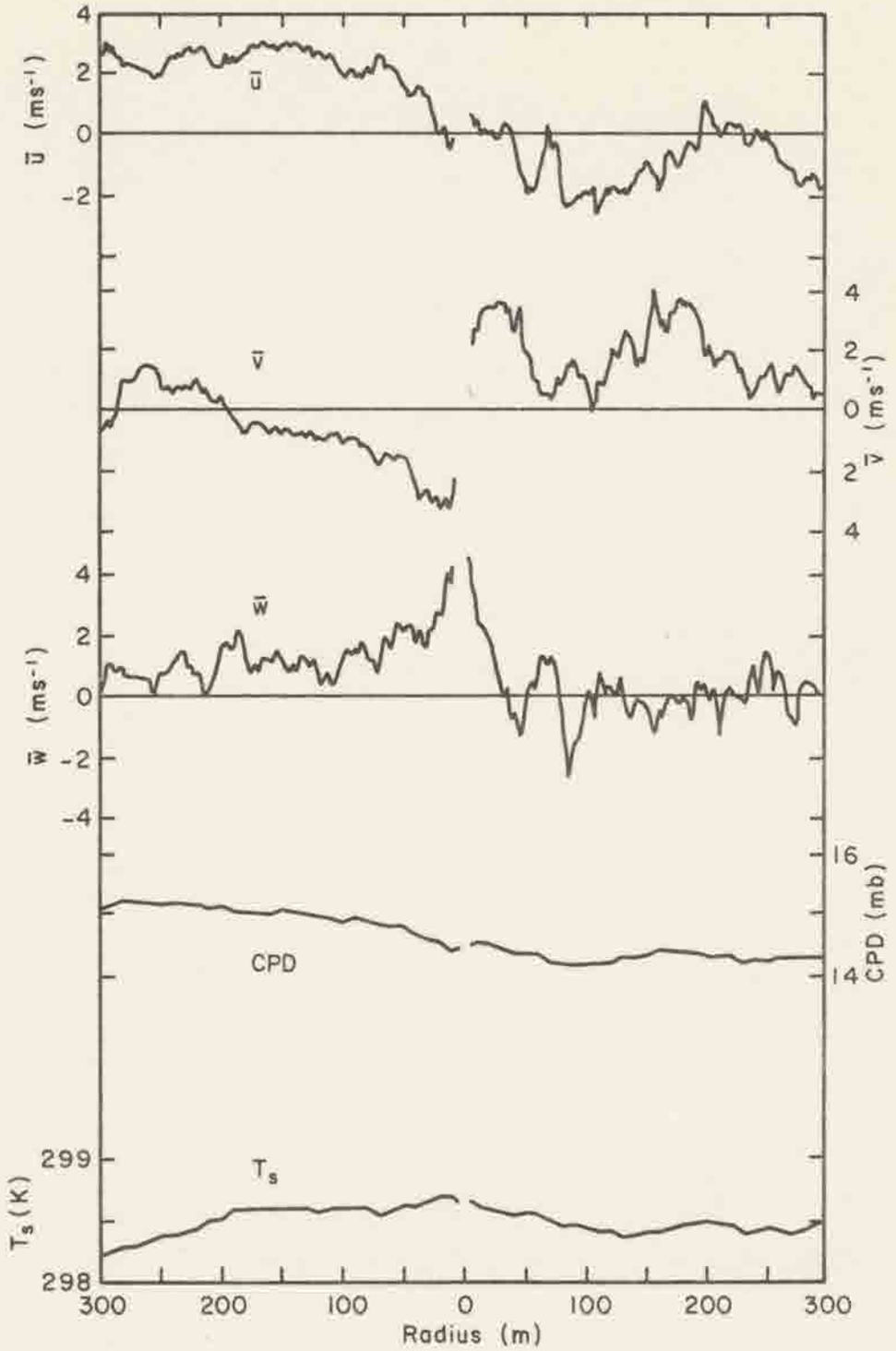

Fig. 23. As in Fig. 20 except for penetration 4. Penetration altitude was 474m; penetration heading was 120°.

the most noticeable difference is the smaller deviations of temperature and pressure near the center of the vortex. The general decreasing trend in CPD from the front to the back side of the waterspout is due to a slight gain in aircraft altitude of $\sim$ 8m from r (front) = 350m to r (back) = 300m. This masks the pressure drop in the spout somewhat making it difficult to calculate its actual magnitude. A reasonable number might be $\sim$ -0.4mb.

Temperature values at small radii increase only approximately 0.1 K above T_s at r (front) = 150m. The smaller anomalies in both T_s and CPD are probably due to a combination of two factors. The first is a penetration likely made farther off center than any previous one, and the second is the coincidence of the waterspout's decay, hence the weakening of its pressure, temperature, and wind fields, with the penetration event.

4.3 Case II

The second case study is composed of data obtained from two penetrations of an anticyclonic waterspout. The waterspout was encountered on the same flight on which the Case I waterspout was penetrated but about one hour later ($\sim$ 1315 EDT). Four actual penetrations were flown on the funnel, but only the first two provided quality data in and outside the vortex. The waterspout was selected for study for several reasons:

1) its sense of rotation was anticyclonic;

2) wind and CPD values were the strongest measured during the the 1974 program;

3) the funnel was tilted up to 30° out of the local vertical, thus providing kinematic and thermodynamic data from a moderately contorted funnel; and

4) a nearby rainshower all but engulfed the vortex in its dying stage.

A second waterspout initially existed ∿ 0.5km WSW of the first and was penetrated once before it dissipated.

The two waterspouts developed out of a line of cumulus congestus oriented ENE-WSW and located ∿ 8km north of the island chain. The individual cell(s) (Fig. 24) from which the funnel emanated were situated ∿ 16km directly north of the Key West Airport and were among the strongest in the entire cloudline. The waterspouts' birth was undocumented; the aircraft first reached the area with moderate rain already falling immediately west of the funnels. In addition, both waterspouts had already evolved to the spray vortex stage with complete visible funnels from cloud to sea.

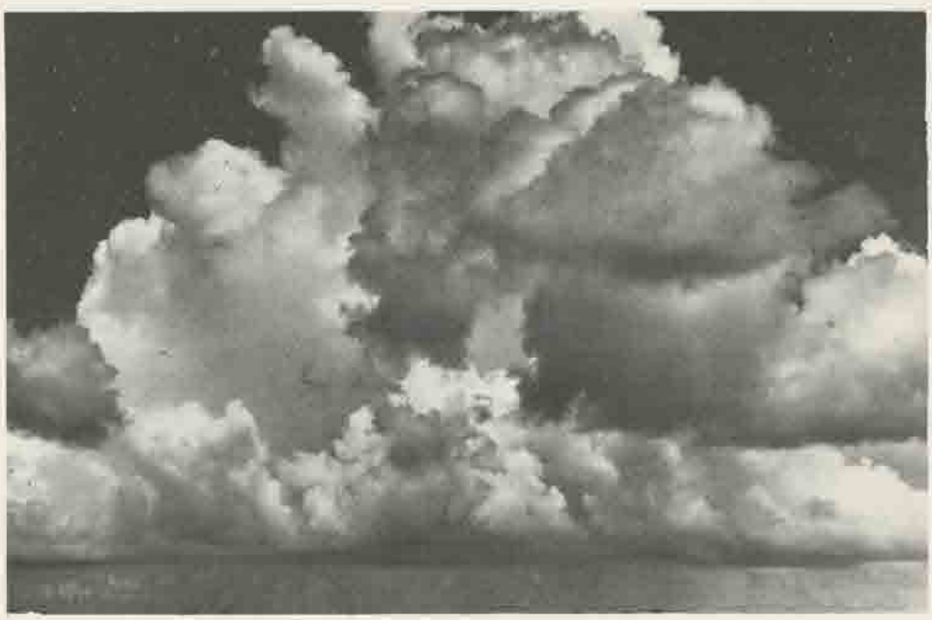

Fig. 24. Photograph of the cloud line from which the Case II waterspout developed. The funnel clouds extended from the solid cloud base in the lower portion of the photo.

Penetration 1. The first penetration was flown at a heading of 250°. The waterspout was translating to the west-northwest (∿ 280°) at about 4-5ms^{-1}. At the altitude and time of penetration, funnel tilt was measured as ∿ 30° towards a 330° heading.

a. Three Dimensional Wind Profiles. Figure 25 shows the relative radial, tangential, and vertical velocities in and up to 180m outside the visible funnel. Due to the penetration heading, the back side of the waterspout is to the WSW and is also the rain shower side of the funnel. The pronounced tangential wind field extends to radii of ∿ 150m on either side. Maximum measured values of $\bar{v}$ are 13ms^{-1} at front side radii of ∿ 4 and 5m, and 10.6ms^{-1} at back side radii of ∿ 6 and 8m.

The vertical velocity trace shows front side near-funnel environmental values of ∿ 1ms^{-1} increasing to maxima of ∿ 5.5 to 6.0ms^{-1} at smallest funnel radii. There is a strong decrease in $\bar{w}$ immediately to the rear of r = 0 and then a subsequent increase to a broad area of strong upward motion, on the order of 5ms^{-1}, centered around r (back) = 100m. At r (back) = 150m the vertical velocity decreases abruptly, but remains positive.

Radial velocities show weak inflow on both sides of the funnel that increases to ∿ -2 to -3ms^{-1} at small radii. This characteristic of the $\bar{u}$ profile is considered more typical of the convergent flow usually assumed to exist around a vortex, even above the surface boundary layer. At r = 150m the relative radial inflow peaks at ∿ -4ms^{-1}. This may be the approximate boundary of the nearby rain shower at the penetration altitude.

b. Temperature and Pressure Profiles. The CPD profile shown in Fig. 25 reveals a moderate pressure drop at the small waterspout radii.

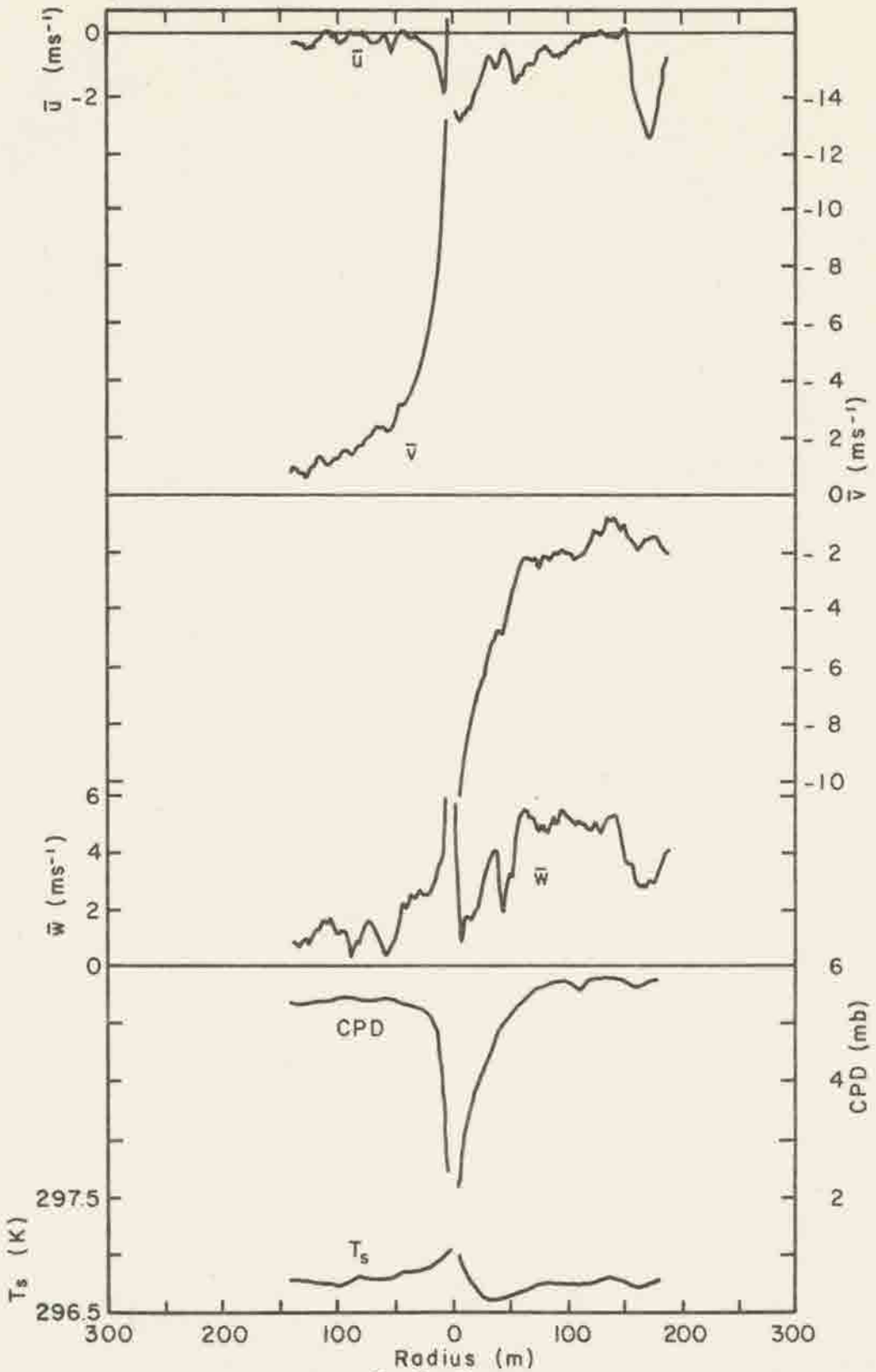

Fig. 25. Radial profiles of $\bar{u}$, $\bar{v}$, $\bar{w}$, CPD, and T_s for the Case II anticyclonic waterspout, penetration 1. Penetration altitude was 676m; penetration heading was 250°.

The maximum drop from values at r(front) = 100 m is ≃ 3.3 mb. Again, the pressure differential of ∿ 0.4 mb between outside funnel CPD values on front and back sides is due to an aircraft altitude change of ∿ 5m during the penetration. The difference between the magnitude of the radial pressure gradient ($\partial p/\partial r$) on front and back sides may be partially due to the slope of funnel and/or to the rapid vertical acceleration of the aircraft as it penetrates the vortex.

The temperature profile shows the characteristic increase at small funnel radii. The maximum temperature anomaly is ∿ 0.3K above outside funnel environmental values. The relative minima at r(back) = 30m may be correlated with the abrupt decrease in $\bar{w}$ in that vicinity or may be due to partial wetting of the sensor upon passage thru the funnel.

Penetration 2. The second penetration was made 1.5min after the first and at a heading of 160°. Funnel tilt at the penetration altitude was estimated to be ∿20° towards a heading of ∿ 350°. The waterspout's translational velocity at the penetration altitude was assumed the same as the motion of the spray vortex, ∿ 5ms^{-1} towards 280°.

a. Three Dimensional Wind Profiles. The values of $\bar{v}$ and CPD were the largest measured during the 1974 field program. The tangential wind profile (Figure 26) exhibits the familiar vortex profile. The maximum values of $\bar{v}$ are 17.2 ms^{-1} at r(front) ≃ 5m and 22.0 ms^{-1} at r(back) ≃ 3m. This penetration graphically reveals the waterspout's location on a relative wind shear boundary, possibly the quasi-vertical vortex sheet hypothesized by Golden (1974a).

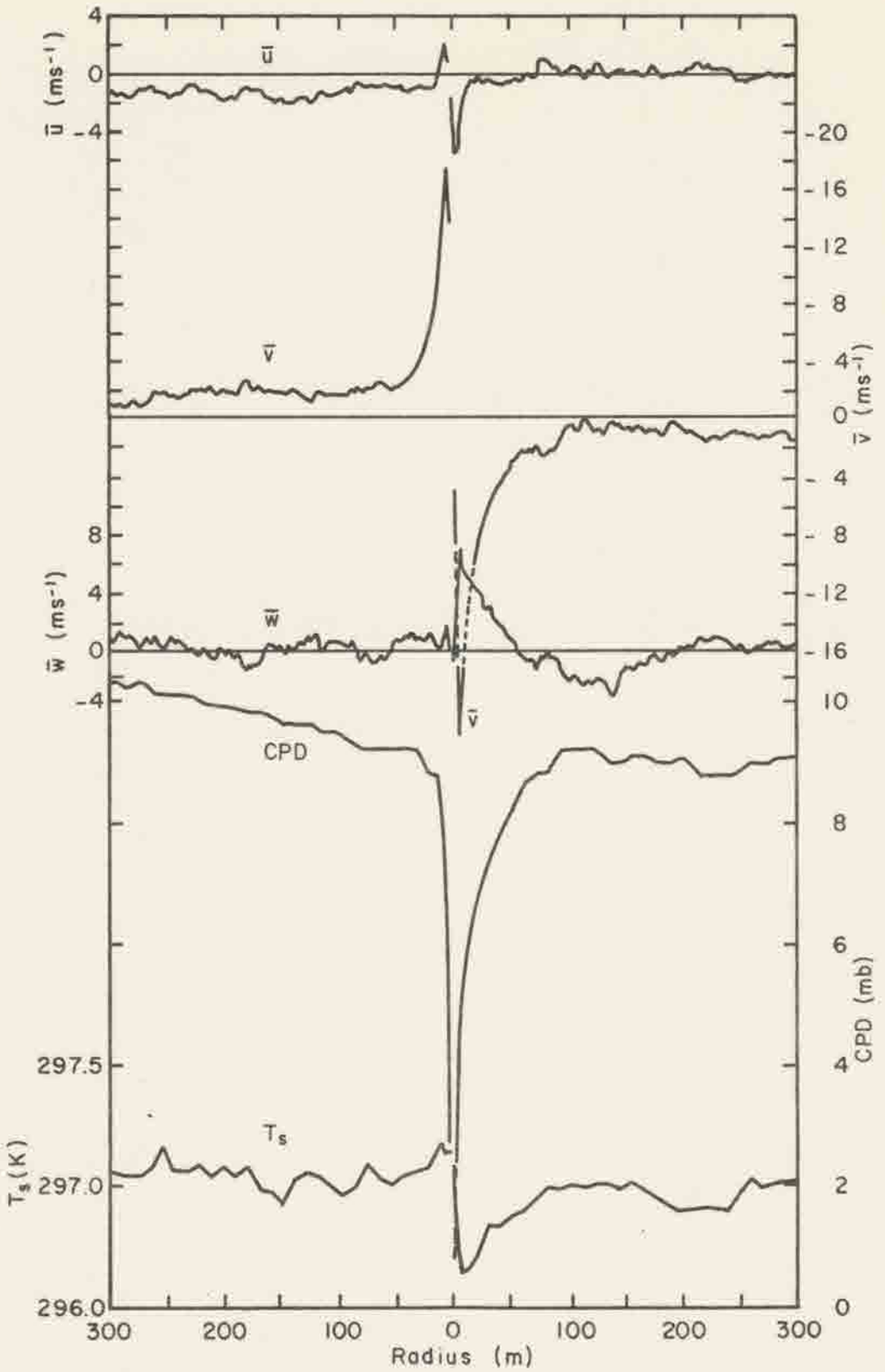

Fig. 26. As in Fig. 25 except for penetration 2. Penetration altitude was 643m; penetration heading was 160°.

Relative radial velocities are negative on the vortex's front side indicating inflow of ~ -1 to $-2ms^{-1}$. In the funnel itself, there is a small area of outflow at r(front) $\simeq$ 5-7m and strong inflow of $-5ms^{-1}$ at r(back) $\simeq$ 3-6m. Beyond r(back) $\simeq$ 75m, relative outflow exists.

Outside the waterspout, vertical velocities are on the order of $1ms^{-1}$. The maximum in-funnel measured vertical velocity is $\sim 7.3ms^{-1}$, and there is an indication of decreased upwards velocities near r = 0. Notice the asymmetry in the vertical velocity profile across the vortex. The highest values are located at back side radii, while only a maximum $1.7ms^{-1}$ was measured at r(front) $\simeq$ 5m.

b. Temperature and Pressure Profiles. The CPD measured during the penetration was -8.4 mb, the strongest waterspout pressure drop documented during the 1974 program. Since the AADS-2B essentially passed very close to the vortex center, the CPD is considered to reflect nearly the entire vortex pressure drop at the penetration altitude. Again, the back side decrease in $\partial p/\partial r$ compared to the front is probably due to the aircraft's vertical acceleration as it responds to the funnel vertical velocities. That is, at front side radii, the airplane has not yet responded to the upward velocities, and the CPD trace is undoubtedly more accurate than on the back. This characteristic response of the airplane has since been documented by aircrew observations and movies of funnel penetrations.

The temperature profile shows an increase of $\sim$ 0.2K at front side radii. However, a temperature drop of $\sim$ 0.6K is measured

immediately upon funnel penetration, and, as previously mentioned, may be due to partial wetting of the sensor by waterspout condensate.

4.4 Case III

The last waterspout to be discussed is another anticyclonically rotating vortex. The funnel was one of two that formed over Turkey Basin (north of Saddlebunch Keys) just prior to the Case II waterspout event; both funnels are shown in Figure 27. The data presented here was obtained from a penetration through the westerly most waterspout. The penetration was made within $\sim$ 1m of the visible funnel's center. Its tilt was calculated as $\sim 20^{o}$ towards a heading of $\sim 65^{o}$. Translational velocity was $\sim$ 3-4 ms^{-1} towards the west.

Profiles of winds, temperature, and pressure (Figure 28) are similar to the other penetration data. The penetration was chosen because of its distinct vertical velocity profile. A pronounced region of downward relative vertical velocity is seen to exist at the center of the vortex. Close examination of the original digital data revealed no spurious voltages at this point and reinforced the validity of the negative $\bar{w}$ values. The minimum value measured is $-\ 0.8ms^{-1}$, and the area of diminished vertical velocity has a diameter of $\sim$ 8m centered at r = 0. These measurements substantiate conclusively the occurrence of downward, sinking air motions at the center of the waterspout vortex in, at least, some situations. The suggestion that the downflow at the center of geophysical vortices may not exist at all times has been previously advanced, for example, by Morton (1966) and Dessens (1972). At any rate, post mortem comparisons of this waterspout funnel and all others encountered

Fig. 27. Photograph of the Case III waterspouts over Turkey Basin. Photo looks ENE. Left-most funnel cloud is the penetrated waterspout.

failed to reveal any major differences in physical appearances, circulation features, or life cycle evolution. Unfortunately, after this penetration the aircraft left the vicinity for another waterspout, and further information on the funnel's life cycle was never attained.

Tangential and radial velocities show the typical flow fields around and in the vortex. Again, the funnel is located at an apparent shear zone in the relative horizontal winds. The front side tangential velocity peak appears slightly eroded and of a broader, turbulent extent.

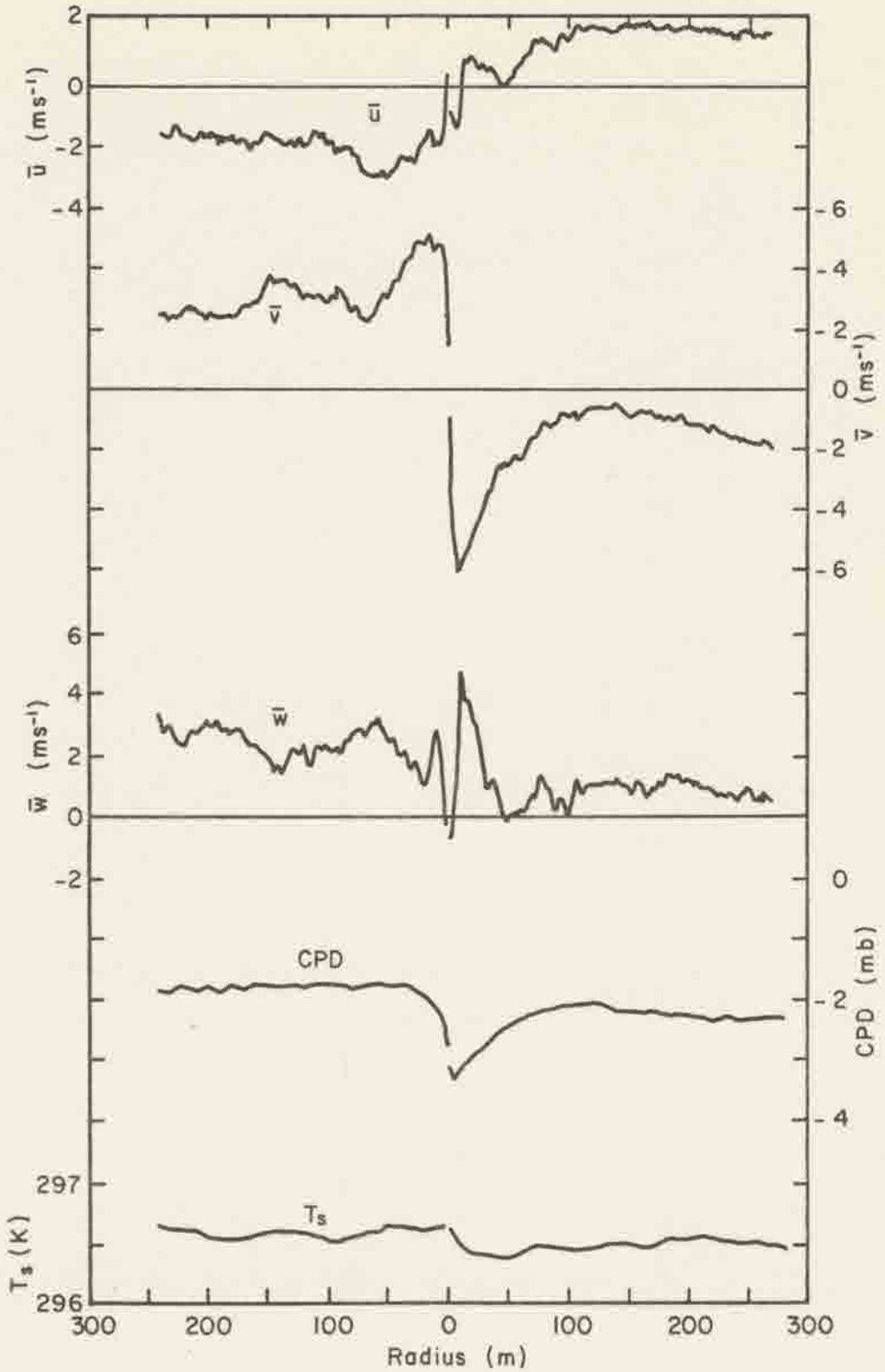

Fig. 28. Radial profiles of $\bar{u}$, $\bar{v}$, $\bar{w}$, CPD, and T_s for the Case III waterspout. Penetration altitude was 779m; penetration heading was 270°.

Radial velocities increase in inflow intensity around front side (upwind) radii of ∿ 50 to 60m. At back side radii the general relative radial flow is outward. This characteristic radial profile is seen in Case I data, and appears to be a result of the funnel translating at a slower rate than the environmental winds.

Temperature and pressure profiles are again similar to previous data. The maximum CPD in the vortex is measured as ∿ - 1.6 mb. As in previous CPD profiles, the front side of the curve is considered more accurate than the back due to the airplane's delayed response to the waterspout vertical motion field. The T_s profile shows a slight increase, then decrease, in values as the airplane passes through the visible funnel. The decrease is possibly because of partial wetting of the temperature sensor.

5. THE MATHEMATICAL MODEL

The first task in formulating a meaningful mathematical model of the waterspout is the choice of a suitable coordinate system in which to represent the waterspout's physical and kinematic properties in the simplest, most enlightening manner. As discussed in Section 4.1 and the Appendix, an appropriate coordinate system for a small scale, columnar vortex such as the waterspout is one that translates with the vortex over the earth's surface and whose vertical axis coincides with the funnel's axis of rotation. Such requirements suggest a cylindrical coordinate system (r, θ, z) arranged coaxially with the tilted, moving funnel. Therefore, the set of hydrodynamic equations that describe waterspout behavior must apply in the new coordinate system. The Appendix describes the transformation of the equation of motion from the standard meteorological rectangular cartesian system to the waterspout cylindrical system.

5.1 Governing Equations

Basic Set. In the new waterspout coordinate system the three scalar components of the vector equation of motion (momentum equation) take the form of equations (A-15) in the Appendix. The vector $\vec{V} = u\hat{r} + v\hat{\theta} + w\hat{k}$ is the velocity in the waterspout coordinate system, and u, v, w are radial, tangential (circumferential), and vertical waterspout velocities, respectively. The differential operations, ∇^2 and $\vec{\nabla} \cdot \vec{V}$, take the usual form in cylindrical coordinates. The effective gravity at sea level is $\vec{g}_e$, and the earth's angular rotation rate is $\vec{\omega}$. The variables p, ρ and μ are, respectively, the air pressure, density, and dynamic viscosity. Terms on the left of (A-15) represent inertial

forces, and on the right, pressure gradient, gravity, Coriolis, and molecular friction forces, respectively. All forces are represented as per unit mass.

Important assumptions leading to the derivation of (A-15) are:

1) the only external real forces acting on an air parcel are those of gravitational attraction, pressure gradients, and molecular friction;

2) the variable gravitational attraction is replaced by a constant value of $\vec{g}_e$ at sea level that includes the centrifugal force term $-\vec{\omega} \times \vec{\omega} \times \vec{R}$;

3) the curvature of the earth's surface is neglected;

4) waterspout translational velocities are assumed constant during each penetration;

5) the relationship between the dynamic viscosity μ and the coefficient of bulk viscosity λ is $\mu = -3/2\ (\lambda)$; and

6) the dynamic viscosity is assumed constant, i.e., does not vary with temperature and pressure.

Besides the equation of motion which expresses the basic physical law of conservation of momentum, the laws of conservation of mass and energy are necessary to describe a flow field as a function of time and space. An equation of continuity expresses the law of mass conservation, and the first law of thermodynamics expresses the principle of thermodynamic energy conservation. An equation of state for a particular fluid describes the relationship between the basic thermodynamic variables: pressure, temperature, and density.

In waterspout cylindrical coordinates the continuity equation takes the vector form

$$\frac{d\rho}{dt} + \rho \vec{\nabla} \cdot \vec{V} = 0 \tag{16}$$

and the scalar form

$$\frac{\partial \rho}{\partial t} + \frac{1}{r} \frac{\partial \rho u}{\partial r} + \frac{1}{r} \frac{\partial \rho v}{\partial \theta} + \frac{\partial \rho w}{\partial z} = 0. \tag{17}$$

The thermodynamic energy equation derives its form from the first law differentiated with respect to time

$$\frac{dT_s}{dt} = \frac{1}{\rho c_p}\frac{dp}{dt} + \frac{1}{c_p}\frac{dQ}{dt} \tag{18}$$

where T_s is an air parcel's temperature as measured by the AADS-2B, c_p is the specific heat of dry air at constant pressure, and dQ/dt represents diabatic processes, e.g., condensation, radiational cooling, etc. A form of (18) can be derived that accounts for important changes in an individual air parcel's temperature as it moves through the waterspout's temperature and pressure fields. Following Staley (1965) the vertical momentum equation, less molecular friction and Coriolis forces,

$$\frac{dw}{dt} = -\frac{1}{\rho}\frac{\partial p}{\partial z} - g_{e_z} \tag{19}$$

is combined with (18) and, after some rearrangement, produces

$$\frac{dT_s}{dt} = -\frac{g_{e_z} w}{c_p} + \frac{1}{\rho c_p}\left(\vec{\nabla}_{r,\theta} \cdot \vec{\nabla}_{r,\theta} p\right) - \frac{w}{c_p}\frac{dw}{dt} + \frac{1}{c_p}\frac{dQ}{dt} . \tag{20}$$

$\vec{V}_{r\theta}$ and $\vec{\nabla}_{r\theta}$ are the relative wind and <u>del</u> operator, respectively, in the $r\theta$ plane of the waterspout cylindrical coordinate system. The vertical component of the effective gravity (g_e) is g_{e_z}, where $g_{e_z} = g_e \cos\eta\cos\lambda \approx g_e \cos\gamma$. For simplicity air is assumed on ideal gas.

<u>Inclusion of Turbulence</u>. The flow field of the waterspout has often been regarded to be laminar in nature, at least in comparison with the usually stronger tornado. This concept has largely been based upon photographs and laboratory simulations of atmospheric vortices (Kessler, 1970; Morton, 1966). However, a realistic treatment of the waterspout will most likely require a consideration of turbulent processes. As a result, the equations of motion must be formulated to apply to turbulent flow.

The procedure suggested by Reynolds (1895) involves separating the instantaneous variables (velocity, pressure, density, and temperature) of a turbulent flow field into a mean value and a deviational value or fluctuation such that

$$\begin{aligned} \vec{V} &= \bar{\vec{V}} + \vec{V}' \\ p &= \bar{p} + p' \\ \rho &= \bar{\rho} + \rho' \\ T_s &= \bar{T}_s + T_s' \ . \end{aligned} \tag{21}$$

Bars denote averages, and primes indicate turbulent fluctuations from the mean. The mean of a variable (a) can be defined as a time or spatial average by

$$\bar{a} = \frac{1}{L} \int_{s-L}^{s+L} a \, ds \tag{22}$$

where L is the time/space averaging interval taken over s (time, linear, area, or volume dimensions). This averaging process must satisfy four postulates in order that Reynolds' method of modifying the momentum equations to turbulent flow be valid (Kampe de Feriet, 1951):

$$\begin{aligned} &\overline{a + b} = \bar{a} + \bar{b} \\ &\overline{ka} = k\bar{a}, \text{ where k is a constant} \\ &\overline{\bar{a}b} = \bar{a}\bar{b} \\ &\overline{\lim a_n} = \lim \bar{a}_n \\ \text{or} \quad &\overline{\frac{\partial a}{\partial s}} = \frac{\partial \bar{a}}{\partial s} \ . \end{aligned} \tag{23}$$

From (23) three additional postulates can be derived:

$$\bar{\bar{a}} = \bar{a}$$

$$\bar{a}' = 0 \qquad (24)$$

and $\overline{ab} = \bar{a}\bar{b} + \overline{a'b'}$.

Since the measurements in Chapter 4 show maximum deviations in density (ρ) due to non-turbulent processes (waterspout core pressure drop and temperature increase) to be only 0.1 to 1% of ambient, and Mach numbers (ratio of wind speed to speed of sound) of the vortex flow field to be much less than 1 ($\sim$ 0.05), density fluctuations (ρ') are considered negligible.

The equation of continuity is also employed in its imcompressible form $\vec{\nabla}\cdot\vec{V}=0$ in the Reynolds' derivation. By showing density deviations to be negligible, as above, the assumption of incompressibility has already been inferred. However, the entire equation of continuity should be analyzed term by term to assure the validity of assuming incompressible flow in the waterspout.

The equation of continuity for the moving waterspout coordinate system (16) can be written as

$$\frac{1}{\rho}\frac{\partial\rho}{\partial t} + \frac{1}{\rho}(\vec{V}\cdot\vec{\nabla}\rho) + \vec{\nabla}\cdot\vec{V} = 0 \ , \qquad (25)$$

where $\vec{V}$ is the vector air velocity relative to the moving system. Incompressibility implies $d\rho/dt=0$; however, if it can be shown that the sum of the magnitudes of ρ^{-1} $(\partial\rho/\partial t)$ and ρ^{-1} $(\vec{V}\cdot\vec{\nabla}\rho)$ is much less than the magnitude of the terms in $\vec{\nabla}\cdot\vec{V}$ during each individual penetration, then an approximate incompressible situation may be assumed for the duration of each penetration.

In the moving system partial time derivatives of density are due to waterspout intensity changes and advective changes from the

translational motion of the waterspout. Photographs of funnels show little, if any, visible change during separate penetrations. If visible changes are indications of waterspout intensity changes, then a quasi-steady situation may be assumed to exist during the duration of each penetration, i.e., on the order of 0.5 to 1 min. Sinclair (1973) made similar assumptions in treating the life cycle of desert dust devils as a series of quasi-steady state intervals. The second contribution to ρ^{-1} $(\partial\rho/\partial t)$ arising from the translation of the waterspout through the environment is assumed negligible since horizontal (with respect to the earth's surface) variations in the near-waterspout environmental density are essentially nonexistant. As a result, ρ^{-1} $(\partial\rho/\partial t)$ is approximately zero.

The second term in equation (25), $\rho^{-1}(\vec{V} \cdot \vec{\nabla}\rho)$ represents changes in an air parcel's density due to advection by the waterspout winds through the density field. Maximum values of $\vec{\nabla}\rho$ occur in the waterspout core due to pressure deficits and temperature changes. The magnitude of the advection term can be calculated from characteristic scales of waterspout velocity, length, and density such that ρ^{-1} $(\vec{V} \cdot \vec{\nabla}\rho) \sim \frac{V_o \nabla\rho}{\rho_o L} \simeq 10^{-2}\ s^{-1}$.

The individual terms in $\vec{\nabla} \cdot \vec{V}$ are on the order of $0.1 - 1.0\ s^{-1}$; hence in comparison with ρ^{-1} $(\partial\rho/\partial t)$ and ρ^{-1} $(\vec{V} \cdot \vec{\nabla}\rho)$, $\vec{\nabla} \cdot \vec{V}$ is one to two orders of magnitude larger than the remaining two terms in the continuity equation. As a result, the assumption of incompressible flow in the waterspout is accurate to at least an order of magnitude, and $\vec{\nabla} \cdot \vec{V} = 0$.

Reynolds' procedure for deriving the equations of turbulent motion calls for the substitution of equations (21) into equation

(A-15), remembering that $\rho' \simeq 0$. The postulates in equations (23) and (24), along with the imcompressible form of the continuity equation for the mean flow field, $\vec{\nabla} \cdot \vec{V}$, are utilized in the modification procedure which follows standard textbook examples, e.g., White, 1974 and Schlichting, 1968.

The final forms of the scalar components of the equation of turbulent motion are then written out in full as

$$\frac{\partial \bar{u}}{\partial t} + \bar{u}\frac{\partial \bar{u}}{\partial r} + \frac{\bar{v}}{r}\frac{\partial \bar{u}}{\partial \theta} + \bar{w}\frac{\partial \bar{u}}{\partial z} - \frac{\bar{v}^2}{r} = -\frac{1}{\bar{\rho}}\frac{\partial \bar{p}}{\partial r} - g_{e_r} + 2(\omega_z \bar{v} - \omega_\theta \bar{w})$$
$$+ \frac{\mu}{\bar{\rho}}\left[\frac{\partial^2 \bar{u}}{\partial r^2} + \frac{1}{r}\frac{\partial \bar{u}}{\partial r} + \frac{1}{r^2}\frac{\partial^2 \bar{u}}{\partial \theta^2} + \frac{\partial^2 \bar{u}}{\partial z^2} - \frac{\bar{u}}{r^2} - \frac{2}{r^2}\frac{\partial \bar{v}}{\partial \theta}\right] - \frac{1}{\bar{\rho}}\left[\frac{\partial \overline{\rho u'^2}}{\partial r}\right.$$
$$\left. + \frac{1}{r}\frac{\partial \overline{\rho u'v'}}{\partial \theta} + \frac{\partial \overline{\rho u'w'}}{\partial z} + \frac{\overline{\rho u'^2}}{r} - \frac{\overline{\rho v'^2}}{r}\right]$$

$$\frac{\partial \bar{v}}{\partial t} + \bar{u}\frac{\partial \bar{v}}{\partial r} + \frac{\bar{v}}{r}\frac{\partial \bar{v}}{\partial \theta} + \bar{w}\frac{\partial \bar{v}}{\partial z} + \frac{\overline{uv}}{r} = -\frac{1}{\bar{\rho} r}\frac{\partial \bar{p}}{\partial \theta} - g_{e_\theta} + 2(\omega_r \bar{w} - \omega_z \bar{u})$$
$$+ \frac{\mu}{\bar{\rho}}\left[\frac{\partial^2 \bar{v}}{\partial r^2} + \frac{1}{r}\frac{\partial \bar{v}}{\partial r} + \frac{1}{r^2}\frac{\partial^2 \bar{v}}{\partial \theta^2} + \frac{\partial^2 \bar{v}}{\partial z^2} - \frac{\bar{v}}{r^2} + \frac{2}{r^2}\frac{\partial \bar{u}}{\partial \theta}\right] - \frac{1}{\bar{\rho}}\left[\frac{\partial \overline{\rho u'v'}}{\partial r}\right. \qquad (26)$$
$$\left. + \frac{1}{r}\frac{\partial \overline{\rho v'^2}}{\partial \theta} + \frac{\partial \overline{\rho v'w'}}{\partial z} + \frac{2\overline{u'v'}}{r}\right]$$

$$\frac{\partial \bar{w}}{\partial t} + \bar{u}\frac{\partial \bar{w}}{\partial r} + \frac{\bar{v}}{r}\frac{\partial \bar{w}}{\partial \theta} + \bar{w}\frac{\partial \bar{w}}{\partial z} = -\frac{1}{\bar{\rho}}\frac{\partial \bar{p}}{\partial z} - g_{e_z} + 2(\omega_\theta \bar{u} - \omega_r \bar{v})$$
$$+ \frac{\mu}{\bar{\rho}}\left[\frac{\partial^2 \bar{w}}{\partial r^2} + \frac{1}{r}\frac{\partial \bar{w}}{\partial r} + \frac{1}{r^2}\frac{\partial^2 \bar{w}}{\partial \theta^2} + \frac{\partial^2 \bar{w}}{\partial z^2}\right] - \frac{1}{\bar{\rho}}\left[\frac{\partial \overline{\rho u'w'}}{\partial r} + \frac{1}{r}\frac{\partial \overline{\rho v'w'}}{\partial \theta}\right.$$
$$\left. + \frac{\partial \overline{\rho w'^2}}{\partial z} + \frac{\overline{\rho u'w'}}{r}\right] .$$

The additional terms in the right most set of brackets in equation (26) are the spatial derivatives of the well-known Reynolds' stresses. They involve the product of turbulent velocity fluctuations and represent spatial variations of momentum fluxes arising from the

turbulent flow field (Tennekes and Lumley, 1972). As Schlichting points out, the Reynolds' stresses can be described as an apparent viscosity of the mean flow that adds to the molecular viscosity to produce an increase in the total viscosity.

The final $\bar{u}$, $\bar{v}$, $\bar{w}$ profiles (Chapter 3) are considered representative of the waterspout's average three-dimensional wind field during each penetration. However, the data probably do not accurately depict, at least, the important scales of turbulent motion in the waterspout vortex. This is due to complicated interrelations of instrument response times, analog to digital data conversions, and short sampling times. As a result, it is necessary to replace the terms in equation (26) containing velocity fluctuations (primes) with terms containing mean velocity values (bars). One standard semi-empirical assumption first suggested by Boussinesq in 1877 (Schlichting, 1968) is the eddy-viscosity hypothesis. Following the law of viscosity for Newtonian fluids, the relationship between Reynolds' stresses and the mean velocity components is exemplified by

$$-\overline{\rho u'v'} = \bar{\rho}\, K_\theta \frac{\partial \bar{u}}{r\partial\theta} \tag{27}$$

where K_θ is the eddy viscosity that varies spatially (denoted by its subscript) according to the form of (27).

Using (27), equation (26) is rewritten in the form:

$$\frac{\partial \bar{u}}{\partial t} + \bar{u}\frac{\partial \bar{u}}{\partial r} + \frac{\bar{v}}{r}\frac{\partial \bar{u}}{\partial \theta} + \bar{w}\frac{\partial \bar{u}}{\partial z} - \frac{\bar{v}^2}{r} = -\frac{1}{\bar{\rho}}\frac{\partial \bar{p}}{\partial r} - g_{e_r} + 2(\omega_z \bar{v} - \omega_\theta \bar{w})$$

$$+ \frac{\mu}{\bar{\rho}}\left[\frac{\partial^2 \bar{u}}{\partial r^2} + \frac{1}{r}\frac{\partial \bar{u}}{\partial r} + \frac{1}{r^2}\frac{\partial^2 \bar{u}}{\partial \theta^2} + \frac{\partial^2 \bar{u}}{\partial z^2} - \frac{\bar{u}}{r^2} - \frac{2}{r^2}\frac{\partial \bar{v}}{\partial \theta}\right] + \frac{1}{\bar{\rho}}\left[\frac{\partial}{\partial r}\left(\bar{\rho}K_r \frac{\partial \bar{u}}{\partial r}\right)\right.$$

$$\left. + \frac{1}{r}\frac{\partial}{\partial \theta}\left(\frac{\bar{\rho}K_\theta}{r}\frac{\partial \bar{u}}{\partial \theta}\right) + \frac{\partial}{\partial z}\left(\bar{\rho}K_z \frac{\partial \bar{u}}{\partial z}\right) + \frac{\bar{\rho}K_r}{r}\frac{\partial \bar{u}}{\partial r} - \frac{\bar{\rho}K_\theta}{r^2}\frac{\partial \bar{v}}{\partial \theta}\right]$$

$$\frac{\partial \bar{v}}{\partial t} + \bar{u}\frac{\partial \bar{v}}{\partial r} + \frac{\bar{v}}{r}\frac{\partial \bar{v}}{\partial \theta} + \bar{w}\frac{\partial \bar{v}}{\partial z} + \frac{\overline{uv}}{r} = -\frac{1}{\bar{\rho} r}\frac{\partial \bar{p}}{\partial \theta} - g_{e_\theta} + 2(\omega_r \bar{w} - \omega_z \bar{u})$$
$$+ \frac{\mu}{\bar{\rho}}\left[\frac{\partial^2 \bar{v}}{\partial r^2} + \frac{1}{r}\frac{\partial \bar{v}}{\partial r} + \frac{1}{r^2}\frac{\partial^2 \bar{v}}{\partial \theta^2} + \frac{\partial^2 \bar{v}}{\partial z^2} - \frac{\bar{v}}{r^2} + \frac{2}{r^2}\frac{\partial \bar{u}}{\partial \theta}\right] + \frac{1}{\bar{\rho}}\left[\frac{\partial}{\partial r}\left(\bar{\rho} K_r \frac{\partial \bar{v}}{\partial r}\right)\right.$$
$$\left. + \frac{1}{r}\frac{\partial}{\partial \theta}\left(\frac{\bar{\rho} K_\theta}{r}\frac{\partial \bar{v}}{\partial \theta}\right) + \frac{\partial}{\partial z}\left(\bar{\rho} K_z \frac{\partial \bar{v}}{\partial z}\right) + \frac{2\bar{\rho} K_r}{r}\frac{\partial \bar{v}}{\partial r}\right] \qquad (28$$

$$\frac{\partial \bar{w}}{\partial t} + \bar{u}\frac{\partial \bar{w}}{\partial r} + \frac{\bar{v}}{r}\frac{\partial \bar{w}}{\partial \theta} + \bar{w}\frac{\partial \bar{w}}{\partial z} = -\frac{1}{\bar{\rho}}\frac{\partial \bar{p}}{\partial z} - g_{e_z} + 2(\omega_\theta \bar{u} - \omega_r \bar{v})$$
$$+ \frac{\mu}{\bar{\rho}}\left[\frac{\partial^2 \bar{w}}{\partial r^2} + \frac{1}{r}\frac{\partial \bar{w}}{\partial r} + \frac{1}{r^2}\frac{\partial^2 \bar{w}}{\partial \theta^2} + \frac{\partial^2 \bar{w}}{\partial z^2}\right] + \frac{1}{\bar{\rho}}\left[\frac{\partial}{\partial r}\left(\bar{\rho} K_r \frac{\partial \bar{w}}{\partial r}\right)\right.$$
$$\left. + \frac{1}{r}\frac{\partial}{\partial \theta}\left(\frac{\bar{\rho} K_\theta}{r}\frac{\partial \bar{w}}{\partial \theta}\right) + \frac{\partial}{\partial z}\left(\bar{\rho} K_z \frac{\partial \bar{w}}{\partial z}\right) + \frac{\bar{\rho} K_r}{r}\frac{\partial \bar{w}}{\partial r}\right] .$$

Equations (28) are the three momentum equations for turbulent, incompressible motion applicable to a tilted, cylindrical coordinate system moving with the waterspout over the earth's surface.

5.2 Simplified Governing Equations

Before an order of magnitude analysis is performed on the governing equations, a few simplifications can be made thus reducing the complexity of the equations.

Incompressibility and Negligible Density Variations. This has already been discussed in Section 5.1. The measurements of temperature and core pressure deficit indicate maximum variations of ρ to be approximately 0.1 to 1% of ambient values, and Mach numbers are calculated to much less than 1 ($\sim$ 0.05). The complete continuity equation (25) is analyzed to show that the terms in $\vec{\nabla} \cdot \vec{V}$ have magnitudes approximately one order larger than the magnitude of ρ^{-1} $(d\rho/dt)$.

Steady State Assumption. If local time derivatives $(\frac{\partial \bar{u}}{\partial t}, \frac{\partial \bar{v}}{\partial t}, \frac{\partial \bar{w}}{\partial t})$ in the moving system could be shown to be negligible, all data

collected during each penetration would be a function only of the spatial coordinates. That is, it would be allowable to assume that each penetration's measurements are obtained instantaneously, i.e., time is no longer a variable. Since the time interval represented by the penetration profiles ranges from five to about fifteen seconds, it is only necessary to invoke steady state conditions for that period.

Despite this seemingly simple task, the measurements provide no suitable manner of showing that sufficient steady state conditions exist, such that the magnitudes of the local time derivatives are negligible compared to the other terms in (28). Visual observations, however, indicate very little noticeable changes in the general features of the funnel. This is not to say smaller scale phonemena, such as turbulent eddies, are not apparent in and moving thru the vortex system. Nevertheless, time variations in the mean velocity components over a period of ten to twenty seconds are probably quite small.

Following Sinclair's (1966) method of analyzing the assumption for dust devils, an order of magnitude comparison of local time derivative terms with other inertial terms can be made. For example, on comparing $\partial\bar{u}/\partial t$ with $\bar{v}^2/r$, using characteristic values of velocity (V_o), radius (R), and time increment (Δt) for the moderate to strong waterspouts presented in this study, time variations in the radial velocity ($\Delta\bar{u}$) can be approximated. For characteristic velocity V_o = 15 ms^{-1}, radius R = 5 m, and Δt = 15 s, $\Delta\bar{u} \sim \frac{(15\ ms^{-1})^2(15\ s)}{5\ m} = 675\ ms^{-1}$ for both terms to have the same order of magnitude. Using characteristic values from a weaker waterspout of V_o = 5 ms^{-1} and R = 5 m, and considering the shortest reasonable characteristic time increment

Δt = 5 s, $\Delta\bar{u}$ must be approximately 25 ms^{-1} for both terms to balance order of magnitudes. Either value of $\Delta\bar{u}$ over the characteristic time interval is very large and in light of the waterspout measurements, appears highly improbable. As a result of the above calculations and visual observations, a steady state is assumed to exist during each penetration. This follows Sinclair's (1966) and Golden's (1974) assumptions of dust devil and waterspout life cycles, respectively, being approximated by a series of quasi-steady states.

Coriolis Acceleration. Values of $\vec{\omega}_r$, $\vec{\omega}_\theta$, and $\vec{\omega}_z$ are generally of the order 10^{-4} (Key West latitude equals 24.6°N). Multiplication by characteristic values of waterspout radial, tangential, and vertical winds places the magnitude of the Coriolis terms at 10^{-3}. This is easily two orders of magnitude less than other terms (e.g., $\bar{v}^2/r$) in the equations of motion, and to a good approximation, the effects of the earth's rotation on waterspout motion can be neglected.

Another method of considering the effects of the earth's rotation on rotating waterspout flow is through use of the Rossby number (Ro) which is a ratio of inertial to Coriolis forces such that Ro = $(V^2/L)/(2\Omega V) = V/2\Omega L$ (Morton, 1966). V and L are characteristic velocities and lengths or in a waterspout, characteristic tangential wind speeds and diameters. Ω is the rotation rate of the earth, 7.29×10^{-5} s^{-1}. Small Rossby numbers (0.1-1) occur for synoptic scale disturbances; large Rossby numbers (10^5) characterize small scale motion such as wing tip vortices. For typical waterspout motion, ranges of V and L can be taken as 10-20 ms^{-1} and 10-20 m, respectively. Ro is then approximately 10^3-10^4, which gives a good indication that background (Coriolis) rotation has little effect on waterspout flow.

It should not be assumed that Coriolis forces can likewise be neglected when considering the mesoscale forcing processes that produce a favorable environment for waterspout formation and sustenance.

Acceleration Due to Gravity. In a tilted waterspout, components of gravity in the radial and tangential directions arise. Even with only a tilt angle (γ) of 10°, g_{e_r} and g_{e_θ} in (28) can equal unity. However, assuming a hydrostatic balance in the waterspout environment, there will be an equal and opposite component of the vertical pressure gradient in the radial and tangential directions that will cancel the effects of g_{e_r} and g_{e_θ}. These pressure gradient components are included in the pressure terms ($\partial\bar{p}/\partial r$ and $r^{-1}(\partial\bar{p}/\partial\theta)$ in (28). In the waterspout core, hydrostatic equilibrium may not exist. For a 10% departure from hydrostatic balance in a funnel tilted 30°, the effects of tilt on the radial and tangential flow could approach ± 1 ms^{-2}. Unfortunately, the data presented here virtually preclude the possibility of determining hydrostatic balance within an error of 10%. In addition, only when a strongly tilted waterspout ($\tilde{>}30°$) combines with significant non-hydrostatic gradients would the effect on the radial/tangential motion be of concern. As a result, we neglect this effect and eliminate g_{e_r} and g_{e_θ} from (28). The (assumed) equal and opposite radial and tangential components of the vertical pressure gradient are likewise eliminated; however, for clarity and simplicity, the form of the pressure gradient terms in (28) are retained in their present form and are directly applicable to the AADS-2B pressure measurements.

Molecular Viscosity. The terms describing the affects of molecular friction on the total viscosity of the waterspout flow

field are assumed to be insignificant in comparison to the turbulence terms in (28). This is based on the coefficient of dynamic viscosity (μ) being several orders of magnitude less than the coefficients of eddy viscosity ($K_{r,\theta,z}$). Physically stated, turbulence provides almost the entire frictional forcing in atmospheric motions.

Eddy Viscosity. Due to the lack of information describing the functional forms of K_r, K_θ, and K_z in terms of the measurement data, a single constant coefficient of eddy viscosity (K) is assumed. This constant K is considered relevant for the characteristic waterspout flow near, but below, cloud base. It should be realized that assumptions of a constant eddy viscosity coefficient are somewhat unrealistic and that eddy viscosity is likely as three-dimensional as are velocity fields. However, for the purposes of an order of magnitude analysis, a constant K should suffice.

Based on the above six assumptions, (28) can be modified to a simpler form suitable for an extensive order of magnitude analysis based on the measurement data,

$$\bar{u}\frac{\partial\bar{u}}{\partial r}+\frac{\bar{v}}{r}\frac{\partial\bar{u}}{\partial\theta}+\bar{w}\frac{\partial\bar{u}}{\partial z}-\frac{\bar{v}^2}{r}=-\frac{1}{\bar{\rho}}\frac{\partial\bar{p}}{\partial r}+K\left[\frac{\partial^2\bar{u}}{\partial r^2}+\frac{1}{r^2}\frac{\partial^2\bar{u}}{\partial\theta^2}+\frac{\partial^2\bar{u}}{\partial z^2}+\frac{1}{r}\frac{\partial\bar{u}}{\partial r}-\frac{1}{r^2}\frac{\partial\bar{v}}{\partial\theta}\right] \tag{29}$$

$$\bar{u}\frac{\partial\bar{v}}{\partial r}+\frac{\bar{v}}{r}\frac{\partial\bar{v}}{\partial\theta}+\bar{w}\frac{\partial\bar{v}}{\partial z}+\frac{\overline{uv}}{r}=-\frac{1}{\bar{\rho}r}\frac{\partial\bar{p}}{\partial\theta}+K\left[\frac{\partial^2\bar{v}}{\partial r^2}+\frac{1}{r^2}\frac{\partial^2\bar{v}}{\partial\theta^2}+\frac{\partial^2\bar{v}}{\partial z^2}+\frac{2}{r}\frac{\partial\bar{v}}{\partial r}\right]$$

$$\bar{u}\frac{\partial\bar{w}}{\partial r}+\frac{\bar{v}}{r}\frac{\partial\bar{w}}{\partial\theta}+\bar{w}\frac{\partial\bar{w}}{\partial z}=-\frac{1}{\bar{\rho}}\frac{\partial\bar{p}}{\partial z}-g_{e_z}+K\left[\frac{\partial^2\bar{w}}{\partial z^2}+\frac{1}{r^2}\frac{\partial^2\bar{w}}{\partial\theta^2}+\frac{\partial^2\bar{w}}{\partial z^2}+\frac{1}{r}\frac{\partial\bar{w}}{\partial z}\right].$$

These three equations represent the final forms of the momentum equations in a tilted cylindrical coordinate system, and together with (20) and $\vec{\nabla} \cdot \vec{V} = 0$, form a complete set of governing equations for steady, incompressible, turbulent waterspout motion.

6. ORDER OF MAGNITUDE ANALYSES

Data from six of the seven penetrations presented in Chapter 4 were used in the order of magnitude analyses. Penetration 4 of Case I was discarded because of the lack of a visible condensation funnel and uncertainty in knowing where the aircraft pierced the vortex circulation. Most terms in equation (29) were calculated as a function of the radial and vertical coordinates for each of the six penetrations. Gross order of magnitude estimates of derivatives with respect to θ were attempted with little success. Radial variations of $\bar{u}$, $\bar{v}$, $\bar{w}$, $\bar{T}_s$, and $\bar{p}$ should be considered more accurate than vertical variations, since the measurements have the greatest spatial detail in the radial direction. Vertical variations can only be determined from successive funnel penetrations separated by relatively large altitude increments and long time intervals.

6.1 Derivative Computations

Radial Derivatives. Only wind, temperature, and pressure measurements extending to radii of 50 m from the waterspout center were utilized for the order of magnitude calculations. Generally, the important variations in the terms of (29) were found to occur at radii less than 20 m. Measured values of $\bar{u}$, $\bar{v}$, $\bar{w}$, $\bar{T}_s$. and $\bar{p}$ were plotted as a function of radius for each penetration. Curves were fit by hand to the plotted points, and new data sets were subsequently tabulated at radial intervals of one meter from the new profiles. As discussed in Chapter 4 the measurements, including temperature and pressure, are considered to typify mean waterspout values with the important turbulent fluctuations remaining unmeasured.

Radial derivatives were computed using a centered difference scheme such that

$$\left.\frac{\partial \bar{u}}{\partial r}\right|_{r=a} \simeq \frac{\bar{u}(a + \frac{x}{2}) - \bar{u}(a - \frac{x}{2})}{x} \tag{30}$$

where $x = 1$ m and $r \leq 49.5$ m. Since the measurements were obtained along the aircraft penetration track which was usually not along a constant radius vector hence through the waterspout center, care must be taken in interpreting the data. (See Section 4.1 and Fig. 14). For example, in using (30), $\bar{u}(a + x/2)$ may be that value of $\bar{u}$ at $r = 5$ m and $\theta = 47°$ (measured as in standard cylindrical coordinates), while $\bar{u}(a - x/2)$ might be the radial velocity at $r = 4$ m and $\theta = 63°$. If the waterspout was symmetric about $r = 0$, no errors would arise; however, the measurements in this paper have shown that pronounced asymmetries can and probably do exist in the mean flow fields. Nevertheless, the errors due to this problem are considered negligible for order of magnitude calculations and in light of other errors from the AADS-2B and data reduction procedure.

A second error arises due to horizontal penetrations of waterspouts with $\lambda \neq 0$. The aircraft enters and leaves the vortex at different altitudes (with respect to the waterspout vertical). For a funnel diameter of 30 m and $\lambda = 20°$, the change in altitude along the waterspout vertical amounts to approximately 10 m. While an appreciable amount, this difference is neglected in the present calculations since vertical wind shears over similar vertical increments are probably quite small near cloud base.

Second-order partial derivatives were also calculated using the centered differencing scheme (30). Values of $\bar{u}$, for example,

where replaced with values of $\partial\bar{u}/\partial r$ at one meter increments of radius.

Radial profiles of pressure and temperature were modified based on the following premises. Whether the Rosemount total temperature sensor element is dampened upon passage through a visible funnel or not remains essentially unknown. The characteristic drop in temperature immediately following some penetrations as shown in these data, suggests that this may be so. As a result, for the order of magnitude calculations, only the front (left) side profiles of T_s (Chapter 4) were used along with the assumption of axial symmetry. Similarly, pressure profiles on the back (right) side of the penetration may be partially affected by aircraft motions, i.e., rapid vertical accelerations. The fact that the aircraft "delays" its response to vortex winds until in the vicinity of the back side of the funnel has been seen in movie films and witnessed by crew members. As a result, only the front (left) side profiles of $\bar{p}$ were used along with the axisymmetric assumption.

Finally, to smooth the somewhat noisy pressure values for derivative calculations, a 5 m running mean was used with the last two pressure points nearest the vortex center retained as their original values. Values of the density (ρ) were assumed constant through the vortex since calculations of ρ in the funnel core deviate from ambient values only by approximately one percent. The constant value of density ($\bar{\rho}$) was calculated for each penetration from data obtained outside the waterspout.

Tangential Derivatives. An attempt was made to estimate derivatives with respect to θ. The technique compared values of

$\bar{u}$, $\bar{v}$, $\bar{w}$ at equal radii on the left and right sides of the funnel along the penetration track and related the differences to a mean asymmetry at that radius. This method proved unsound. The values of the derivatives increased unreasonably as the distance between data points on the left and right funnel sides decreased, i.e., converged on the pseudo-center. Actually, accurate computations of tangential derivatives from a single funnel pass are virtually impossible due to the very nature of the penetration. Because of this lack of accurate values of derivatives with respect to θ, the assumption of axial symmetry was made, i.e., all terms involving $r^{-1}\partial/\partial\theta$ are much smaller than the other terms in (29).

Vertical Derivatives. The difficulty in obtaining accurate vertical variations of wind, temperature, and pressure in the waterspout arises from the inability of an airplane or any *in situ* vehicle to probe the vortex vertical structure in a continuous, uninterrupted manner. One aircraft can successively penetrate the funnel at different altitudes, but each penetration is separated by a finite time interval that probably must invoke non-steady state considerations in the vortex's dynamics. In a way this problem is similar to that involved in computing tangential derivatives. At least two successive penetrations are necessary to calculate vertical derivatives.

Three attempts were made to compute vertical derivatives of waterspout wind, temperature, and pressure. Two involved successive penetrations (2) of the same funnel. The third used data from two penetrations separated by three unusable penetrations and a time interval of approximately 4.3 min. Derivatives were calculated from

$$\left.\frac{\partial \bar{u}}{\partial z}\right|_{\substack{z=h \\ r=a}} = \frac{\bar{u}_{z_u} - \bar{u}_{z_1}}{(z_u - z_1/\cos\gamma} \tag{31}$$

where $\bar{u}_{z_u}$ and $\bar{u}_{z_1}$ are radial velocities at equal radii (a) at the upper penetration altitude z_u and the lower penetration altitude z_1, respectively. The funnel tilt is given by γ. Values of $\bar{u}$ (or $\bar{v}$ or $\bar{w}$) are assumed to vary linearly between $\bar{u}_{z_u}$ and $\bar{u}_{z_1}$. In addition, $z = h = 0.5\,[(z_u - z_1)/\cos\gamma]$. Because only two penetrations were used to calculate first-order derivatives with respect to z, it was not possible to compute derivatives of order two. The assumption of axial symmetry has been made, since each penetration may pass on different sides of the funnel. Values of z for each penetration were calculated from static pressure measurements P_S and the pressure-height sounding from Key West for the particular day. As pointed out in Chapter 2, measurements of P_S may be in error by as much as $\sim$ 30 m. With most vertical distances separating the penetrations on the order of 30 to 70 m, errors in $z_u - z_1$ could possibly approach 100%. The mean density ($\bar{\rho}$) in the vertical pressure gradient term was determined from an average of the density at the two different penetration altitudes.

6.2 Results of the Order of Magnitude Computations

Case I. Wind, pressure, and temperature data for three Case I penetrations are shown in Figs. 29-31. As previously noted, all profiles are limited to radii of 50 m either side of the waterspout center but along the aircraft penetration track.

a. Radial Momentum Equation. Radial variations of the apparent important terms in the radial momentum equation are shown in Figs.

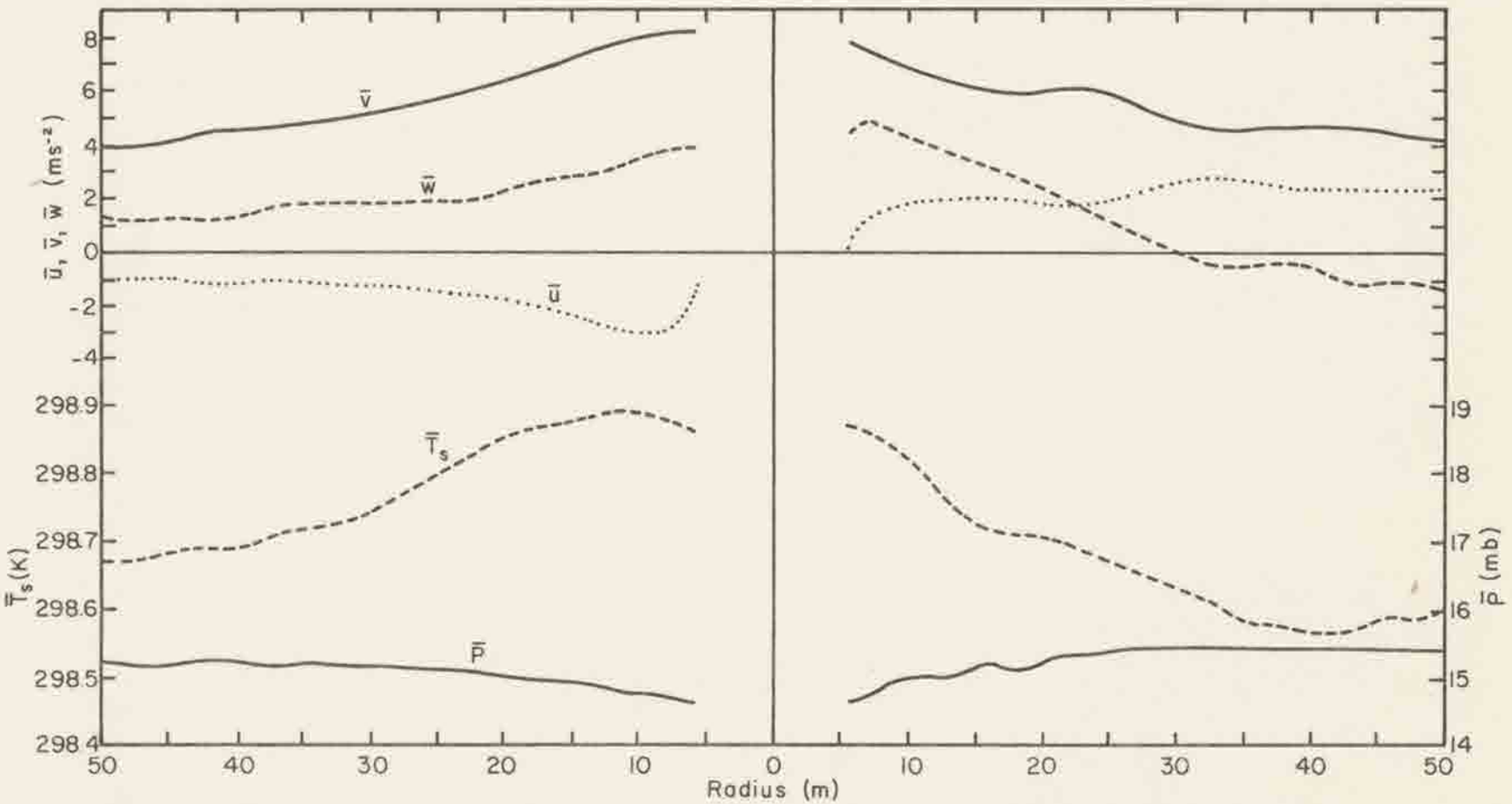

Fig. 29. Radial profiles of waterspout three-dimensional winds, pressure, and temperature for penetration 1 of Case I. The gap in the data near r = 0 is the result of an off-center funnel penetration. See Fig. 20 for profiles extending to radii of ~ 200 m.

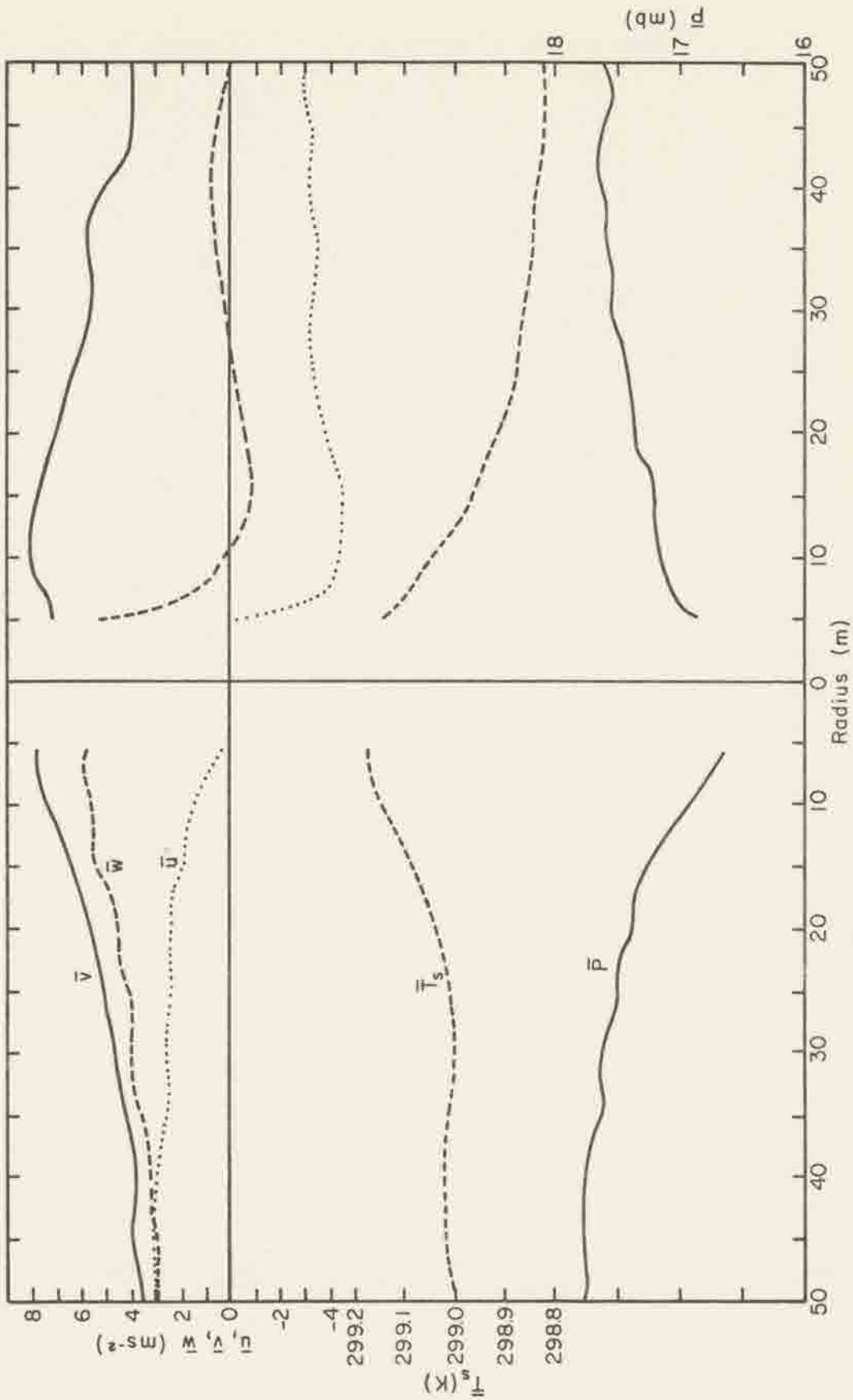

Fig. 30. As in Fig. 29 except for penetration 2 of Case I. See Fig. 21 for profiles extending to radii of ~ 300 m.

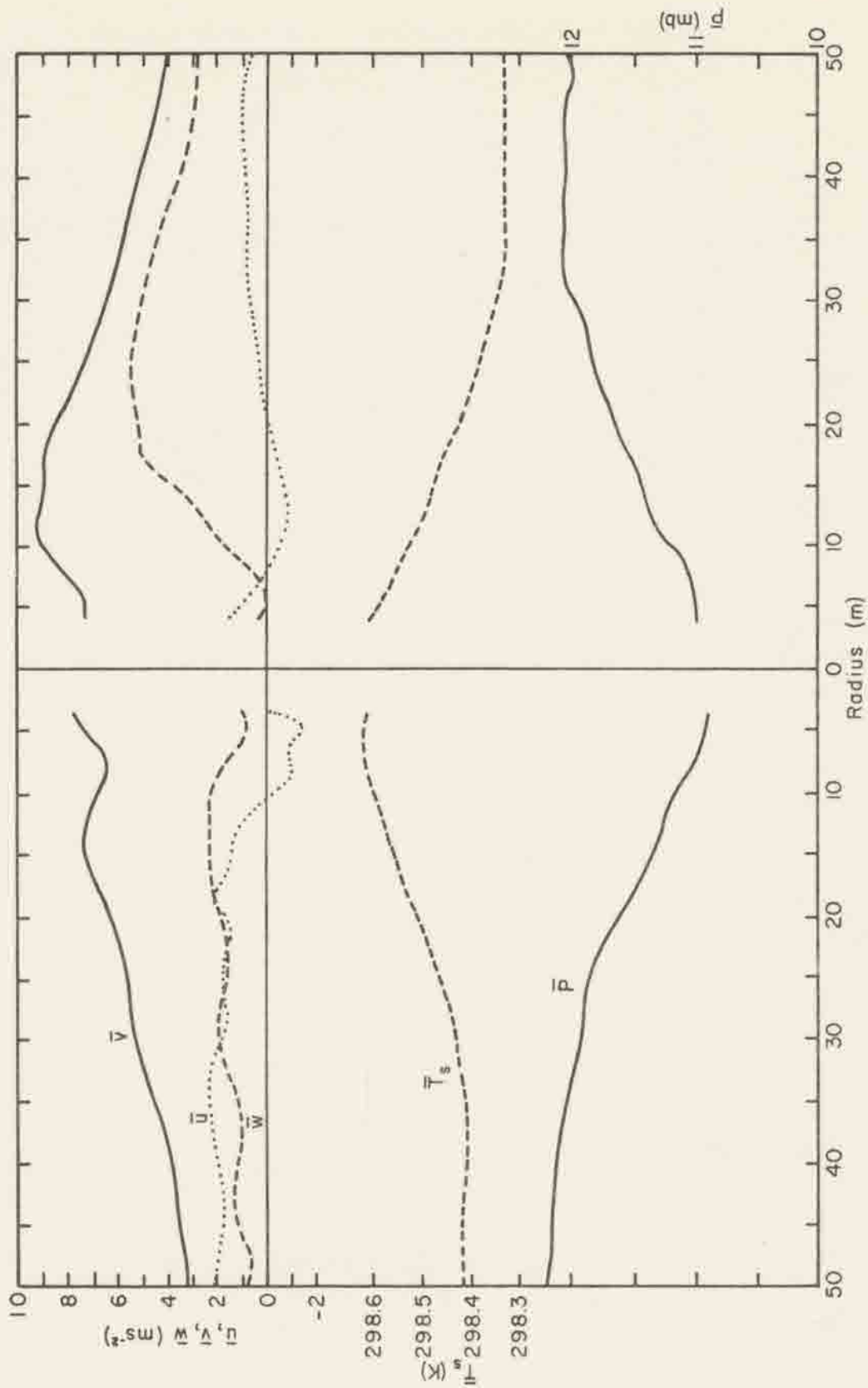

Fig. 31. As in Fig. 29 except for penetration 3 of Case I. See Fig. 22 for profiles extending to radii of ∿ 250 m.

32-34 for the three penetrations. The assumption that derivatives with respect to θ are everywhere negligible has been made. In fact, asymmetric motion almost certainly exists in the waterspout vortex as suggested by the measurement data. Whether the asymmetries are appreciable is difficult to ascertain from single penetration data.

In all three cases the important feature of the measurements is the domination of the equation by the centripetal acceleration ($\bar{v}^2/r$) and the pressure gradient ($\bar{\rho}^{-1}\partial\bar{p}/\partial r$) at radii generally less than 40 m. Only in penetration 3 does the inertial term representing the vertical advection of radial momentum ($\bar{w}\ \partial\bar{u}/\partial z$) reach comparable magnitudes. However, as pointed out in the previous section, vertical derivatives calculated from penetrations 2 and 3 are likely subject to large errors and unrepresentative values due to the long time lapse between penetrations ($\sim$ 4.3 min). Excluding $\bar{w}\ \partial\bar{u}/\partial z$ in penetration 3, the centripetal acceleration and pressure gradient terms are usually one, sometimes two, order(s) of magnitude larger than the remaining inertial terms. Thus the cyclostrophic relation ($\bar{v}^2/r = \bar{\rho}^{-1}\partial\bar{p}/\partial r$) may be used as a valid first approximation to the radial momentum equation for the waterspout vortex near cloud base.

A closer look at the profiles shows that at radii greater than about 10-15 m, the centripetal acceleration and pressure gradient are approximately equal. However, at smaller radii, the centripetal acceleration exceeds the pressure term by as much as $\sim$ 8.1 ms^{-2} (penetration 1). The difference is accentuated by apparent decreases in the pressure gradient in the last one to two meters near r = 0. This decrease is in part due to the retention of the last two values of the CPD when the profiles were smoothed by the 5 m running mean.

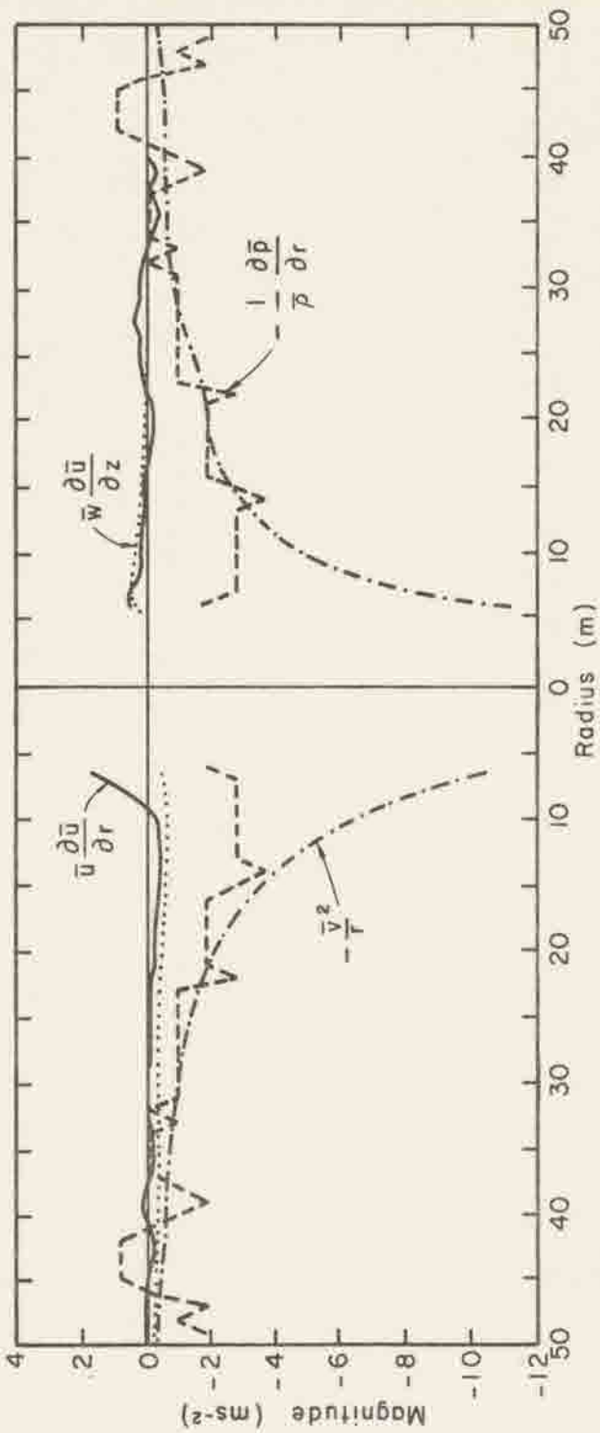

Fig. 32. Radial profiles of the magnitude of terms in the r momentum equation (see (29)) for penetration 1 of Case I.

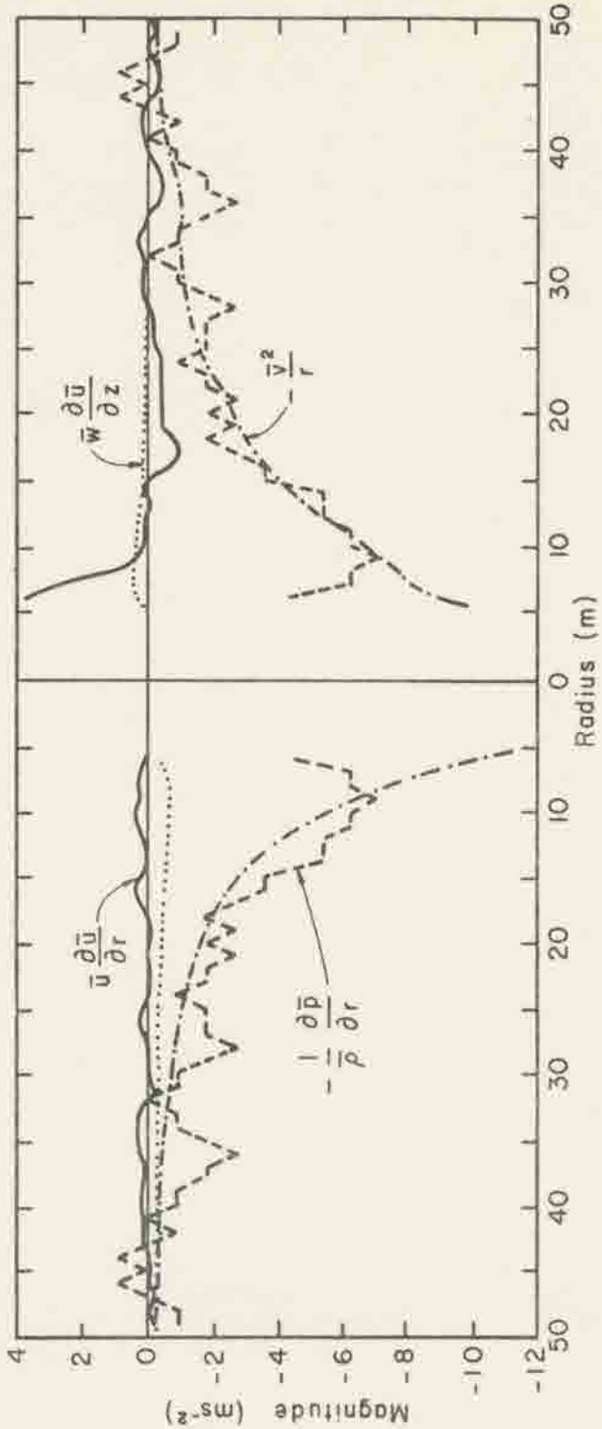

Fig. 33. As in Fig. 32 except for penetration 2 of Case I.

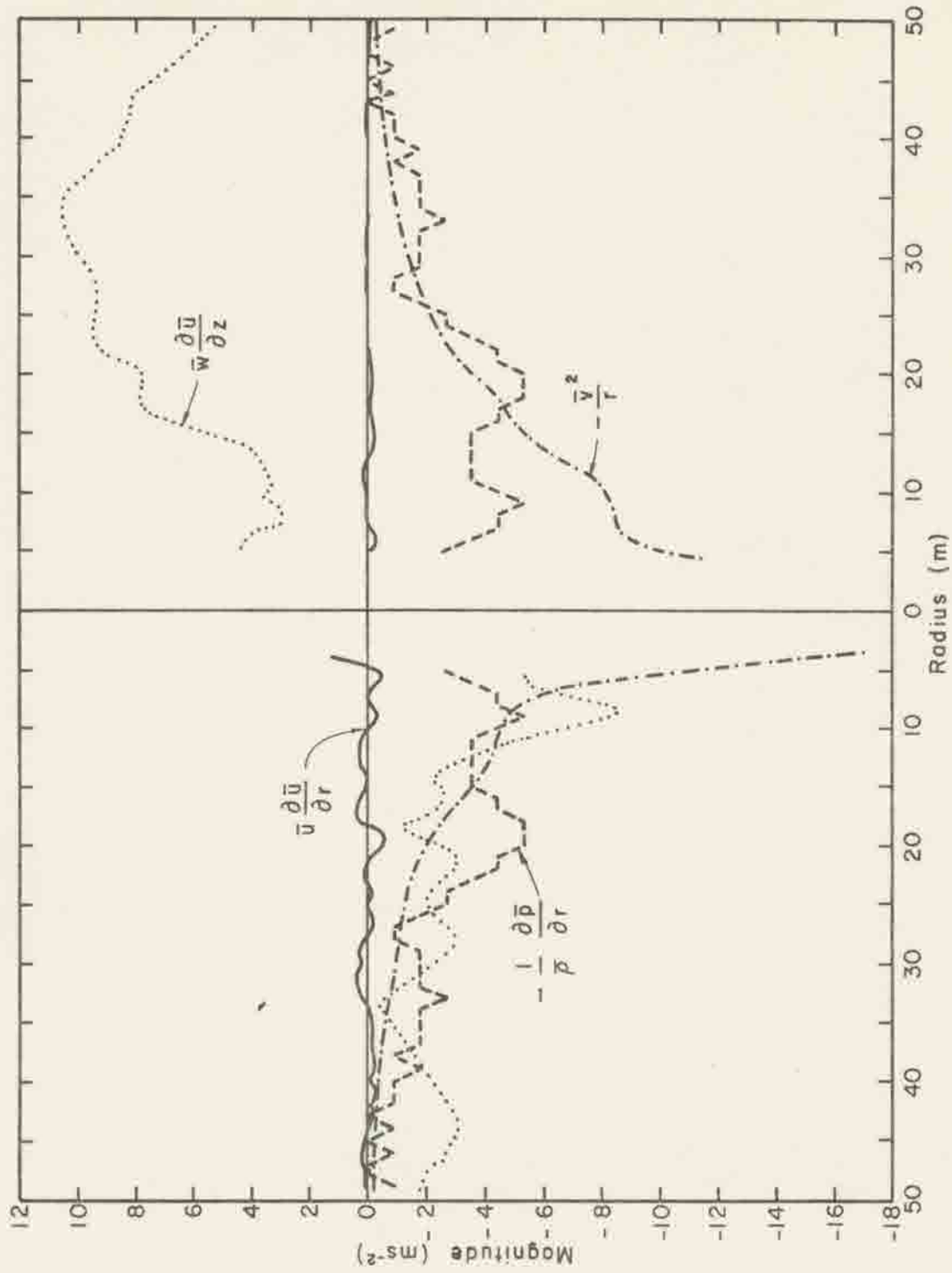

Fig. 34. As in Fig. 32 except for penetration 3 of Case I.

Despite this effect the general discrepancy suggests the existence of a radial outflow and a resulting divergence of angular momentum from the vortex core. Bellamy-Knight's (1970) similarity solutions for an unsteady two-cell vortex showed that a decrease in the radial inflow with time, hence a decrease in the convergence of angular momentum, allowed the outward viscous (turbulent) diffusion of vorticity (angular momentum) to gradually destroy the swirl of the vortex. While this process may have been occurring in the waterspout (funnel decay began thirty seconds after penetration 3), it is by no means obvious. Although relative radial outflow appears in parts of the vortex during each penetration, and there is slight evidence for an increase in the radius of maximum tangential velocities in penetration 3, no timewise reduction in the maximum tangential velocities occurs. What seems more likely, unfortunately, is the occurrence of errors in the pressure gradient due to errors in determining values of waterspout radii (r). In addition, as noted before, calculations of $\bar{u}$ at small radii can be subject to large errors.

The relative importance of several terms in the radial component of equation (29) is depicted in Table 5 for each penetration. Ratios of the radial advection of radial momentum ($\bar{u}\ \partial\bar{u}/\partial r$), the vertical advection of radial momentum ($\bar{w}\ \partial\bar{u}/\partial z$), and the centripetal acceleration ($\bar{v}^2/r$) to the radial pressure gradient are listed at various radii. The radial momentum transport term ratio is generally very small and fluctuates about zero. Only near the vortex core does it approach values as high as 79% of the pressure gradient. All values near the core (except the small values in penetration 3) are negative

Table 5. Ratio of terms in the radial momentum equation to the pressure gradient force for penetrations 1, 2, and 3 of Case 1.

r	Pressure Gradient Force $-\frac{1}{\bar{\rho}}\frac{\partial \bar{p}}{\partial r}$	Ratio of Term to Pressure Gradient Force (per Unit Mass) $\bar{u}\frac{\partial \bar{u}}{\partial r}$	$\bar{w}\frac{\partial \bar{u}}{\partial z}$*	$-\frac{\bar{v}^2}{r}$
(m)	($m\ s^{-2}$)			
		Case I, Pent 1		
40.5	-0.446	-0.07	0.58	1.12
25.5	-0.892	0.08	0.36	1.40
20.5	-1.785	0.10	0.22	1.09
15.5	-2.231	0.15	0.22	1.50
10.5	-2.677	0.11	0.21	2.22
9.5	-2.677	0.03	0.22	2.55
8.5	-2.677	-0.16	0.21	2.92
7.5	-2.677	-0.40	0.19	3.35
6.5	-2.231	-0.79	0.17	4.63
-	-	-	-	-
6.5	-2.231	-0.24	-0.19	3.98
7.5	-2.677	-0.13	-0.16	2.69
8.5	-2.677	-0.11	-0.16	2.28
9.5	-2.677	-0.08	-0.15	1.93
10.5	-2.677	-0.05	-0.14	1.64
15.5	-2.231	0	-0.10	1.08
20.5	-1.785	0.05	-0.07	1.00
25.5	-0.892	-0.23	-0.08	1.46
40.5	-0.446	0	-0.02	1.19
		Case I, Pent 2		
40.5	-0.445	-0.34	0.58	0.81
25.5	-1.779	-0.10	0.18	0.57
20.5	-2.224	-0.03	0.18	0.67
15.5	-3.557	-0.10	0.14	0.73
10.5	-6.226	-0.05	0.09	0.80
9.5	-6.671	-0.05	0.09	0.89
8.5	-6.671	-0.04	0.08	1.05
7.5	-6.226	-0.05	0.08	1.29
6.5	-5.337	-0.03	0.07	1.75
-	-	-	-	-
6.5	-5.337	-0.64	-0.08	1.58
7.5	-6.226	-0.34	-0.07	1.37
8.5	-6.671	-0.12	-0.06	1.12
9.5	-6.671	-0.05	-0.06	1.02
10.5	-6.226	-0.04	-0.06	1.02
15.5	-3.557	0.09	-0.06	1.08
20.5	-2.224	0.17	-0.06	1.10
25.5	-1.779	0.14	-0.04	0.88
40.5	-0.445	-0.18	-0.02	1.30
		Case I, Pent 3		
40.5	-0.894	0.16	2.56	0.40
25.5	-2.236	0.02	0.94	0.54
20.5	-4.918	0.06	0.58	0.38
15.5	-4.024	-0.05	0.65	0.84
10.5	-4.024	-0.01	1.55	1.11
9.5	-4.918	0.05	1.62	0.96
8.5	-4.918	0.03	1.75	1.01
7.5	-4.471	-0.01	1.63	1.26
6.5	-4.024	0.03	1.41	1.69
5.5	-3.130	0.10	1.74	2.93
-	-	-	-	-
5.5	-3.130	0.05	-1.37	3.01
6.5	-4.024	0.04	-0.97	2.15
7.5	-4.471	-0.00	-0.66	1.91
8.5	-4.918	-0.02	-0.61	1.71
9.5	-4.918	-0.02	-0.72	1.68
10.5	-4.024	-0.03	-0.83	1.98
15.5	-4.024	0.03	-1.54	1.28
20.5	-4.918	0.00	-1.61	0.68
25.5	-2.236	-0.01	-4.19	0.92
40.5	-0.894	-0.04	-9.41	0.70

* Likely subject to large errors in sign and magnitude

($\bar{u}\ \partial\bar{u}/\partial z$ positive) indicating opposition to the outward inertial forces of centripetal acceleration, i.e., increasing the radial momentum in the direction of the pressure gradient force. The ratio of $\bar{w}\ \partial\bar{u}/\partial z$ to the pressure gradient is consistent in opposite signs on either side of the vortex. Because each penetration was made through different quadrants and at various altitudes in the vortex, and therefore apparent inflow ($u < 0$) may be compared to apparent outflow ($u > 0$) in calculating $\partial\bar{u}/\partial z$, these values probably have consistent errors in both sign and magnitude. Finally, the ratio of centripetal acceleration to the pressure gradient shows how closely the two terms dominate the balance of forces in the radial direction. The closeness of fit of the two curves (Figs. 32-34) decreases with decreasing radius however, but their general shape is still in good agreement. Nothing has been said as yet of the turbulent transport terms. They will be covered in a following section that discusses calculations and concepts of the eddy viscosity (K).

b. Tangential Wind Profiles. The striking feature of the tangential wind velocities (Figs. 29-31) is the drastic departure from the irrotational potential vortex flow where vr = const. This type of flow regime is often used to approximate vortex flow outside of the radius of maximum tangential winds. For example the Rankine model (Leverson, et al., 1977) describes a tangential flow field by solid body rotation, $vr^{-1} = c_1$, in the vortex core (i.e., inside the radius of maximum winds) and potential flow outside the radius of maximum winds. The shape of the measured tangential winds in all three penetrations indicates that relative angular momentum is not being strictly conserved (vr = const) in this portion of the

waterspout, but that it increases with radius. As Davies-Jones (1976) and Scorer (1958) point out, a fluid parcel displaced outwards in a cyclostrophic tangential flow field where the angular momentum increases with radius will experience a restoring force to its original position by the pressure gradient force. Such a vortex is stable to radial oscillations. However, in this case, waterspout radial pressure gradients do not balance centripetal accelerations, and an outwardly displaced parcel would continue to move towards greater radii. This is manifest by apparent areas of relative outflow.

The sharp discontinuous maxima in the tangential wind profiles often seen in theoretical inviscid flow models of concentrated vortices are not apparent in Figs. 29-31. This point in the profile, where the maximum tangential winds are found, is the boundary between the inner solid rotating core and the irrotational outer shell. Erosive characteristics similar to those seen in Figs. 29-31 were found by Sinclair (1973b) in measurements of dust devil winds. He pointed out that turbulent mixing in the core-shell region acts to erode the extrema in the $\bar{v}$ profiles.

c. Tangential Momentum Equation. Radial variations of the inertial terms in the angular ($\hat{\theta}$) momentum equation are shown in Fig. 35 for the three Case I penetrations. The assumption is made that all derivatives with respect to θ in equations (29) are negligible. The dominant term is the "Coriolis" term ($\overline{uv}/r$), which arises automatically in the transformation to cylindrical coordinates. It is a force directed in the θ direction when there is both radial and tangential flow. Positive values of $\overline{uv}/r$ indicate an opposition (sustenance) to cyclonic (anticyclonic) flow.

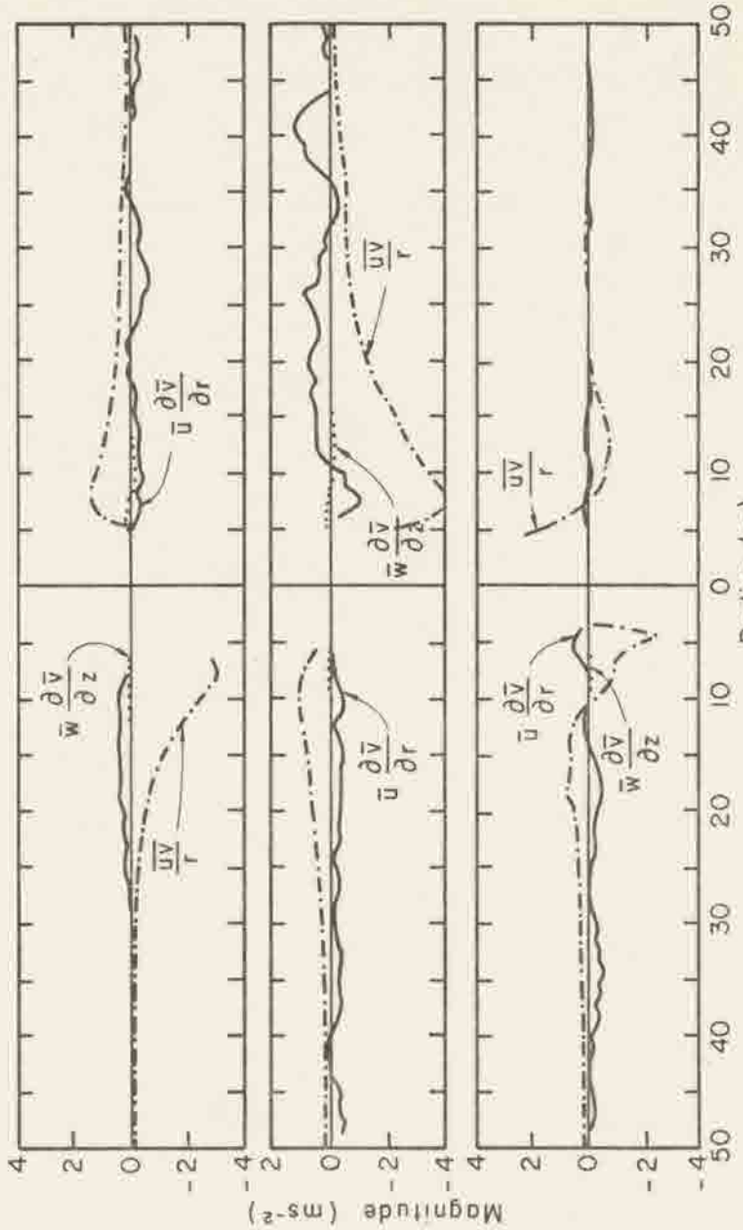

Fig. 35. Radial profiles of the magnitude of the inertial terms in the θ momentum equation (see (29)) for penetrations 1 (top), 2 (center), 3 (bottom) of Case I.

Because of the characteristic profile of $\bar{v}(r)$ such that usually $\partial\bar{v}/\partial r < 0$ for cyclonic flow outside the radius of maximum winds, the angular momentum transport term in the radial direction ($\bar{u}\ \partial\bar{v}/\partial r$) will be opposite in sign to $\overline{uv}/r$. In other words, when the "Coriolis" term is positive or opposing the cyclonic swirl, $\bar{u}\ \partial\bar{v}/\partial r$ will be negative or assisting in increasing the positive angular momentum at some outer radius. In Fig. 35 values of $\bar{u}\ \partial\bar{v}/\partial r$ are approximately $\pm$ 0.2 to $\pm$ 0.6 ms^{-2} at large radii but increase to as much a -1.1 ms^{-2} at small radii (penetration 2). Values of $\overline{uv}/r$ near the core reach -4.0 ms^{-2} (penetration 2).

The magnitude of the vertical advection term ($\bar{w}\ \partial\bar{v}/\partial z$) is of the order 0.05 ms^{-2} but can reach values of 0.1 ms^{-2} near the vortex core. No preference for sign accompanies these small values. An approximate value for $\partial\bar{v}/\partial\bar{z}$ in all three penetrations is approximately 0.02 ms^{-2}. Therefore, the data suggests vertical variations of the tangential velocity are very small at this level in the waterspout. However, caution should be used in interpreting this result in light of the large vertical increments (Δz) used in calculating $\partial/\partial z$. Typical values of Δz are 30 to 70 m.

d. Vertical Momentum Equation. Finally, a rough comparison of important terms in the vertical momentum equation are shown in Fig. 36 for the three penetrations. It should be recalled that "vertical" pertains to the waterspout vertical axis, in this case tilted $\sim$ 15° from the local vertical. Because of the requirement of at least two penetrations to calculate vertical derivatives, values for $\partial/\partial z$ actually apply at a distance midway between penetration altitudes. However, it is assumed that they also apply at both

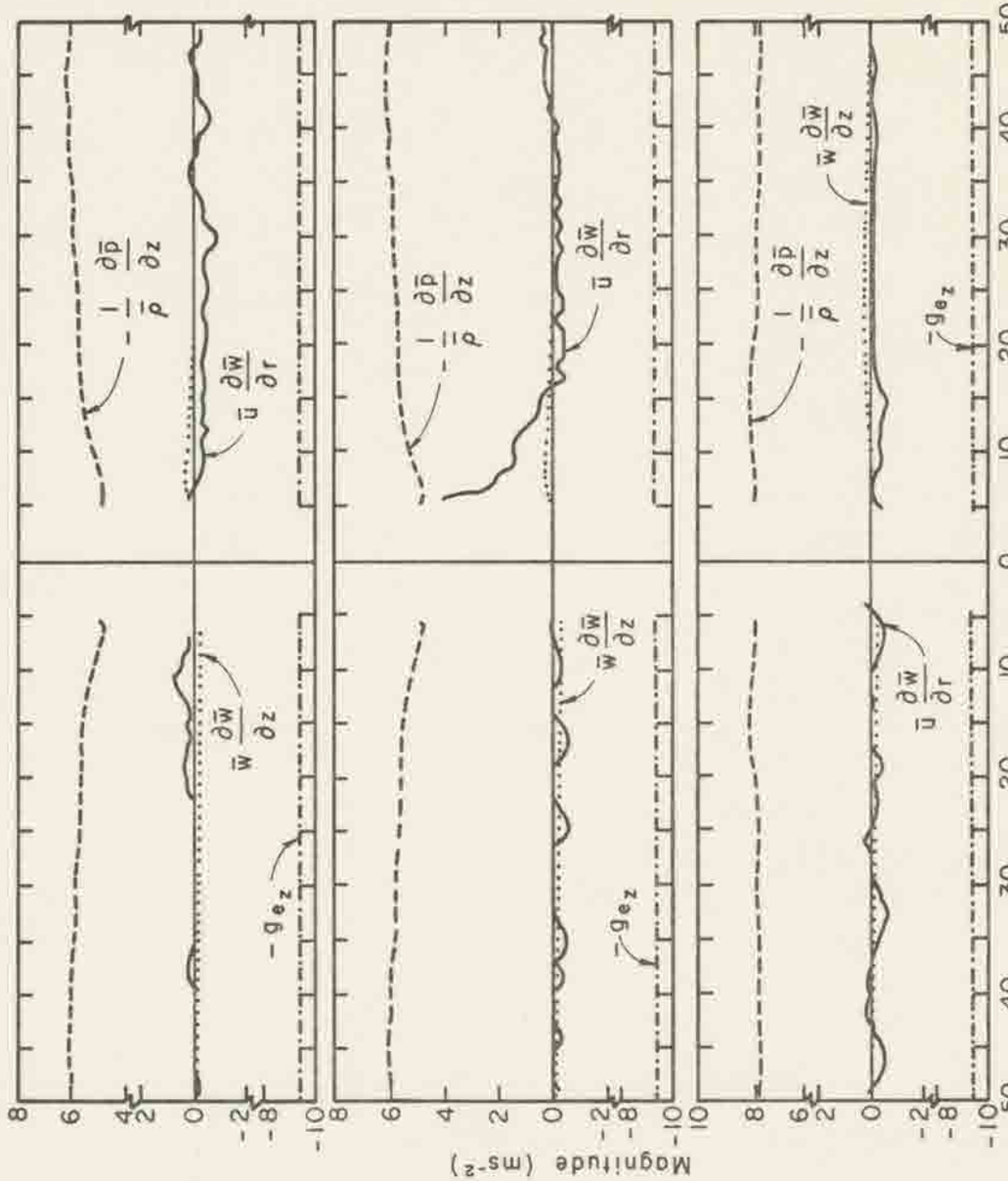

Fig. 36. Radial profiles of the magnitude of terms in the z momentum equation (see (29)) for penetration 1 (top), 2 (center), and 3 (bottom) of Case I.

penetration altitudes, and, as a result, profiles of the tilted vertical pressure gradient ($\bar{\rho}^{-1}\partial\bar{p}/\partial z$) and the vertical advection of vertical momentum are identical for penetrations 1 and 2. In addition, values of $\partial\bar{p} \simeq \Delta\bar{p}$ are calculated from the fine static pressure (P_F), and as pointed out in Chapter 2 should contain errors of no more than $\simeq$ 0.1 mb. The vertical increment (Δz) could contain large errors approaching 100% as noted in Section 6.1 of this chapter. Furthermore, errors in measuring the waterspout tilt (γ) by 10° could produce errors in g_{e_z} of 6-7%.

Remembering these potential errors, the pressure gradient approximately balances the gravitational acceleration in the three penetrations (only two actual profiles of $\bar{\rho}^{-1}\partial\bar{p}/\partial z$). The value of $-g_{e_z}$ is -9.46 ms^{-2} while the pressure gradient is approximately 5-6 ms^{-2} in the first two penetrations and about 8 ms^{-2} calculated from penetrations 2 and 3. The shape of the pressure gradient curve in penetrations 1 and 2 suggests the possibility of a lessening of the gradient near the tilted vortex axis. Despite the fact that the tilt of the vortex would reduce the pressure change per unit length along the vortex axis compared to a hydrostatic atmosphere, such a strong reduction as shown in Fig. 36 must be described by other explanations. The most likely is measurement errors.

Despite large errors, both $\bar{\rho}^{-1}\partial\bar{p}/\partial z$ and g_{e_z} exceed the inertial terms, $\bar{u}\,\partial\bar{w}/\partial r$ and $\bar{w}\,\partial\bar{w}/\partial z$, by an order of magnitude at most radii. Only in penetration 2 does the term for the radial advection of vertical momentum ($\bar{u}\,\partial\bar{w}/\partial r$) attain comparable values (approximately 4.0 ms^{-2} at a radius of 6 m). Its role at that point is the reduction of upward vertical momentum by the inward advection of air

parcels with lower vertical velocities. It acts in combination with gravity to oppose the upward vertical pressure gradient. Finally, $\bar{w}\,\partial\bar{w}/\partial z$ is of the order $\pm$ 0.2 ms^{-2}, with typical values of the vertical variation of $\bar{w}$ of about $\pm$ 0.06 ms^{-2} both near and far from the waterspout core. It cannot be said with conclusive evidence that $\bar{w}$ either increases or decreases with height in this waterspout, only that it appears to change very little over vertical distances of tens of meters.

Case II. Measurements of $\bar{u}$, $\bar{v}$, $\bar{w}$, $\bar{T}_s$, and $\bar{p}$ indicate the Case II waterspout was in general more intense than either Case I or Case III (also see Chapter 4). Profiles of wind, temperature, and pressure for penetrations 1 and 2 (Case II) are shown in Figs. 37 and 38. Negative values of $\bar{v}$ indicate anticyclonic rotation.

a. Radial Momentum Equation. Radial profiles of the inertial, centripetal acceleration, and pressure gradient terms are depicted in Figs. 39 and 40. As in previous penetrations the centripetal acceleration and pressure gradient terms dominate the radial equation; however, the discrepancy between the two terms is generally less in Case I. In penetration 1 the pressure gradient term is slightly larger than the centripetal acceleration, reaching a maximum of -39 ms^{-2} at 4 = 5.5 m. In penetration 2 the pressure gradient exceeds the centripetal acceleration on the left side of the funnel, but is equalled and exceeded by the centripetal acceleration between 2.5 m $\leq r \leq$ 5 m on the right side. At radii less than (right) = 3.5 m, $-\bar{v}^2/r$ decreases negatively rapidly as expected in the vortex core. Of course, both $\bar{v}^2/r$ and $\bar{\rho}^{-1}\partial\bar{p}/\partial r$ should go to zero at r = 0. The maximum values of $-\bar{v}^2/r$ and $-\bar{\rho}^{-1}\partial\bar{p}/\partial r$ in Case II penetration 2

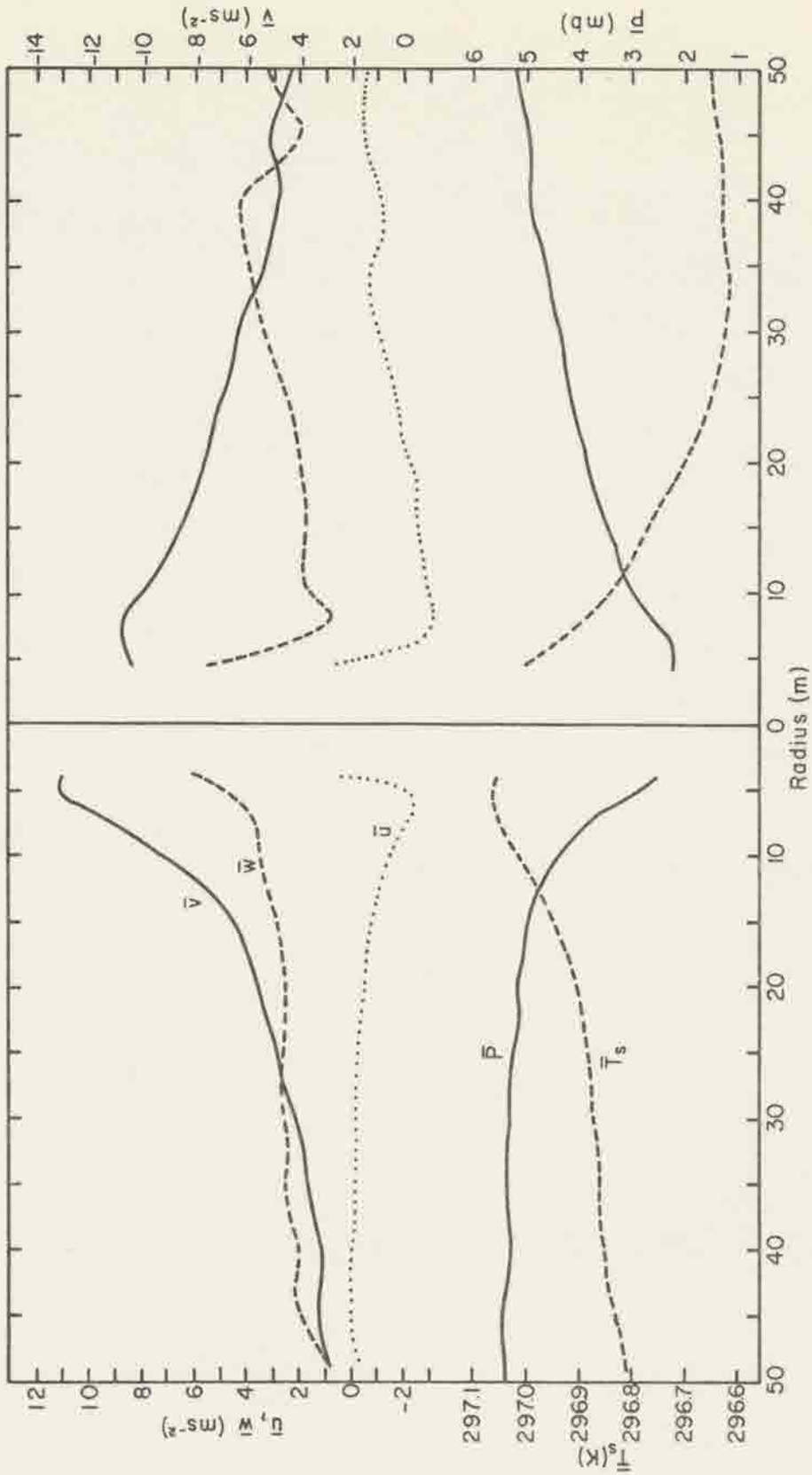

Fig. 37. As in Fig. 29 except for penetration 1 of the anticyclonic Case II waterspout. See Fig. 25 for profiles extending to radii of ~ 150 m.

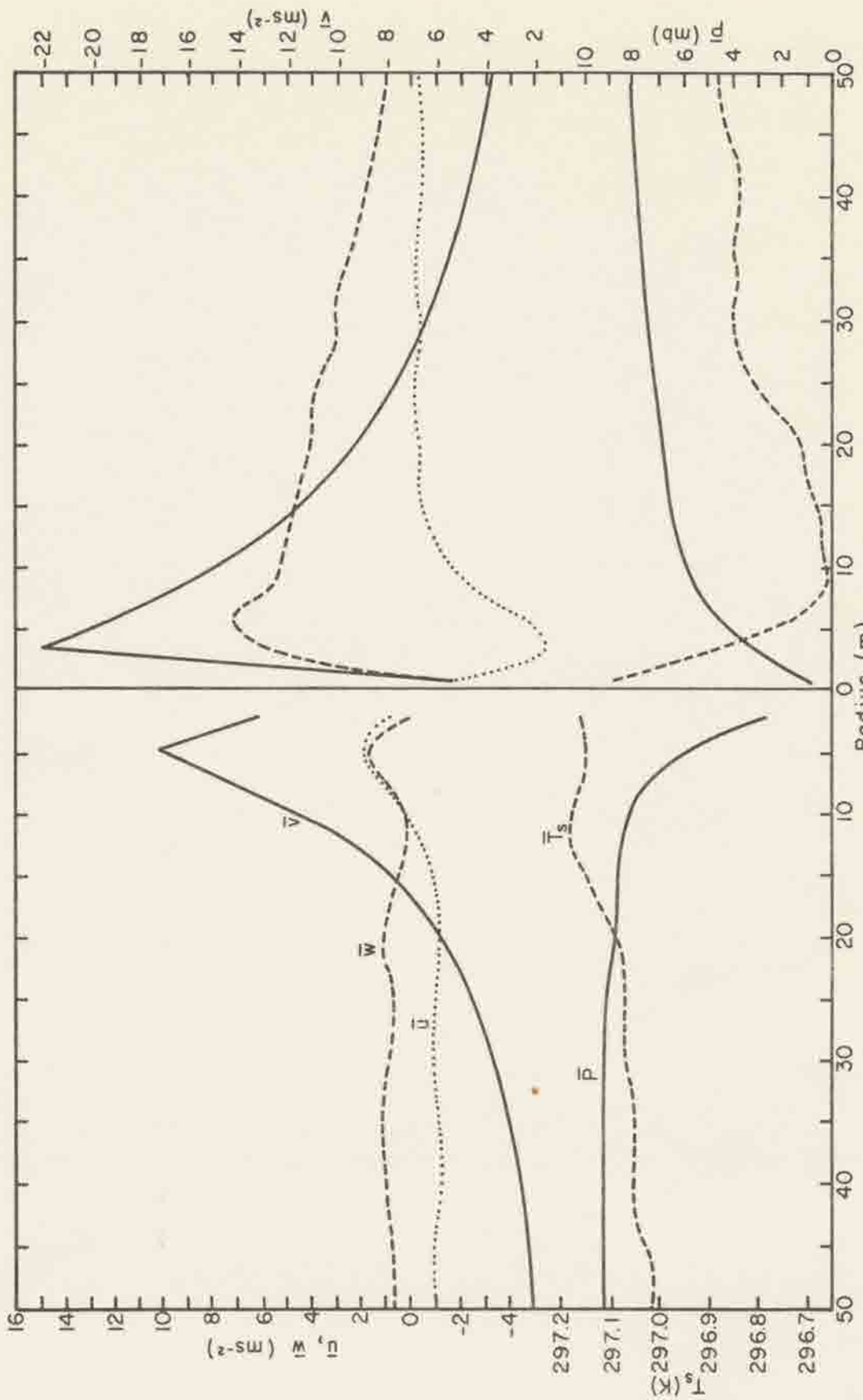

Fig. 38. As in Fig. 29 except for penetration 2 of the anticyclonic Case II waterspout. See Fig. 26 for profiles extending to radii of ∿ 300 m.

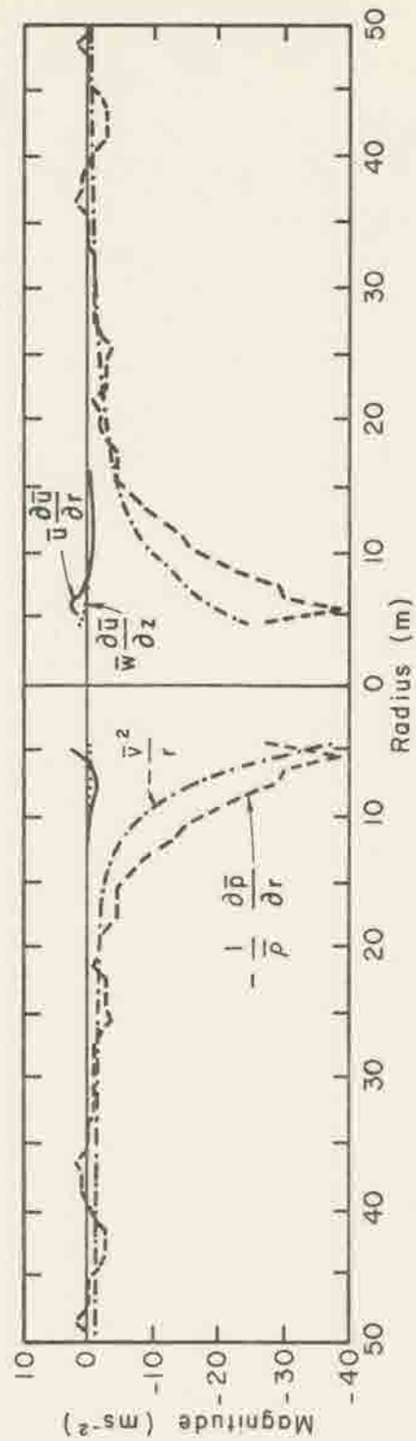

Fig. 39. As in Fig. 32 except for penetration 1 of the anticyclonic Case II waterspout.

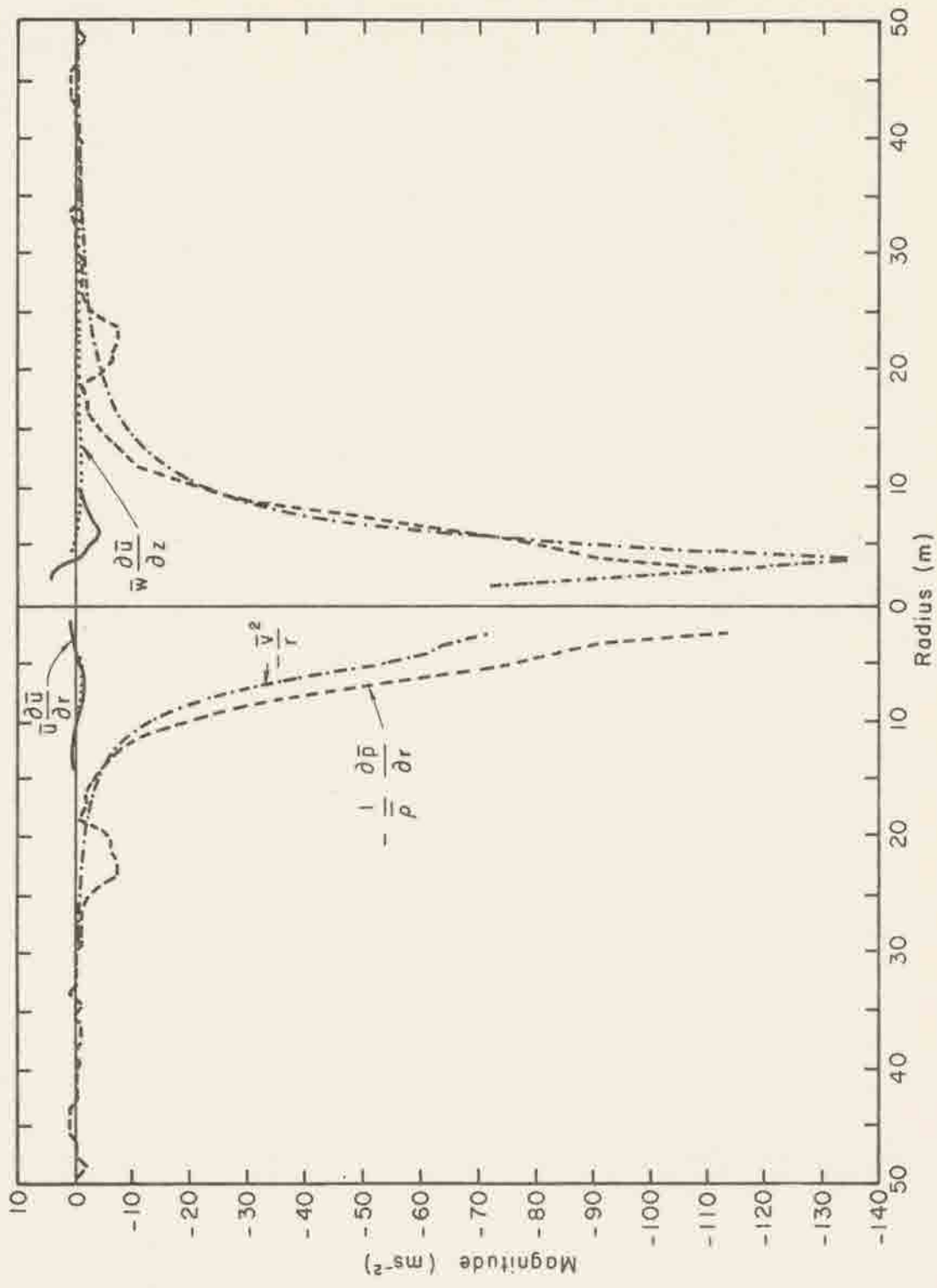

Fig. 40. As in Fig. 32 except for penetration 2 of the anticyclonic Case II waterspout.

are the largest calculated from the field measurements, $-137\ ms^{-2}$ and $-113\ ms^{-2}$, respectively.

The radial inertial terms remain relatively small in both penetrations 1 and 2. Only at radii generally less than six to seven meters in penetration 1 and three to four meters in penetration 2 does $\bar{u}\ \partial\bar{u}/\partial r$ exceed $+ 1.0\ ms^{-2}$. At these small radii $\bar{u}\ \partial\bar{u}/\partial r$ acts with the radial pressure gradient to advect radial momentum inward. The vertical transport of $\bar{u}$ momentum ($\bar{w}\ \partial\bar{u}/\partial z$) remains very small, as in previous penetrations. However, as pointed out before, vertical derivatives could be unrepresentative of actual changes with altitude.

The ratios of the two inertial terms and the centripetal acceleration to the radial pressure gradient are shown in Table 6. Comparison with Table 5 for the weaker cyclonic waterspout substantiates even more the use of the cyclostrophic relation ($\bar{v}^2/r = \bar{\rho}^{-1}\partial\bar{p}/\partial r$) as a valid first approximation for the horizontal flow field in a waterspout vortex, at least above the surface boundary layer.

b. Tangential Wind Profiles. The shape of the tangential wind profile in penetration 1 departs from the pure potential vortex similar to Case I penetrations. The departure is one such that relative angular momentum increases with radius outside the radius of maximum $\bar{v}$. The $\bar{v}$ profile at the right (back) side shows an approximate linear decrease with radius rather than an exponential change typical of the potential vortex.

In contrast to all previous penetrations, penetration 2 (Fig. 38) exhibits a tangential wind field closely resembling the Rankine vortex. It is interesting to note that the largest values of tangential

Table 6. Ratio of terms in the radial momentum equation to the pressure gradient force for penetrations 1 and 2 of Case II.

r (m)	Pressure Gradient Force $-\frac{1}{\bar{\rho}}\frac{\partial \bar{p}}{\partial r}$ ($m\ s^{-2}$)	Ratio of Term to Pressure Gradient Force (per Unit Mass) $\bar{u}\frac{\partial \bar{u}}{\partial r}$	$\bar{w}\frac{\partial \bar{u}}{\partial z}$*	$-\frac{\bar{v}^2}{r}$
		Case II, Pent 1		
40.5	-0.908	0.002	-0.08	0.25
25.5	-3.633	0.01	-0.01	0.24
20.5	-1.817	0.01	-0.03	0.82
15.5	-4.542	0.02	-0.004	0.57
10.5	-15.442	0.02	0.01	0.47
9.5	-19.076	0.02	0.01	0.50
8.5	-23.618	0.03	0.01	0.53
7.5	-29.068	0.02	0.01	0.56
6.5	-29.976	0.01	0.01	0.75
5.5	-39.060	-0.03	0.01	0.79
4.5	-27.251	-	0.01	1.39
-	-	-	-	-
4.5	-27.251	-	-0.05	0.87
5.5	-39.060	-0.05	-0.02	0.51
6.5	-29.976	-0.06	-0.01	0.58
7.5	-29.068	-0.02	0.001	0.52
8.5	-23.618	0	0.004	0.560
9.5	-19.076	0.02	0.01	0.57
10.5	-15.442	0.02	0.01	0.57
15.5	-4.542	0.03	0.06	0.99
20.5	-1.817	0.25	0.11	1.47
25.5	-3.633	0.06	0.05	0.49
40.5	-0.908	0.16	0.07	0.62
		Case II, Pent 2		
39.5	-0.906	0.07	-0.08	0.18
25.5	-1.812	0	-0.02	0.43
20.5	-6.342	0	-0.01	0.25
15.5	-2.718	-0.04	-0.01	1.35
10.5	-17.215	0.001	0.01	0.69
9.5	-23.558	0.01	0.01	0.68
8.5	-31.712	0.01	0.01	0.67
7.5	-47.115	0.01	0.01	0.59
6.5	-57.988	0.01	0.01	0.64
5.5	-72.485	0.004	0.01	0.69
4.5	-81.545	-0.003	0.005	0.75
3.5	-90.606	-0.01	-	0.72
2.6	-113.257	-0.01	-	0.64
-	-	-	-	-
2.6	-113.257	-0.04	-	1.03
3.5	-90.606	-0.003	-	1.51
4.5	-81.545	0.02	-0.02	1.14
5.5	-72.485	0.05	-0.01	0.92
6.5	-57.988	0.06	-0.003	0.87
7.5	-47.115	0.07	0.001	0.82
8.5	-31.712	0.04	0.003	0.96
9.5	-23.558	0.04	0.01	1.03
10.5	-17.215	0.03	0.01	1.14
15.5	-2.718	0.01	0.09	2.92
20.5	-6.342	0.005	0.03	0.62
25.5	-1.812	-0.01	0.10	1.19
39.5	-0.906	-0.02	0.10	0.63

* Likely subject to errors in sign and magnitude

and core pressure deficit measured during the field program occur in this penetration. On the left (front) side the profile outside the radius of maximum $\bar{v}$ is closely approximated by a $vr^{0.98} = c$ curve. The right side $\bar{v}$ profile outside $\bar{v}_{max}$ deviates slightly more from the Rankine vortex. However, the curve vr is closely proportional to ln r. The vr = k ln r relationship, where k is a constant, has been suggested before (Hoffman and Joubert, 1963). In this case the proportionality constant (k) for r (right) = 3.5 m to 50 m is -56.6 ms^{-1} with a standard deviation of ± 6.0. For radii r (right) = 3.5 to 20.5 m, k = -62.7 ms^{-1} (standard deviation, ± 1.2).

Despite only several data points within the waterspout core, approximate solid body rotation ($vr^{-1} = c$) appears to exist in penetration 2. The deviation is greater at left side radii than right side, but only one data point (r= 2.2) was available for curve fitting as opposed to two on the right side. The mean value of the constant (c) in $vr^{-1} = c$ on the right side of the core is -6.82 s^{-1} with a standard deviation of ± 0.15 s^{-1}. On the left side of the core $\bar{c}$ = -4.53 with a standard deviation of ± 0.92 s^{-1}. If the profile is completed from r (right) = 2.2 m to r = 0 where $\bar{v} \equiv 0$, the deviation from a $vr^{-1} = c$ curve is less. In that case $\bar{c}$ (standard deviation) is -5.80 s^{-1} (± 0.15). Since by the definition of solid body rotation, $c = \omega = vr^{-1}$ where ω is the angular velocity, the core of this waterspout is rotating anticyclonically at an approximate rate of (5.80 + 6.82) x 0.5 = 6.3 rad s^{-1} or 60 revolutions min^{-1} (1 revolution s^{-1}). If this rotation rate remains constant out to r (left) = 5 m, this implies a theoretical $\bar{v}_{max}$ of $\sim$ 31.5 ms^{-1} or about 14 ms^{-1} stronger than the measured $\bar{v}_{max}$. It

is likely, however, that the tangential velocity peak is eroded by turbulence and/or measurement errors.

c. Tangential Momentum Equation. Figure 41 presents radial profiles of the inertial terms ($\bar{u}\ \partial\bar{v}/\partial r$, $\bar{w}\ \partial\bar{v}/\partial z$) and the "Coriolis" term ($\overline{uv}/r$) in the tangential equation of motion. Note the different ordinate scales for each section of the figure. In penetration 1, $\overline{uv}/r$ and $\bar{u}\ \partial\bar{v}/\partial r$ generally dominate. The term $\overline{uv}/r$ reaches its maxima of 5.6 ms^{-2} at r (left) = 5.5 m and 4.6 ms^{-2} at r (right) = 6.5 m. The radial angular momentum transport term ($\bar{u}\ \partial\bar{v}/\partial r$) is of the same order as the "Coriolis" term, reaching maximum values of -2.3 ms^{-2} at r (left) = 6.5 m and -1.7 ms^{-2} at r (right) = 10 m. Negative values of $\bar{u}\ \partial\bar{v}/\partial r$ imply a retardation of the anticyclonic flow through an inward transport of air from larger radii with less angular momentum, while a positive $\overline{uv}/r$ acts to enhance the anticyclonic swirl. The vertical transport of angular momentum increases at small radii primarily due to the concentrated vertical motion field in the waterspout. Magnitudes of $\partial\bar{v}/\partial z$ are of the same order as the Case I waterspout ($\sim$ 0.02 ms^{-2}) at radii greater than about 20 m, but increase to as high as 0.36 ms^{-2} at r (left) = 4.5 m.

The relatively high values bordering the vortex core may be partially due to apparent intensity canges in the waterspout during the penetrations. As seen in Figs. 37 and 38, maximum values of almost all measured variables increased for the second penetration. Although the first had a larger off-center distance, corresponding values of $\bar{v}$ and $\bar{p}$, for example, at the same radii increase substantially from the first to the second penetration. In penetration 2 those larger values are especially evident on the

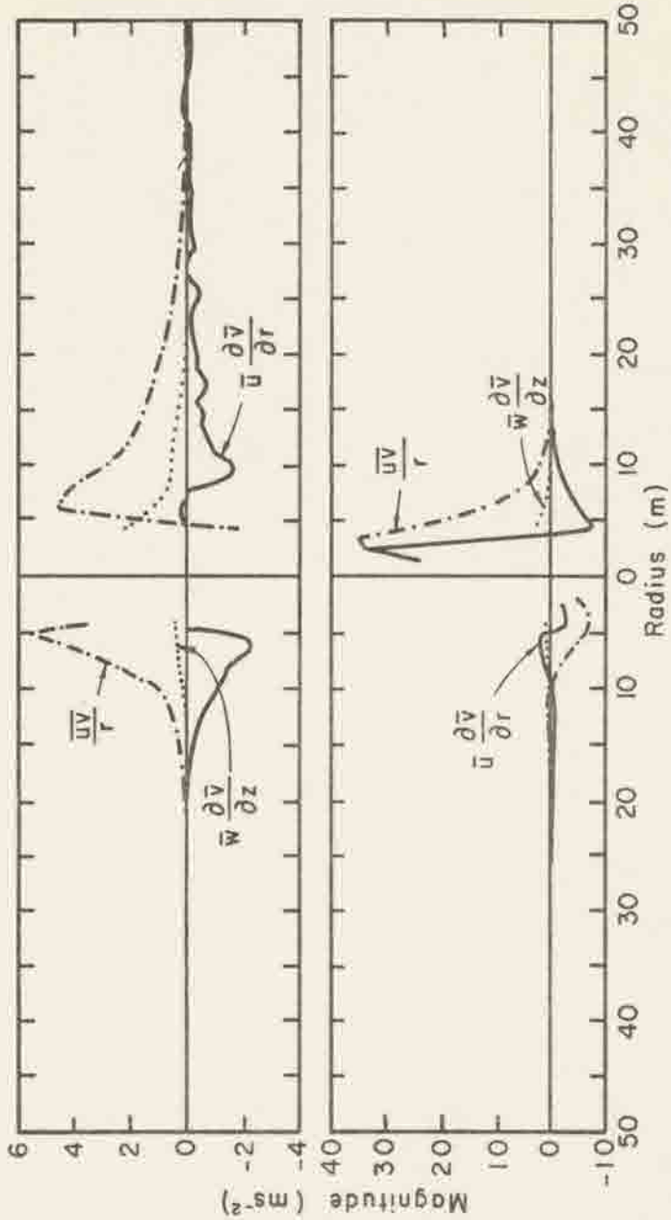

Fig. 41. As in Fig. 35 except for penetration 1 (top) and 2 (bottom) of the anticyclonic Case II waterspout.

right (back) side of the vortex. Values of $\overline{uv}/r$ and $\bar{u}\,\partial\bar{v}/\partial r$ reach maximum values of $\sim 34\ ms^{-2}$ at the radius of highest tangential winds (~ 3 m). Both terms contribute significantly to the maintenance of the anticyclonic swirl both in and outside of the vortex core. In the core on the left (front) side the two terms act against the anticyclonic flow, although at lesser magnitudes, primarily due to smaller and positive radial velocities.

d. Calculations of the Eddy Viscosity. Several attempts were made to calculate an approximate coefficient of eddy viscosity (K). In Chapter 5 a unique, constant K was assumed for waterspout vortex motion based primarily on the fact that adequate formulation of a functional relationship for K_r, K_θ, K_z based on the available measurements proved unlikely. By calculating values of the turbulence terms in equation (29) and solving for K from the equations, an approximate range of values for waterspout motion could be determined. This technique involved dividing the algebraic sum of the inertial and pressure gradient terms by the algebraic sum of mostly second-order derivatives of the velocity field. As a result relatively large numerators were divided by occasionally quite small denominators. Rounding errors and the occasional cancelling of turbulence terms often relegated the K values to appreciable variations in sign and magnitude. Nevertheless, it was hoped that a rough idea of the magnitude of the eddy viscosity could be gleaned from the data.

Values of K at various radii were calculated from Case II penetrations using the tangential momentum equation. This was done so as to use first and second order radial variations of $\bar{v}$, considered the most accurately measured wind component. Axial symmetry was

assumed, and due to lack of quantitative measurements, second order derivatives with respect to z were assumed zero. An attempt to calculate K using the radial momentum equation was made, but values fluctuated widely over radial intervals of 1 m, ranging from -3600 m^2 s^{-1} to 2100 m^2 s^{-1}. Due to measurement inaccuracies in $\bar{u}$, these values were considered meaningless.

Table 7 lists average K values at various radii for Case II penetrations 1 and 2. Average values outside the core range from $\sim$ 0 to $\sim$ 20 m^2 s^{-1}. Inside the core (penetration 2) a mean K is -6.7 m^2 s^{-1}. The negative sign (or any sign at any radius) is not dependent upon the direction of tangential flow. For example, if Case II was a cyclonic waterspout with the same flow field as penetration 2, K_{core} would still be negative. The turbulence terms (and

TABLE 7

Calculated Mean Values of Eddy Viscosity (K)(m^2 s^{-1})

	Left ($4.5 \text{ m} \leq r \leq 25.5 \text{ m}$)	Right ($8.5 \text{ m} \leq r \leq 25.5 \text{ m}$)
Penetration 1 (anticyclonic)	1.9	6.4
	$K_{\text{at } \bar{v}_{max}} = 54.5$	
	($5.5 \text{ m} \leq r \leq 25.5 \text{ m}$)	($3.5 \text{ m} \leq r \leq 25.5 \text{ m}$)
	1.0	14.3
Penetration 2 (anticyclonic)	($5.5 \text{ m} \leq r \leq 15.5 \text{ m}$)	($4.5 \text{ m} \leq r \leq 13.5 \text{ m}$)
	-0.24	20.9
	$K_{core} = -6.7$	

inertial terms) would change sign, but the affect of K_x(turbulence terms) in the waterspout core (or elsewhere) would remain the same. In the case of penetration 2, the sign of K_{core}x(turbulence terms)$_{core}$ is positive, indicating an opposition to the anticyclonic swirl.

The values of K in Table 7 appear reasonable in light of other order of magnitude calculations made for convective vortices. Sinclair (1966) made similar calculations from desert dust devil data to arrive at values of 5 - 15 $m^2 s^{-1}$. Golden (1974a) calculated a value of 100 $m^2 s^{-1}$ for a strong waterspout using characteristic velocity and dimension values. Values of K suggested by Table 7 would range from 1 to 20 $m^2 s^{-1}$ for weak to moderately intense waterspouts with values from approximately 5 to 20 $m^2 s^{-1}$ in regions of strongest wind and wind shear. It is considered that calculations from other penetrations made during the field program would probably yield similar but slightly smaller values of K.

Figure 42 is a graph of the radial profiles of the inertial, pressure gradient, and gravity terms in the vertical momentum equation from penetrations 1 and 2 of Case II. As in Case I, $\bar{\rho}^{-1}\partial\bar{p}/\partial z$ and g_{e_z} dominate the equation. The suggestion of a decreasing vertical pressure gradient near the vortex core may be partly due to apparent intensity changes in the waterspout between penetrations and to differences in the off-center penetration distance for each penetration. Only near the radius of $\bar{v}_{max}$ and in the core (penetration 2) does $\bar{u}\ \partial\bar{w}/\partial r$ approach the magnitude of $\bar{\rho}^{-1}\partial\bar{p}/\partial z$ and g_{e_z}. At r (right) = 1.5 m, $\bar{u}\ \partial\bar{w}/\partial r$ reaches -11.0 ms^{-2} acting in consort with the vertical pressure gradient to drive the upward vertical motion at smaller radii.

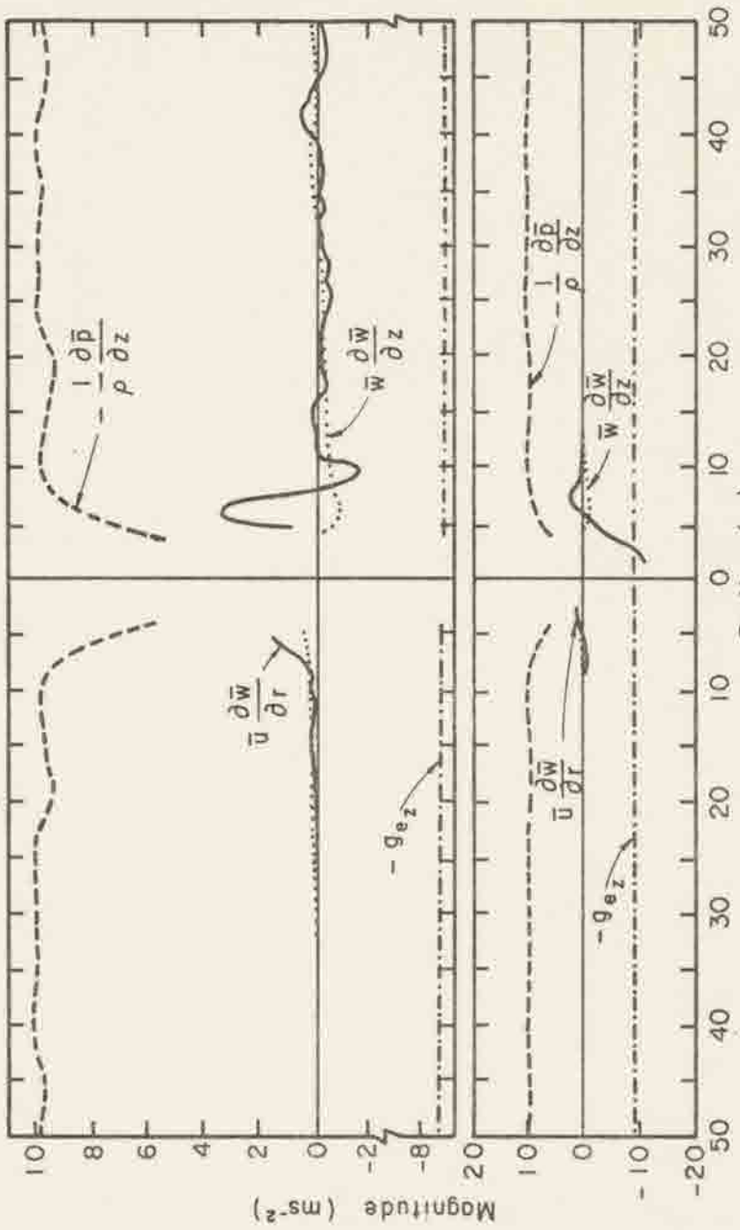

Fig. 42. As in Fig. 36 except for penetrations 1 (top) and 2 (bottom) of the anticyclonic Case II waterspout.

Case III - Central Core Downdraft. Figure 43 is a detailed plot of the Case III penetration data (see Fig. 28, Chapter 4). The area of subsiding (negative $\bar{w}$) motion in the vortex core is clearly evident. Although several other penetrations suggest reduced positive vertical motion in the core (Case I penetration 3 and Case II penetration 2), Case III is the only penetration in which a definite downdraft was detected by the alpha vane. As discussed in Chapter 4, the visible appearance of the funnel differed little from other penetrated funnels during the field program. The funnel did not extend more than 100 m below cloud base which was at a relatively high 780 m (see Fig. 27). No disturbance was visible on the water surface; however, several small mangrove keys were scattered beneath the funnel and may have concealed the surface disturbance.

No drastic differences from other penetrations are apparent in the three-dimensional wind profiles of Fig. 43. The radius of maximum $\bar{w}$ is displaced slightly outwards from the radius of $\bar{v}_{max}$. Case I penetration 3 is somewhat similar in that respect. The tangential wind profile is smooth, departs markedly from a Rankine vortex, and has values of $\bar{v}_{max}$ appreciably eroded. The temperature profile shows very little warming in the vortex at r (left), but a drop of $\sim$ 0.3 K immediately upon passage at r (right).

The concept of central subsiding motion in concentrated vortices is well known and has been extensively modeled and simulated (see reviews by Lewellen and Davies-Jones, 1976). A few of the numerical and laboratory models (Fitzjarrald, 1973; Harlow and Stein, 1974; and Ward, 1972) appear more realistic of many observed characteristics of geophysical vortices. These models basically describe the axial

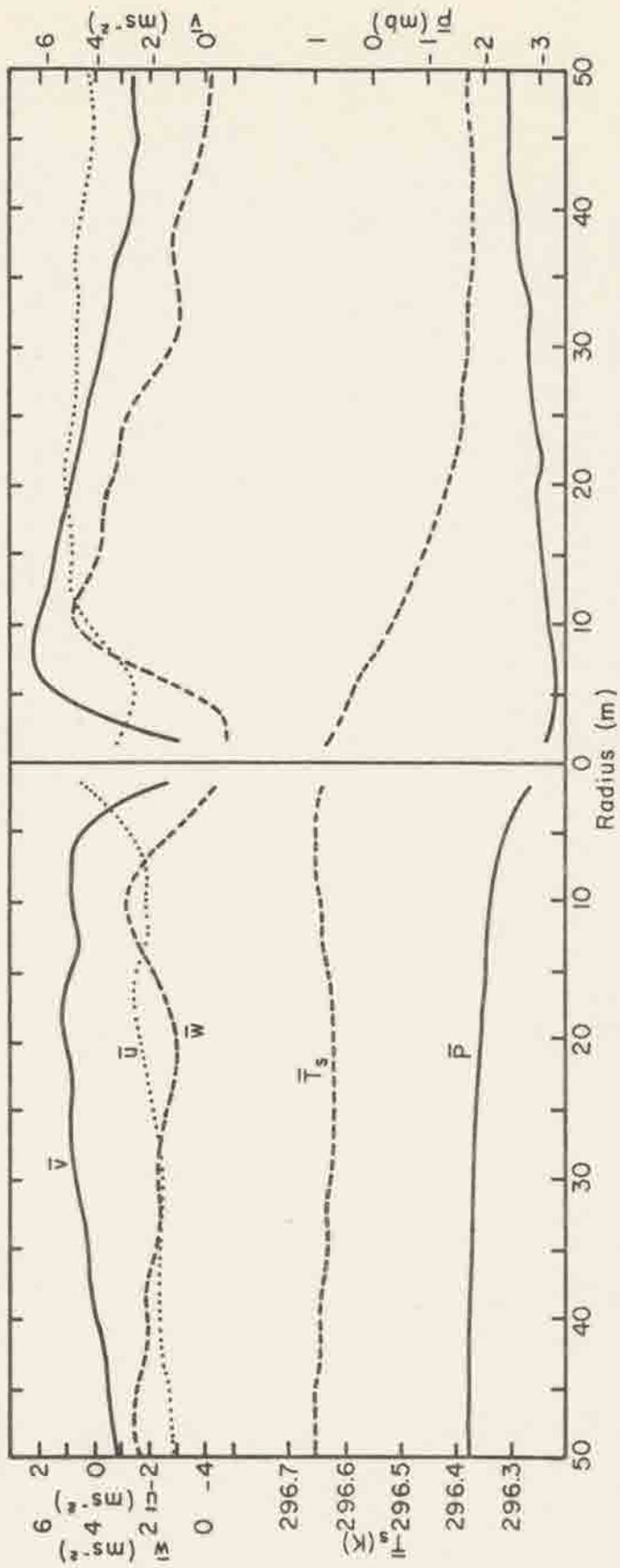

Fig. 43. Radial profiles of three-dimensional winds, pressure, and temperature for the anticyclonic Case III waterspout. See Fig. 28 for profiles extending to ~ 250 m.

downflow in terms of the magnitude of a circulation to convection ratio or swirl ratio. As the circulation increases, vertical pressure gradients develop that oppose upward vertical motion in the vortex core. A stagnation point on the axis (r = 0) develops, forcing a "vortex jump" or "breakdown" region, upstream of which laminar flow with a high helix angle exists and downstream of which turbulent flow and reversed (downward) axial motion occurs. As the circulation increases, the stagnation point moves down the vortex and the turbulent vortex core radius increases. Stable multiple vortices can develop at a critical swirl ratio as shown by Ward (1970) and Davies-Jones (1973).

Direct observations of axial downflow in natural vortices are less numerous. Sinclair (1966, 1973b) and Kaimal and Businger (1970) measured downward or reduced upward vertical velocities in and above the boundary layer of desert dust devils. Values of $\bar{w}$ occasionally reached -5 ms^{-1} (Sinclair, 1973b). Golden (1974a) (see Chapter 3) used smoke flare streaklines to detect downward vertical motions in large waterspouts.

The minimum value of $\bar{w}$ measured in Case III is -0.8 ms^{-1}; the area of negative $\bar{w}$ extends over an approximate 7 m diameter. It is quite possible that the rapid sampling time of the waterspout by the aircraft reduced the actual maximum downward velocity measured. At any rate, axial downflow in that portion of a waterspout near cloudbase is verified by the measurements. The lack of occasional substantiating evidence in the other measurements may be partly due to off-center penetrations. It also seems likely that downward vertical velocities do not exist in all portions of all waterspouts in all stages of their life cycles.

6.3 Reduced Set of Modeling Equations

Momentum and Continuity Equations. Calculated values for each term in the three component momentum equations are tabulated for each penetration in Table 8. The values listed below each term indicate the order of magnitude range (ms^{-2}) for the corresponding term and penetration. Equations (32), (33) and (34) result from assumed axial symmetry and other assumptions discussed in Chapter 5. The range of values for the turbulence terms multiplied by the eddy viscosity (K) values (1-20 m^2 s^{-1}) is grouped under those terms in the equations. The turbulence terms include second-order derivatives with respect to height (z). As noted before, these cannot be evaluated from the penetration data. However, at this level in the waterspout these terms are probably quite small compared with derivatives with respect to r. As a result, justification for their omission in calculating the effects of turbulence appears reasonable. All calculations are based on measurements inside a radius of 50 m and within $\sim$ 150 m below cloud base (see Section 6.2). However, due to off-center penetrations, most ranges do not include data from the waterspout core. Only in Case II penetration 2 (C II P 2) and Case III (C III) were core measurements available.

Inspection of Table 8 shows once again the dominant influence of an approximate balance between the radial pressure gradient and the centripetal acceleration in the radial momentum equation at this level in the waterspout vortex. All terms in the tangential momentum equation are in approximate balance. However, in C II P 2, where core measurements were made in a moderately intense waterspout, the radial advection term, "Coriolis" term, and turbulence terms are much larger

Table 8. Order of magnitude ranges for terms of the momentum equations computed from six individual waterspout penetrations. The Penetration number is listed at the left, e.g., CIP1 is Case I Penetration 1.

$$\bar{u}\frac{\partial \bar{u}}{\partial r} + \bar{w}\frac{\partial \bar{u}}{\partial z} - \frac{\bar{v}^2}{r} = -\frac{1}{\bar{\rho}}\frac{\partial \bar{p}}{\partial r} + K\left[\frac{\partial^2 \bar{u}}{\partial r^2} + \frac{1}{r}\frac{\partial \bar{u}}{\partial r} + \frac{\partial^2 \bar{u}}{\partial z^2}\right] \quad (32)$$

CIP1	0-1.8	0-0.6	0.3-11.0	0-3.6	0-5	($m\ s^{-2}$)
CIP2	0-3.8	0-0.6	0.3-11.2	0-7.1	0-10	
CIP3	0-1.4	0.4-10.5	0.2-16.9	0-5.4	0-28	
CIIP1	0-2.8	0-1.3	0.2-37.9	0-39.1	0-21	
CIIP2	0-6.7	0-1.3	0.1-137.0	0-113.3	0-13	
CIII	0-0.5	-	0.1-5.9	0-12.0	0-8	

$$\bar{u}\frac{\partial \bar{v}}{\partial r} + \bar{w}\frac{\partial \bar{v}}{\partial z} + \frac{\overline{uv}}{r} = K\left[\frac{\partial^2 \bar{v}}{\partial r^2} + \frac{2}{r}\frac{\partial \bar{v}}{\partial r} + \frac{\partial^2 \bar{v}}{\partial z^2}\right] \quad (33)$$

CIP1	0-0.6	0-0.1	0.1-3.0	0-3	($m\ s^{-2}$)
CIP2	0-1.1	0-0.1	0.2-4.0	0-5	
CIP3	0-0.6	0-0.1	0-2.4	0-7	
CIIP1	0-2.3	0-2.2	0-5.6	0-22	
CIIP2	0-32.2	0-2.2	0-34.1	0-129	
CIII	0-2.0	-	0-1.5	0-5	

$$\bar{u}\frac{\partial \bar{w}}{\partial r} + \bar{w}\frac{\partial \bar{w}}{\partial z} = -\frac{1}{\bar{\rho}}\frac{\partial \bar{p}}{\partial z} - g_{e_z} + K\left[\frac{\partial^2 \bar{w}}{\partial r^2} + \frac{1}{r}\frac{\partial \bar{w}}{\partial r} + \frac{\partial^2 \bar{w}}{\partial z^2}\right] \quad (34)$$

CIP1	0-0.9	0-0.3	4.8-6.1	9.5	0-7	($m\ s^{-2}$)
CIP2	0-3.9	0-0.3	4.8-6.1	9.5	0-17	
CIP3	0-0.6	0-0.3	7.6-8.1	9.5	0-10	
CIIP1	0-3.5	0-0.8	5.8-10.1	8.5	0-17	
CIIP2	0-11.0	0-0.8	5.8-10.1	9.2	0-15	
CIII	0-1.6	-	(10)*	9.2	0-17	

*Estimation

than the vertical advection term. These maximum values were calculated at or inside the radius of maximum winds where both $\bar{v}$ and $\partial\bar{v}/\partial r$ are large. Finally, the vertical pressure gradient and gravitational terms have greatest influence on the vertical motion field over the breadth and height of the vortex just below cloud base, but turbulence and radial advection terms can have equal or greater influence near and/or in the core. It should be pointed out that generally the maximum and minimum range values do not occur at the exact same location in the vortex, but are found within radii of $\sim$ 10 m.

Vertical derivatives are smaller compared to other terms. This may be partly due to calculations of vertical derivatives using large vertical increments (Δz) on the order of tens of meters. Taking this into account, it seems likely that actual inertial terms involving vertical derivatives might approach and equal the ranges of the radial advection terms.

The range of values for the terms in the momentum equations for weak to moderately intense waterspouts can be summarized as:

$$\underset{0\text{-}10}{\bar{u}\frac{\partial\bar{u}}{\partial r}} + \underset{0\text{-}10}{\bar{w}\frac{\partial\bar{u}}{\partial z}} - \underset{0\text{-}1}{\frac{\bar{v}^2}{r}} = \underset{0\text{-}1}{-\frac{1}{\bar{\rho}}\frac{\partial\bar{p}}{\partial r}} + K\underset{0\text{-}30\ (ms^{-2})}{\left[\frac{\partial^2\bar{u}}{\partial r^2} + \frac{1}{r}\frac{\partial\bar{u}}{\partial r} + \frac{\partial^2\bar{u}}{\partial z^2}\right]} \tag{35}$$

$$\underset{0\text{-}30}{\bar{u}\frac{\partial\bar{v}}{\partial r}} + \underset{0\text{-}5}{\bar{w}\frac{\partial\bar{v}}{\partial z}} + \underset{0\text{-}30}{\frac{\overline{uv}}{r}} = K\underset{0\text{-}20\ (ms^{-2})}{\left[\frac{\partial^2\bar{v}}{\partial r^2} + \frac{2}{r}\frac{\partial\bar{v}}{\partial r} + \frac{\partial^2\bar{v}}{\partial z^2}\right]} \tag{36}$$

$$\bar{u}\frac{\partial \bar{w}}{\partial r} + \bar{w}\frac{\partial \bar{w}}{\partial z} = -\frac{1}{\bar{\rho}}\frac{\partial \bar{p}}{\partial z} - g_{\ell_z} + K\left[\frac{\partial^2 \bar{w}}{\partial r^2} + \frac{1}{r}\frac{\partial \bar{w}}{\partial r} + \frac{\partial^2 \bar{w}}{\partial z^2}\right] . \qquad (37)$$

0-10 0-1 5-10 10 0-20 (ms^{-2})

It is apparent that further simplification of the component momentum equations is needless, and equations (35), (36), and (37) should be considered necessary to describe the waterspout vortex flow field above the surface boundary layer. Notice that vertical derivatives may be larger than indicated, and that inertial and turbulent effects must be retained and considered together in any detailed vortex modelling attempt. It should also be realized that the order of magnitude values will likely be much higher near the water surface and that different balance of forces will apply there.

The continuity equation and corresponding order of magnitude range for each term per each penetration show that equation (38) is an appropriate form for incompressible vortex flow.

$$\frac{\partial \bar{u}}{\partial r} + \frac{\bar{u}}{r} + \frac{\partial \bar{w}}{\partial z} = 0 \qquad (38)$$

CIP1	0-0.8	0-0.4	0-0.1	(s^{-1})
CIP2	0-1.6	0-0.5	0-0.1	
CIP3	0-1.3	0-0.3	0-0.1	
CIIP1	0-2.1	0-0.4	0-0.2	
CIIP2	0-1.9	0-2.4	0-0.2	
CIII	0-0.5	0-0.6	-	

Again note that values of $\partial \bar{w}/\partial z$ are most likely conservative because of the method of calculation.

Energy Equation. The thermodynamic energy equation (20) can be expanded to:

$$\bar{u}\frac{\partial \bar{T}_s}{\partial r} + \bar{w}\frac{\partial \bar{T}_s}{\partial z} = -\frac{g_e \bar{w}}{c_p} + \frac{1}{\bar{\rho} c_p}\left(\bar{u}\frac{\partial \bar{p}}{\partial r}\right) - \frac{\bar{w}}{c_p}\left[\bar{u}\frac{\partial \bar{w}}{\partial r} + \bar{w}\frac{\partial \bar{w}}{\partial z}\right] + \frac{1}{c_p}\frac{dQ}{dt} \quad . \qquad (39)$$

Mean value bars have been added to properly represent the AADS-2B measurements. Axial symmetry and steady state conditions have been assumed.

Equation (39) states that the time rate of change of an air parcel's temperature (K s^{-1}) (assumed to occur primarily from radial and vertical advection) is described by the effects of the terms on the right-hand side. The first term describes the expansional cooling (heating) a parcel undergoes as it moves vertically in a hydrostatic atmosphere. The second term is the expansional temperature change a parcel undergoes as it is advected radially in a changing pressure field. The third term represents the effects on expansion of a vertical pressure field that deviates from hydrostatic equilibrium (see equation (19)). The last term represents diabatic heating effects. Since the formulation of (39) is made for unsaturated motion the diabatic term should include water phase changes in the waterspout.

An order of magnitude analysis was completed for each term in (39) based on the waterspout wind, pressure, and temperature measurements within radii of 50 m. The ranges for each penetration are

$$\bar{u}\frac{\partial \bar{T}_s}{\partial r} + \bar{w}\frac{\partial \bar{T}_s}{\partial z} = -\frac{g_e \bar{w}}{c_p} + \frac{1}{\bar{\rho} c_p}\left(\bar{u}\frac{\partial \bar{p}}{\partial r}\right) - \frac{\bar{w}}{c_p}\left[\bar{u}\frac{\partial \bar{w}}{\partial r} + \bar{w}\frac{\partial \bar{w}}{\partial z}\right] + \frac{1}{c_p}\frac{dQ}{dt}$$

						$\left(\times 10^{-2}\right.$
CIP1	0-3	0-4	0-5	0-1	0-0.3	0-1
CIP2	0-9	0-4	0-6	0-3	0-0.4	$\left.0\text{-}1 \quad \text{Ks}^{-1}\right)$
CIP3	0-4	0-3	0-5	0-1	0-0.5	0-0.5
CIIP1	0-6	0.5-2	1-5	0-9	0-1	0-2
CIIP2	0-2	0.5-2	0-7	0-50	0-4	0-2
CIII	0-3	-	0-4	0-1	-	0-0.5
All	0-10	0-5	0-10	0-50	0-5	0-2

The last row summarizes the range of values for weak to moderate waterspouts. The values of $c_p^{-1}\, dQ/dt$ may be in error since only condensational effects were included. The maximum values for the diabatic term were estimated using a mean moist lapse rate at atomspheric temperatures and pressures characteristic of the near cloud base environment, and mean vertical velocities for each penetration. As expected, additional processes other than strictly vertical ascent can have important effects on the thermodynamic structure of the waterspout vortex. In addition, strong changes in vortex intensity would require inclusion of local derivatives of $\bar{T}_s$, $\bar{p}$, and $\bar{w}$ in equation (39).

Final Equations. Equations (35) thru (39) constitute a reduced set of the governing equations for waterspout vortex motion below cloud base and above the surface boundary layer.

7. SUMMARY AND CONCLUSIONS

An extensive field program was carried out in the Florida Keys in September, 1974, to provide actual measurements of the vortex circulation and thermodynamic structure of waterspouts. A specially instrumented aircraft penetrated visible funnels and provided the first complete measurements of the vortex structure near cloud base. Data from seven penetrations are presented, and an extensive order of magnitude analysis of the governing equations using data from six of the penetrations is performed.

Conclusions from this study are summarized as follows:

1. Suitably instrumented and stressed aircraft are capable of successfully penetrating weak to moderately intense waterspouts and obtaining measurements of the vortex flow and thermodynamic fields. By this method measurements in the radial direction are spatially detailed: however, the vertical structure can only at best be coarsely resolved. Improved penetration techniques and faster responding instrumentation should supply data of greater accuracy than that presented here.

2. Waterspout wind, temperature, and pressure structure in the near cloud base environment can be described as follows:

   a. The vortex is defined by a concentrated region of strong tangential and vertical velocities upon which is superimposed radial velocities of slightly lesser magnitude. Maximum values of $\bar{v}$ range from $\sim$5 m s^{-1} to 22 m s^{-1}, while largest values of $\bar{w}$ range from +2 m s^{-1} to $\sim$+8 m s^{-1}. In the weaker waterspouts $\bar{v}_{max} \approx \bar{w}_{max}$, but the departure of $\bar{v}_{max}$ above $\bar{w}_{max}$ increases with more intense waterspouts. Radial velocities exhibit maximum values of $\sim$+2 m s^{-1} to -5 m s^{-1}. The average radial velocity profile shows inward motion of $\sim$-1 m s^{-1} to -3 m s^{-1}; however, the environmental winds can apparently disrupt the convergent velocities and produce regions of either outflow or amplified inflow.

   b. The measurements indicate general upward vertical motion near the core (one-cell cortex); however, several penetrations suggest reduced positive

vertical velocities, and in one case, a definite downdraft of -0.8 m s^{-1} was measured at a radius of 1.5 m. The lack of more evidence of the central core downdraft (two-cell vortex) in the measurements may be due to consistent, but small, off-center penetrations by the aircraft.

c. The tangential velocity radial profiles do not in general fit the Rankine-combined vortex model very well. Profiles of $\overline{v}$ show an increase in relative angular momentum outward of the radius of maximum $\overline{v}$ (non-zero relative vorticity). The closest fit to the Rankine model occurs in the strongest waterspout penetrated. Few core measurements of $\overline{v}$ are available; however, those that are indicate a region rotating approximately in solid body fashion with a rotation rate that decreases from r = 0 to $r_{\overline{v}_{max}}$. The $\overline{v}_{max}$ extrema are appreciably eroded from that predicted by the (inviscid) Rankine model.

d. The temperature structure exhibits increases on the order of 0.1 to 0.5 K from distant radii to the waterspout core. Such a small relative warming in or near the core gives little evidence for either rising or sinking air motion on the vertical axis. Warm boundary-layer air is certainly transported vertically by the waterspout circulation system, remaining essentially undiluted due to the vortex's resistance to entrainment/detrainment. By the same token, axial downflow could warm an air parcel adiabatically, the amount depending on its initial temperature and pressure. No apparent decrease in temperature has been detected in the vortex core.

e. The pressure structure indicates core deviations of -0.6 to -8.4 mb. The measured tangential wind maxima, assuming cyclostrophic flow, account for as little as 25% to as much as $\sim$94% of the measured core pressure deficits with an average value of 63% for all six penetrations.

3. Anticyclonic waterspouts of the weak to moderate intensity appear to occur as often as cyclonic ones. Of the 15 waterspouts penetrated during the field program, 4 rotated cyclonically, 7 anticyclonically, and 4 in an undetected direction.

4. The order of magnitude analysis shows that the cyclostrophic relation ($\overline{v}^2/r = \overline{\rho}^{-1}\, \partial\overline{p}/\partial r$) provides a valid first approximation to the complete radial momentum equation. Likewise, the hydrostatic assumption appears valid near the core, but the lack of accurate and numerous

> measurements in the core and along the vertical axis precludes knowledge of the vertical momentum balance there. In general, retention of the inertial terms necessitates likewise retention of the turbulence terms in all three momentum equations. The continuity equation for incompressible, axisymmetric flow is valid. The derivation and order of magnitude analysis of a thermodynamic energy equation shows that in addition to strictly vertical ascent; non-vertical ascent, non-hydrostatic effects, and condensation processes can be important in considering parcel temperature changes in the waterspout.

The data and conclusions in this paper should provide additional useful insights into waterspout structure and dynamics. Together with previous field measurements of other naturally occurring vortices (e.g., Sinclair, 1966), these results can form a solid foundation upon which new and more accurate concepts and models of geophysical vortices can be built.

Of utmost importance in the area of future research is the necessity for continued efforts at detailed observations of concentrated atmospheric vortices. Such observations should include not only the atmospheric structure antecedent to and concurrent with the occurrence of such vortices, but also examinations of the detailed circulation and energetics of the parent cloud-vortex system. The frequently occurring and usually more docile waterspout (particularly Florida Keys and Gulf Coast types) should continue subject to detailed observational programs; the goal(s) being not so much a determination of maximum kinematic and thermodynamic anomalies, but more a quantitative description of the hydrodynamic processes and life cycle dynamics that in general should be transferrable, at least qualitatively, to the tornado. These efforts should be directed to the entire waterspout system - - from parent cloud to surface boundary layer.

REFERENCES

Agee, E. M., C. Church, C. Morris, and J. Snow, 1975: Some synoptic aspects and dynamic features of vortices associated with the tornado outbreak of 3 April 1974. Mon. Wea. Rev., 103, 318-333.

Axford, D. N., 1968: On the accuracy of wind measurements using an inertial platform in an aircraft, and an example of a measurement of the vertical mesostructure of the atmosphere. J. Appl. Meteor., 7, 645-666.

Bellamy-Knights, P. G., 1970: An unsteady two-cell vortex solution of the Navier-Stokes equations. J. Fluid Mech., 41, 673-687.

Bellamy-Knights, P. G., 1971: Unsteady multicellular viscous vortices. J. Fluid Mech., 50, 1-16.

Blechman, J. B., 1975: The Wisconsin tornado event of April 21, 1974: Observations and theory of secondary vortices. Proceedings Ninth Conference on Severe Local Storms, Norman, Oklahoma, Amer. Meteor. Soc., 344-349.

Bode, L., L. M. Leslie, and R. K. Smith, 1975: A numerical study of boundary effects on concentrated vortices with application to tornadoes and waterspouts. Quart. J. R. Met. Soc., 101, 313-324.

Bunker, A. F., 1955: Turbulence and shearing stresses measured over the North Atlantic Ocean by an airplane-acceleration technique. J. Meteor., 12, 445-455.

Burgers, J. M., 1948: A mathematical model illustrating the theory of turbulence. Advan. Appl. Mech., 1, 197-199.

Byers, H. R. and R. R. Braham, 1949: The Thunderstorm. U.S. Gov't. Print. Office, Washington, D.C., 287 pp.

Clemons, G. H., 1969: Detailed radar observations and recent climatology of waterspouts in the Key West area. Proceedings Sixth Conference on Severe Local Storms, Chicago, Illinois, AMS, unpublished manuscript.

Davies-Jones, R. P., 1973: The dependence of core radius on swirl ratio in a tornado simulator. J. Atmos. Sci., 30, 1427-1430.

Davies-Jones, R. P., 1976: Laboratory simulations of tornadoes. Proceedings of the Symposium on Tornadoes, Institute for Disaster Research, Texas Tech. University, Lubbock, Texas, 151-174.

REFERENCES (cont'd)

Dessens, J., 1972: Influence of ground roughness on tornadoes: a laboratory simulation. J. Appl. Meteor., 11, 72-75.

Dutton, J. A., 1967: Belling the CAT in the sky. Bull. Amer. Meteor. Soc., 48, 813-820.

Fitzjarrald, D. E., 1973: A laboratory simulation of convective vortices. J. Atmos. Sci., 30, 894-902.

Fujita, T. T., 1970: The Lubbock tornadoes: A study of suction spots. Weatherwise, 23, 160-173.

Fujita, T. T., 1975: New evidence from April 3-4, 1974 tornadoes. Proceedings Ninth Conference on Severe Local Storms, Norman, Oklahoma, Amer. Meteor. Soc., 248-255.

Garza, C., Jr., 1971: A study of funnel cloud occurrences in the Beaumont-Port Arthur-Orange area in Texas. NOAA Tech. Memo. NWS TM SR-52, Southern Region Headquarters, Ft. Worth, Texas, 11 pp.

Gerrish, H. P., 1967: Tornadoes and waterspouts in the South Florida area. Proceedings 1967 Army Conference on Tropical Meteorology, Coral Gables, Florida.

Goddard, Brent B., 1962: The development of aircraft investigations of squall lines from 1956-1960. National Severe Storms Project, Report No. 2, Washington, D.C.

Golden, J. H., 1970: The Lower Florida Keys waterspout project, May-September, 1969. Bull. Amer. Meteor. Soc., 51, 235-236.

Golden, J. H., 1971: Waterspouts and tornadoes over South Florida. Mon. Wea. Rev., 99, 146-154.

Golden, J. H., 1973a: Some statistical aspects of waterspout formation. Weatherwise, 26, 108-117.

Golden, J. H., 1973b: The life cycle of the Florida Keys waterspout as the result of five interacting scales of motion. Ph.D. dissertation, Florida State University, 371pp.

Golden, J. H., 1974a: Life cycle of Florida Keys' waterspouts, NOAA Tech. Memo. ERL NSSL-70, National Severe Storms Laboratory, Norman, Oklahoma, 147 pp.

Golden, J. H., 1974b: The life cycle of Florida Keys' waterspouts. I. J. Appl. Meteor., 13, 676-692.

Golden, J. H., 1974c: Scale interaction implications for the waterspout life cycle. II. J. Appl. Meteor., 13, 693-709.

REFERENCES (cont'd)

Golden, J. H., 1976: An assessment of windspeeds in tornadoes. Proceedings of the Symposium on Tornadoes, Institute for Disaster Research, Texas Tech. University, Lubbock, Texas, 5-42.

Golden, J. H. and D. Purcell, 1976: Airflow characteristics around the Union City tornado, Chapter 14, The Union City, Oklahoma tornado of 24 May 1973. NOAA Tech. Memo. ERLTM-NSSL-80, Rodger Brown, editor, National Severe Storms Laboratory, Norman, Oklahoma.

Gordon, A. H., 1951: Waterspouts. Weather, 6, 364-371.

Gutman, L. N., 1957: Theoretical model of a waterspout. Bull. Academy of Sciences of U.S.S.R. (Geophysical Series). Pergamon Press translation, 1, 87-103.

Haltiner, G. J. and F. L. Martin, 1957: Dynamical and Physical Meteorology, New York, McGraw-Hill, 470 pp.

Harlow, F. H. and L. R. Stein, 1974: Structural analysis of tornado-like vortices. J. Atmos. Sci., 31, 2081-2098.

Hess, S. L., 1959: Introduction to Theoretical Meteorology. New York, Holt, Rinehart, and Winston, 362 pp.

Hoecker, W. H., 1960: Wind speed and air flow patterns in the Dallas tornado of April 2, 1957. Mon. Wea. Rev., 88, 167-180.

Hoffman, E. R. and P. N. Joubert, 1963: Turbulent line vortices. J. Fluid Mech., 16, 395-411.

Holmes, R. M., 1972: An airborne instrument system for atmospheric boundary-layer research. Boundary-Layer Meteor., 3, 59-76.

Hsu, C. T. and B. Fattahi, 1975: Tornado funnel formation from a tornado cyclone. Proceedings Ninth Conference on Severe Local Storms, Norman, Oklahoma, Amer. Meteor. Soc., 358-363.

Hyde, W. D., 1971: Waterspouts off Cyprus, 14 January 1970. Meteor. Magazine, 100, 112-117.

Kaimal, J. C. and J. A. Businger, 1970: Case studies of a convective plume and a dust devil . J. Appl. Meteor., 9, 612-620.

Kampé de Fériet, J., 1951: Averaging processes and Reynolds equations in atmospheric turbulence. J. Meteor., 8, 358-361.

Kessler, E., 1970: Tornadoes. Bull Amer. Meteor. Soc., 51, 926-936.

Kuo, H. L., 1966: On the dynamics of convective atmospheric vortices. J. Atmos. Sci., 23, 25-42.

REFERENCES (cont'd)

Kuo, H. L., 1971: Axisymmetric flows in the boundary layer of a maintained vortex. J. Atmos. Sci., 28, 20-41.

Lenschow, D. H. and W. T. Pennell, 1974: On the measurement of in-cloud and wet-bulb temperatures from an aircraft. Mon. Wea. Rev., 102, 447-454.

Leslie, L. M., 1971: The development of concentrated vortices: a numerical study. J. Fluid Mech., 48, 1-21.

Leverson, V. H., P. C. Sinclair, and J. H. Golden, 1977: Waterspout wind, temperature, and pressure structure deduced from aircraft measurements, Mon. Wea. Rev., 105, 725-733.

Lewellen, W. S., 1976: Theoretical models of the tornado vortex. Proceedings of the Symposium on Tornadoes, Institute for Disaster Research, Texas Tech. University, Lubbock, Texas, 107-143.

Lewis, W. and P. J. Perkins, 1953: Recorded pressure distribution in the outer portion of a tornado vortex. Mon. Wea. Rev., 81, 379-385.

Lilly, D. K., 1965: Experimental generation of convectively driven vortices. Geofisica Internacional, 5, 43-48.

Lilly, D. K. and P. J. Kennedy, 1973: Observations of a stationary mountain wave and its associated momentum flux and energy dissipation. J. Atmos. Sci., 30, 1135-1152.

Long, R. R., 1958: Vortex motion in a viscous fluid. J. Meteor., 15, 108-112.

Long, R. R., 1961: A vortex in an infinite viscous fluid. J. Fluid Mech., 11, 611-623.

Malkus, J. S., 1954: Some results of a trade-cumulus cloud investigation. J. Meteor., 11, 220-237.

Maxworthy, T., 1972: On the structure of concentrated, columnar vortices. Astro. Acta., 17, 363-374.

Mehta, K. C., J. E. Minor, J. R. McDonald, B. R. Manning, J. J. Abernathy, and U. F. Koehler, 1975: Engineering aspects of the tornadoes of April 3-4, 1974. Committee on Natural Disasters, National Academy of Sciences, Washington, D.C., 110 pp.

Morton, B. R., 1966: Geophysical vortices. Progress in Aeronautical Sciences, Vol. 7, New York, Pergamon Press, 145-194.

Outram, T. S., 1904: Storm of August 20, 1904. Mon. Wea. Rev., 32, 365-366.

REFERENCES (cont'd)

Phillips, P. E., 1950: Flight through cloud funnel of waterpout. Meteor. Mag. 79, 24-25.

Price, S. and R. J. Sasaki, 1963: Some tornadoes, waterspouts, and other funnel clouds of Hawaii. Mon. Wea. Rev., 91, 175-190.

Reynolds, O., 1895: On the dynamical theory of incompressible viscous fluids and the determination of the criterion. Phil. Trans. Roy. Soc. London, A186, 123-164.

Rossman, F. O., 1958: Differences in the physical behavior of tornadoes and waterspouts. Weather, 13, 259-263.

Rossow, V. J., 1970: Observations of waterspouts and their parent clouds. NASA Tech. Note D-5854, NASA, Washington, D.C., 63 pp.

Schlichting, H., 1968: Boundary Layer Theory. New York, McGraw-Hill, 747 pp.

Scorer, R. S., 1958: Natural Aerodynamics. London, Pergamon Press, 312 pp.

Sinclair, P. C., 1966: A quantitative analysis of the dust devil. Ph.D. dissertation, University of Arizona, 292 pp.

Sinclair, P. C., 1969a: General characteristics of dust devils. J. Appl. Meteor., 8, 32-45.

Sinclair, P. C., 1969b: Vertical motion and temperature structure of severe convective storms. Preprints Sixth Conference on Severe Local Storms, Chicago, Illinois, Amer. Meteor. Soc., 346-350.

Sinclair, P. C., 1973a: Severe storm air velocity and temperature structure deduced from penetrating aircraft. Preprints Eighth Conference on Severe Local Storms, Denver, Colorado, Amer. Meteor. Soc., 25-32.

Sinclair, P. C., 1973b: The lower structure of dust devils. J. Atmos. Sci., 30, 1599-1619.

Sinclair, P. C., 1974: Severe storm turbulent energy structure. Preprints Sixth Conference on Aerospace and Aeronautical Meteorology, El Paso, Texas, Amer. Meteor. Soc., 13 pp.

Sinclair, P. C., 1977: Waterspout penetrations by instrumented aircraft. J. Appl. Meteor. (to be published 1978).

Staley, D. O., 1966: The lapse rate of temperature following an air parcel. Quart. J. Roy. Meteor. Soc. 92, 147-150.

REFERENCES (cont'd)

Steiner, R. and R. H. Rhyne, 1962: Some measured characteristics of severe storm turbulence. National Severe Storms Project, Rept. No. 10, U.S. Dept. of Commerce, Washington, D.C.

Sullivan, R. D., 1959: A two-cell vortex solution of the Navier-Stokes equations. J. Aerospace Sci., 26, 767-768.

Tennekes, H. and J. L. Lumley, 1972: A First Course in Turbulence. Cambridge, Mass., MIT Press. 300 pp.

Turner, J. S. and D. K. Lilly, 1963: The carbonated-water tornado vortex. J. Atmos. Sci., 20, 468-471.

Ward, N. B., 1964: The Newton, Kansas tornado cyclone of May 24, 1962. Proceedings of the Eleventh Weather Radar Conference, Boulder, Colorado, Amer. Meteor. Soc., 410-415.

Ward, N. B., 1970: The exploration of certain features of tornado dynamics using a laboratory model. NOAA Tech. Memo ERLTM-NSSL 52, National Severe Storms Laboratory, Norman, Oklahoma.

Ward, N. B., 1972: The exploration of certain features of tornado dynamics using a laboratory model. J. Atmos. Sci., 29, 1194-1204.

White, F. M., 1974: Viscous Fluid Flow. New York, McGraw-Hill, 725 pp.

Ying, S. J. and C. C. Chang, 1970: Exploratory model study of tornado-like vortex dynamics. J. Atmos. Sci., 27, 3-14.

Zipser, R. A., 1976: Photogrammetric studies of a Kansas tornado and a Hawaiian tornadic-waterspout. M.S. Thesis, Dept. of Meteorology, Univ. of Oklahoma, Norman, Oklahoma, 75 pp.

APPENDIX

The derivation of an equation of motion for the waterspout vortex must begin from first principles, these being Newton's three laws of motion. From Newton's second law, the fundamental relationship describing the dynamics of the atmosphere is

$$\sum \vec{F} = m\vec{a} = m\frac{d\vec{V}}{dt} \quad . \tag{A-1}$$

According to (A-1) the net external real forces acting on a fluid element can be described in terms of the accelerations they produce. This law is valid in an inertial or nonaccelerating coordinate system. The center of the earth can be assumed the origin of such a system since its acceleration with respect to the "fixed" stars is considered insignificant for dynamical studies on the earth's surface (Hess, 1959). However, a coordinate system with its origin fixed at (or near) the earth's surface is a noninertial system since it rotates (accelerates significantly) with respect to the earth's center. The expression of Newton's second law for the motion of an air parcel in such a system is then written as

$$\frac{d\vec{V}}{dt} = \vec{g} - \frac{1}{\rho}\vec{\nabla}p - \vec{\omega} \times (\vec{\omega} \times \vec{R}) - 2\vec{\omega} \times \vec{V} + \frac{\mu}{\rho}\left[\nabla^2\vec{V} + \frac{1}{3}\vec{\nabla}(\vec{\nabla}\cdot\vec{V})\right] \quad . \tag{A-2}$$

The left side of the equation is the acceleration of an air parcel relative to the earth's surface. The first two and the last terms on the right side represent the net external real forces (per unit mass) exerted on the parcel; namely, gravitation, pressure gradients, and friction, respectively. The third and fourth terms on the right are the familiar centrifugal and Coriolis forces respectively, apparent forces that arise upon conversion of (A-1) into a noninertial rotating

coordinate system. The earth's angular velocity ($\vec{\omega}$) is considered constant, and $\vec{R}$ is the mean radius of the earth. The dynamic viscosity (μ) of air is assumed constant and equal to -3/2 its bulk viscosity (λ).

Several coordinate transformations must be made to the scalar components of (A-2) to express it in a suitable waterspout coordinate system. The author believes one appropriate system is a cylindrical system (r, θ, z) translating over the earth's surface with the vortex. In this manner the waterspout axis of rotation coincides with the cylindrical z axis, and velocities and acceleration in the r, θ, and z directions represent vortex radial, tangential, and vertical motions respectively. Notice that this system can be a tilted one, corresponding to natural funnel tilt. In such a case, r and θ are not necessarily horizontal directions, and z is not vertical, i.e., not parallel to the local vertical.

Three transformations are separately employed to arrive at the desired waterspout coordinate system. Actually, four can be considered since a transformation is made from the commonly used rectangular cartesian system (hereafter designated with R subscripts) described by Haltiner and Martin (1957) to the aircraft measurement cartesian system (subscript f). As discussed in Section 2.2 the AADS-2B measurement coordinate system is one in which the positive x_f and y_f axes point toward the tail and right wind respectively, and are orthogonal to the earth's local vertical. It is a coordinate system fixed in space (at flight altitude) with respect to a reference point on the earth's surface. The three-dimensional winds (u_f, v_f, w_f) are measured in this coordinate system and therefore are relative to the surface of the earth.

Written in component form (adding R subscripts for the rectangular cartesian system), (A-2) becomes

$$\frac{du_R}{dt} = -\frac{1}{\rho}\frac{\partial p}{\partial x_R} + 2(\omega_{z_R} v_R - \omega_{y_R} w_R) + \frac{\mu}{\rho}\left[\nabla_R^2 u_R + \frac{1}{3}\frac{\partial}{\partial x_R}(\vec{\nabla}_R \cdot \vec{\nabla}_R)\right]$$

$$\frac{dv_R}{dt} = -\frac{1}{\rho}\frac{\partial p}{\partial y_R} + 2(\omega_{x_R} w_R - \omega_{z_R} u_R) + \frac{\mu}{\rho}\left[\nabla_R^2 v_R + \frac{1}{3}\frac{\partial}{\partial y_R}(\vec{\nabla}_R \cdot \vec{\nabla}_R)\right] \quad \text{(A-3)}$$

$$\frac{dw_R}{dt} = -\frac{1}{\rho}\frac{\partial p}{\partial z_R} - g_{e_{z_R}} + 2(\omega_{y_R} u_R - \omega_{x_R} v_R) + \frac{\mu}{\rho}\left[\nabla_R^2 w_R + \frac{1}{3}\frac{\partial}{\partial z_R}(\vec{\nabla}_R \cdot \vec{\nabla}_R)\right].$$

The centrifugal force term, $-\vec{\omega} \times (\vec{\omega} \times \vec{R})$, in (A-2) has been combined with the gravitational term $(\vec{g})$ in the customary manner to produce a new term known as the effective gravity $(\vec{g}_e)$.

In transforming (A-3) to the AADS-2B coordinate system the transformation equations take the form

$$\begin{aligned} x_R &= x_f \cos\psi + y_f \sin\psi \\ y_R &= x_f \cos\psi + y_f \sin\psi \\ z_R &= z_f \end{aligned} \quad \text{(A-4)} \qquad \begin{aligned} x_f &= x_R \cos\psi - y_R \sin\psi \\ y_f &= x_R \sin\psi + y_R \cos\psi \\ z_f &= z_R \end{aligned} \quad \text{(A-5)}$$

where ψ = aircraft true heading + 90° (Fig. A-1). All terms remain essentially in the same form since the coordinate transformation is between two equivalent cartesian systems. However, since $\omega_{x_R} = 0$, $\omega_{y_R} = \omega \cos\phi$, and $\omega_{z_R} = \omega \sin\phi$ (where ϕ = latitude and $\omega = |\vec{\omega}|$), then by (A-5) $\omega_{x_f} = -\omega \cos\phi \sin\psi$, $\omega_{y_f} = \omega \cos\phi \cos\psi$, and $\omega_{z_f} = \omega \sin\phi$.

The second coordinate transformation is from the AADS-2B system to a system translating with the waterspout. In considering a translating coordinate system on or near the earth's surface, the curvature of the earth enters into the analytical computations. For example, as the aircraft flies over the earth, the directions of u_f, v_f, and w_f are

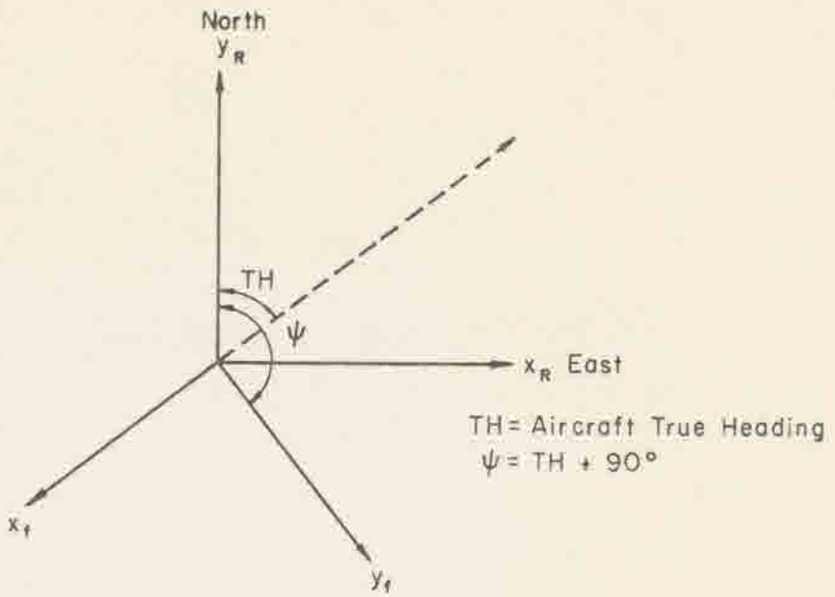

Figure A-1. Relation of rectangular cartesian and AADS-2B measurement coordinates in the horizontal plane for an arbitrary aircraft heading.

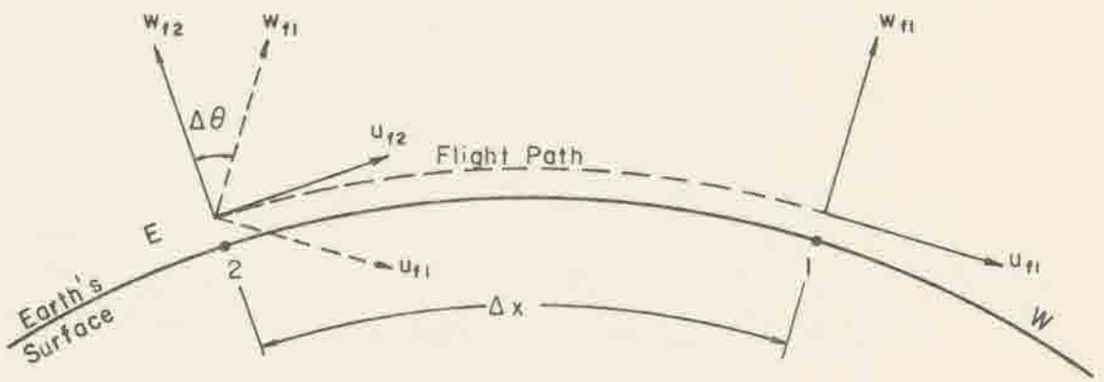

Figure A-2. Curvature effect of the earth's surface on AADS-2B measured winds (in the x_f, z_f plane).

continuously changing (Fig. A-2). If these changes in direction of the measured air motions and the changes in orientation of the translating coordinate system were ignored, the earth's surface could be treated as a plane, thus simplifying the development of exact governing equations for waterspout vortex motion. It might intuitively seem that for dimensions of motion so limited in direction as they are in this study, the curvature effect could be ignored. The greatest error in relating AADS-2B derived winds to a moving coordinate system assumed to unchange in its orientation occurs as the aircraft flies at a constant $90^{o}/270^{o}$ heading, or along a latitude circle. (At any point on earth, the curvature of the surface overflown at a constant heading will be greatest along the local latitude circle.) Referring to Fig. A-2, if the coordinate system is oriented as over point 1, and the final wind measurements made along the flight path are positioned as shown over point 2, the angular difference $\Delta\theta$, or angular error due to curvature, is approximated by $\Delta x/R$, where $R = a\cos\phi$ ($a \equiv$ earth's mean radius). With a typical Δx of $\sim$ 4km, R = 6371km, and $\phi = 24.5^{o}$, the maximum $\Delta\theta$ encountered is $\sim 0.04^{o}$, or a change in typical measured winds (u_f, v_f, w_f) of <0.1%. This error is much less than measurement and instrumentation errors (see Section 2.4). Therefore, the assumption of treating the earth's surface as a plane is justifiable for this study.

For the coordinate system translating relative to a fixed system, the transformation equations describing the positions of any point in space are

$$x_f = x_s + h_f \qquad y_f = y_s + k_f \qquad z_f = z_s \qquad \text{(A-6)}$$

$$x_s = x_f - h_f \qquad y_s = y_f - k_f \qquad z_s = z_f \qquad \text{(A-7)}$$

where the subscript s denotes the moving waterspout system (Fig. A-3). For our purposes, the relative motion between the two coordinate systems is limited to the x_f, y_f plane; hence, $z_f = z_s$ and vice versa. The x_s, y_s, z_s axes remain parallel to x_f, y_f, z_f at all times. In addition, the relative motion of the two coordinate systems is assumed constant in speed and direction during each penetration. The new coordinate system moves with the waterspout and has its origin at the altitude of penetration and on the funnel's axis of rotation.

The third coordinate transformation places the moving cartesian system at the correct tilt of the funnel. The funnel's tilt (γ) is defined as the angle formed by the axis of rotation of the waterspout and the local vertical (Fig. A-4) and may be directed at any heading during a penetration. That is, during the field program, no preference was given to tilt orientation with respect to the aircraft's penetration heading. The transformation involves two rotations of the (s) coordinate axes (see Fig. 13 a and b, Chapter 4). The first is a rotation around the y_s axis through the angle λ ($\lambda>0$ for a right-handed rotation; $\lambda<0$ for left). The second rotation is around the x' axis through the angle η (η>right; $\eta<0$ left). The end result is a cartesian coordinate system (double prime superscript) whose z" axis is tilted γ degrees from the vertical.

The transformation equations for the operation are obtained by multiplying the two transformation matrices for each rotation. Thus,

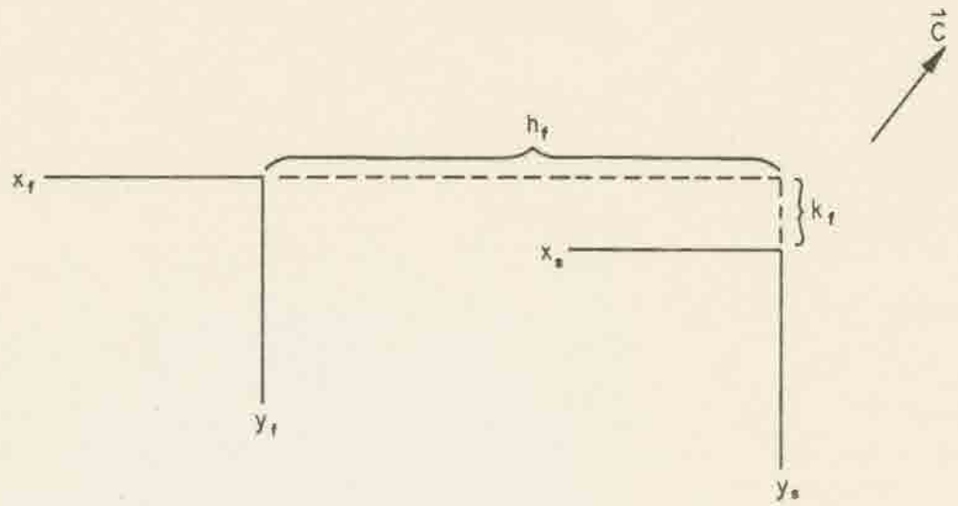

Figure A-3. Relation of AADS-2B measurement and (waterspout) translating coordinates in the horizontal plane.

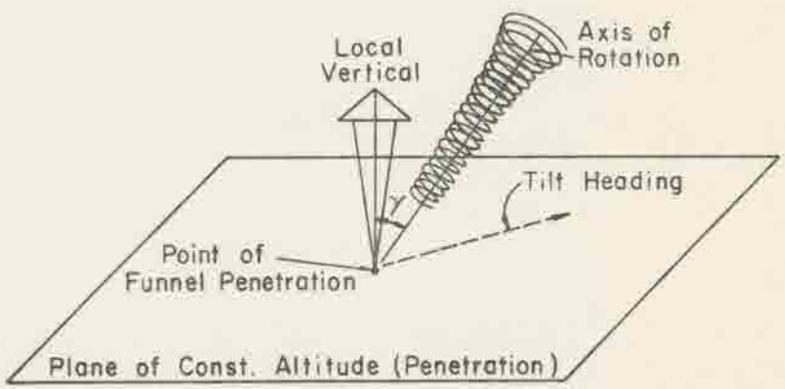

Figure A-4. Diagram illustrating the geometry of a waterspout funnel tilted from the local vertical.

$$\begin{pmatrix} x'' \\ y'' \\ z'' \end{pmatrix} = \begin{pmatrix} 1 & 0 & 0 \\ 0 & \cos\eta & -\sin\eta \\ 0 & \sin\eta & \cos\eta \end{pmatrix} \begin{pmatrix} \cos\lambda & 0 & \sin\lambda \\ 0 & 1 & 0 \\ -\sin\lambda & 0 & \cos\lambda \end{pmatrix} \begin{pmatrix} x_s \\ y_s \\ z_s \end{pmatrix}$$

$$= \begin{pmatrix} \cos\lambda & 0 & \sin\lambda \\ \sin\eta \sin\lambda & \cos\eta & -\sin\eta \cos\lambda \\ -\cos\eta \sin\lambda & \sin\eta & \cos\eta \cos\lambda \end{pmatrix} \begin{pmatrix} x_s \\ y_s \\ z_s \end{pmatrix}. \qquad \text{(A-8)}$$

Then

$$\begin{aligned} x'' &= x_s \cos\lambda + z_s \sin\lambda \\ y'' &= x_s \sin\eta \sin\lambda + y_s \cos\eta - z_s \sin\eta \cos\lambda \\ z'' &= x_s \cos\eta \sin\lambda + y_s \sin\eta + z_s \cos\eta \cos\lambda \end{aligned} \qquad \text{(A-9)}$$

and

$$\begin{aligned} x_s &= x'' \cos\lambda + y'' \sin\eta \sin\lambda - z'' \cos\eta \sin\lambda \\ y_s &= y'' \cos\eta + z'' \sin\eta \\ z_s &= x'' \sin\lambda - y'' \sin\eta \cos\lambda + z'' \cos\eta \cos\lambda \ . \end{aligned} \qquad \text{(A-10)}$$

The scalar equations of motion for the tilted system are as in (A-3) except velocities are now u", v", and w" and all derivatives are with respect to the new coordinates x", y", z". However, since we are working in a coordinate system tilted out of the vertical, components of $\vec{g}_e$ will now exist in the x" and y" directions as well as in the z" direction. From (A-9) it can be seen that

$$\begin{aligned} g_{e_{x''}} &= g_e \sin\lambda \\ g_{e_{y''}} &= -g_e \sin\eta \cos\lambda \\ g_{e_{z''}} &= g_e \cos\eta \cos\lambda \end{aligned} \qquad \text{(A-11)}$$

since $g_{e_{x_s}} = g_{e_{y_s}} = 0$ and $g_{e_{z_s}} = g_e$. Then the three components of the equation of motion in the tilted system simply take the form

$$\frac{du''}{dt} = -\frac{1}{\rho}\frac{\partial p}{\partial x''} - g_{e_{x''}} + 2(\omega_{z''}v'' - \omega_{y''}w'') + \frac{\mu}{\rho}\left[\nabla''^2 u'' + \frac{1}{3}\frac{\partial}{\partial x''}(\vec{\nabla}'' \cdot \vec{V}'')\right]$$

$$\frac{dv''}{dt} = -\frac{1}{\rho}\frac{\partial p}{\partial y''} - g_{e_{y''}} + 2(\omega_{x''}w'' - \omega_{z''}u'') + \frac{\mu}{\rho}\left[\nabla''^2 v'' + \frac{1}{3}\frac{\partial}{\partial y''}(\vec{\nabla}'' \cdot \vec{V}'')\right] \qquad \text{(A-12)}$$

$$\frac{dw''}{dt} = -\frac{1}{\rho}\frac{\partial p}{\partial z''} - g_{e_{z''}} + 2(\omega_{y''}u'' - \omega_{x''}v'') + \frac{\mu}{\rho}\left[\nabla''^2 w'' + \frac{1}{3}\frac{\partial}{\partial z''}(\vec{\nabla}'' \cdot \vec{V}'')\right].$$

The final coordinate transformation is made from the tilted cartesian system to a cylindrical system (r, θ, z) with both origins and z axes coinciding as per typical textbook example. The variables (r, θ, z) are related to (x", y", z") by the transformation equations (Fig. A-5)

$$\begin{aligned} x'' &= r\cos\theta & r &= (x''^2 + y''^2)^{\frac{1}{2}} \\ y'' &= r\sin\theta \qquad \text{(A-13)} & \theta &= \tan^{-1}(y''/x'') \\ z'' &= z & z &= z''. \end{aligned}$$

Differentiating with respect to time gives

$$\begin{aligned} u'' &= u\cos\theta - v\sin\theta & u &= u''\cos\theta + v''\sin\theta \\ v'' &= u\sin\theta + v\cos\theta \qquad \text{(A-14)} & v &= -u''\sin\theta + v''\cos\theta \\ w'' &= w & w &= w'' \end{aligned}$$

where u, v, and w correspond to the radial, tangential, and vertical waterspout velocities, respectively. The unit vectors $\hat{r}$, $\hat{\theta}$, $\hat{k}$ are related to the cartesian unit vectors, $\hat{i}''$, $\hat{j}''$, $\hat{k}''$ just as the velocity components in equations (A-14). Values of r increase positively outward from r = 0, and values of θ increase positively in the direction of a right-hand rotation about the z axis. The positive z direction is in the normal meteorological sense, i.e., towards increasing altitude.

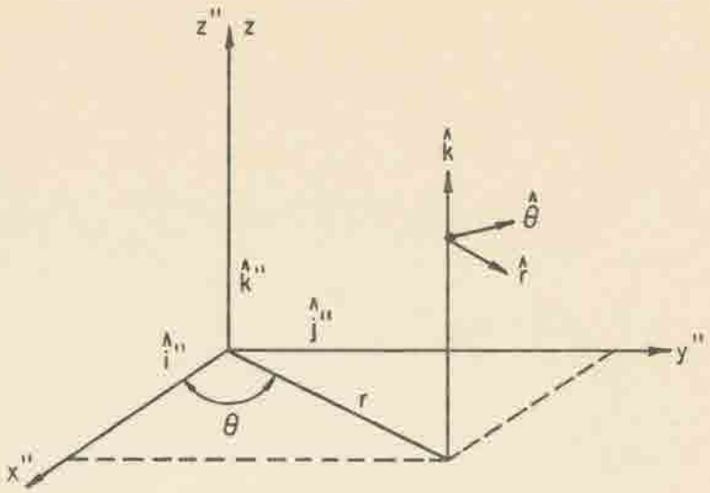

Figure A-5. Directions and unit vectors in cartesian and cylindrical coordinate systems.

Using the transformation equations (A-13) and (A-14), (A-12) becomes

$$\frac{du}{dt} - \frac{v^2}{r} = -\frac{1}{\rho}\frac{\partial p}{\partial r} - g_{e_r} + 2(\omega_z v - \omega_\theta w) + \frac{\mu}{\rho}\left[\nabla^2 u + \frac{1}{3}\frac{\partial}{\partial r}(\vec{\nabla}\cdot\vec{V})\right]$$

$$\frac{dv}{dt} + \frac{uv}{r} = -\frac{1}{\rho r}\frac{\partial p}{\partial \theta} - g_{e_\theta} + 2(\omega_r w - \omega_z u) + \frac{\mu}{\rho}\left[\nabla^2 v + \frac{1}{3r}\frac{\partial}{\partial \theta}(\vec{\nabla}\cdot\vec{V})\right]$$

$$\frac{dw}{dt} = -\frac{1}{\rho}\frac{\partial p}{\partial z} - g_{e_z} + 2(\omega_\theta u - \omega_r v) + \frac{\mu}{\rho}\left[\nabla^2 w + \frac{1}{3}\frac{\partial}{\partial z}(\vec{\nabla}\cdot\vec{V})\right].$$

The chain rule and equations (A-13) and (A-14) are used to derive the usual expressions for the differential operators d/dt, ∇^2, and $\vec{\nabla}\cdot\vec{V}$ in cylindrical coordinates. (A-15) is the final form of the equation of motion in cylindrical coordinates translating and tilted with the waterspout funnel.

Reprinted from MONTHLY WEATHER REVIEW, Vol. 105, No. 6, June 1977
American Meteorological Society
Printed in U. S. A.

Waterspout Wind, Temperature and Pressure Structure Deduced from Aircraft Measurements

VERNE H. LEVERSON AND PETER C. SINCLAIR

Department of Atmospheric Science, Colorado State University, Fort Collins 80523

JOSEPH H. GOLDEN[1]

Environmental Research Laboratories, NOAA, Boulder, Colo. 80302

(Manuscript received 13 August 1976, in revised form 28 February 1977)

ABSTRACT

During September 1974 in the Lower Florida Keys, the first successful penetrations of mature waterspouts were accomplished by a specially instrumented research aircraft. Throughout the course of each penetration, the measurement system recorded the temperature, the pressure and the three-dimensional velocity field near and within the visible funnel. Multiple penetrations of both cyclonic and anticyclonic waterspouts in various life-cycle stages were achieved. The results indicate that the waterspout funnel structure exhibits 1) a warm central core region, 2) positive vertical velocities of 5–10 m s^{-1} outside of the warm core, and 3) tangential velocities and horizontal pressure gradients with characteristics similar to but with magnitudes greater than those of the dust devil. A scale analysis of each term in the governing equations of motion suggests a simplified set of modeling equations. The simple Rankine-combined vortex model with cyclostrophic flow explains approximately 75% of the total measured pressure deficit. This compares favorably with Sinclair's (1966, 1973) earlier results for the dust devil vortex.

1. Introduction

The tornado continues to be one of the most enigmatic and elusive meteorological phenomena to understand. Every year, especially during the spring and summer months, the entire United States east of the Rockies is susceptible to the onslaught of tornadoes. Davies-Jones and Kessler (1974) reported that from 1953–72 an average of 113 persons were killed annually by tornadoes with a corresponding average annual property loss of $75 million. During the same period, only lightning caused a higher average annual number of human fatalities from severe storms. The worst tornado outbreak to affect the United States in recorded history occurred on 3–4 April 1974. Though well forecast, 148 tornadoes were responsible for over 300 deaths in about a 16 h period (Fujita, 1976). The continued urbanization of large parts of the United States increases the risk of tornado devastation in those areas each year. Furthermore, it must be recognized that our basic understanding of tornado structure and behavior is not complete; improvement in this understanding requires among other things more direct tornado observations.

The only direct quantitative assessments of tornado flow fields to date have been obtained by photogrammetric analysis of fortuitous eyewitness and news-media photography of tornadoes (Hoecker, 1960; Fujita, 1976; Agee *et al.*, 1975). Subsequent analyses of tornado damage and debris configurations on the ground (e.g., cycloidal suction swaths) have yielded useful but sometimes conflicting surface wind speed estimates (Fujita, 1970; Mehta *et al.*, 1971). The pressure and temperature profiles through tornadoes remain virtually unknown. Some success at purposefully intercepting, tracking and photographing tornadoes and their attendant cloud structures from a radio-equipped van on the ground has been reported (Golden and Morgan, 1972). Rotational and vertical flow components have been photogrammetrically derived in the debris and cloud-tags around a large tornado intercepted in Oklahoma (Golden and Purcell, 1974).

Because of the lack of accurate and sufficient tornado measurements, relatively slow progress has been made in numerical and laboratory modeling of small-scale convective vortices which have tornado-like features (e.g., Gutman, 1957; Kuo, 1966, 1969; Leslie, 1971; Ying and Chang, 1970; Ward, 1972). However, our analyses and those of others (Lilly, 1965) indicate that some of the assumptions inherent in these and other modeling attempts remain open to doubt until they can be checked with more quantitative observational data.

Improved understanding of tornado structure will not be forthcoming until we obtain much better mea-

[1] Research completed while this author was associated with National Severe Storms Laboratory, NOAA, Norman, Okla. 73069.

FIG 1. Subcloud severe storms measurement aircraft. The North American T-6 aircraft has been extensively modified to carry the AADS-2B system. The boom structure positions some of the sensing probes ahead of the aircraft to minimize fuselage-wing flow and pressure effects. The boom supports the Rosemount temperature sensor, pitot-static tube and the α, β vane system. The α and β vane units, along with the gyro-referenced platform, provide data on the vertical and lateral air motions near and within the severe storms. The vanes are constructed of lightweight balsawood and are internally mass balanced to improve the response characteristics. The boom is of aluminum-stainless steel construction and has a natural frequency of 11 Hz.

surements of the vortex wind, pressure and temperature fields. Because of the intensity and relatively short duration of the tornado vortex we do not have adequate instrumentation to accomplish the necessary observations. In order to guide us in the development of these observational systems and techniques, we have been studying a close relative to the tornado—the waterspout.[2] Golden (1974a,b) has given evidence which indicates strongly that waterspouts and tornadoes are qualitatively the same, but differ in only certain quantitative characteristics. These differences encompass vortex size and intensity, structure of the mesoscale environment, and intensity and organization of the parent convection. Preliminary measurements by Golden (1974a,b) and Church *et al.* (1973) have indicated from observations in Key West, Fla., where waterspouts frequently occur (Golden, 1970), that waterspout horizontal winds above the spray vortex maximum are approximately 25–35 m s^{-1} and the funnel core is slightly warmer than the environment.

The purpose of this paper is to provide some new data and insights on the distribution of wind, pressure and temperature near and within the waterspout funnel. The measurements are considered to be the first obtained by the direct penetration of the visible funnel with an instrumented research aircraft. The aircraft measurement system (Sinclair, 1973a, 1974b) was developed by the Severe Storm Measurement and Analysis Group (SSMAG) of the Atmospheric Science Department, Colorado State University (CSU). During the period 15–27 September 1974 the aircraft system was deployed to Key West. During this period, 16 waterspout funnels were penetrated up to 17 successive times each.

[2] We define the waterspout as an intense columnar vortex (usually containing a funnel cloud) of small horizontal extent which occurs over a body of water (Golden, 1971).

2. Airborne measurement technique

a. System requirements

In order to formulate a waterspout model which is physically more realistic than, for example, Gutman's (1957) numerical model, a measurement program of considerable detail as well as scope is required. Initially, this measurement program has been based primarily on the direct probing of the waterspout funnel, the parent cloud and the immediate environment of the funnel-cloud system. This requires the use of sophisticated airborne systems that are capable of accurately measuring physical and kinematic variables across and within the boundaries of the waterspout funnel. In addition, it is mandatory that measurements be made at several levels within the waterspout-cloud system and the environment in a systematic manner that permits optimum space-time interpretation of the data.

In addition to the multiple-level sampling requirements of the airborne platform, the measurement systems should be capable of recording the temperature, pressure, moisture, liquid water content and the three-dimensional velocity and turbulence structure of both the environment and the waterspout funnel-cloud system. The accuracy and space resolution of these measurements must be such that they are compatible with modeling requirements and possible cloud modification design requirements. For example, our past experience in cumulus-type cloud penetration measurements and modeling requirements indicates that the waterspout funnel-cloud system will probably require temperature and air velocity measurement accuracies of at least ± 0.1°C and ± 0.5 m s^{-1}, respectively. Also, adequate space resolution of data collected from an aircraft platform near and within the waterspout funnel requires instrument response times of 0.1 s. This virtually eliminates the use of the aircraft itself as part of the measurement system in the sensing of the wind velocity components in these regions of the waterspout.

b. System design

Over the past five years, several airborne measurement systems have been developed by SSMAG at Colorado State University. These systems have been or are presently being used to measure the three-dimensional velocity, temperature, pressure and humidity fields near and within severe storms. The

technology and some of the hardware of three Airborne Atmospheric Data Systems (AADS) [the North American T-6/T-28 AADS-2B, the Canadair T-33, AADS-3B (Sinclair 1969b) and the F-101B, AADS-4A (Sinclair, 1973a)] have been utilized in developing the waterspout project airborne measurement system. The AADS-2B (Fig. 1) in its present configuration is capable of obtaining direct measurements of the three-dimensional velocity field, temperature and pressure near and within the waterspout-cloud system. The measurement system is designed so as to be independent of the aircraft sensitivity to atmospheric motions and/or pilot-induced motions. The measurement technique (Sinclair, 1969b) requires knowledge of the motion of the air relative to the airplane ($V_{a,p}$) and the motion of the airplane relative to the ground ($V_{p,g}$) in order to calculate the atmospheric motion with respect to the ground ($V_{a,g}$); thus

$$\mathbf{V}_{a,g}=\mathbf{V}_{a,p}+\mathbf{V}_{p,g},$$

which for the vertical component ($w_{a,g}$) can be expressed as

$$w_{a,g}=V_T\alpha+V_T\beta\phi-V_T\theta+\int_0^t a_z dt+w_{p,g}(0)+L\dot{\theta},$$

where V_T is the true airspeed; α the angle of attack; θ, β and ϕ the pitch, yaw and roll angles, respectively; a_z the vertical acceleration of the aircraft; $w_{p,g}(0)$ the vertical motion of the aircraft at time $t=0$; $\dot{\theta}$ the pitch rate; and L the accelerometer displacement from the angle of attack measurement point. The measurement of α and β are made with lightweight, but durable, flow vanes. The aircraft pitch and roll angles and the pitch rate (ϕ) are measured with high precision vertical and rate gyros. Accelerations are measured by a three-axis accelerometer system at the aircraft center of gravity and the true airspeed is calculated from measurements of total ram and static pressures. Relatively fine structure of the turbulent velocity spectrum (0.04–10 Hz) can be obtained from the data which are recorded on a 1000 character per second, digital, incremental magnetic tape recorder. The AADS-2B permits detailed measurements of the visible funnel structure. That is, approximately 15–30 data points of all parameters are recorded for an average funnel diameter of 25 m. All funnel penetrations are made with a minimum of aircraft control and power changes. Ideally, the approach to the visible funnel proceeds from an initial point ~0.5 km upwind to the funnel boundary in a constant altitude mode. The funnel penetration is made with essentially constant attitude fixed controls at a constant altitude. A similar 0.5 km downwind track is accomplished after funnel penetration. This procedure allows space-time referencing of the AADS-2B and detection of the wind, pressure and temperature fields surrounding the visible funnel. The idealized flight track, however, must usually be modified to accomodate cloud and precipitation development.

Most of the AADS-2B system is mounted below the right wing of the T-6 aircraft in a modified T-33 drop tank (Fig. 1). The α, β vane system and pitot tube are mounted at the front of the instrumentation boom which extends from the nose of the drop tank to a point ahead of the plane of the propellor. Since vertical accelerations of the aircraft may range from ± 1–$3g$ incremental, it is imperative that only certain (many are negative g-limited) military stressed aircraft are used in and near the waterspout funnel. In addition, the aircraft must be fully aerobatic in order to recover easily from all possible attitudes. All commercial aircraft fail to meet either these airframe and maneuverability requirements or the instrumentation load capacity and low speed requirements, or both. These safety requirements and performance capabilities, while well-recognized by aircraft oriented organizations, have not always been appreciated by atmospheric research groups (RAND, 1968). We consider this type of system a necessary requirement for obtaining accurate pressure, temperature and wind measurements in the waterspout environment.

3. Penetration case studies

During the 12-day period from 16 September–27 September 1974, a total of 16 waterspouts were penetrated by the instrumented aircraft. The life-cycle stages of the penetrated waterspouts included all of Golden's (1974a,b,c) five documented stages except the spiral stage. Multiple penetrations were made on 7 of the 16 waterspouts, and in one case two cyclonic waterspouts were penetrated 26 successive times with no apparent effect on the vortex structure. The majority of the waterspouts ranged from weak to moderate in intensity, i.e., maximum upward vertical velocities <10 m s^{-1} and maximum tangential velocities <30 m s^{-1} at penetration attitudes of >400 m MSL.

In this section, three representative penetrations are presented in terms of horizontal profiles of vertical velocity, horizontal velocity, temperature and core pressure deficit. All velocities are measured relative to a cylindrical coordinate system fixed to and moving with the waterspout. The measurement technique has been designed such that the aircraft penetration track and the boom-vane system longitudinal axis pass through the spout center along the radial coordinate. That is, only the radial velocity component requires significant correction due to the combined motion of the waterspout and the aircraft. As a result, the transverse horizontal velocity v presented in this paper represents the waterspout's tangential velocity.

a. Cylonic waterspout

The first cyclonic waterspout was one of two adjacent cases documented at midday on 20 September. Both

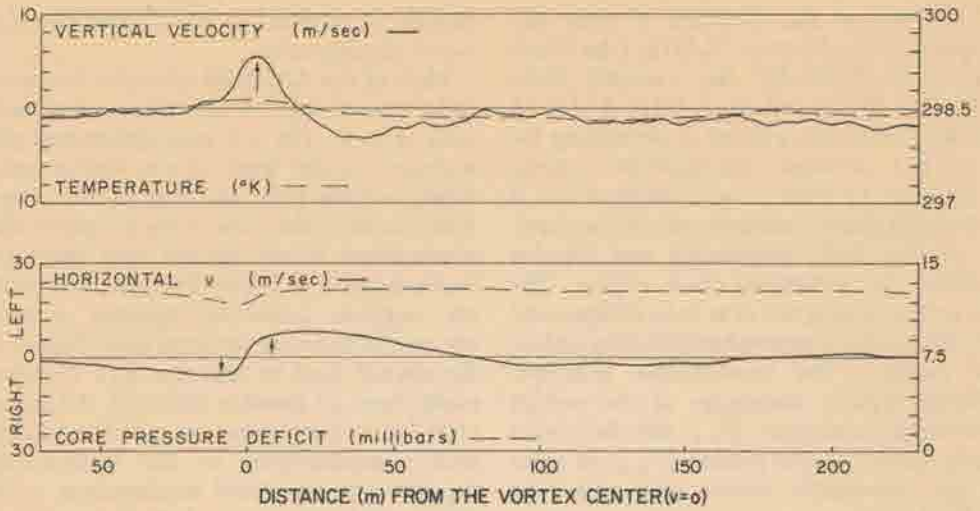

FIG. 2. Profiles of vertical velocity, horizontal velocity, temperature and pressure for a cyclonic waterspout along the penetration flight path. Horizontal velocities are directed to the left or right of the aircraft's direction of flight. Pressure is the deviation from an environmental reference pressure far from the funnel. The cyclonic waterspout occurred 20 September 1974. Penetration altitude was approximately 490 m, and the funnel diameter at the time of penetration was approximately 10–14 m.

spouts existed at the dark spot stage (Golden, 1973a) with funnel clouds extending down from cloud base approximately 100–150 m. The two waterspouts did not form simultaneously; the second was initially sighted approximately 16 min into the first waterspout's total lifetime of 23 min. The demise of the second spout occurred approximately 6 min after the first vortex decay.

Fig. 2 illustrates the horizontal profiles of vertical velocity, tangential velocity, temperature and core pressure deficit through the visible funnel. Each trace encompasses 5 s of data sampling.

The vertical velocity trace shows a singular, broad, quasi-symmetric peak of upward motion existing in the funnel, with maximum values of 5.8 m s^{-1}. A 2.9 m s^{-1} downdraft immediately behind the funnel rapidly (~1 s) approaches the near-waterspout environmental value of approximately −1 m s^{-1}. During the next 8 s of flight (not shown), the vertical velocity approaches zero before the aircraft penetrates the second waterspout.

The cyclonic flow of the waterspout is clearly shown in the tangential wind velocity profile[3] (Fig. 2). A broad circulation is evident, with the wind velocities decreasing slowly outward from the radius of maximum winds. Slight asymmetry in the v profile exists because v_{max} on the front and back sides (with respect to the penetration) of the waterspout is 5.4 and 8.5 m s^{-1}, respectively.

The temperature structure of the waterspout exhibits a positive anomaly of ~0.3 K that coincides with the maximum updraft velocities. This increase in temperature is similar to that found in dust devils (Sinclair 1966, 1973b) and results from the upward transport of warmer air from lower levels. Differing only in magnitude, this temperature profile, with a single positive peak, is similar to most other waterspouts penetrated.

The maximum core pressure deficit of ~1.3 mb coincides with the defined vortex center of $v=0$. Slightly less coincidence is shown between the minimum core pressure and the maximum positive values of temperature and vertical motion. These preliminary results, as well as the succeeding examples, show for the first time from direct measurements that the waterspout structure can be characterized by a warm, low-pressure vortex. This structure is very similar to that found by Sinclair (1966, 1973b, 1974a) for the upper levels of desert dust devils. Thus, two geophysical vortices formed by quite different initiating mechanisms exhibit similar structual characteristics. We suspect that comparable *in-situ* measurements near and within the tornado funnel will also show a warm, low-pressure vortex.

b. Intensifying anticyclonic waterspouts

The first of two penetrations through an anticyclonic waterspout is shown in Fig. 3. Again, only 5 s of data sampling is given in order to more clearly show the symmetry and coincidence of the temperature, pressure and wind profiles near and within the visible vortex. This waterspout was not penetrated until it had reached the spray vortex stage of its life cycle with a fully extended funnel from cloud base to sea surface. A second waterspout was penetrated after the one shown in Fig. 3, but it was significantly weaker and

[3] Note that all wind velocities are to be considered relative winds with respect to the vortex center, and that reference to front (forward) and near (back) sides of the waterspout is with respect to the aircraft penetration track.

was engulfed by a moderate rain shower after one penetration. The stronger waterspout (Fig. 3) lasted approximately 7 min after the first sighting. During the decay stage of the vortex, the rain shower almost completely wrapped around the funnel, and the upper one-third of the funnel was tilted about 60° from the vertical.

The vertical velocity profile shows an ambient, near-waterspout value of ~1.5 m s^{-1}. This rising motion increases gradually (in ~0.7 s) to a maximum of 6.8 m s^{-1} near the apparent waterspout center. Immediately after penetration an abrupt downdraft of 4.9 m s^{-1} was encountered. The remainder of the trace shows a return to the ambient upward vertical motions characteristic of the waterspout-cloud base environment. The weak subsidence in the funnel core inferred from previous observations (Golden, 1971, 1973a) may have been smoothed out because of small waterspout sizes and penetration speeds.

The waterspout's tangential wind velocity (v) field is marked by broad-scale circulation characteristics and slight asymmetry. The maximum values of v are 5.2 m s^{-1} on the forward side and 9.3 m s^{-1} on the rear of the waterspout.

The temperature and core pressure deficit traces exhibit maximum anomalies of +0.3 K and −3.2 mb, respectively. These values occur almost simultaneously with the maximum vertical velocity and lie approximately midway between the two v maxima.

c. Mature anticyclonic waterspout

The profiles in Fig. 4 are the results of a penetration of the same anticyclonic waterspout 1.5 min after the penetration shown in Fig. 3. In that amount of time the waterspout parameters have markedly intensified. This intensification can be due to either a strengthening of the mature vortex prior to decay or to an off-center penetration of the funnel during the first penetration (Fig. 3). The latter possibility would have reduced the magnitude of variation of all measured variables (except u) below that of the core values.

The vertical velocity trace shows a characteristic 1–2 m s^{-1} value in the near-waterspout environment prior to penetration. As the boom-vane system on the aircraft (Fig. 1) penetrates the spout, there is a rapid, almost instantaneous, increase in the vertical motion to a maximum value of ~ 8 m s^{-1}. From this maximum, the vertical velocity decreases much more slowly to the rear of the funnel. A distinct downdraft of ~3.5 m s^{-1} was again encountered on the backside following the penetration, in a region of developing heavy rain-showers.

The tangential wind velocities measured during this penetration were the strongest recorded during the 12-day program. The maximum values for v were 13.1 and 28.1 m s^{-1} for the front and back sides of the spout, respectively. Once again, asymmetry of the clockwise circulation is apparent. This asymmetric flow that has appeared in each of the presented cases appears to be due to one or both of the following factors: 1) neglect of the yaw accelerations of the aircraft during the penetrations, and 2) the slope of the waterspout funnel with respect to the aircraft penetration heading. Preliminary integration of the aircraft yaw accelerations has shown that a significant reduction in the measured asymmetry of the tangential wind profiles can be accomplished. It is anticipated that funnel slope corrections will also yield similar results. These corrections will be incorporated in a more detailed paper at a later date. However, taking into account the asymmetry of the flow, the tangential

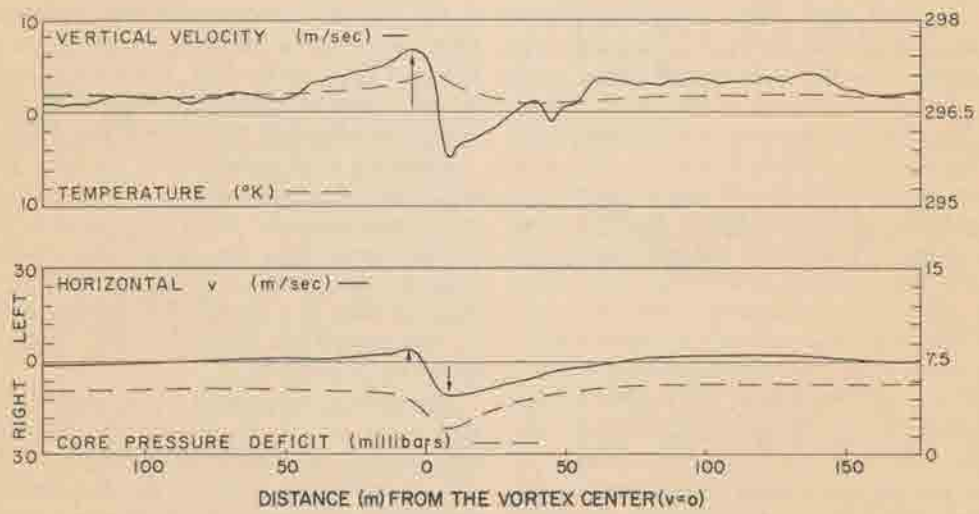

FIG. 3. As in Fig. 2 except for an intensifying anticyclonic waterspout. The anticyclonic waterspout occurred 20 September 1974. Penetration altitude was approximately 670 m and the funnel diameter at the time of penetration was approximately 15–20 m.

wind data indicate that the waterspout vortex closely approximates a Rankine-combined vortex. This will be further discussed in a following section.

The waterspout's temperature exhibits a sinusoidal variation with a positive core anomaly of 0.2 K that drops ~0.5 K to a minimum on the back side of the funnel. This profile differs from our other penetration data. Several explanations may be responsible for rapid cooling outside of the funnel, i.e., a slightly wet sensor, evaporative cooling, or vortex entrainment of cooler air from the rain shower within 3–4 funnel diameters of the visible spout.

The core pressure deficit shows an abrupt drop of 8.5 mb in pressure from the environment to the center of the funnel with a less rapid recovery on the back side of the funnel. This core of minimum pressure demonstrates good spatial correlation with the temperature maximum, the waterspout center where $v=0$, and the beginning of the rapid vertical velocity rise. The maximum values of v occur at 4–5 mb below the reference pressure, i.e., in the region of large $\partial p/\partial r$.

4. Scale analysis

To facilitate a quantitative description and to help formulate a model of the waterspout dynamic characteristics, the equations of motion have been reduced to a simplified set by a scale or order-of-magnitude analysis of each term. Characteristic magnitudes are obtained as representative values from the three case studies presented. The three scalar components of the vector equation of motion for steady-state, incompressible flow with constant eddy viscosity in cylindrical coordinates may be written

$$u\frac{\partial u}{\partial r}+\frac{v}{r}\frac{\partial u}{\partial \theta}+w\frac{\partial u}{\partial z}-\frac{v^2}{r}=-\frac{1}{\rho}\frac{\partial p}{\partial r}+K\left[\frac{\partial^2 u}{\partial r^2}+\frac{1}{r}\frac{\partial u}{\partial r}+\frac{1}{r^2}\frac{\partial^2 u}{\partial \theta^2}+\frac{\partial^2 u}{\partial z^2}\right], \quad (1)$$

$$u\frac{\partial v}{\partial r}+\frac{v}{r}\frac{\partial v}{\partial \theta}+w\frac{\partial v}{\partial z}+\frac{uv}{r}=-\frac{1}{\rho r}\frac{\partial p}{\partial \theta}+K\left[\frac{\partial^2 v}{\partial r^2}+\frac{2}{r}\frac{\partial v}{\partial r}+\frac{1}{r^2}\frac{\partial^2 v}{\partial \theta^2}+\frac{\partial^2 v}{\partial z^2}\right], \quad (2)$$

$$u\frac{\partial w}{\partial r}+\frac{v}{r}\frac{\partial w}{\partial \theta}+w\frac{\partial w}{\partial z}=-\frac{1}{\rho}\frac{\partial p}{\partial z}-g+K\left[\frac{\partial^2 w}{\partial r^2}+\frac{1}{r}\frac{\partial w}{\partial r}+\frac{1}{r^2}\frac{\partial^2 w}{\partial \theta^2}+\frac{\partial^2 w}{\partial z^2}\right], \quad (3)$$

where u, v, w are the mean wind components in the r, θ, z directions, respectively, p is the mean pressure, ρ the mean ambient air density, g the acceleration of gravity, and K a constant coefficient of eddy viscosity. Note also that the Coriolis acceleration terms are omitted since for small vortices such as waterspouts, dust devils, etc., they are known to be several orders of magnitude smaller than the remaining terms (Sinclair, 1966, 1969a).

Characteristic values for the components of the three-dimensional wind field are chosen from the strongest case presented in this paper, that shown in Fig. 4. This is done so as to represent realistic values of a moderately intense waterspout. The characteristic values selected are $v=25$ m s^{-1}, $w=8$ m s^{-1} and $u=1$ m s^{-1}. The value of u is based upon estimates from a large waterspout made by Golden (1974a) and applied to this somewhat weaker case. We take $r=40$ m, where r is the vortex scale radius (not necessarily the visible funnel), and $z\approx 40$ m, where z is the vertical distance between two successive funnel penetrations. These values are chosen from visual observations and the reduced data. Finally, a core pressure deficit Δp of 8.5 mb is selected.

In applying these characteristic values to each term of the r equation of motion, the inertial term for the centripetal acceleration (v^2/r) and the radial pressure gradient term are at least three orders of magnitude larger than the next largest term. Therefore, the r equation of motion can be approximated by $v^2/r=-\rho^{-1}\times(\partial p/\partial r)$ which is simply the cyclostrophic wind relation. This same reduction of the r equation has also been accomplished by Golden (1974a) from analysis of photographic data of the waterspout funnel and spray vortex. Sinclair (1966) has also shown for the dust devil vortex near the ground that the cyclostrophic relation accounts for most of the balance within the r equation (disregarding friction). While the assumption of cyclostrophic motion does give a fair estimate of the radial pressure distribution, and hence may be helpful in deducing total pressure drops in violent systems such as the tornado, the departure from cyclostrophic "balance" is in essence the basic feature of the waterspout and dust devil vortex flow. Consequently, other terms in the r equation must be retained in order to adequately describe and model these flow fields.

Assuming axial symmetry in the wind and pressure fields, the θ equation can be used to obtain an approximate mean value for K. A scale analysis of the three inertial terms and the three eddy viscosity terms indicates that $K\approx 40$ m^2 s^{-1}. This compares favorably with the value $K\approx 100$ m^2 s^{-1} found by Golden (1974a) for waterspouts and Sinclair's (1966) values of $\bar{K}=5$–15 m^2 s^{-1} for dust devils.

The vertical component of the equation of motion after scale analysis shows that the pressure gradient term is of the same order of magnitude as the acceleration of gravity, i.e., the vertical flow field is approximately in hydrostatic balance. However, the departures from hydrostatic balance produce many important waterspout features. If the terms with the largest

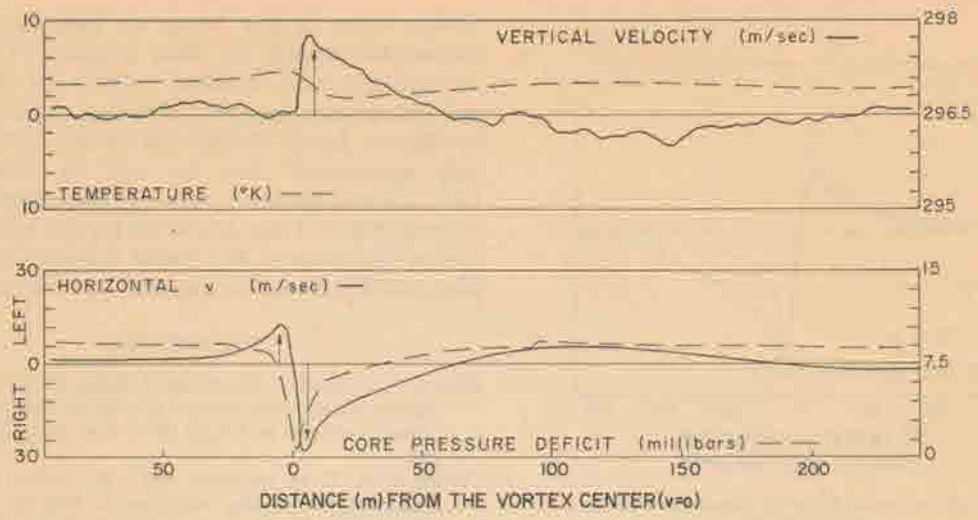

FIG. 4. As in Fig. 3 except for a mature anticyclonic waterspout. Penetration altitude was approximately 645 m and the funnel diameter at the time of penetration was approximately 15–20 m.

order of magnitude (shown in brackets below each term) are retained, the equation can be written

$$\underset{[0.1]}{u\frac{\partial w}{\partial r}}+\underset{[0.1]}{w\frac{\partial w}{\partial z}}=\underset{[10]}{-\frac{1}{\rho}\frac{\partial p}{\partial z}}\underset{[10]}{-g}+\underset{[0.1]}{K\frac{\partial^2 w}{\partial r^2}}+\underset{[0.1]}{K\frac{1}{r}\frac{\partial w}{\partial r}}. \quad (4)$$

Whether the two inertial terms may be appreciable remains to be investigated from a more detailed analysis of successive, multi-level funnel penetrations. A more detailed analysis is now being conducted in order to ascertain the importance of each term as a function of the radial and vertical coordinates. This will reveal the regions near and within the waterspout circulation where each term has significant importance.

5. Rankine-combined vortex

To obtain some idea of how well the waterspout measurements may be explained by a simple model, consider a steady circular vortex (cyclostrophic motion) with the tangential velocity described by a Rankine vortex, i.e., solid rotation in the core and irrotational motion outside of the core. Fig. 5 illustrates the closeness with which the Rankine vortex fits the tangential wind velocity trace of the mature anticyclonic waterspout (Section 3c). Adjusting for the asymmetric flow, the fit chosen seems to best represent the data. From the vortex core, where $v=0$, to the radius of maximum tangential winds, where $v=25$ m s^{-1}, the Rankine vortex exhibits a flow field in solid rotation, i.e., the tangential velocity is directly proportional to the radius of $v=c_1 r$. Outside the radius of maximum winds, the v field is one of irrotational motion or $v=c_2 r^{-1}$ (c_1 and c_2 are constants). The tangential field of motion closely approximates the $v=c_2 r^{-1}$ relationship on the front side of the funnel and $v=c_2 r$ relationship through the waterspout core. On the back side, however, the velocity trace beyond $v_{max}=28$ m s^{-1} departs markedly from the Rankine model, i.e., the v measurements more closely approach that of a $v=c_3 r^{-\frac{1}{2}}$ profile until an approximate value of 10 m s^{-1} is reached ($r\approx 28$ m). From this radius, v decreases linearly to zero at ~ 58 m.

The scale analysis of the r equation of motion indicates that the cyclostrophic relation is a valid first approximation for describing the tangential flow field in the upper levels of the waterspout funnel. If we use the Rankine-combined vortex to describe the tangential wind distribution, the cyclostrophic relation requires a total presure deficit of 6.23 mb. The measured waterspout pressure deficit was 8.50 mb. The simple cyclostrophic-Rankine-combined vortex model is thus capable of explaining approximately 75% of the total measured pressure deficit. This compares very favorably with Sinclair's (1966, 1973b) dust devil measurements which showed that this same simple model was capable of explaining approximately 75% of the total mean pressure drop from the environment to the dust devil center. With respect to the waterspout and the dust devil results, the discrepancy between the measured pressure deficit and that calculated from the simple cyclostrophic vortex model is attributed to the neglect of radial inflow and vertical motion in the model. Since radial inflow and vertical motion are characteristic of the waterspout structure at all altitudes, calculations of a core pressure deficit from the tangential wind field alone will obviously be less than the true value. In this case, inaccuracies based on the somewhat arbitrary fitting of the Rankine vortex must also certainly exist. Also, terms in the r equation of motion containing u may be of larger magnitude than that analyzed, particularily the inertial and turbulence terms containing $\partial u/\partial z$.

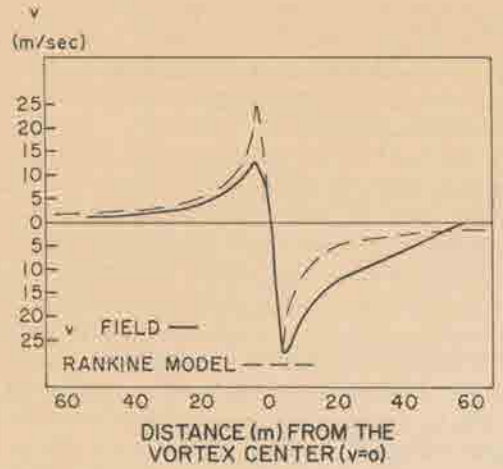

FIG. 5. Rankine model fit to the horizontal velocity profile of Fig. 4.

6. Conclusions

The waterspout velocity, temperature and pressure fields obtained by an airborne measurement system have been presented and examined to produce an integrated picture of the waterspout vortex structure in the near-cloud base environment. The data show that in the waterspout funnel there exist 1) a core of rising motion of 5–10 m s^{-1}, 2) a horizontal circular flow field that is broader in weaker waterspouts and spatially concentrated in more intense waterspouts, 3) a central core region ~0.3 K warmer than the environment, and 4) a core pressure deficit on the order of ~1–10 mb depending on waterspout intensity. Based on these data, some simplifications to the cylindrical, incompressible equations of motion have been made by an order-of-magnitude scale analysis of each term. While the present form of the reduced equations represent only a rough approximation, it has been shown that the cyclostropic relation and a Rankine-combined vortex model account for a considerable portion of the measured total pressure deficit. A more detailed measurement program was conducted during the 1975 waterspout season in order to document more fully the dynamic structure of larger and more intense waterspouts. Hopefully, these studies will lead to a greater insight into the waterspout's more energetic relative, the tornado.

Acknowledgments. The authors express their appreciation to the National Oceanic and Atmospheric Administration for their support under Grant 04-5002-8 which made this work possible and to the Nuclear Regulatory Commission for partial support in the data analysis phase of the research. Also we extend our gratitude to Mr. George Faraldo, Airport Manager of Key West International Airport, and Mr. Richard Urbanak, Meteorologist-in-Charge of the Weather Service Office in Key West, for their assistance and cooperation during the field program. The capable maintenance and technical support of the aircraft and instrumentation systems during the field program by Messrs. Jerrell Wilkey and Donald Hill are gratefully appreciated. Also we wish to thank Messrs. Lyle Lilie and Thomas Grove for their expert assistance in preparation of the AADS-2B for the field program. Special thanks go to Mr. David Younkin, the reserach pilot, and Ms. Karen Greiner who typed the manuscript.

REFERENCES

Agee, E., C. Church, C. Morris and J. Snow, 1975: Some synoptic aspects and dynamic features of vortices associated with the tornado outbreak of 3 April 1974. *Mon. Wea. Rev.*, **103**, 318–333.

Church, C. R., C. M. Ehresman and J. H. Golden, 1973: Instrumentation for probing waterspouts. *Preprints Eight Conf. Severe Local Storms*, Denver, Colo., Amer. Meteor. Soc., 169–172.

Davies-Jones, R. P., and E. Kessler, 1974: Tornadoes. *Weather and Climate Modification*, W. N. Hess, Ed., Wiley, 842 pp. (see Chap. 16).

Fujita, T. T., 1970: The Lubbock tornadoes: A study of suction spots. *Weatherwise*, **23**, 160–173.

——, 1976: Graphic examples of tornadoes. *Bull. Amer. Meteor. Soc.*, **57**, 401–412.

Golden, J. H., 1970: The lower Florida Keys waterspout project, May–Sept., 1969. *Bull. Amer. Meteor. Soc.*, **51**, 235–236.

——, 1971: Waterspouts and tornadoes over South Florida. *Mon. Wea. Rev.*, **99**, 146–154.

——, 1973a: The life cycle of the Florida Keys waterspout as the result of five interacting scales of motion. Ph.D. dissertation, Florida State University, 371 pp.

——, 1973b: Some statistical aspects of waterspout formation. *Weatherwise*, **26**, 108–117.

——, 1974a: Life cycle of Florida Keys waterspout. NOAA Tech. Memo. ERL-NSSL-70, National Severe Storms Lab., 247 pp.

——, 1974b: The life cycle of Florida Keys waterspout, I. *J. Appl. Meteor.*, **13**, 676–692.

——, 1974c: Scale interaction implications for the waterspout life cycle. II. *J. Appl. Meteor.*, **13**, 693–709.

——, and B. J. Morgan, 1972: The NSSL-Notre Dame tornado intercept program, spring 1972. *Bull. Amer. Meteor. Soc.*, **53**, 1178–1180.

——, and D. Purcell, 1974: Velocity and morphological analysis of Union City, Oklahoma tornado, May 24, 1973. *Trans. Amer. Geophys. Union*, **56**, p. 1130 (abstract).

Gutman, L. N., 1957: Theoretical model of a waterspout. *Bull. Acad. Sci. USSR Geophys. Ser.*, **1**, 87–103.

Hoecker, W. H., 1960: Wind speed and air flow patterns in the Dallas tornado of April 2, 1957. *Mon. Wea. Rev.*, **88**, 167–180.

Kessler, E., 1970: Tornadoes. *Bull. Amer. Meteor. Soc.*, **51**, 966–936.

Kuo, H. L., 1966: On the dynamics of convective atmospheric vortices. *J. Atmos. Sci.*, **23**, 25–42.

——, 1969: Axially-symmetric flows in the boundary layer of a maintained vortex. Planetary Circulation Project, Rep. No. 15, Dept. Geophys. Sci., University of Chicago, 57 pp.

Leslie, L. M., 1971: The development of concentrated vortices: A numerical study. *J. Fluid Mech.*, **48**, 1–21.

Lilly, D. K., 1965: Experimental generation of convectively driven vortices. *Geofis. Intern.*, **5**, 43–48.

Mehta, K. C., J. R. McDonald, J. E. Minor and A. J. Sanger, 1971: Response of structural systems to the Lubbock storm. Storm Res. Rep. 03, Institute for Disaster Research, 428 pp.

RAND, 1968: Weather modification progress and the need for interactive research. Tenth Annual Report, NSF.

Sinclair, P. C., 1966: A quantitative analysis of the dust devil. Ph.D. dissertation, University of Arizona, 292 pp.

——, 1969a: General characteristics of dust devils. *J. Appl. Meteor.*, **8**, 32–45.

——, 1969b: Vertical motion and temperature structure of severe convective storms. *Preprints Sixth Conf. Several Local Storms*, Chicago, Ill., Amer. Meteor. Soc., 346–350.

——, 1973a: Severe storm air velocity and temperature structure deduced from penetrating aircraft. *Preprints Eighth Conf. Severe Local Storms*, Denver, Colo., Amer. Meteor. Soc., 25–32.

——, 1973b: The lower structure of dust devils. *J. Atmos. Sci.*, **30**, 1599–1619.

——, 1974a: Vertical transport of desert particulates by dust devils and clear thermals. *Proc. Atmosphere-Surface Exchange of Particulate and Gaseous Pollutants*, Richland, Wash., Atomic Energy Commission, 497–527.

——, 1974b: Severe storm turbulent energy structure. Preprints *Sixth Conf. Aerospace and Aeronautical Meteor.*, El Paso, Tex., Amer. Meteor. Soc., 36–39.

Ward, N. B., 1972: The exploration of certain features of tornado dynamics using a laboratory model. *J. Atmos. Sci.*, **29**, 1194–1204.

Ying, S. J., and C. C. Chang, 1970: Exploratory model study of tornado-like vortex dynamics. *J. Atmos. Sci.*, **27**, 3–14.

Reprinted from Preprint Volume, Ninth Conference on Severe Local Storms, Oct. 21-23, 1975, Norman, Okla. Published by Amer. Meteor. Soc., Boston, Mass.

WATERSPOUT WIND, TEMPERATURE, AND PRESSURE STRUCTURE DEDUCED FROM AIRCRAFT MEASUREMENTS

Verne H. Leverson and Peter C. Sinclair

Colorado State University
Fort Collins, Colorado

Joseph H. Golden

National Severe Storms Laboratory
Norman, Oklahoma

1. INTRODUCTION

The tornado continues to be one of the most enigmatic and elusive meteorological phenomena to understand. Every year, especially during the spring and summer months, the entire United States east of the Rockies is susceptible to the onslaught of tornadoes. Kessler (1970) reported that from 1955-1969 an average of 125 persons were killed annually by tornadoes with a corresponding average annual property loss of $75 million. During the same period, only lightning caused a higher average annual number of human fatalities from severe storms. The past two years have seen record numbers of U.S. tornadoes; in 1973 there were 1104 tornado sightings with 89 associated deaths and about $300 million in property damage. The worst tornado outbreak to affect the United States in the past 90 years occurred on April 3-4, 1974. Though well forecast, nearly 150 tornadoes were responsible for 300 deaths in just an 18-hour period (Fujita, 1974). The continued urbanization of large parts of the United States increases the risk of tornado devastation in those areas each year. Furthermore, it must be recognized that our basic understanding of tornado structure and behavior is rather poor; improvement in this understanding requires more direct tornado observations. The synthesis of these new tornado observations should assist the development of improved tornado warnings and protective building design measures.

The only direct quantitative assessments of tornado flow fields to date have been obtained by photogrammetric analysis of fortuitous eyewitness and news-media photography of tornadoes (Hoecker, 1960, Fujita, 1974). Subsequent analyses of tornado damage and debris configurations on the ground (e.g., cycloidal suction swaths) have yielded useful but sometimes conflicting surface windspeed estimates (Fujita, 1970, Mehta et. al., 1971). The pressure and thermal profiles through tornadoes remain virtually unknown. Direct observations of tornadoes are still very difficult to obtain because of our inability to make pinpoint forecasts, and this situation is likely to continue for sometime into the future. Some success at purposefully intercepting, tracking and photographing tornadoes and their attendant cloud structures from a radio-equipped van on the ground have been reported (Golden and Morgan, 1972). Rotational and vertical flow components have been photogrammetrically derived in the debris and cloud-tags around a large tornado intercepted in Oklahoma (Golden and Purcell, 1974a).

Some progress has been made in numerical and laboratory modelling of small scale convective vortices (e.g. Gutman, 1957, Kuo, 1966, 1969, Leslie, 1971, Ying and Chang, 1970, and Ward, 1972). However, some of the assumptions inherent in these modelling attempts remain open to doubt until they can be checked with more quantitative observational data (Lilly, 1965). In particular, feasible modification schemes are not easily promulgated because of the lack of sufficient quantitative information on the vortex-parent cloud structure and energetics.

Golden (1974a, b) has given evidence which indicates strongly that waterspouts and tornadoes are qualitatively the same, but differ in only certain quantitative characteristics. These differences encompass vortex size and intensity, structure of the mesoscale environment and intensity and organization of the parent convection. Moreover, Golden (1973a) has shown that waterspouts are much more amenable to close-range field observations than tornadoes. Waterspouts occur more frequently in a small area of the Florida Keys than anywhere else in the world (Golden, 1973b), and nearly 400 waterspouts have been documented there during one May-September season (Golden, 1970). Golden (1974a, b) used photogrammetric analysis of aircraft film data to derive horizontal windspeeds through waterspout spray vortices and vertical windspeeds in the funnel walls. The first successful attempts at probing waterspout funnels with a sensor package towed behind a light aircraft (Golden, 1970) were made by Church et. al. (1973). The Purdue waterspout probe gave some interesting temperature profiles through the waterspout core and its near environment, but unstable oscillations encountered during funnel penetration prevent accurate measurement of winds and pressure (Church et. al., 1973).

The purpose of this paper is to provide some new data and insights as to the distribution of wind, pressure, and temperatue near and within the waterspout funnel. The measurements are considered to be the first obtained by the direct

penetration of the visible funnel with an instrumented research aircraft. The aircraft measurement system (Sinclair, 1973a, 1974b) was developed by the Severe Storm Measurement and Analysis Group (SSMAG) of the Atmospheric Science Department, Colorado State University (CSU). During the period September 15-27, 1974 the aircraft system was deployed to Key West, Florida. During this period, 16 waterspout funnels were penetrated up to 17 successive times each.

2. AIRBORNE MEASUREMENT TECHNIQUE

2.1 System Requirements

In order to formulate a waterspout model which is physically more realistic than current models, a measurement program of considerable detail as well as scope is required. Initially, this measurement program has been based primarily on the direct probing of the waterspout funnel, the parent cloud, and the immediate environment of the funnel-cloud system. This requires the use of sophisticated airborne systems that are capable of accurately measuring physical and kinematic variables across and within the boundaries of the waterspout funnel. In addition, it is mandatory that measurements are made at several levels within the waterspout-cloud system and the environment in a systematic manner that permits optimum space-time interpretation of the data.

In addition to the multiple level sampling requirements of the airborne platform, the measurement systems should be capable of recording the temperature, pressure, moisture, liquid water content and the three-dimensional velocity and turbulence structure of both the environment and the waterspout funnel-cloud system. The accuracy and space resolution of these measurements must be such that they are compatible with modelling requirements and possible cloud modification design requirements. For example, our past experience in severe storm penetration measurements and modelling requirements indicates that the waterspout-cloud system will require similar temperature and air velocity measurement accuracies, i.e., ± 0.1°C and ± 0.5 m sec^{-1}, respectively. Also, adequate space resolution of data collected from an aircraft platform near and within the waterspout funnel requires instrument response times of 0.1 sec. This virtually elimates the use of the aircraft itself as part of the measurement system in the sensing of the wind velocity components in these regions of the waterspout.

2.2 System Design

Over the past five years, several airborne measurement systems have been developed by SSMAG at Colorado State University. These systems have been or are presently being used to measure the three dimensional velocity, temperature, pressure and humidity fields near and within severe storms. The technology and some of the hardware of three Airborne Atmospheric Data Systems (AADS): the North American T-6/T-28 AADS-2B, the Canadair T-33, AADS-3B (Sinclair 1969b) and the F-101B, AADS-4A (Sinclair 1973a) has been utilized in developing the waterspout project airborne measurement system. The AADS-2B (Figure 1) in its present configuration is capable of obtaining direct measurements of the three-dimensional velocity field, temperature, and pressure near and within the waterspout-cloud system. The measurement system is designed so as to be independent of the aircraft sensitivity to atmospheric motions and/or pilot induced motions. The measurement technique (Sinclair, 1969b) requires knowledge of the motion of the air relative to the airplane ($V_{a,p}$) and the motion of the airplane relative to the ground ($V_{p,g}$) in order to calculate the atmospheric motion with respect to the ground ($V_{a,g}$), thus:

$$V_{a,g} = V_{a,p} + V_{p,g}$$

which for the vertical component ($w_{a,g}$) can be expressed as

$$w_{a,g} = V_T\alpha + V_T\beta\phi - V_T\theta + \int_o^t a_z dt + w_{p,g}(o) + L\dot{\theta}$$

where V_T is the true airspeed; α the angle of attack; θ, β, and ϕ the pitch, yaw, and roll angles, respectively; a_z the vertical acceleration of the aircraft; $w_{p,g}(o)$ the vertical motion of the aircraft at time $t = o$; $\dot{\theta}$ the pitch rate; and L the accelerometer displacement from the angle of attack measurement point. The measurement of α and β are made with lightweight, but durable, flow vanes. The pitch (θ), pitch rate ($\dot{\theta}$), and roll (ϕ) angles are measured with high precision vertical and rate gyros. Accelerations are measured by a three-axis accelerometer system at the aircraft c.g., and the true airspeed is calculated from measurements of total ram and static pressures. Relatively find structure of the turbulent velocity spectrum (0.04 to 10 cycles sec^{-1}) can be obtained from the data which is recorded on a 1000 character per second, digital, incremental magnetic tape recorder. The AADS-2B will permit detailed measurements of the visible funnel structure. That is, approximately 15-30 data points of all parameters are recorded for an average funnel diameter of 25 m. All funnel penetrations are made with a minimum of aircraft control and power changes. Ideally, the approach to the visible funnel proceeds from an I.P. approximately 1/4 mile upwind to the funnel boundary in a constant altitude mode. The funnel penetration is made with essentially constant attitude fixed controls at a constant altitude. A similar 1/4 mile downwind track is accomplished after funnel penetration. This procedure allows space-time referencing of the AADS-2B and detection of the wind, pressure, and temperature fields surrounding the visible funnel. The idealized flight track must be, however, usually modified to accomodate cloud and precipitation development.

Most of the AADS-2B system is mounted below the right wing of the T-6 aircraft in a modified T-33 drop tank (Figure 1). The α-β vane system and pitot tube are mounted at the front of the instrumentation boom which extends from the nose of the drop tank to the point ahead of the plane of the propellor. Since vertical accelerations of the aircraft may range from $\pm$ 1-3g incremental, it is imperative that only certain (many are negative g-limited) military stressed aircraft are used in and near the waterspout funnel. In addition, the aircraft must be fully aerobatic in order to recover easily from all possible attitudes. All commercial aircraft fail to meet either these airframe and maneuverability requirements or the instrumentation load capacity and low speed

Figure 1; Sub-Cloud Severe Storms Measurement Aircraft

The North American T-6 aircraft has been extensively modified to carry the AADS-2B system. The boom structure positions some of the sensing probes ahead of the aircraft to minimize fuselage-wing flow and pressure effects. The boom supports the Rosemount temperature sensor, pitot-static tube and the α-β vane system. The α and β vane units, along with the gyro referenced platform, provide data on the vertical and lateral air motions near and within the severe storms. The vanes are constructed of lightweight balsawood and are internally mass balanced to improve the response characteristics. The boom is of aluminum-stainless steel construction and has a natural frequency of 11 cps.

requirements, or both. These safety requirements and performance capabilities, while well-recognized by aircraft oriented organizations, have not always been appreciated by atmospheric research groups (RAND Report, 1968). We consider this type of system a necessary requirement for obtaining accurate pressure, temperature, and wind measurements in the waterspout environment.

3. PENETRATION CASE STUDIES

During the twelve day period from 16 September thru 27 September, a total of 16 waterspouts were penetrated by the instrumented aircraft. The life cycle stages of the penetrated waterspouts included all of Golden's (1974a, b,c) five documented stages except the spiral stage. Multiple penetrations occurred on 7 of the total 16, and in one case two cyclonic waterspouts were penetrated twenty-six successive times. The majority of the waterspouts ranged from weak to moderate in intensity, i.e., maximum vertical velocities ≤ 10 m-sec^{-1} and maximum tangential velocities ≤ 30 m-sec^{-1}.

In this section, three representative penetrations are presented in terms of horizontal profiles of vertical velocity, tangential velocity, temperature, and core pressure deficit. Of the three selected penetrations one is cyclonic, the other two anticyclonic. The two anticyclonic traces are successive penetrations of the same waterspout.

3.1 Cyclonic Waterspout

The first cyclonic waterspout was one of two adjacent cases documented at midday on September 20. Both spouts existed at the dark spot stage (Golden, 1973a) with funnel clouds extending down from cloud base approximately 100-150 . The

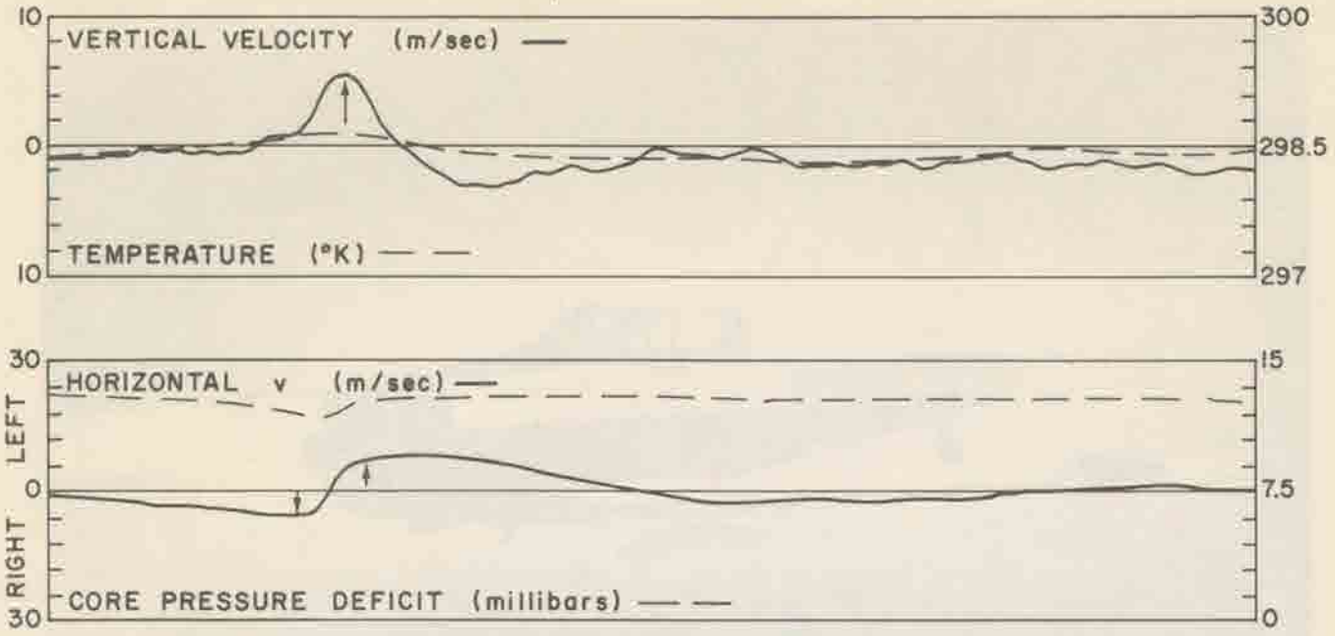

Figure 2: Cyclonic Waterspout

two waterspouts did not form simultaneously; the second was initially sighted approximately 16 minutes into the first waterspout's total lifetime of 23 minutes. The demise of the second spout occurred approximately 6 minutes after the first vortex decay.

Figure 2 illustrates the horizontal profiles of vertical velocity, tangential velocity, temperature, and core pressure deficit through the visible funnel. Each trace encompasses five seconds of data sampling.

The vertical velocity trace shows a singular, broad quasi-symmetric peak of upward motion existing in the funnel, with maximum values of 5.8 m sec^{-1}. A 2.9 m sec^{-1} downdraft immediately behind the funnel rapidly ($\sim$ 1 sec) approaches the near-waterspout environmental value of approximately -1 m-sec^{-1}. During the next 8 seconds of flight, (not shown), the vertical velocity approaches zero before the aircraft penetrates the second waterspout.

The cyclonic flow of the waterspout is clearly shown in the tangential wind velocity profile[1] (Figure 2). A broad circulation is evident, with the wind velocities decreasing slowly outward from the radius of maximum winds. Slight asymmetry in the v profile exists because v_{MAX} on the front and back sides (with respect to the penetration) of the waterspout is 5.4 and 8.5 m-sec^{-1}, respectively.

The temperature structure of the waterspout exhibits a positive anomaly of approximately .3°K that coincides with the maximum updraft velocities. This increase in temperature results from the upward transport of warmer air from lower levels. Differing only in magnitude, this temperature profile, with a single positive peak, is similar to most other waterspouts penetrated during the field program.

The maximum core pressure deficit of approximately 1.3 mb. coincides with the defined vortex center of v = 0. Slightly less coincidence is shown between the minimum core pressure and the maximum positive values of temperature and vertical motion. These preliminary results, as well as the succeeding examples, show for the first time from direct measurements, that the waterspout structure can be characterized by a warm, low pressure vortex. This structure is very similar to that found by Sinclair (1966, 1973b, 1974a) for the upper levels of desert dust devils.

3.2 Intensifying Anticyclonic Waterspout

The first of two penetrations through an anticyclonic waterspout is shown in Figure 3. Again, only five seconds of data sampling are given in order to more clearly show the symmetry and coincidence of the temperature, pressure, and wind profiles near and within the visible vortex. This waterspout was not penetrated until it had reached the spray vortex stage of its life cycle with a fully extended funnel from cloud base to sea surface. A second waterspout was penetrated after the one shown in Figure 3, but it was significantly weaker and was engulfed by a moderate rain shower after one penetration. The stronger waterspout (Figure 3) lasted approximately seven minutes after the first sighting. During the decay stage of the vortex, the rain shower almost completely wrapped around the funnel, and the upper one third of the funnel was tilted about 60° from the vertical.

The vertical velocity profile shows an ambient, near-waterspout value of approximately 1.5 m-sec^{-1}. This rising motion increases gradually,

[1] Note that: (1) all wind velocities are to be considered relative winds with respect to the vortex center, and (2) reference to front (forward) and near (back) sides of the waterspout is with respect to the aircraft penetration track.

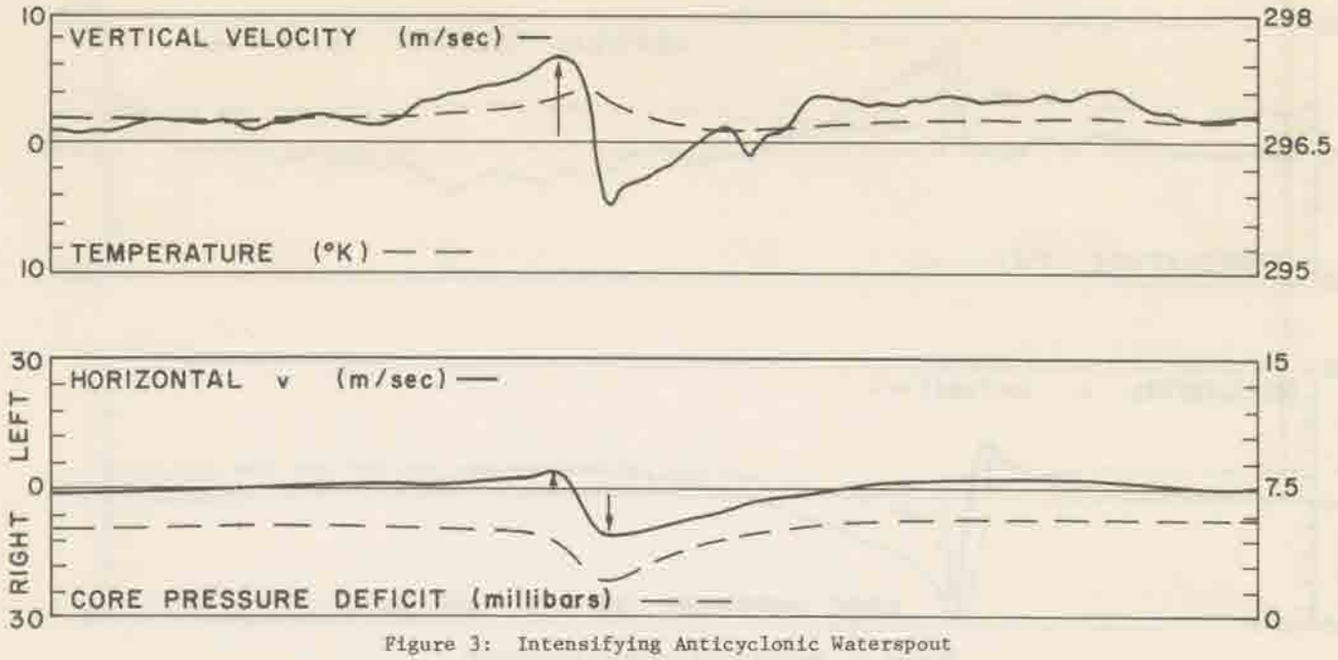

Figure 3: Intensifying Anticyclonic Waterspout

in approximately .7 second, to a maximum 6.8 m-sec^{-1} near the apparent waterspout center. Immediately after penetration an abrupt downdraft of 4.9 m-sec^{-1} was encountered. The remainder of the trace shows a return to the ambient upward vertical motions characteristic of the waterspout-cloud base environment.

The waterspout's tangential wind velocity (v) field is marked by broad-scale circulation characteristics and slight asymmetry. The maximum values of v are 5.2 m-sec^{-1} on the forward side and 9.3 m-sec^{-1} on the rear of the waterspout.

The temperature and core pressure deficit traces exhibit maximum anomalies of .3°K and 3.2 mb, respectively. These values occur almost simultaneously with the maximum vertical velocity and lie approximately midway between the two v maxima.

3.3 Mature Anticyclonic Waterspout

The profiles in Figure 4 are the results of a penetration of the same anticyclonic waterspout 1.5 minutes after the penetration shown in Figure 3. In that amount of time the waterspout parameters have markedly intensified. This intensification can be due to either a strengthening of the mature vortex prior to decay or to an off-center penetration of the funnel during the first penetration (Figure 3). The latter possibility would have reduced the magnitude of all of the measured variables below that of the core values.

The vertical velocity trace shows a characteristic 1-2 m-sec^{-1} value in the near-waterspout environment prior to penetration. As the boom-vane system on the aircraft (Figure 1) penetrates the spout, there is a rapid, almost instantaneous, increase in the vertical motion to a maximum value of approximately 8 m-sec^{-1}. From this maximum, the vertical velocity decreases much more slowly to the rear of the funnel. A definite downdraft of ~3.5 m-sec^{-1} was again encountered on the backside following the penetration, in a region of developing heavy rainshowers.

The tangential wind velocities measured during this penetration were the strongest recorded during the twelve day program. The maximum values for v were 13.1 m-sec^{-1} and 28.1 m-sec^{-1} for the front and backsides of the spout, respectively. Once again, asymmetry of the clockwise circulation is apparent. This asymmetric flow that has been documented for more than one case, may be partially due to the response characteristics of the gust vane-gyro reference platform. This uncertainty will be removed in a more detailed paper at a later date. However, taking into account the asymmetry of the flow, the tangential wind data indicates that the waterspout vortex closely approximates a Rankine-Combined vortex. This will be further discussed in a following section.

The waterspout's temperature exhibits a sinusoidal variation with a positive core anomaly of .2°K that drops approximately .5°K to a minimum on the back side of the funnel. This profile differs from our other penetration data. Several explanations may be responsible for rapid cooling outside of the funnel, i.e. (1) a slightly wet sensor, (2) evaporative cooling, or (3) vortex entrainment of cooler air from the rain shower within 3-4 funnel diameters of the visible spout.

The core pressure deficit shows an abrupt drop of 8.5 mb in pressure from the environment to the center of the funnel with a less rapid recovery on the backside of the funnel. This core of minimum pressure demonstrates good spatial correlation with: (1) the temperature maximum, (2) the waterspout center where v = 0, and (3) the beginning of the rapid vertical velocity rise. The maximum values of v occur at 4-5 mb. below the reference pressure, i.e. in the region of large $\partial p/\partial r$.

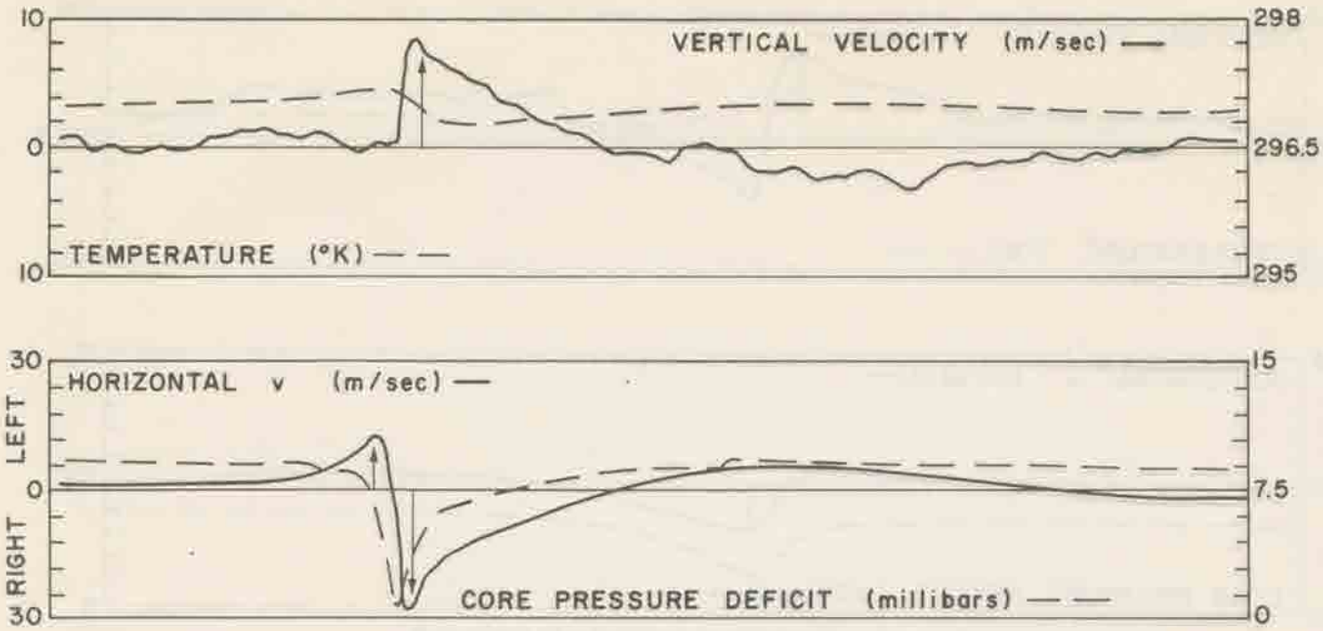

Figure 4: Mature Anticyclonic Waterspout

4. SCALE ANALYSIS

To faciliitate a quantitative description and to help formulate a model of the waterspout dynamic characteristics, the equations of motion have been reduced to a simplified set by a scale analysis of each term. Characteristic magnitudes are obtained as representative values from the three case studies presented in this paper. The three scalar components of the vector equation of motion for steady state, incompressible flow with constant eddy viscosity in cylindrical coordinates may be written:

$$u\frac{\partial u}{\partial r} + \frac{v}{r}\frac{\partial u}{\partial \theta} + w\frac{\partial u}{\partial z} - \frac{v^2}{r} = \frac{1}{\rho}\frac{\partial p}{\partial r} + K\left[\frac{\partial^2 u}{\partial r^2} + \frac{1}{r}\frac{\partial u}{\partial r} + \frac{1}{r^2}\frac{\partial^2 u}{\partial \theta^2} + \frac{\partial^2 u}{\partial z^2}\right] \quad (1)$$

$$u\frac{\partial v}{\partial r} + \frac{v}{r}\frac{\partial v}{\partial \theta} + w\frac{\partial v}{\partial z} + \frac{uv}{r} = -\frac{1}{\rho r}\frac{\partial p}{\partial \theta} + K\left[\frac{\partial^2 v}{\partial r^2} + \frac{2}{r}\frac{\partial v}{\partial r} + \frac{1}{r^2}\frac{\partial^2 v}{\partial \theta^2} + \frac{\partial^2 v}{\partial z^2}\right] \quad (2)$$

$$u\frac{\partial w}{\partial r} + \frac{v}{r}\frac{\partial w}{\partial \theta} + w\frac{\partial w}{\partial z} = -\frac{1}{\rho}\frac{\partial p}{\partial z} - g + K\left[\frac{\partial^2 w}{\partial r^2} + \frac{1}{r}\frac{\partial w}{\partial r} + \frac{1}{r^2}\frac{\partial^2 w}{\partial \theta^2} + \frac{\partial^2 w}{\partial z^2}\right] \quad (3)$$

where u, v, and w are the mean wind components in the r, θ, and z directions, respectively, p is the mean pressure, ρ is the mean ambient air density, g is the acceleration of gravity, and K is a constant coefficient of eddy viscosity. All velocities are measured relative to a cylindrical coordinate system fixed to and moving with the waterspout. The measurement technique has been designed such that the aircraft penetration track and the boom-vane system longitudinal axis pass through the spout center along the radial coordinate. That is, only the radial velocity component requires significant correction due to the combined motion of the waterspout and the aircraft. Note also that the Coriolis acceleration terms are omitted since for small vortices such as waterspouts, dust devils, etc., they are known to be several orders of magnitude smaller than the remaining terms (Sinclair, 1966, 1969a).

Characteristic values for the components of the three dimensional wind field are chosen from the strongest case presented in this paper, Figure 4. This is done so as to represent realistic values of a moderately intense waterspout. The characteristic values selected are $v = 25$ m-sec^{-1}, $w = 8$ m-sec^{-1}, and $u = 1$ m-sec^{-1}. The value of u is based upon estimates from a large waterspout made by Golden (1974a) and applied to this somewhat weaker case. We take $r = 40$ m, where r is the vortex scale radius (not necessarily the visible funnel), and $z \sim 150$ m, where is the vertical distance between two successive funnel penetrations. These values are chosen from visual observations and the reduced data. Finally, a core pressure deficit, Δp, of 8.5 mb is selected.

In applying these characteristic values to each term of the r equation of motion, the inertial term for the centripetal acceleration, v^2/r, and the radial pressure gradient term are at least three orders of magnitude larger than the next largest term. Therefore, the r-equation of motion can be approximated by $v^2/r = 1/\rho\ [\partial p/\partial r]$ which is simply the cyclostrophic wind relation. This same reduction of the r-equation has also been accomplished by Golden (1974a) from analysis of photographic data of the waterspout funnel and spray vortex. Sinclair (1966), has also shown for the dust devil vortex near the ground that the cyclostrophic relation accounts for most of the balance within the r-equation (disregarding friction). While the assumption of cyclostrophic motion does give a fair estimate of the radial pressure

distribution, and hence may be helpful in deducing total pressure drops in violent systems such as the tornado, the departure from cyclostrophic "balance" is in essence the basic feature of the waterspout and dust devil vortex flow. Consequently, other terms in the r-equation must be retained in order to adequately describe and model these flow fields.

Assuming axial symmetry in the wind and pressure fields, the θ-equation can be used to obtain an approximate value for K for dust devils. A scale analysis of the three inertial terms and the three eddy viscosity terms, indicates that $K \simeq 40\ m^2 sec^{-1}$. This compares favorably with the value $K \sim 100 m^2\ sec^{-1}$ found by Golden (1974a) for waterspouts and Sinclair's (1966) values of $K=5\text{-}15 m^2 sec^{-1}$.

The vertical component of the equation of motion after scale analysis shows that the pressure gradient term is of the same order of magnitude as the acceleration of gravity, i.e., the vertical flow field is approximately in hydrostatic balance. If the terms with the three largest orders of magnitude (shown in [] below each term) are retained, the equation can be written as:

$$u\frac{\partial w}{\partial r} + w\frac{\partial w}{\partial z} = -\frac{1}{\rho}\frac{\partial p}{\partial z} - g + K\frac{\partial^2 w}{\partial r^2} + K\frac{1}{r}\frac{\partial w}{\partial r} \quad (4)$$

$$[0.1] \quad [0.1] \quad [10] \quad [10] \quad [0.1] \quad [0.1]$$

Whether the two inertial terms may be appreciable remains to be investigated from successive, multi-level funnel penetrations. A more detailed analysis is now being conducted in order to ascertain the importance of each term as a function of the radial and vertical coordinates. This will reveal the regions near and within the waterspout circulation where each term has significant importance.

5. RANKINE-COMBINED VORTEX

To obtain some idea of how well the waterspout measurements may be explained by a simple model, consider a steady circular vortex (cyclostrophic motion) with the tangential velocity described by a Rankine vortex, i.e., solid rotation in the core and irrotational motion outside of the core. Figure 5 illustrates the closeness with which the Rankine vortex fits the tangential wind velocity trace of the mature anticyclonic waterspout (Sec. 3.3.). Adjusting for the asymmetric flow, the fit chosen seems to best represent the data. From the vortex core, where $v = 0$, to the radius of maximum tangential winds, where v is 25 $m\text{-}sec^{-1}$, the Rankine vortex exhibits a flow field in solid rotation, i.e., the tangential velocity is directly proportional to the radius or $v = c_1 r$. Outside the radius of maximum winds, the v field is one of irrotational motion or $v = c_2 r^{-1}$ (c_1 and c_2 are constants). The tangential field of motion closely approximates the $v = c_2 r^{-1}$ relationship on the front side of the funnel and the $v = c_2 r$ relationship through the waterspout core. On the back side, however, the velocity trace beyond v_{MAX} (28 $m\text{-}sec^{-1}$) departs markedly from the Rankine model, i.e., the v measurements more closely approach that of a $v = c_3 r^{-\frac{1}{2}}$ profile until an approximate value of 10 $m\text{-}sec^{-1}$ reached ($r \simeq 28m$). From this radius, v

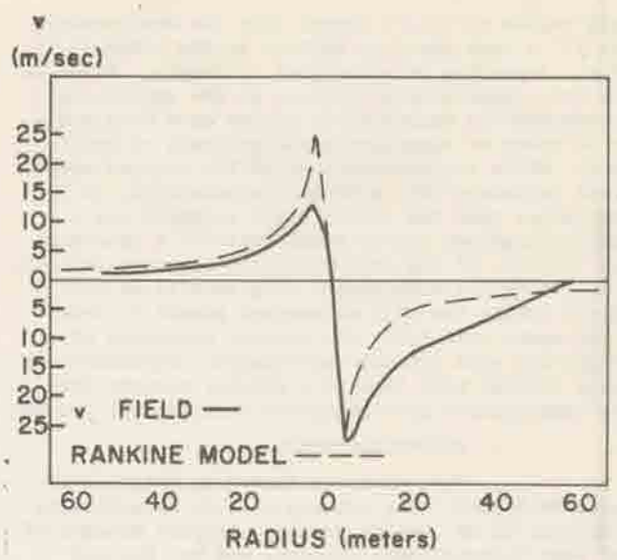

Figure 5: Rankine Model Fit To Mature Anticyclonic Waterspout

decreases linearly to zero at approximately 58 meters.

The scale analysis of r-equation of motion indicates that the cyclostrophic relation is a valid first approximation for describing the tangential flow field in the upper levels of the waterspout funnel. If we use the Rankine-Combined vortex to describe the tangential wind distribution, the cyclostrophic relation requires a total pressure deficit of 6.23 mb. The measured waterspout pressure deficit was 8.50 mb. The simple cyclostrophic-Rankine-Combined vortex model is thus capable of explaining approximately 74% of the total measured pressure deficit. This compares very favorably with Sinclair's (1966, 1973b) dust devil measurements which showed that this same simple model was capable of explaining approximately 75% of the total mean pressure drop from the environment to the dust devil center. This apparent discrepancy is attributed to the neglect of radial inflow and vertical motion in the cyclostrophic vortex model. Since radial inflow and vertical motion are characteristic of the waterspout structure at all altitudes, calculations of a core pressure deficit from the tangential wind field along will obviously be less than the true value. In this case, inaccuracies based on the somewhat arbitrary fitting of the Rankine vortex must also certainly exist. Also, terms in the r-equation of motion containing u may be of larger magnitude than that analyzed, particularly the inertial and turbulence terms containing $\partial u/\partial z$.

6. CONCLUSIONS

The waterspout velocity, temperature, and pressure fields obtained by an airborne measurement system have been presented and examined to produce an integrated picture of the waterspout vortex structure in the near-cloud base environment. The data shows that in the waterspout funnel there exists: (1) a core of rising motion of 5-10 $m\text{-}sec^{-1}$, (2) a horizontal circular flow field that is broader in weaker waterspouts and spatially concentrated in more intense waterspouts, (3) a central

core region of ~0.3°K warmer than the environment, and (4) a core pressure deficit on the order of ~1-10 mb. depending on waterspout intensity. Based on the data, some simplifications to the cylindrical, incompressible equations of motion have been made by an order of magnitude scale analysis of each term. While the present form of the reduced equations represent only a rough approximation, it has been shown that the cyclostropic relation and a Rankine-Combined vortex model explains a considerable portion of the measured total pressure deficit. A more detailed measurement program will be conducted during the 1975 waterspout season in order to document more fully the dynamic structure of larger and more intense waterspouts. Hopefully, these studies will lead to a greater insight into the waterspout's more energetic relative, the tornado.

7. . ACKNOWLEDGEMENTS

This work was funded by NOAA under Grant 04-5002-8. The authors wish to extend their gratitude to Mr. George Faraldo, Airport Manager of Key West International Airport, and Mr. Richard Urbanak, MIC of the WSO in Key West, for their generous assistance and cooperation during the field program.

8. REFERENCES

Church, C.R., C.M. Ehresman, and J.H. Golden, 1973: Instrumentation for probing waterspouts. Proc. Eighth Conf. on Severe Local Storms, Denver, CO, Oct. 15-17.

Fujita, T.T., 1970: The Lubbock tornadoes: A study of suction spots. Weatherwise, 23, 160-173.

Fujita, T.T., 1974: Jumbo tornado outbreak of 3 April. Weatherwise, 27, 116-119.

Golden, J.H., 1970: The lower Florida Keys waterspout project, May-Sept., 1969. BAMS, 51, 235-236.

Golden, J.H. and B.J. Morgan, 1972: The NSSL-Notre Dame tornado intercept program, spring 1972. BAMS, 53, 1178-1180.

Golden, J.H., 1973a: The life cycle of the Florida Keys waterspout as the result of five interacting scales of motion. Ph.D. Dissertation, Florida State U., 371 pp.

Golden, J.H., 1973b: Some statistical aspects of waterspout formation. Weatherwise, 26,108-117.

Golden, J.H., 1974a: Life cycle of Florida Keys waterspouts. NOAA Tech. Memo. ERL-NSSL-70, Natl. Severe Storms Lab., Norman, OK.

Golden, J.H., 1974b: The life cycle of Florida Keys waterspouts. I. JAM, 13, 676-692.

Golden, J.H., 1974c: Scale interaction implications for the waterspout life cycle. II. JAM 693-709.

Golden, J.H. and D. Purcell, 1974d: Velocity and morphological analysis of Union City, OK tornado, May 24, 1973. EOS Abstract, 56,No. 12.

Gutman, L.N., 1957: Theoretical model of a waterspout. Bull. Acad. Sci. USSR (Geophys. Ser.) Pergamon Press translation, N.Y. Vol. 1, 87-103.

Hoecker, W.H., 1960: Wind speed and air flow patterns in the Dallas tornado of April 2, 1957. Mon. Wea. Rev., 88, 167-180.

Kessler, E., 1970: Tornadoes. BAMS, 51, 926-936.

Kuo, H.L., 1966: On the dynamics of convective atmospheric vortices. JAS, 23, 25-42.

Kuo, H.L., 1969: Axially-symmetric flows in the boundary layer of a maintained vortex. Planetary Circulation Project Rept. No. 15, Dept. of the Geophys. Sci., U. of Chicago, IL, 57 pp.

Leslie, L.M., 1971: The development of concentrated vortices.: A numerical study. J. Fluid. Mech., 48, 1-21.

Lilly, D.K., 1965: Experimental generation of convectively driven vortices. Geofis. Intern., 5, 43-48.

Mehta, K.C., J.R. McDonald, J.E. Minor, and A.J. Sanger, 1971: Response of structural systems to the Lubbock storm. Texas Tech. U., Storm Res. Rept. 03, 1971.

RAND Report, 1968: Weather modification progress and the need for interactive research. Tenth Annual Rept., NSF.

Sinclair, P.C., 1966: A quantitative analysis of the dust devil. Ph.D. Dissertation, Dept. of Meteor., U. of Arizona, 292 pp.

Sinclair, P.C., 1969a: General characteristics of dust devils. JAM, 8, 32-45.

Sinclair, P.C., 1969b: Vertical motion and temperature structure of severe convective storms. Sixth Conf. on Severe Local Storms, Chicago, IL.

Sinclair, P.C., 1973a: Severe storm air velocity and temperature structure deduced from penetrating aircraft. Proc. Eighth Conf. on Severe Local Storms, Denver, CO, Oct. 15-17.

Sinclair, P.C., 1973b: The lower structure of dust devil. JAS, 30, 1599-1619.

Sinclair, P.C., 1974a: Vertical transport of desert particulates by dust devils and clear thermals. Proc. Atmosphere-Surface Exchange of Particulate and Gaseous Pollutants, Richland, Wash., AEC.

Sinclair, P.C., 1974b: Severe storm turbulent energy structure. Proc. Sixth Conf. on Aerospace and Aeronautical Meteor., El Paso, TX, Nov. 12-15.

Ward, N.B., 1972: The exploration of certain features of tornado dynamics using a laboratory model. JAS, 29, 1194-1204.

Ying, S.J. and C.C. Chang, 1970: Exploratory model study of tornado-like vortex dynamics. JAS, 27, 3-14.